CRANIODENTAL ADAPTATION AND HOMOPLASY IN EARLY MAMMALS

by

Anthony Maxwell Harper

A dissertation submitted to Johns Hopkins University in conformity with the requirements for the degree of Doctor of Philosophy

Baltimore, Maryland

September, 2019

Abstract

For the first two-thirds of their over 180-million-year history, mammals left a sparse fossil record. Often the only direct evidence of these early forms are small and unassociated craniodental fragments. Despite these limitations, the three chapters of this thesis support the effectiveness of this type of material for estimating the functional and autecological capacities in Mesozoic mammals, through high resolution imaging and morphometric analysis of the molariform dentition.

Each of the three chapters is a self-contained study addressing separate topics relating to the evolution of dental and petrosal morphology. The common thread between all sections is that variation in craniodental structure among Mesozoic lineages is greater than would be expected based only on the disparity seen among extant small mammals. This is a result of both the more "modern" dynamics of dental evolution in more Mesozoic mammalian lineages than historically appreciated (Chapters 1 and 3), and the more "primitive" morphology of the inner ear, even in groups very closely related to extant crown therians (Chapter 2). In both cases, the craniodental morphologies described are outside the range of variation seen in extant species.

Chapter 1 describes several new specimens from the herbivorous stem-therian mammal *Reigitherium*, from the Late Cretaceous of Patagonia. These newly available specimens demonstrate that the herbivorous molar morphology seen in *Reigitherium* is

derived from the more plesiomorphic tuberculosectorial pattern seen in the South American endemic group Meridiolestida.

Chapter 2 presents descriptions and analysis of the internal structure of three stem therian petrosal bones from the Late Jurassic of North America, and middle Cretaceous of Mongolia. Within the comparative context of labyrinthine endocast evolution, it can be determined that many of the advanced features of modern therian hearing likely developed only after their divergence from their common ancestor with the fossil groups described here.

Finally, Chapter 3 presents a macroevolutionary analysis of lower molariform shape change across a large sample of early mammaliaforms, using high-level morphometric methods. The results of this analysis suggest that the stochastic processes controlling the shape evolution of lower molariforms in crown Mammalia are shared across a wide range of "triconodont", "symmetrodont", and "tribosphenic" Mesozoic taxa.

Dissertation Adviser

Gabriel S. Bever

Dissertation Readers

Guillermo W. Rougier
Brian M. Davis
Adam D. Sylvester

When I lay asleep, then did a sheep eat at the ivy-wreath on my head—it ate, and said thereby: "Zarathustra is no longer a scholar."

It said this, and went away clumsily and proudly. A child told it to me.

I like to lie here where the children play, beside the ruined wall, among thistles and red poppies.

A scholar am I still to the children, and also to the thistles and red poppies. Innocent are they, even in their wickedness.

But to the sheep I am no longer a scholar: so willeth my lot—blessings upon it!

F. Nietzsche
Thus Spoke Zarathustra: Chapter 38 – On Scholars

Acknowledgments

Even during the darkest times in my academic and professional career, I have had the incredible good fortune of being able to look up toward several brilliant constellations. In the paleontological sphere these stars include the amazing people at the Los Angeles County Museums, especially Xiaoming Wang, Luis Chiappe, and Shelly Cox, who gave me my start as a volunteer in VP. I am also thankful for the kindness and patience shown by my supervisors Mark Roeder, Bruce Lander (both at Paleoenvironmental Associates), and Aaron Kaye (Badlands National Park) during my first part-time jobs in this field.

Since joining the JHU anatomy program it has been an amazing experience contributing to three field seasons in the Big Horn Basin of Wyoming with Amy Chew, Shawn Zack, and Tonya Penkrot. And I will also fondly remember driving across central Patagonia looking for huesitos with Leandro Canessa, Andy Lires, Willy Turrazini, and Luca Appella-Guiscafre. Gracias por aguantarme.

I have also been embarrassingly fortunate to have accumulated such an immense number of other friends, teachers and inspirations in paleontology, without whom this dissertation would have been impossible. Topping this list are Don Prothero, Michael Novacek, Rich Cifelli, ZheXi Luo, Annalisa Berta, Brian Davis, John Wible, Gabriel Bever, Eric Ekdale, David Weishampel, Cara Burres-Jones, Beth Strassler, Kena Fox-Dobbs, Paul Koch, Greg Wilson, Aneila Hogan, Yue Zhang, and Jessica Martin. To these folks I apologize for not knowing not to express how much your hard work and kindness has meant to me in this project, short of quoting G. G. Simpson the most prominent paleomammalologist, who in recommending his field to introverts like me wrote: “one of

the great values of paleontology is that it enables us to live in our own complex minds not just a few score years but more than three billion years."[1] Thank you for making those years so memorable.

Above all, I am grateful for the direction provided by the brightest stars in my graduate career - David Archibald, Ken Rose, and Guillermo Rougier. It's been a long strange trip. Thank you.

I also want to thank all my friends and teachers in the Earth sciences, starting especially with David Douglass, Bruce Carter, Ling O'Connor, and Gerry Lewis, at Pasadena City College's Geology Department, and the PCC Dana Club. As an undergraduate at UC Santa Cruz it was also a lot of fun taking part in several geology classes, and the 2007 Summer field season in the Inyo/White Mountains, thanks to the impressive organizational capabilities of Hide Schwatrz, Casey Moore, and Chris Pluhar (currently at Fresno State). I am also grateful to Gary Girty (SDSU), Ben Passey, and Naomi Levin (both currently at University of Michigan) for letting me into their exceptional graduate courses, and for allowing me to work on various non sequitur projects.

Outside of the classroom, I am also extremely lucky to have received advice and encouragement from Thomas Bown, Judy King (CSU Dominguez Hills), Andy Evans (Geologist at AECOM), and Kimberly "Rain" Miner (Geoscientist at the Army Geospatial Research Lab). Thank you all for providing me with a compass in this strange world. Once this dissertation is finished I hope to see you in the field soon.

The last decade and a half has also brought me into sympatric association with an amazing variety of biologists. The classes taught by Russell DiFiori (Pasadena City College), Tod Reeder, Marshall Hedin, Ken Burns, Michael Simpson, and Robert Zeller (SDSU) have been amazing experiences, for which I am extremely grateful. As a wildlife biologist at the San Diego Natural History Museum, working with my role models Scott Tremor, Phil Unit, Drew Stokes, Lori Hardgrove, Brad Holingsworth, and Melissa Stepek, has been one of the greatest times of my life. And my former supervisors Punkaj Kapahi (currently at Buck Institute), Viceca Sapin (Caltech), and Sandra Garver (SDSU anatomy), have also been inspirations to me throughout my academic career. Additionally, I have benefited immeasurably from the kindness of Patrick Luckett (JHU), Geoffrey Manley (University of Oldenburg), Steve Gliessman (UC Santa Cruz), Richard Etheridge, Mike Van Patten, Bob Mangan (the last three at SDSU), Phil Rundel (UCLA), Cindy Corbitt (University of Louisville), Samantha Young (Grossmont College), Yvea Moore (Crissy Field), and Isaac Simpson (Halibut for Humanity). Thank you all for making life so interesting.

I will also be forever grateful for the expertise and patience that my teachers in the rarified spheres of math and other technical fields have shown me; starting especially with Anna Osipova, my high school math teacher who convinced me to "stick with it." Likewise, this project would not have been possible without the superhuman commitment towards teaching shown by my graduate statistics professors Doug Deutschman and Matt Edwards at SDSU; and Gary Rosner, Robert Scharpf, Fernando Pineda, Frank Curriero, and Adam Sylvester at JHU. What little illustration skill I have is entirely due to the amazing talents of

Tim Phelps, Ian Suk, Juan Garcia, and Gary Lees in the Johns Hopkins Art as Applied to Medicine Department; and the fact that this dissertation exists at all is due to Arlene Daniel (JHU Functional Anatomy and Evolution). To the many people I have missed here, please know that I am very sorry that I will never be able to list everyone who has indispensably helped me along my academic and professional trajectory. To everyone who has ever gotten behind me and helped push, thank you.

Finally, because the best part of being a mammal is having a mom, I thank first and foremost my mom Lynn, and her mom Mary Ann ("Mimi"). Thank you for letting me pick apart those owl pellets, and everything else.

[1]In: Laporte, L. 2000. George Gaylord Simpson: Paleontologist and Evolutionist. Columbia University Press

Publications and Coauthors

The material in Chapter 1 is published as:

> Harper, T., A. Parras, and G. W. Rougier. *Reigitherium* (Meridiolestida, Mesungulatoidea) an enigmatic Late Cretaceous mammal from Patagonia, Argentina: morphology, affinities, and dental evolution. Journal of Mammalian Evolution (2018). https://doi.org/10.1007/s10914-018-9437-x

This work was accomplished with the expert help and advice of the following coauthors:

> Ana Parras, INCITAP (CONICET-UNLPam), Facultad de Ciencias Exactas y Naturales, Universidad Nacional de La Pampa, Uruguay 151, 6300 Santa Rosa, La Pampa, Argentina
>
> Guillermo W. Rougier, Department of Anatomical Sciences and Neurobiology, University of Louisville, 511 S. Floyd St., Louisville, KY 40202, USA

In particular, the sections "Study Area and Sample Provenance" and "Geological Background" in Chapter 1 were written by Ana Parras, one of the original discoverers of the Anfiteatro locality.

The material in Chapter 2 is also published at PLOS One as:

> Harper, T., and G.W. Rougier. Petrosal morphology and cochlear function in Mesozoic stem therians. PLOS One 14 (2019). e0209457. https://doi.org/10.1371/journal.pone.0209457

with Guillermo W. Rougier as second author.

Each of the three chapters are formatted according to the guidelines provided by the journal where they are published or are planned to be published. Chapter 3 and the bibliography for the introduction and summary are formatted according to the guidelines for the Journal of Vertebrate Paleontology.

Contents

List of Tables

List of Figures

1 Introduction

Modern mammals are an unrepresentative sample of their past biodiversity. This is a product of the highly unbalanced survival of both major lineages of crown Mammalia in the modern fauna, and the relatively recent common ancestry of therian mammals, the group representing the vast majority of all living species (Rose, 2006; also see Tarver and Donoghue, 2011; Mitchell, 2015). Despite these biases, the relatively small body-size of a "typical" mammalian species (both in terms of abundance and diversity) represents a major point of continuity between the the modern fauna and the earliest known mammals in the Mesozoic (Clauset and Redner, 2009; Cooper and Purvis, 2010; Smith et al., 2010; Smith and Lyons 2011; Slater, 2013; Saarinen et al., 2014; Baker et al., 2015). The large number of apomorphies uniting all extant small mammals in the clade Theria (Rowe, 1988) does however call into question the usefulness of extant small-bodied taxa as representatives of mammals generally, especially the most ancient forms. The major goal of this dissertation is to allow the available material evidence of the earliest mammals to speak for itself regarding the functional limitations and ecological restrictions experienced during the first two-thirds of mammalian history.

The nature of the fossil record also imposes its own sampling restrictions. Being relatively rare members of Mesozoic "microvertebrate" assemblages, the variety of diagnostic material referred to early mammals is usually limited to unassociated fragments of the dentition, mandible, and cranium (e.g. Simpson, 1928, 1929; Kielan-Jaworowska et al., 2004). All three chapters of this dissertation therefore leverage the information available in isolated craniodental remains through the use of high-resolution visualization techniques, and "high-level" (sensu Evans et al., 2007) comparative methods compatible with the wide

range of morphologies seen across the the earliest mammals and their near relatives. Specifically, the application of dental topography metrics (Evans et al., 2013) in Chapter 1, and spherical harmonic morphometric registration (Shen, et al., 2009) in Chapter 3, are shown to be effective for the analysis of a wider range of dental morphology than traditional homology-based techniques would be capable of. All three chapters utilize high-resolution micro-CT imaging and/or surface scanning for the rendering and reconstruction of extremely small mammalian craniodental specimens.

This digitized sample of early mammalian fossils is used to qualify and revise several hypotheses about the function and adaptive significance of craniodental characteristics seen in some of the most obscure early mammalian taxa from both the Northern and Southern Hemispheres. In Chapter 1, a collection of newly discovered dental and mandibular specimens referable to the South American Late Cretaceous "pretribosphenic" mammal *Reigitherium* is described and quantitatively compared with contemporary and later therian mammals. The conclusions of this chapter support the nested position of *Reigitherium* within a Cretaceous-Cenozoic, South American radiation of occasionally large-bodied and herbivorously adapted "pretribosphenic" mammals termed the mesungulatoids, and demonstrates the uniquely complicated dental topography attained by *Reigitherium* in the Late Cretaceous. In Chapter 2, the internal morphology of the petrosal bone in three northern mammalian specimens (from North America and Asia) is described. Here, high-resolution micro-CT imaging is used to generate detailed labyrinthine endocasts which illustrate the extent and connectivity of several venous structures associated with the cochlear apparatus. These three petrosal specimens, belonging to the Late Jurassic triconodontid *Priacodon fruitaensis* (Rougier et al., 1996) and the Aptian-Albian Mongolian fossils known as the Höövör petrosals (Wible et al., 1995), are some of the most plesiomorphic three-

dimensionally preserved cranial remains referable to crown mammals. As such, this chapter focuses on physiological implications of the size, and vascularization of the cochlear canal, along with references to the soft tissue anatomy of the inner ear seen in extant model taxa. The derived characteristics, but plesiomorphic geometry, of the Höövör Petrosals in particular support their close relationship with modern therian mammals, but likely very limited capacity for high-frequency hearing. Finally, Chapter 3 provides a large-scale analysis of the tempo and mode of morphological transformation seen for a wide sample of early mammaliaforms. This chapter uses the surface reconstructions of representative lower molariforms as an evolutionary proxy for feeding adaptation generally. Because of the wide range of morphologies involved, this macroevolutionary analysis relies on several computational techniques which require minimal assumptions regarding a priori homological correspondence among the sampled specimens, and permit a wide range of possible covariance structures to be estimated throughout the evolutionary history of the sampled taxa. This chapter also incorporates new observations on the internal petrosal anatomy of the northern hemisphere taxa described in Chapter 2 and several South American endemic taxa into the morphological character matrix used to scale branch lengths for the required input phylogeny in this analysis. The results support the lack of punctuational change in evolutionary mode within the clade Theria, and provides some ambiguous support for the much more inclusive clade Theriimorpha having a unique variational dynamics of lower molariform shape change relative to all other sampled mammaliaform taxa.

A common theme among these chapters is the unrepresentative nature of modern small crown therians as living analogs of their earliest ancestors. This is both because of the uniquely complex herbivorous nature of the dentition seen in the Cretaceous South American stem therians described in Chapter 1; and the relatively plesiomorphic condition

of the auditory apparatus in the northern stem therian taxa described in Chapter 2. In both of these chapters, the newly described morphology is outside of the range of variation seen in crown therians. These two chapters emphasize the importance of the deliberate inclusion of relatively under-studied taxa (e.g., stem therians), and under-represented biogeographical regions (e.g., the Southern Hemisphere) for an unbiased understanding of craniodental adaptation and function in the earliest mammals. Chapter 3 therefore utilizes one of the most inclusive datasets available for the macroevolutionary analysis of lower molariform shape in Mesozoic mammaliaforms; and, in this context, fails to support the unique nature of dental evolution within the therian clade. The pattern of craniodental adaptation and homoplasy in modern therian mammals can therefore be seen as an extension of evolutionary processes beginning much earlier in the Mesozoic. However, because of the long amounts of time involved, these processes are no longer recognizable in samples composed solely of extant taxa.

The following paragraphs provide a brief introduction to the particular problems tackled by the three chapters of this dissertation. Additional comments on methodology, anatomy and systematics used in this dissertation are provided in the final summary section.

The strange case of *Reigitherium*

During the 1984 field expeditions of the Museo Argentino de Ciencias Naturales led by José Bonaparte, a small enigmatic molar specimen was collected from the Upper Cretaceous Los Alamitos Formation in Rio Negro, Argentina. Although fragmentary, this specimen was recognized as a mammal because of its surface complexity, and was accessioned as the type specimen of *Reigitherium bunodontum* by Bonaparte, (1990). Based on this limited evidence

Bonaparte identified this type specimen as an upper molar and insightfully suggested the sister relationship of *Reigitherium* with *Mesungulatum houssayi*, the first Mesozoic mammal recovered from South America. During the following decade, subsequent sampling efforts in the Upper Cretaceous La Colonia Formation in Chubut, Argentina (Rougier et al., 2009), recovered additional material referable to *Reigitherium*. This included a mandibular specimen described by Pascual et al, (2000), preserving enough of the dentition to demonstrate the lower molar identity of the holotype specimen. These authors also hypothesized the phylogenetic placement of *Reigitherium* within Docodonta, a diverse Mesozoic clade outside of the mammalian crown group and otherwise unrecorded in the Southern Hemisphere (but see abstract by Martin et al., 2013).

While both docodonts and *Reigitherium* show highly complicated, and often crenulated, molar morphologies, the descriptions provided in Chapter 1 present several new upper and lower dental elements for *Reigitherium* newly recovered from the La Colonia Formation (Rougier et al., 2009), which support its membership within the South American clade of "pretribosphenic" mammals termed the meridiolestidans (Rougier et al., 2011, 2012). Being an endemic lineage of stem therians, the meridiolestidans were relatively neglected in prior reviews of the mammalian dentition. Within the Cretaceous, however, the level of morphological adaption towards an increasingly herbivorous diet is taken further within the meridiolestidan lineage than in crown therians or any other trechnotherian taxon (mammals characterized by highly triangulated molar cusps, or their derivatives; Paez-Arango, 2008). This is in addition to the presence of several remarkable similarities seen between meridiolestidans and the earliest therians, such as seen in molar dental formula and the absence of Meckel's groove. Within Meridiolestida, the material described in Chapter 1 additionally supports the sister-relationship of the shrew-sized *Reigitherium* with the sheep-

sized, Early Paleocene meridiolestidan *Peligrotherium* (Paez-Arango, 2008). Through the use of high-level (sensu Evans et al., 2007) dental topography metrics, the level of herbivorous adaptation apparent in these two taxa is shown to be greater than that seen in even the most hervbivorously adapted therian mammals known from the Cretaceous, and is within the numerical range seen in the herbivorous marsupials likely replacing the meridiolestidans during the Cenozoic.

Morphology and performance of the early mammalian ear

Most small therians today have an extraordinary capacity for high-frequency airborne sound detection (Manley, 2018). At the level of sensorineural transduction, this capacity is facilitated by physiological and anatomical features present in the cochlear apparatus and surrounding structures within the otic capsule (Luo et al., 2016). The apomorphic distribution of these characters, relative to monotremes and sauropsid amniotes, also points to the origins of high-frequency adaptation somewhere among the early ancestors of the exclusively therian lineage; i.e., among the stem therians (Manley, 2017). Chapter 2 presents descriptions of the petrosal bone (the major component of the ossified otic capsule in mammals) in three early stem therian specimens.

The use of high-resolution micro-CT renderings of these specimens identifies osteological correlates of several of the functionally significant therian soft-tissue cochlear structures. In particular, the virtual labyrinthine endocasts figured in this chapter demonstrate the presence of the secondary bony lamina in both *Priacodon fruitaensis* and the Höövör petrosals. The Höövör specimens additionally show other derived features, such as a general reduction of venous sinuses within the pars cochlearis of the petrosal, but the first

appearance of a small venous conduit supplying the abneural side of the cochlear canal. Based on the location and connectivity of this neomorphic canal, its contents can be reliably reconstructed as the vein of the cochlear aqueduct, the major venous drainage for all contents of the pars cochlearis in therian mammals today (Axelsson, 1988). The appearance of this structure in the Höövör petrosals is hypothesized to be related to the increasing size and reliance on the stria vascularis as the major endolymph secreting organ within the ancestral therian lineage.

In extant therians the stria vascularis is the sole endolymph secreting organ, and is responsible for the production of the highly positive endocochlear electrical potential required for the reception of high-frequencies (Manley, 2017). The presence of bony laminae in living therians also supports the macromechanical form of cochlear tuning seen only in mammals (Manley, 2000). The presence of these features in the earliest stem therians could therefore be taken to imply the "modern" high-frequency capabilities of the earliest therians. However, the generally plesiomorphic geometry of the cochlear endocast and lack of primary bony lamina in the short, straight cohlear canal of the stem therian petrosals described here suggest that neither a wide enough octave range, nor high enough maximum detectable frequency, were present to allow these forms to detect ultrasonic frequencies. The appearance of the apomorphic cochlear features described in our sample could therefore be related to increasing sensitivity and resolution within an ancestral frequency range, but were not sufficient for the highly precise mechanisms of sound source localization seen in extant therian mammals.

Physical models of molariform shape evolution

The dentition in Mesozoic mammaliaforms varies in different directions, and to different extents, than their extant toothed representatives - the therian mammals. In the case of the lower molariform series this can be seen in the wide differences in formula (up to nine molars in some dryolestoids) and crown morphology (linear, triangular, tribosphenic) seen across many Mesozoic lineages. The stark contrasts and limited preservation in the fossil record of mammaliaforms creates many obstacles for investigators interested in quantitatively representing the complete range of this morphological diversity in a single coordinate system. A major part of the problem is the ambiguity of biological correspondence between structures expressed on the molariform crown surface, and the required assumptions of strict (point-wise) homology between registration points used in the most common morphometric techniques. The macroevolutionary analysis of lower molariform shape presented in Chapter 3 uses several morphometric techniques and probabilistic models originally formalized in the physical sciences, which therefore require fewer a priori assumptions of biological "sameness", or evolutionary covariance between the structures analyzed. In particular, the application of the spherical harmonic registration protocol for lower molariform surfaces outlined in this chapter is shown to be successful at accommodating a wider range of shape variation than more traditional sliding-semilandmark based techniques.

Using these spherical harmonic shape specifiers, different macroevolutionary scenarios of molariform shape change are contrasted as multivariate Brownian motion processes evolving over mammaliaform phylogeny (Polly, 2004; Clavel et al., 2015). Because of the predominance of extinct taxa included in this sample, the time-calibrated phylogeny used to account for autocorrelation in molariform shape in this analysis was generated using

a Bayesian total-evidence estimation procedure and updated morphological character data including inner ear characters described in Chapter 2.

The most supported models resulting from this analysis all suggest the lack of a punctuational shift in evolutionary mode soley within the northern tribosphenic (therian) lineage. Given the fact that the function of the tribosphenic molar requires the precise interlocking of the corresponding upper molar protocone with the basined talonid of the lower (Polly et al., 2005), and the overwhelming success of therian mammals today, this lack of a therian-specific evolutionary mode for lower molar shape change may seem surprising. However, given the presence of many independent groups showing dental modifications for elaborate mastication and omnivory (such as *Reigitherium* and other meridiolestidans) these models show that the processes influencing the principal components of lower molariform shape likely began earlier in time and in a much more inclusive group than just the crown clade Theria.

Chapter 1: *Reigitherium* (Meridiolestida, Mesungulatoidea) an enigmatic Late Cretaceous mammal from Patagonia, Argentina: morphology, affinities, and dental evolution

ABSTRACT

New dental and dentary fossils collected in the Upper Cretaceous La Colonia Formation in central Patagonia provide new evidence on the morphology, feeding ecology, and relationships of the enigmatic mammal *Reigitherium*. The newly discovered specimens described here include elements of the upper dentition and several partial dentaries, elucidating fundamental questions of serial homology and postcanine dental formula (four premolars and three molars). This new evidence supports a nested position of *Reigitherium* within the advanced meridiolestidan clade Mesungulatoidea. Apomorphic features of the upper and lower molariform elements include intense enamel crenulation circumscribed within the primary trigon and trigonid, elevated cingulids, and the neomorphic appearance of cusps/cuspulids, all of which increase overall crown complexity. A Dental Topography Analysis comparing *Reigitherium* and its sister taxon *Peligrotherium* to Cretaceous and Cenozoic therians demonstrates functional similarity between the mesungulatoids and South American marsupial taxa that succeed them in the small-to medium-sized herbivore niche during the Paleocene. Previous taxonomic attributions of *Reigitherium* are discussed and comparisons with other meridiolestidans highlight the remarkable radiation of this group in the Cretaceous of South America.

INTRODUCTION

Concurrent with the initial division and differentiation of the Late Cretaceous lineages of the crown group Theria in the Northern Hemisphere (Archibald and Deutschman 2001; Grossnickle and Polly 2013; Halliday and Goswami 2016; Grossnickle and Newham 2016), the mammalian fauna of South America had already achieved a state of prominent diversity within microvertebrate fossil assemblages (Rougier et al. 2010). The most abundant and diverse of these Late Cretaceous Gondwanan endemic mammals are referable to a monophyletic grouping of stem therians termed the Meridiolestida (Rougier et al. 2011). These species therefore represent an independent phylogenetic experiment with which to compare the trajectory of mammalian evolution in northern continents before and near the K-Pg boundary (e.g., Jernvall et al. 1996; Woodburne et al. 2014).

Morphological comparisons using meridiolestidans are also particularly valuable because of the specific craniodental similarities between meridiolestidans and hypothetical reconstructions of the therian common ancestor, such as the reduction to three molars and an enlarged and triangular fifth-from-last successor tooth (blade-like in early therians, but pyramidal in the Meridiolestida; McKenna 1975; Prothero 1981; Luckett 1993; Rougier et al. 2012). Because of their likely derivation from Jurassic dryolestoids (or a related pretribosphenic group with similar dental formulae and crown morphology), many of these similarities are likely the result of convergence and/or parallelism, in addition to shared ancestry (Gould 2002). These features, combined with the retention of stem therian symplesiomorphies, have also underwritten much of the confusion seen in the taxonomic history of the better known meridiolestidan taxa. For example, the fossorial *Necrolestes* (Rougier et al. 2012; Wible and Rougier 2017) has been variously interpreted as an aberrant

metatherian or eutherian, and the large herbivorous *Peligrotherium* (Bonaparte et al. 1993; Gelfo and Pascual 2001) was first assigned to the eutherian family Periptychidae.

The latest Cretaceous meridiolestidan *Reigitherium* (Figs. 1 and 2) has been the subject of an altogether different battery of alternative interpretations. While originally described as a dryolestoid by Bonaparte (1990), several later authors ascribed it to a stem mammaliaform group far distant from the crown clade Theria (Pascual et al. 2000). This diversity of opinion has been enabled by the limited material and highly derived morphology presented by this taxon, which has been commented on by Kielan-Jaworowska et al. (2004) as warranting an ordinal distinction from Docodonta. These authors subsequently assigned *Reigitherium* to Mammalia (sensu lato), subclass and order incertae sedis.

Additionally, while being distinctive at the generic level, the ornamented and labially distended morphology seen in the molariforms of *Reigitherium* have made diagnosis of the principal anatomical axes (mesiodistal, labiolingual etc.) and the upper versus lower attribution of isolated dental elements uniquely problematic. The apomorphic complexity and ambiguity manifest in the dentition of *Reigitherium* have caused the misidentification of its holotype, a lower right molar recovered from the Los Alamitos Formation (described as an upper left molariform in its initial description by Bonaparte 1990). The later report of three sequential lower postcanines (p3, p4, and m1 based on current interpretations) preserved in situ by a dentary fragment recovered from the La Colonia Formation made clear the lower molar identity of the type specimen (Pascual et al. 2000). However, based on this evidence these authors transferred *Reigitherium* (within a monotypic family) from Dryolestoidea to Docodonta, a clade currently unrecorded from South America (however, see Martin et al. 2013).

Expanded samples of isolated dental and gnathic remains recovered from two localities in the La Colonia Formation during field expeditions organized by one of us (GWR) in collaboration with the Museo Paleontológico Egidio Feruglio (MPEF) corroborate the original taxonomic assignment of *Reigitherium* as a dryolestoid (or dryolestoid-like) mammal, and further underscore its eccentric position outside the range of dental morphologies known in any other stem therian lineage (Patterson 1956; Hershkovitz 1971; Kielan-Jaworowska et al. 2004). These new and better preserved specimens also greatly clarify major aspects of cusp homology, dental formula, and the phylogenetic placement of *Reigitherium* among the advanced meridiolestidans. This report summarizes the provenance and anatomy of these new specimens, and provides explicit comparisons with the dentition of better known meridiolestidans and other crown mammals.

Fig. 1 Reconstruction of upper postcanine series. Schematic illustrations of upper left penultimate and ultimate premolars and molars in **A** *Peligrotherium*; **B** *Coloniatherium*; and **C** *Reigitherium*

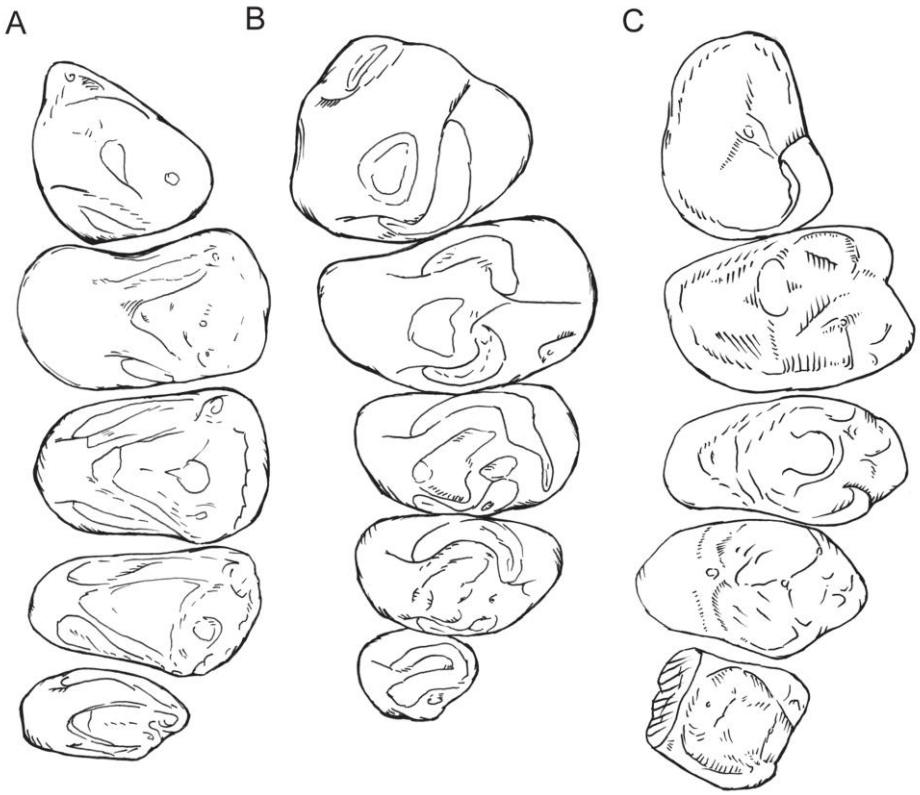

Fig. 2 Reconstruction of lower postcanine series. Schematic illustrations of lower right penultimate and ultimate premolars and molars in **A** *Peligrotherium*; **B** *Coloniatherium*; and **C** *Reigitherium*

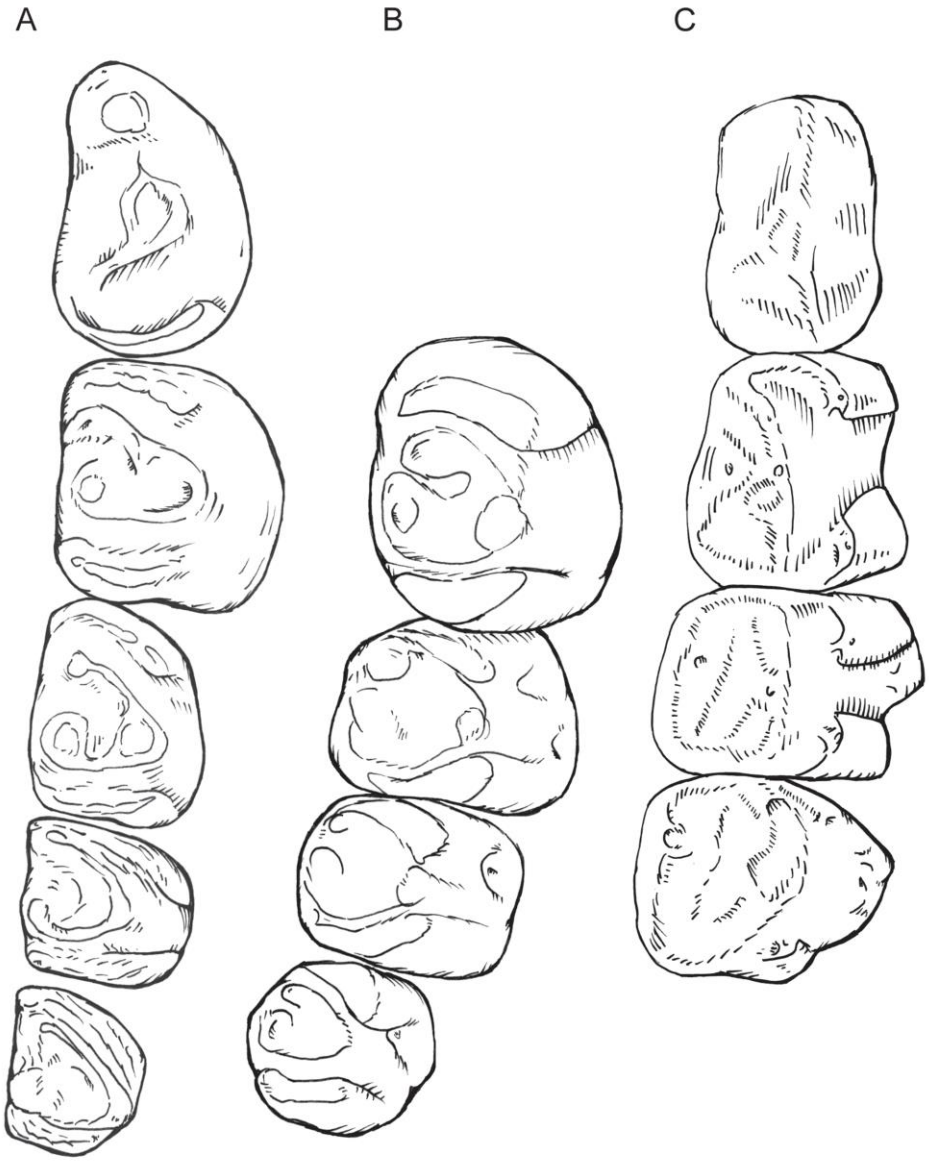

Study Area and Sample Provenance. The new specimens come from middle strata of the La Colonia Formation (second facies association of Pascual et al. 2000), in the "Anfiteatro" area, located at the southeastern slope of the Sierra de La Colonia, in the vicinity of Cerro Bayo, Chubut Province (Argentina). The exposed sedimentary rocks in this area are characterized by the predominance of massive or laminated claystones and siltstones, with intercalations of massive, laminated or cross-bedded sandstones (see "Norte de Cerro Bayo 1" and "Norte de Cerro Bayo 2" sections, in Gasparini et al. 2015).

Mammal remains were collected from intercalated, very thin lenses (< 0.2 m) of scarce lateral extension, located ~70 m from the bottom of the outcrops as part of a column sampling in search of microfossils. The lenses have a pelitic-sandy matrix with abundant gypsum, and consist of millimeter-scale remains of aquatic and terrestrial vertebrates, mainly fishes, but also and in very low proportion mammals, amphibians, and reptiles. The specimens are mostly concentrated in a bed of ~1 to 4 cm in thickness, are disarticulated and chaotically oriented, and most of them are fragmented with rounded and polished broken surfaces showing a high degree of alteration. The fossils are poorly sorted by size, with complete isolated elements smaller than a millimeter preserved together with relatively large isolated dinosaur bones (several tens of centimeters). The taphonomic attributes suggest that the fossil producing layers were formed by hydraulic transport of the fossils previous to their deposition (Varela and Parras 2013; Gasparini et al. 2015). The unsorted composition and thin vertical extent of these lenses suggest that their genesis is attributable to discrete sedimentary events (such as storm surges or mass wasting) in which current velocity rapidly drops to zero. The new specimens described here come from a single lens we call Anfiteatro 1 (coordinates available upon request).

Geological Background. The La Colonia Formation (Pesce 1979) crops out along the south-eastern margin of the Somún Curá Plateau, northern central Chubut Province, Argentina. This stratigraphic unit represents a variety of paleoenvironments including fluvial, marginal marine, and shallow marine deposits (Ardolino and Franchi 1996; Pascual et al. 2000), originating during the initial stages of the Late Cretaceous/Paleocene transgression from the Atlantic Ocean in Patagonia.

At the Sierra de La Colonia area, three facies associations were described as occurring in the La Colonia Formation (Pascual et al. 2000). According to these authors the lowermost facies association is characterized by cross-bedded sandstones and conglomerates deposited in a moderate to low sinuosity fluvial environment. However, Cúneo et al. (2014) interpreted these deposits as representing shoreface sedimentation dominated by bi-modal processes, a product of the initial phase of the Late Cretaceous Atlantic transgression. The second facies association is the thickest and most representative of the La Colonia Formation and contains most of the vertebrate remains, and aquatic and terrestrial plants, so far collected (e.g., Pascual et al. 2000; Rougier et al. 2009b; O´Gorman et al. 2013; Cúneo et al. 2014; Gasparini et al. 2015). It is composed mostly of massive and laminated claystone-siltstone with intercalations of massive, laminated, or cross-bedded sandstones deposited in marginal marine environments, such as estuaries, tidal flats, littoral lagoons or coastal plains, influenced by both freshwater stream flows from the continent and tidal currents from the sea (Ardolino and Delpino 1987; Page et al. 1999; Pascual et al. 2000; Gasparini et al. 2015). From sedimentological characteristics together with ecological requirements of the well-preserved collected fauna (mostly terrestrial, fresh, and brackish water taxa), Gasparini et al. (2015) suggested that deposition would have been mostly in low-energy restricted environments, like muddy flood plains, marshes, and ponds cut by meandering channels,

probably in the central mixed-energy zone within an estuary. Alternatively, sedimentary deposits outcropping between Cerro Bosta locality and the Cañadón del Irupé/Quebrada del Helecho were interpreted by Cúneo et al. (2014) as a barrier-island/lagoon complex occurring along irregular clastic coastal plains bathed by shallow seas.

The uppermost facies association is composed of laminated claystones containing remains of bivalves and it was regarded as deposited in the upper part of an intertidal flat environment (Pascual et al. 2000). Toward the northeast in Telsen area, Guler et al. (2014) recognized, based on the composition of palynological assemblages and sedimentological data, a progressive upward-shallowing trend for this upper part of the La Colonia Formation, consisting in shoreface to offshore deposits at the bottom and intertidal-flat to supratidal environments toward the top.

Regarding the age of the La Colonia Formation, at the study area the base is marked by the unconformity that separates this unit from the subjacent rocks of the Cerro Barcino Formation of the Chubut Group. Geochronological data from the uppermost part of the Cerro Barcino Formation in the margins of the Río Chubut, south of the study area, gave a U-Pb zircon age of ~97.4 Ma, constraining the Chubut Group to an age not younger than the Cenomanian (Suárez et al. 2014). Therefore, the age of the base of the La Colonia Formation depends on the time span encompassed by the unconformity below, but could not be older than Cenomanian. On the other hand, Ardolino and Franchi (1996), based on micropaleontological data, regarded the upper part of this unit as Campanian-Maastrichtian in age. Recently, Guler et al. (2014), based on palynological data, suggested an age not older than Paleocene for the uppermost part of the unit in the Telsen area. In short, the La Colonia Formation was deposited in the Late Cretaceous, most probably during the Campanian–Maastrichtian, with the uppermost strata extending to the Paleocene. The Late

Cretaceous Los Alamitos Formation is also interpreted as being of Campanian–Maastrichtian age and yielded the type specimen of *Reigitherium bunodontum*, an isolated molar (Bonaparte 1990; see below). The facies yielding mammals in the Los Alamitos Formation reflects shallow lacustrian to lagoonal environments with a likely near-shore location and laterally interdigitating with marine sediments (Andreis 1987; Andreis et al. 1989). Both the La Colonia and Los Alamitos formations were deposited as part of the epeiric sea environment formed by the fragmented archipelago developed in what it is present-day northern Patagonia during the Late Cretaceous-Paleocene Atlantic transgression (Malumián and Caramés 1995; Goin et al. 2016) and the invasion of the extensive Kawas sea (Riccardi 1987; Hugo and Leanza 2001). Based on faunal composition it is likely, but not certain, that the specimens from La Colonia Formation are younger than those from both the Los Alamitos Formation and the contemporaneous (or near contemporaneous) Allen Formation in northernmost Patagonia (Rougier et al. 2009a).

MATERIALS AND METHODS

A few isolated mammalian teeth were found by one of us (AP) during the processing of sediment samples in search of microfossils. The sediment was soaked and washed in a screen with a 6.2 mm aperture that removed the bulk of the pelitic fraction and then separated in fractions using screens with 4, 2, and 1 mm of mesh size. The picking was done manually under binocular microscope and mammalian specimens were recovered from all fractions. Variations of this procedure were used more recently (GWR and collaborators) to process larger samples aimed at microvertebrate collection, such as using a deflocculant:

sodium silicate (Na_2SiO_3) with a 1.4-7 specific density, which was very helpful to shorten the pre-wash soaking of the sediment. The final mesh size was reduced to 0.65 mm.

Systematic analyses including *Reigitherium* and nine other taxa referable to Mesungulatoidea, Meridiolestida, and/or Dryolestoidea were conducted using phylogenetic estimations based on both Maximum Parsimony and Bayesian (maximum a posteriori) optimality criteria. These tree searches were implemented with the programs PAUP* version 4.0 (Swofford 2002) and MrBayes version 3.2 (Ronquist et al. 2012) using standard parameterizations, as described below. Convergence diagnostics were checked for the Bayesian analysis using programs packaged with the program BEAST (Drummond et al. 2015).

Quantification of high-level morphological features in the lower second molars from a comparative sample of tribosphenic mammals, *Reigitherium*, and *Peligrotherium* are reported below in the context of a Dental Topographic Analysis (Evans et al. 2007; Boyer 2008; Bunn et al. 2011). Dental metrics were measured from surface files generated from surface scans and CT imaging. Because all surface information is subsampled to approximately 10,000 triangular faces before further processing, no systematic difference in topography is detectable between data generated from either method. The Bissekty eutherians were micro-CT scanned at 27 micrometer resolution using the GE Explore Locus rodent CT scanner housed at the Moores Cancer Institute at the University of California, San Diego. The marsupial taxa and *Peligrotherium* were scanned using a HDI Advance white light surface scanner. Finally, the specimen of *Reigitherium* used was converted to a surface file from approximately 9-micrometer resolution micro-CT images generated at the Shared Materials Instrumentation Facility (SMIF) at Duke University. All surface files were cropped and edited using default smoothing and re-meshing algorithms implemented by the programs

Amira and Geomagic Wrap. All surface editing protocols followed guidelines recommended by Spradley et al. (2017); and computations were performed with the R package *Mola*R (Pampush et al. 2016). The anatomical terminology employed for the following descriptions follows Keilan-Jaworowska et al. (2004) and Rougier et al. (2009a, 2011, 2012) unless otherwise indicated (Fig. 3).

All data generated or analyzed for this study are included in the supplementary materials associated with this publication, in addition to a table summarizing all new specimens of *Reigitherium* described below. Surface files of all lower second molars included in our Dental Topographic Analysis, and several additional surface models of *Reigitherium*, are available from the corresponding author upon request.

Fig. 3 Crown terminology used here. **A** upper molariform features: ecst, ectostyle (accessory cusp); frenc, frenular crests; mest, metastyle; pa, paracone; past, parastyle; popc, postparacrista; prepc, preparacrista; sty, stylocone. **B** lower molariform features: daccd, distal accessory cuspulid; dcng, distal cingulid; enc, enceinte; frenc, frenular crests; laccd, labial accessory cuspulid; maccd, mesial accessory cuspulid; mcng, mesial cingulid; mtd, metaconid; prd, protoconid

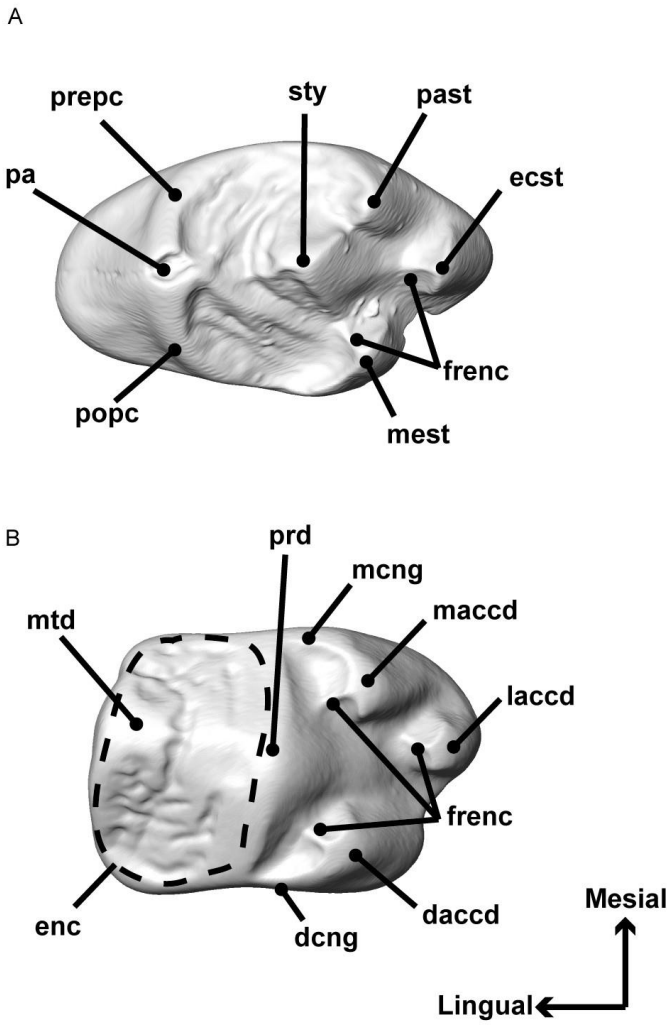

Institutional Abbreviations. CCMGE, Cheryshev's Central Museum of Geological Exploration, St. Petersburg, Russia; FMNH, Field Museum of Natural History, Chicago; MACN- Museo Argentino de Ciencias Naturales "Bernardino Rivadvia," Buenos Aires, Argentina; MLP- Museo de La Plata, La Plata, Argentina; MNHN, Institute de Paléontologie, Muséum National d'Histoire Naturelle, Paris, France; MNRJ – Museo Nacional Rio de Janeiro, Rio de Janeiro, Brazil; MPEF-PV Museo Paleontológico Egidio Feruglio, Chubut, Argentina, Paleontología de Vertebrados; URBAC, Uzbek/Russian/British/American/Canadian joint paleontological expedition specimens; ZIN, Zoological Institute of the Russian Academy of Sciences, St. Petersburg, Russia.

SYSTEMATIC PALEONTOLOGY

Class MAMMALIA Linnaeus 1758

Clade CLADOTHERIA McKenna,1975

Superorder DRYOLESTOIDEA Butler, 1939

Order MERIDIOLESTIDA Rougier et al. 2011

Clade MESUNGULATOIDEA Rougier et al. 2011

Family REIGITHERIIDAE Bonaparte, 1990

Reigitherium Bonaparte, 1990

Type Species. *Reigitherium bunodontum*, Bonaparte, 1990. The specific epithet was changed from *bunodonta* to *bunodontum* by Pascual et al. (2000), to match the neutral gender of the genus.

Holotype. MACN-RN-173: An isolated and fragmentary lower right m2, recovered from the "green-colored bed just below the concretionary top of the Cerrito del Mamifero, middle section of the Los Alamitos Formation" (Bonaparte 1990: 66). West Slope of Cerro Cuadrado locality, Arroyo Verde, Río Negro province, Patagonia, Argentina.

Distribution. Latest Cretaceous (Campanian-Maastrichtian); "Alamitan" South American Land Mammal Age (SALMA). Los Alamitos and La Colonia formations. Río Negro and Chubut provinces, Argentina.

Referred Specimens. MPEF-PV 606: A partial left dentary preserving lower premolars 3-4 and the lower first molar, described by Pascual et al. (2000). Recovered from the "second facies association of the La Colonia Formation, on the southern slopes of the North Patagonian Massif" (Pascual et al. 2000: 402), Chubut province, Patagonia, Argentina.

The new specimens described below were recovered from the El Uruguayo and Anfiteatro 1 localities, upper part of the La Colonia Formation, Chubut province, Patagonia, Argentina. These specimens include: MPEF-PV 2014, dentary fragment; MPEF-PV 2020, dentary fragment; MPEF-PV 2072, P4; MPEF-PV 2237, m2; MPEF-PV2238, M1; MPEF-PV 2317 m1; MPEF-PV 2339, P3; MPEF-PV 2341, M2; MPEF-PV 2343, upper molar; MPEF-PV 2344, P4; and MPEF-PV 2337, dentary fragment; MPEF-PV 2338, dentary fragment; MPEF-PV 2347, c1; MPEF-PV 2349, C1; MPEF-PV 2368, p1; MPEF-PV 2369, M3; MPEF-PV 2372, dentary fragment; MPEF-PV 2373, P4; MPEF-PV 2375, C1; MPEF-PV 2376, p3; respectively. A complete listing of the new La Colonia specimens described

here is available in Supplementary Table 1 in the supplementary materials associated with this report.

Diagnosis. A very small mesungulatoid with simple premolars increasing in size posteriorly to an enlarged molariform fourth premolar; and three complex and mediolaterally extended molars decreasing in size posteriorly. Compared to the better known mesungulatoids *Coloniatherium* (Rougier 2009b) and *Peligrotherium* Paez-Arango 2008), *Reigitherium* is much smaller and shows the presence of several autapomorphic dental specializations: 1) interradicular crests (McDowell 1958) connecting the roots of upper and lower canine and postcanine elements, 2) highly crenulated trigonids and primary trigons, with an enclosing enceinte structure in the lower molars, and 3) neomorphic ectostyles on the upper first and second molars, and neomorphic accessory cuspulids (also seen in *Peligrotherium*) distributed within the labial portion of the lower molariforms.

DESCRIPTIONS

The environment of deposition and method of discovery have both had significant effects on the state of preservation of the fossils described here. Because of the postmortem hydraulic transport of the La Colonia Formation fossils, there has been moderate to extensive rounding of most specimens. Additionally, the bulk sampling and screen washing procedures used to recover and concentrate these specimens may have caused some additional fracturing of the gnathic specimens in particular. The imprint of postmortem wear does obscure many details of texture, use-wear, and unworn morphology in the dental and dentary remains described below; however, it is improbable that the fracturing and

rounding produced by these processes will be mistaken for premortem morphology. Additionally, several of the better preserved dental specimens show no significant postmortem damage. In particular, the newly discovered locality Anfiteatro 1 bears a relative abundance of well-preserved mammalian jaws, which, when combined with previously recovered specimens (Pascual et al. 2000; Rougier et al. 2009b), have proved crucial in the determination of dental formula.

Dentary. Features of the mandibular corpus and base of the ascending ramus can be seen in the specimens, MPEF-PV 2014, MPEF-PV 2337, MPEF-PV 2338, and MPEF-PV 2372 (Figs. 4-7). All of these are fragmentary dentaries, missing the anterior most and posterior most structures of the lower jaw. The MPEF-PV 2337 (Fig. 5) specimen is the most completely preserved and provides the bulk of anatomical detail described below.

The ventral contour of the mandibular corpus is semicircular inferior to the postcanine tooth row and continues posteriorly to form a point of inflection inferior to the base of the ascending ramus, termed the angular notch. An angular process is known to be present in the better known meridiolestidan taxa *Cronopio* and *Peligrotherium* (Paez-Arango 2008; Rougier et al. 2011), and in an unassigned mesungulatoid dentary described by Forasiepi et al. (2012). This phylogenetic bracket, combined with the presence of an angular notch in *Reigitherium*, suggests the presence of an angular process in this species as well.

The anterior region of the ascending ramus shows the base of the coronoid process sloping posteriorly at an angle of approximately 45 degrees. The anterior border of the coronoid process is smoothly convex in a horizontal plane, and lacks evidence of an appositional contact with a coronoid bone. The region of bone directly lateral to the base of the coronoid process is damaged in all available specimens, and what is probably the rostral

margin of the masseteric fossa on the lateral aspect of the coronoid process is obscured. The medial side of the base of the coronoid process and ascending ramus is undamaged and is smoothly flattened in a parasagittal plane, displaying the absence of an anteriorly placed mandibular foramen, Meckel's sulcus, or anteriorly extended pterygoid flange. The lingual surface of the mandibular corpus is also smoothly convex under the tooth row.

The specimens MPEF-PV 2338 and MPEF-PV 2372 (Figs. 6-7) preserve the outline of the mandibular symphysis; however, in both cases its morphology has been partially effaced by postmortem abrasion and fracturing of the anterior dentary. It can still be determined that the symphysis was neither fused nor highly interdigitating, and that it took the form of a horizontally extended oval in medial view. The attachment for the cartilaginous symphysis extended posteriorly to the level of the penultimate premolar, was not medially expanded, and shows no evidence of a symphyseal foramen or connection with Meckel's element.

Fig. 4 *Reigitherium* MPEF-PV 2014. Posterior left dentary fragment (reversed) showing molar alveoli and associated roots. **A** labial view; **B** lingual view; **C** occlusal view. Scale bar is 1 mm

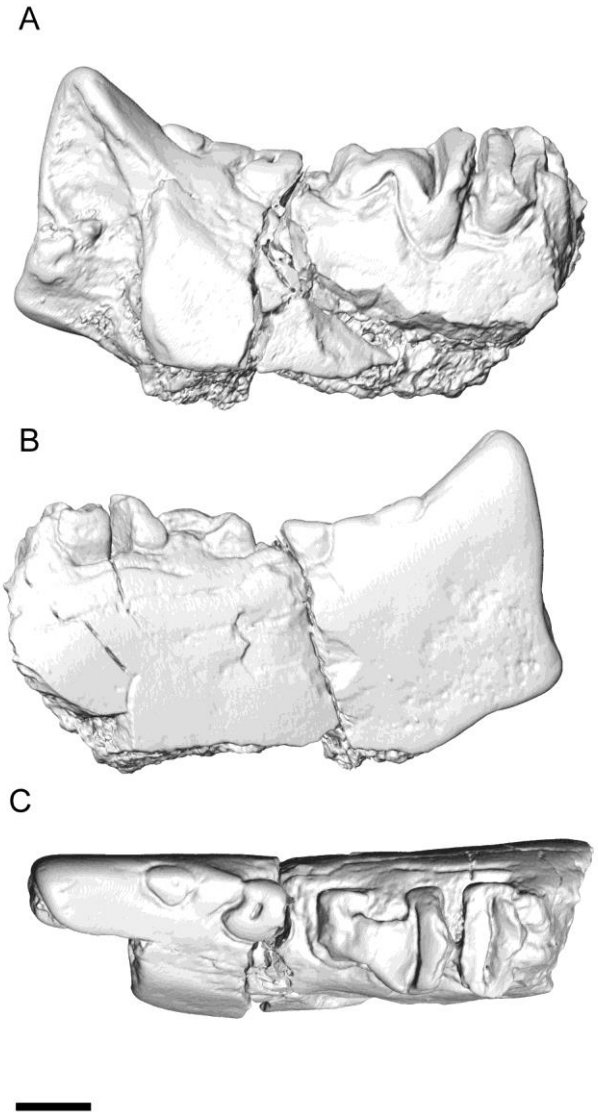

Fig. 5 *Reigitherium* MPEF-PV 2337. Fragmentary left dentary bone (reversed). **A** labial view; **B** occlusal view; **C** lingual view. Scale bar is 1 mm

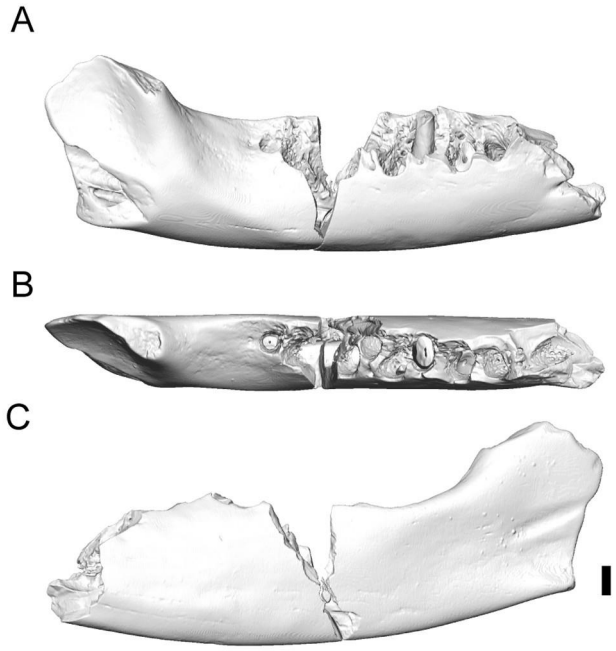

Fig. 6 *Reigitherium* MPEF-PV 2338. Fragmentary right dentary bone (reversed) with p3, p4, and m1. **A** labial view; **B** occlusal view; **C** lingual view. Scale bar is 1 mm

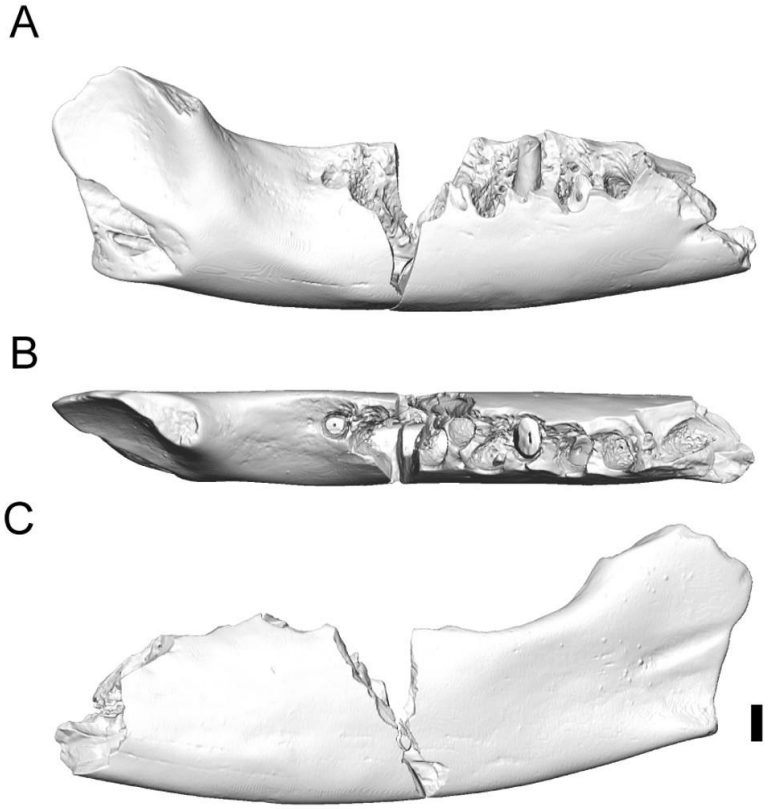

Fig. 7 *Reigitherium* MPEF-PV 2372. Fragmentary left dentary bone (reversed) with p2 and mesial half of p3. **A** lingual view; **B** occlusal view; **C** anterolabial view. Scale bar is 1 mm

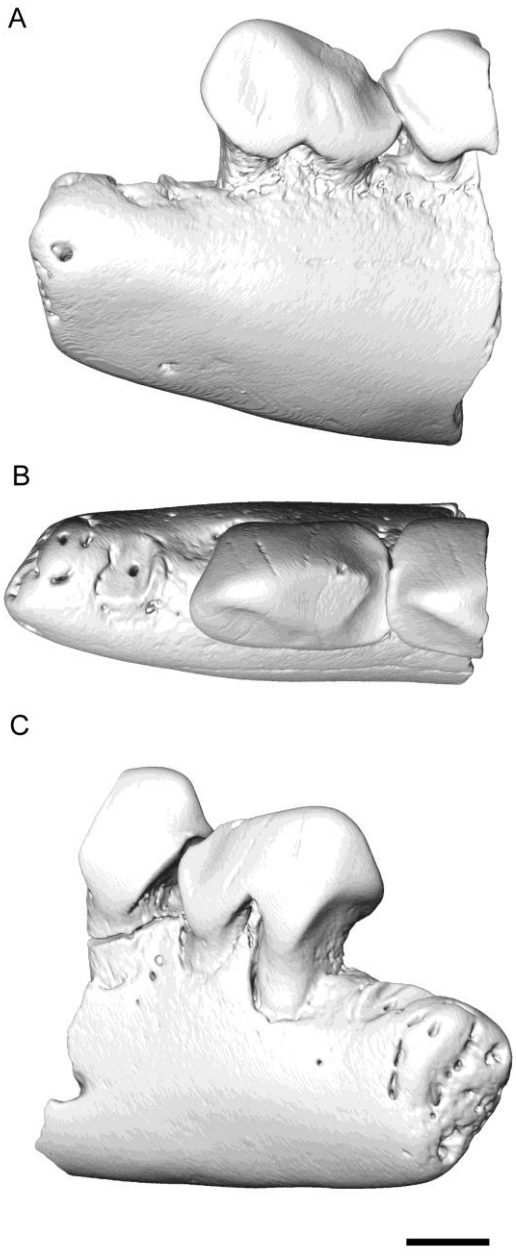

Postcanine Alveoli. Only in specimen MPEF-PV 2338 is there an indication of the dimensions of the distal alveolus of the lower canine. This is preserved on the anterior most margin of the specimen as a mesially facing concavity that shows a wider radius of curvature and more lateral extent than the alveoli corresponding to the mesial and distal roots of p1. The state of preservation of the distal canine alveolus precludes further characterization of the structures accommodating the two-rooted lower canine, but allows the confident identification of the first and subsequent premolar loci. The alignment of several edentulous (MPEF-PV 2014, MPEF-PV 2337; Figs. 4-5) and tooth-bearing (MPEF-PV 2338, MPEF-PV 2372, and MPEF-PV 2020; Figs. 6-8) dentary bone specimens from the La Colonia Formation shows that there is a sum total of 14 postcanine alveoli in the lower jaw. Important features associated with this sequence are the presence of a mental foramen on the lateral dentary surface ventral (or posteroventral) to the fifth alveolus; and a sharp change in alveolar pattern between the eighth and ninth alveolar processes, which is taken to mark the premolar-molar boundary. While the alveoli corresponding to the lower canine are not fully preserved, the anterior most alveolus in this sequence is inferred to be the first postcanine alveolus because of its small size, and location above the shallowest extent of the dentary. It is unlikely that premolar alveoli mesial to the anterior-most alveolus preserved in this sequence would be large enough to support an occlusally relevant dental element, if the gradient of distal alveolar size increase is preserved.

The first two postcanine alveoli are interpreted to correspond to the two-rooted lower first premolar. MPEF-PV 2372 (Fig. 7) best preserves these alveoli, and shows the presence of two subequally sized conical roots. Both roots are circular in cross section, with small circular and centrally placed root canals. The first two alveoli, which accommodate these roots, display subequally high medial and lateral margins, and lack any evidence for

exodaenodonty (the lateral bulging and overhanging of lower molariform crowns, often associated with labial emargination of corresponding alveoli; Rose 2006). The third and fourth postcanine alveoli correspond to the second lower premolar, as can also be seen in MPEF-PV 2238 and MPEF-PV 2372. These two alveoli are subequal in size, and are only slightly wider mediolaterally than the first and second alveoli. The medial and lateral alveolar margins are also subequal in height, similar to p1.

The fifth and sixth postcanine alveoli are associated with the elongate third lower premolar. These alveoli are mediolaterally wider than the preceding alveoli, and assume a generally ovoid, as opposed to circular, outline. Because of the elongate shape of the p3, the raised interradicular alveolar process between the fifth and sixth alveoli is longer mesiodistally than in any other postcanine tooth position. The space between the fifth and sixth alveoli is also longer than the diastemata between any two preserved tooth positions. The seventh and eighth postcanine alveoli correspond to the ultimate (fourth) lower premolar position, and are similar in size, but are larger and more closely approximated than the alveoli corresponding to p3. The specimens MPEF-PV 2337 and MPEF-PV 2020 (Figs. 5 and 8) show that the lateral alveolar border for these two alveoli is significantly lower than the medial alveolar border. Both the seventh and eight postcanine alveoli are mediolaterally elongated, but are slightly less ovoid than the preceding two alveoli.

The ninth through 14th postcanine alveoli show an alternating pattern where alveoli corresponding to mesial roots are enlarged and transversely elongate (beyond just being ovoid in cross section) and alveoli corresponding to distal roots are reduced and circular in cross section. This alternating pattern is characteristic of the molars seen in dryolestids and supports the presence of three lower molars in *Reigitherium*. The known specimens preserving lower molar alveoli are MPEF-PV 2014, MPEF-PV 2020, MPEF-PV 2337, and

MPEF-PV 2338 (Figs. 4, 8, 5, and 6). These specimens show some discrepancies in relative alveolar size and degree of emargination of the lateral alveolar borders, which we interpret as intraspecific variation.

The ninth and tenth postcanine alveoli correspond to the lower first molar position, and can be seen in MPEF-PV 2338, MPEF-PV 2020, and MPEF-PV 2337, while only the tenth alveolus is seen in MPEF-PV 2014. All pertinent specimens show the ninth postcanine alveolus to be the widest mediolaterally in the postcanine tooth row, with a lateral alveolar margin much lower than the corresponding medial alveolar margin. Specimens MPEF-PV 2014, MPEF-PV 2020, and MPEF-PV 2338 also show that the tenth alveolus, while much smaller than the preceding alveolus, also extends labially enough to emarginate its lateral alveolar border. The specimen MPEF-PV 2337 shows a tenth alveolus that is smaller, circular in cross section, and more lingually positioned compared with the other specimens mentioned. This prevents the tenth alveolus from having an emarginated lateral margin in MPEF-PV 2337 or from being visible in lateral view; however, a small depression is present lateral to this alveolus which probably accommodated an interradicular rootlet associated with the m1.

The 11th and 12th postcanine alveoli are best preserved in MPEF-PV 2014 (Fig. 4). The specimen MPEF-PV 2337 also preserves the 11th alveolus, but the 12th alveolus is lost due to a major fracture in the specimen. The 11th postcanine alveolus corresponds to the mesial root of m2, and is transversely elongate and emarginated laterally, similar to the ninth postcanine alveolus. The 12th postcanine alveolus corresponds to the distal root of m2, and is approximately two-thirds the mediolateral width of the preceding alveolus. The 12th postcanine alveolus is also more lingually placed and less laterally emarginated than the 11th postcanine alveolus.

The 13th and 14th postcanine alveoli are the smallest in the molar series, and are also thinner mesiodistally and labiolingually than the alveoli corresponding to the third and fourth premolars. The distal two alveoli are visible in MPEF-PV 2014 and MPEF-PV 2337 (Figs. 4-5) and there is some difference in alveolar cross sectional outline implied by these specimens. The smaller dentary fragment MPEF-PV 2014 shows that the 13th postcanine alveolus is mediolaterally elongate and ovoid in cross section, and is succeeded by a smaller and more circular 14th alveolus. The ultimate alveolus seen in MPEF-PV 2014 is much more obliquely set within the mesiodistally directed crest of a raised buttress of bone. The intersection of this raised buttress with the 13th and 14th alveoli is only seen in MPEF-PV 2014, however. The more complete MPEF-PV 2337 also preserves the penultimate and ultimate alveoli, but shows both of these to be more transversely elongate. The ultimate alveolus is also much more vertically implanted MPEF-PV 2337, and is placed labial to the mesially running buttress on the dentary. Despite these minor topographic variations, these two specimens are of subequal size. Similar variations in the ultimate molar alveoli and root pattern are also present in the larger sample of *Coloniatherium* dentaries from the El Uruguayo locality of the La Colonia Formation (Rougier et al. 2009b; this taxon is present but rare in the sample from the Anfiteatro 1 locality).

While there are no specimens from La Colonia preserving the morphology of the ultimate (third) molar, the conformation of the distal two alveoli in MPEF-PV 2014 and MPEF-PV 2337 demonstrate that the corresponding molar crown would have been significantly narrower than the preceding molars, especially distally. Only MPEF-PV 2337 clearly demonstrates the presence of a retromolar space, mesiolingual to the anterior base of the coronoid process.

Fig. 8 *Reigitherium* MPEF-PV 2020. Cast of left dentary fragment (reversed) showing p4 and m1. **A** occlusal view; **B** labial view. Scale bar is 1 mm

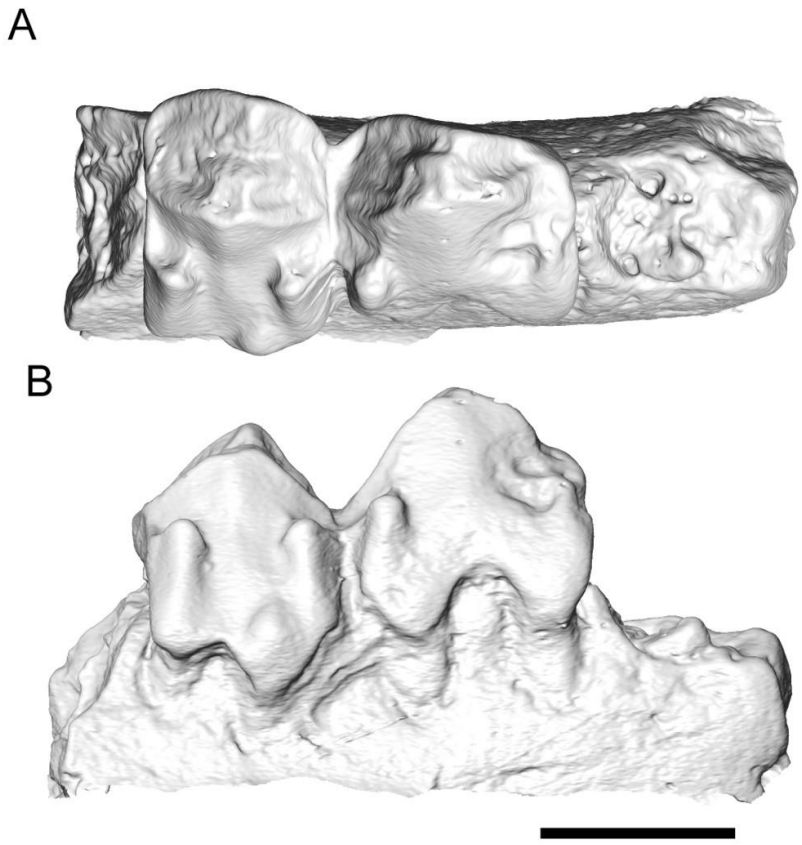

Descriptions of Canine and Postcanine Morphology

The most confusing aspect of the morphology seen in *Reigitherium* is its highly modified dentition. Upper and lower molariform loci show mediolateral elongation associated with the addition of neomorphic structures, and most positions show mesiodistal compression associated with the loss, fusion, and modification of plesiomorphic features compared to the ancestral cladotherian or ``eupantotherian'' condition (Fig. 3). Among the known Cretaceous meridiolestidans, *Reigitherium* is the most autapomorphic and highly specialized taxon. And its morphology has facilitated an unprecedented variety of opinions regarding the assignment of isolated dental elements to the upper versus lower tooth rows, the orientation of these elements along mesiodistal and labiolingual axes, and the differentiation of left versus right elements. It is not surprising, therefore, that alternative phylogenetic hypotheses based on differing fundamental assumptions of cusp homology have produced a wide variety of opinions regarding the location of *Reigitherium* relative to Mammalia generally.

One remarkable feature found in the dentition of *Reigitherium* is the pervasive development of interradicular crests, which form thin raised ridges or nervure structures from the basal dentine surface between the insertions of the surrounding roots. Interradicular crests have been described in several eulipotyphlan taxa such as erinaceids (Butler 1948) and Caribbean soricomorphs (McDowell 1958), with unknown functional significance. In *Reigitherium* all known upper and lower tooth positions represented by adequately preserved specimens show the presence of a linear or furcating interradicular crest, which supports the attribution of isolated elements to this taxon. Further descriptions of each element known from the La Colonia sample are provided below, but because of their complexity newly discovered diagnostic and heuristic features allowing for the

orientation and identification of the isolated molariform elements in *Reigitherium* are reviewed in the following paragraphs.

The fragmentary dentary described by Pacual et al. (2000) demonstrated the presence of labial cuspulids, termed “additional cusps” by these authors, on two molariform tooth positions (here interpreted to be p4 and m1). These structures are here renamed the mesial, distal, and labial accessory cuspulids, corresponding to their position on the crown surface. The expanded sample of upper and lower molariform elements described here further demonstrates the presence of neomorphic cuspulids on m2 (including mesial, distal, and two labial accessory cuspulids), and neomorphic labial cusps on the first and second upper molars as well. These neomorphic cusps/cuspulids allow the orientation of the upper and lower molariforms along the mediolateral axis, but do not resolve the right versus left, and upper versus lower identity of isolated dental elements.

The primary central cusps in the molariforms of *Reigitherium* (cusp ``a" or protoconid in the lower dentition, cusp ``A" or paracone in the upper dentition; Butler 1939; Patterson 1956) are associated with low, sub-linear corrugations that descend from the apex of these cusps to lose distinction among the crenulations present in the primitive trigonid and trigon regions, respectively. These low corrugations show very little relief relative to the underlying crown surface and, because of the lack of high-resolution surface information (such as the 9 micrometer CT data used here), have not been accurately figured in prior descriptions of *Reigitherium*. Because these linear corrugations are associated with the primitive mammalian ``A" and ``a" cusps (paracone and protoconid, also termed eocone and eoconid, respectively; Vandebroek 1961), the presence of extended linear corrugations descending from these primitive cusps allows the upper versus lower differentiation of isolated dental elements.

This is because of the labial position of the protoconid and lingual position of the paracone in tuberculosectorial or ``pre-tribosphenic'' dentitions.

The molariform elements of *Reigitherium* can also be oriented mesiodistally because of the wider mesial curvature, compared with distal curvature, of the crown when seen in occlusal view. The wider mesial curvature of upper molars is caused by the more labial placement of the labial terminus of the mesial cingulum relative to the distal cingulum (as seen in several mesungulatoid meridiolestidan species), and the position of the labial-most neomorphic cusp (ectostyle) slightly anterior to the transverse midline of the upper crown surface. The upper premolars can also be oriented mesiodistally because of the association of the stylocone with the distal cingulum, which is a characteristic seen in all known mesungulatoid taxa. In *Reigitherium*, because of the more distal placement of the distal cingulum, the stylocone is positioned near the distal margin of the crown in both the penultimate and ultimate upper premolars. While the placement of the stylocone along the distal embrasure is a characteristic unknown in the cheek teeth of any other trechnotherian taxon, this orientation is justified for the posterior two premolars known in *Reigitherium*, based on comparisons with the morphology known in mesunguloid taxa, and structural relationships with the in situ lower dentition known in the dentary specimen MPEF-PV 2338.

The lower molars can be oriented mesiodistally because of the position of the labial-most neomorphic cuspulid anterior to the transverse midline of the crown, similar to the upper molars. The lower premolars can be oriented based on their anteriorly skewed profile in lateral view.

Lower Dentition

Lower Canine. The specimen MPEF-PV 2347 (Fig. 9c and f) is a robust, double-rooted, and recurved canine. This specimen appears large when compared to the known gracile anterior extent of the dentary bone (seen in the fragmentary specimen MPEF-PV 2372, which lacks canine alveoli, and MPEF-PV 2338; Figs. 6-7) but the presence of an interradicular crest within the interradicular arch of this tooth suggest it is referable to *Reigitherium*. Additionally, the presence of a distally-facing attritional wear surface on the concave posterior edge of the canine further suggests that this specimen belongs to the mandibular dentition. The mediolateral width across the fractured base of the distal canine root (1.90 mm) is approximately twice that of the known width of the dentary bone across the mesial p1 alveolus. However, it appears likely that the distal root tapered significantly before reaching its accommodating alveolus. The ventrodistal extent of the mandibular symphysis also does not show a bulge or inflation in response to the internal commencement of the distal root of the lower canine.

While two roots of the lower canine are not preserved in the isolated canine MPEF-PV 2347, the orientation of the bi-lobed basal region of the crown indicates that both the mesial and distal roots were procumbent and were most likely concave dorsally. It is also probable that the mesial root is oriented slightly more vertically than the distal root, causing the canine crown to be procumbently situated in the dentary. Underneath the cervical region the interradicular crest connecting the two roots shows a small medially projecting buttress and larger laterally projecting buttress, both of which intersect the mesiodistally oriented interradicular crest at nearly a right angle. The interradicular crest's lateral buttress is labially extended to the labial edge of the crown surface and was possibly enameled to some extent.

This makes it appear as though the lower canine possessed three roots in labial view; however, when viewed ventrally it is clear that the lateral buttress does not project far enough ventrally to be considered an independent root or rootlet.

Two thin crests ascend to the recurved apex of the canine from points mesial to the mesial root and distal to the distal root. These two crests give the canine crown a recurved arrowhead shape in lateral view. The distal crest is sharper and a concave surface develops both on its lingual and labial aspects. The unusual shape of the canine in *Reigitherium* appears proportionately very robust and is reminiscent of the lower canine seen in *Necrolestes* (Wible and Rougier 2017). The canine crown is also slightly curved labiolingually, with a concave lingual aspect and convex labial aspect.

Fig. 9 Upper and lower canines positioned to show morphological correspondence and contact between opposing crown surfaces. **A**,**D** MPEF-PV 2349 upper canine (reversed); **B**,**E** MPEF-PV 2375 tip of upper canine (reversed); **C**,**F** MPEF-PV 2347 tip of lower canine. **A**,**B**,**C** labial view; **D**,**E**,**F** lingual view. Scale bar is 1 mm

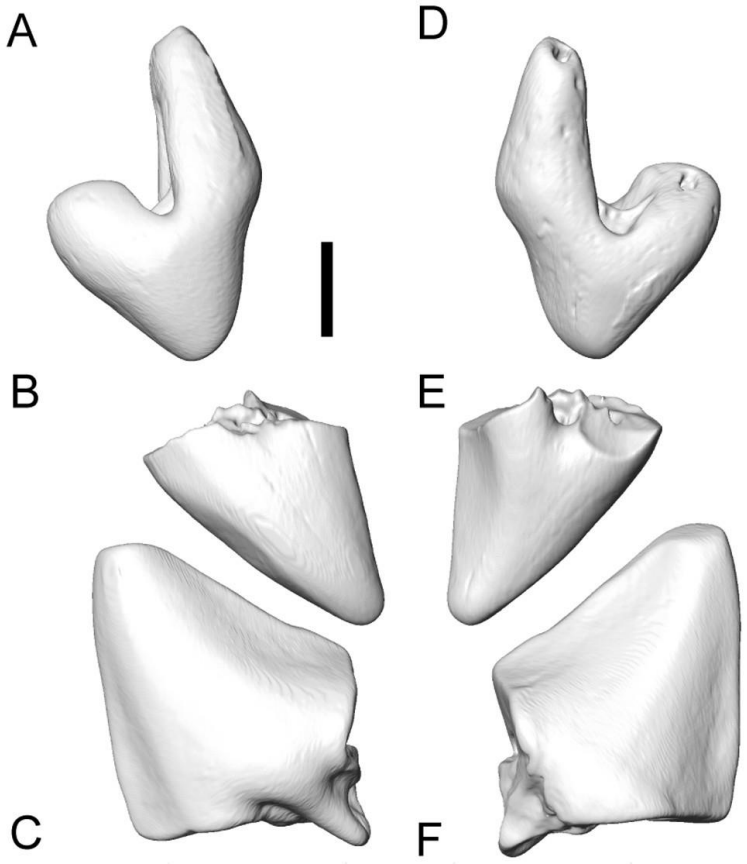

Lower First Premolar. This tooth position is represented by one isolated specimen, MPEF-PV 2368 (Fig. 10). It preserves a complete, and relatively unworn, crown surface but no cervical or root features. This element is referred to here as p1, but may reasonable be homologized with the deciduous p1, which is the first permanent premolar seen in most extant plesiomorphic therian mammals (Luckett 1993). At present we have no data to help us choose between these options.

The first lower premolar is mediolaterally thinner than any other postcanine position known in *Reigitherium*, being approximately 1.31 mm wide and 2.44 mm long mesiodistally. The single cuspid is located over the base of the mesial root, giving it a procumbent triangular profile in lateral view. The occlusal edge of the lateral profile is formed by a thin crest. From the apex of the central cuspid this crest descends along a steep parabolic curve mesially, and along a shallower straighter curve distal to the central cuspid. The outline of the crown in occlusal view is generally ovoid, similar to the two succeeding premolars, and lacks any mesial or distal emarginations or interstitial wear surfaces.

Fig. 10 Figure showing first and third lower premolars. **A**,**D**,**F**,**G** MPEF-PV 2376 lower right p3; **B**,**C**,**F**,**G** MPEF-PV 2368 lower right p1. **A**,**B** labial view; **C**,**D** lingual view; **E**,**F** occlusal view; **G**,**H** ventral view of roots and interradicular crests. Scale bar is 1 mm

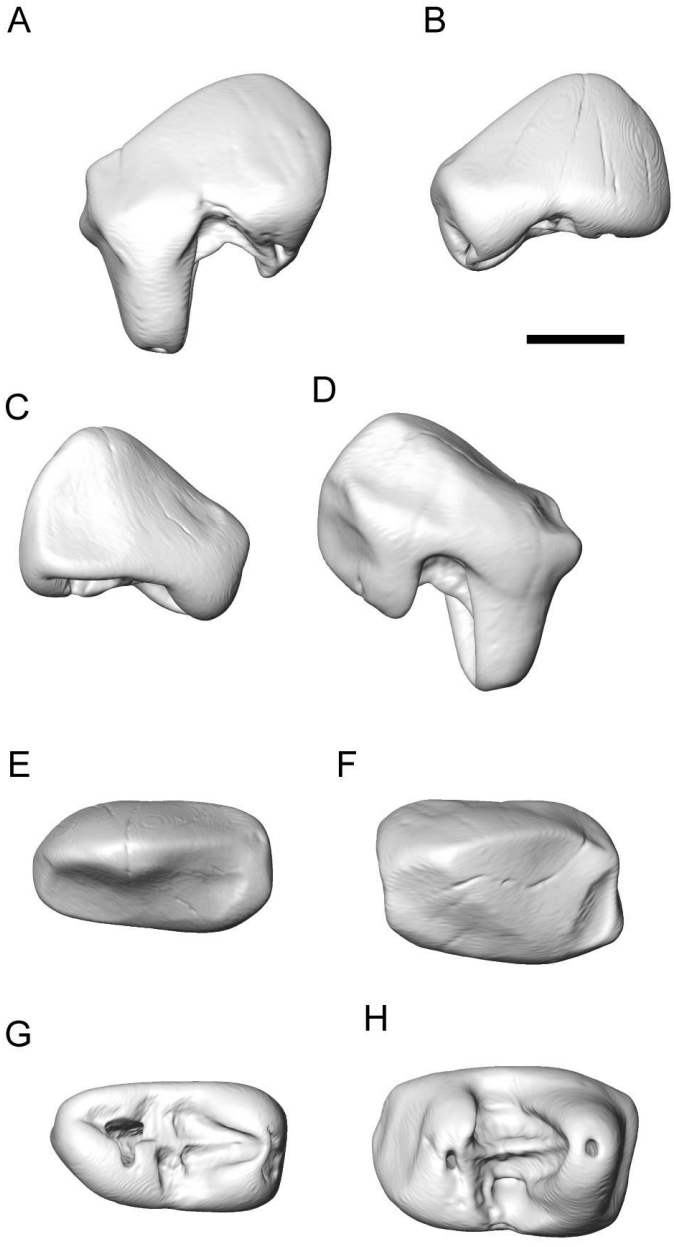

Lower Second Premolar. This element is best preserved in the dentary specimen MPEF-PV 2372 (Fig. 7). This is an anterior left dentary fragment with two alveoli preserved for the lower p1, a complete in situ p2, and the mesial half of the lower p3 in situ. The lower second premolar shows a low, broad, unicuspid crown surface with the apex of the main cuspid (protoconid) placed over its mesial root. This gives the entire crown a mesially skewed triangular profile in lateral or medial view. The posterolingual aspect of the crown supports a poorly defined attritional wear surface.

Lingually, the Dentine Enamel Junction (DEJ) forms two hemispherical lobes that overhang medially the supporting roots. The lingual surface of the crown above these small lobes is fairly smooth, featureless, and vertically oriented. Labially, the DEJ forms a deep interradicular incisure between the mesial and distal roots, which interrupts the labial extension of the DEJ on the lateral aspects of the mesial and distal roots. The lateral rims of the alveolar processes are also proportionally lower than the medial rims to accommodate these lateral extension of the DEJ. In occlusal view the outline of the p2 is generally ovoid, being approximately 2.41 mm long mesiodistally and 1.46 mm wide labiolingually.

The distal surface of p2 forms a distally dipping slope of approximately 33 degrees, ending in a small, horizontal cingulid over the DEJ. The mesial surface of p2 is smoothly convex and mesially facing. However, the basal most extent of the mesial surface is emarginated (indented) to accommodate the distal heel of the preceding (p1) tooth position. This emargination forms a slight ventromesially facing concavity.

The two roots in p2 can be seen in the micro-CT images of MPEF-PV 2372. Both mesial and distal roots are robust, cylindrical, and vertically implanted in their respective alveoli. A mesiodistally directed interradicular crest under the cervix connects both roots.

Lower Third Premolar. This tooth position is best preserved in the MPEF-PV 2338 (Fig. 6) fragmentary dentary specimen. Fragments of the crown surface are also known in MPEF-PV 2372 (Fig. 7) and several other isolated teeth (not figured). As in the preceding tooth position, the apex of the main cuspid on p3 is located above the mesial root. However, the extent of mesial skewing of the p3 crown is much less apparent than in the p2, giving the silhouette of the crown the shape of a blunt arch in lateral and medial views. The p3 is slightly smaller in most dimensions than the preceding tooth, being 2.31 mm long mesiodistally, and 1.38 mm wide labiolingually in MPEF-PV 2338.

The mesial aspect of the p3 shows a sharp crest ascending from a thin mesial cingulid over the mesial root, and intersects the apex of the main cuspid (protoconid). There is a considerable amount of attritional wear medial to this crest on MPEF-PV 2338; however, it is apparent that this crest continues distally on to the posterior aspect of the crown, ending in a slightly larger distal cingulid. The surface of the crown medial and lateral to this longitudinal crest smoothly curves towards the longitudinal midline in the mesial half of the tooth, giving the mesial half of the crown a blade-like appearance. The crown surface medial and lateral to the longitudinal crest forms a flat, posteriorly-facing, vertical wall above the distal root of the tooth. The distal most region of the p3 forms a mediolaterally wide but short distal cingulid.

The DEJ forms labial extensions of the crown surface over both the mesial and distal roots. These extensions are separate at their base, and so do not form a discrete exodaenodont lobe. Additionally, they are both smoothly convex and lack any expression of labial cuspuids. Lingually, the DEJ also forms two hemispherical lobes over the mesial and distal roots. The hemispherical lobe over the distal root is slightly more ventrally extensive. Both roots extend vertically into their respective alveoli. As in the preceding tooth position,

the two roots are connected by a single, straight interradicular crest. In MPEF-PV 2338 there is no expression of a lingually placed accessory rootlet, or extension of the interradicular crest, as figured for this tooth position in Pascual et al. (2000).

Lower Fourth Premolar. Known from specimens MPEF-PV 2020 and MPEF-PV 2338 (Figs. 6,8 and 11), the p4 is a molariform ultimate premolar, longer mesio-distally than wide labiolingually, unlike the succeeding molars. The maximal mesiodistal lengths and labiolingual widths average 2.28 mm and 1.73 mm, respectively.

We adopt the hypothesis (Rougier et al. 2011, 2012) that this element represents the ultimate premolar, as opposed to the first molar, as suggested by Pascual et al. (2000). This discrepancy in dental formula and attribution is based on our comparisons with the morphologically closest dental elements in *Peligrotherium*, and to a lesser extent *Coloniatherium* (see Figs. 1-2). The molariform tooth inferred to be the ultimate premolar in *Peligrotherium* has accumulated much less premortem wear, compared with the three lower molars contained in the exceptionally preserved specimen described by Paez-Arango (2008). This suggests that the tooth in this position had erupted later than its succeeding tooth, and therefore it is likely a successor (as opposed to a first-generation) tooth. Therefore, despite its complexity, we attribute this element to the p4 locus based on its correspondence to the ultimate lower premolar in *Peligrotherium* (based on its inferred replacement pattern) and the alveolar pattern at this location (described above).

The lingual half of the p4 crown in *Reigitherium* shows the plesiomorphic tuberculosectorial morphology of the premolar crown, which has been modified by crenulation of the region representing the trigonid basin. These features are most clearly presented in the dentary specimen MPEF-PV 2338, with the transversely approximated

protoconid and metaconid being clearly visible despite a minor amount of apical wear present on the apex of the protoconid. Anteriorly, the paracristid can be recognized as a salient crest descending mesially from the apex of the protoconid and intersecting with a minor swelling that represents the reduced paraconid. Mesial to the paraconid swelling, the paracristid continues without interruption into a tortuous pre-paraconid crest, which abruptly deflects lingually before itself seamlessly blending into the lingual commencement of the mesial cingulid. Beside the paracristid, several linear wing-like crests can be seen to descend from the apex of the protoconid and metaconid, giving these trigonid cuspids a selenodont-like appearance.

Distal to the protoconid an indeterminate crest (possibly representing the homolog of either the labial half of the protocristid or the cristid obliqua) descends along a direct distal route to terminate just mesial to the distal cingulid. The metaconid has a similar distal crest, with similarly uncertain homology, that descends distolingually before blending seamlessly into the lingual commencement of the distal cingulid. The ultimate lower premolar of *Reigitherium* therefore shows an association of the primary trigonid cusps with the mesial and distal cingulids, a condition that is further accentuated in the lower molars. However, unlike them the ultimate lower premolar still preserves a complete and lingually open trigonid. Also, unlike the molars, the distal margin of the trigonid is wider than the mesial margin. This creates a gradual transition between the mediolaterally compressed premolar morphology and the transversely widened morphology seen in the molars. The lack of closure of the p4 trigonid is the result of the relatively low and shortened form of the crest descending mesially from the metaconid, which loses distinction before being able to blend with the lingual commencement of the mesial cingulid.

The labiolingually thinner region enclosed by the trigonid basin mesial to the protoconid suggests that a molariform upper tooth did not contact the mesial edge of p4 or the embrasure anterior to it. This can be seen as indirect support for the lack of complete molarization in the tooth corresponding to the upper third premolar.

The labial half of p4 forms a smoothly convex lateral slope descending from the labial aspect of the trigonid, supporting two accessory cuspulids. These cuspulids are small but fairly conical (the mesial cuspulid is damaged in the specimen MPEF-PV 2020), and form the labial termini of the mesial and distal cingulids, respectively. Small frenular crests also connect these cuspulids with the lateral aspect of the trigonid, independently of the sharp apical boundaries of the mesial and distal cingulids.

The base of the crown extends further ventrally beneath the mesial and distal margins of the tooth, forming a slight interradicular arch, visible labially. The labial surfaces of the two labiolingually extended roots of this tooth are also visible in lateral view. The lingual surface of the p4 crown forms a fairly flat and featureless sheet oriented in a parasagittal plane. The mesial and distal cingulids do not have any expression on this surface, and the interradicular arch is much shallower in lingual view.

Both roots are expanded mediolaterally at their attachment to the tooth cervix, but deflect labially and taper to have a cylindrical cross section as they extend deeper into their respective alveoli. The apical foramina for both roots are located diametrically opposite the surface expression of the labial cuspulids on the crown. The mesial root is slightly convex along its mesial aspect, but vertically implanted into its alveolus. The distal root is slightly inclined posteriorly (approximately 10 degrees from vertical).

Fig. 11 Lower p4 in MPEF-PV 2338 showing modified trigonid cuspids; pad, paraconid; prd, protoconid; mtd, metaconid; mcngd, mesial cingulid; dcngd, distal cingulid. Scale bar is 1 mm

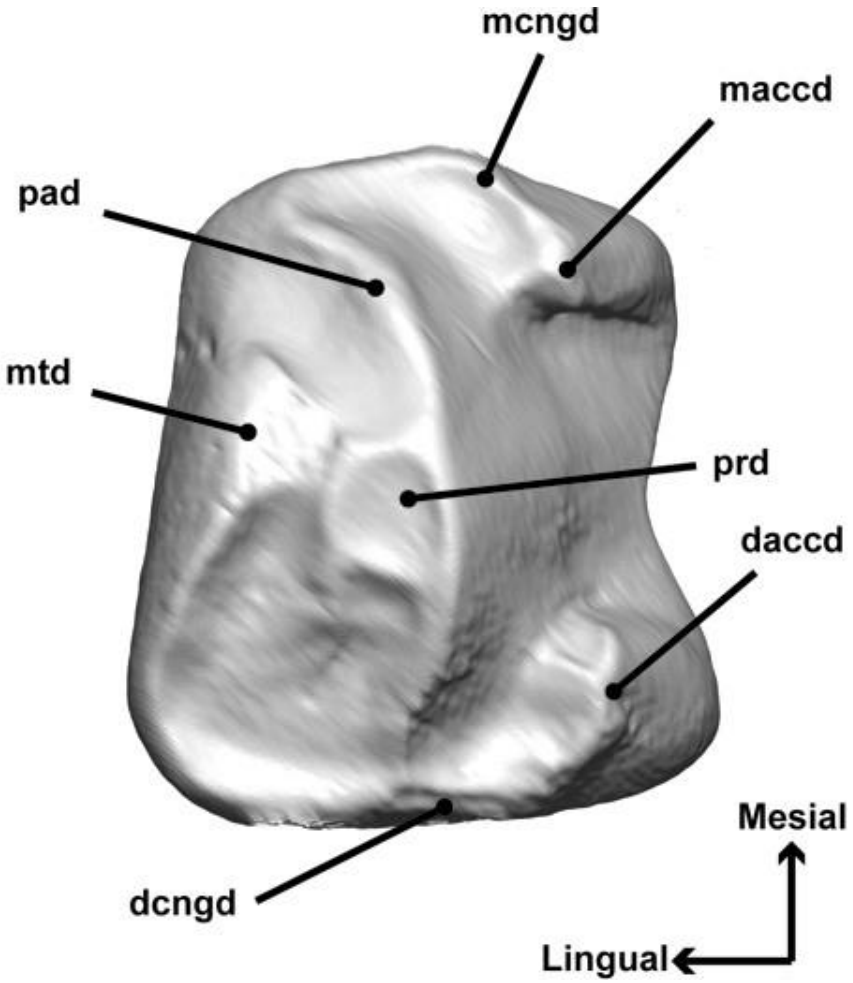

Lower First Molar. The transitional morphology presented by the ultimate lower premolar provides a valuable schematic for interpreting the complexity of the succeeding dentition. In particular, the morphology of the lower molars can be understood as having been derived from the condition seen in the p4 by the further extension and definition of the crest connecting the mesial aspect of the metaconid with the lingual commencement of the mesial cingulid; and the reduction of the paraconid swelling, or its appression onto the metaconid (making this composite structure technically an amphiconid; Yardeni 1942; Patterson 1956). With the confluent connection between the crest descending mesially from the metaconid to the mesial cingulid, a continuous raised loop is developed that circumscribes the crenulated enamel of the trigonid basin. This structure is termed here the enceinte (see Fig. 3b), and is formed from the contiguous circuit of the paracristid, mesial cingulid, mesial crest of the metaconid, distal crest of the metaconid, distal cingulid, and distal crest of the protoconid. The architectural usage of the word enceinte refers to the main defensive line of wall towers and curtain walls surrounding a castle or other fortified location, which is closely analogous to the conformation of trigonid cusps and crests seen is this element. An enceinte is apparent on both known lower molar loci in *Reigitherium* (m3 is unknown), and is vertically highest anteriorly near the trigonid cuspids. Within the boundaries of the enceinte the crown enamel is highly ornamented and (as mentioned by Pascual et al. 2000) contains a mesiodistally oriented sulcus separating the bases of the protoconid and metaconid. The homology of this sulcus is ambiguous, and may correspond to the indentation of the protocristid, or the center of the trigonid basin seen in the lower molars of other meridiolestidan taxa.

The crown of the lower first molar is known in situ from two dentary specimens (MPEF-PV 2020 and MPEF-PV 2338; Figs. 6 and 8) and from a single isolated specimen

(MPEF-PV 2317; Fig. 12). Each of these m1 specimens show a complex crown surface, with minor individual variations, but are all wider labiolingually (average 2.57 mm) than mesiodistally (average 1.73 mm). The lingual half of the crown surface contains the trigonid region, enveloped by an ovoid enceinte. The apex of the protoconid in this region can be seen as a small conical projection independent of the labial wall of the enceinte. Internal to the enceinte the surface of the protoconid shows several low corrugations, two of which run mesially and distally, respectively, and lose definition among the other crenulations of the trigonid region. A third short corrugation runs labially from the protoconid and terminates into the lingual side of the labial portion of the enceinte.

The paraconid is absent in both known lower molar positions in *Reigitherium*. As mentioned above, this is the result of the paracristid being incorporated into the mesial border of the enceinte with the concomitant reduction of the paraconid itself, or its lingual displacement and seamless fusion with the metaconid. The metaconid in m1 is not independent of the lingual wall of the enceinte, which attaches to this cuspid slightly lingual to its apex. Other than this attachment, the metaconid does not show the expression of elongate corrugations like those seen on the protoconid, but is also highly crenulated.

The two trigonid cusps, and the regions of the enceinte immediately labial and lingual to them, are the highest features of the crown surface. This elevated region forms a mediolaterlly directed guiding-ridge, which would have helped to limit motion of the mandible to horizontal translation near centric occlusion. There is also a thin, anterior-posteriorly directed sulcus centrally placed between the protoconid and metaconid; however, this depression is so thin and shallow that it would not have altered the function of the guiding-ridge of the trigonid, which it intersects.

The labial half of the lower first molar is an exodaenodont lobe embellished with several accessory cuspulids. The exodaenodont lobe extends the crown's lateral margin further labially and ventrally than the preceding premolar, and completely obscures the inter-radicular arch and lateral aspect of the roots from lateral view. Similar to the preceding premolar, two cuspulids are placed in the anterior and posterior margins of this lobe and form the labial terminations of the mesial and distal cingulids, respectively. These cuspulids are not as labially positioned as those seen in the ultimate lower premolar, but like the p4 these cingulid cuspulids show lingually directed frenular crests connecting to the lateral aspect of the exodaenodont lobe.

The basal margins of the mesial and distal cingulids project further laterally than their corresponding apical margins, which terminate laterally at the accessory cuspulids described above. This causes the labial aspect of the mesial and distal cingulids to form low, lateroventrally directed buttresses in the intervening space between the cingulid-terminating cuspulids and the lateral border of the crown surface. A third lateral cuspulid is located on the labial margin of the exodaenodont lobe, independent of the cingulids and placed slightly anterior to the transverse midline of the crown. As with the other cuspulids, a frenular crest projects medially for a short distance from this lateral-most cuspulid as well. Ventrally, the inferior extent of the DEJ is deeper under this third cuspulid than elsewhere on the tooth. The lingual surface of the crown is a vertically directed, featureless sheet similar to the condition seen in the preceding tooth position.

The two roots in this position can be seen to extend approximately 2.8 mm into the alveolar sockets in MPEF-PV 2338. The lingual and labial aspects of both roots form a labially convex curve, and both roots become thinner and more circular in cross section as they taper towards small apical foramina. The mesial and distal apical foramina are located

diametrically opposite the apices of the mesial and distal cingulid cuspulids, respectively. Near the cervical region of the m1, both roots fan out lingually to give the base of their insertion into the cervix a transversely elongate cross section. A single, straight interradicular crest connects the mesial and distal roots beneath the m1 cervix. The mesial root is noticeably more robust and vertically implanted than the distal root. The distal root is more gracile and posteriorly inclined by approximately 11 degrees.

Fig. 12 *Reigitherium* lower right first molar MPEF-PV 2317. **A** mesial view; **B** occlusal view; **C** distal view; **D** dorsolabial view; **E** lingual view. Scale bar is 1 mm

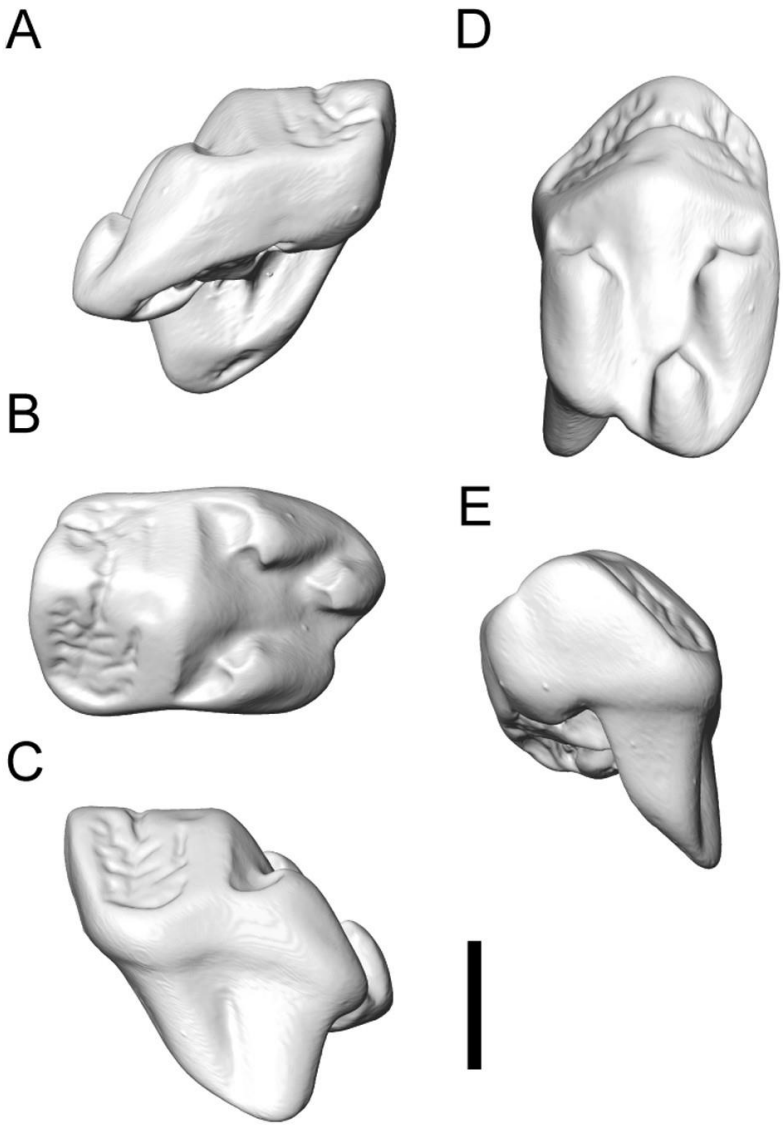

Lower Second Molar. This element is best known in MPEF-PV 2237 (Fig.13), an isolated tooth showing some premortem apical wear, obscuring several locally elevated features. This specimen is inferred to represent the m2 because of the greater discrepancy between the mediolateral width between its mesial and distal borders, and the size of its mesial and distal roots. This tooth is unlikely to represent the crown morphology of the currently unknown m3 of *Reigitherium*, because of the obvious mismatch between its dimensions and the size and positioning of the distal two alveoli, known in MPEF-PV 2014 and MPEF-PV 2337. The m2 is approximately 2.67 mm long mesiodistally, and 1.75 mm wide labiolingually.

The trigonid region is composed of an elevated protoconid and metaconid. Wear on the protoconid prevents the presence of anteroposteriorly or labially directed corrugations from being evaluated; however, there is a still a prominent guiding-ridge connecting the protoconid to the metaconid. Also, as in the preceding molar, there is also an anteroposteriorly directed sulcus intersecting this ridge. As in the m1, the apex of the metaconid participates in the formation of the medial border of the enceinte.

The labial termini of the cingulids are elevated into cuspulids on the lingual border of the exodaenodont lobe. The labial border of the exodaenodont lobe has two additional accessory cuspulids, which are unassociated with either cingulid. The labial-most cuspulid extends the EDJ ventrally beneath it. The other accessory cuspulid, which does not labially bound either cingulid, is positioned near the lateral border of the exodaenodont lobe, posteromedial to the labial most cuspulid. This second accessory cuspulid seems more likely to be the serial homolog of the labial most accessory cuspulid on m1, because of its similar position adjacent to the lateral aspect of the exodaenodont lobe and lateral buttress of the mesial cingulid. The lingual aspects of all four accessory cuspulids also show small frenular crests running lingually from their respective positions.

The mesial root of MPEF-PV 2237 is preserved to a much greater extent than the distal root. However, it is apparent that the mediolateral width of the distal root is at most two-thirds the width of the mesial root, and that it is positioned directly under the distal cingulid. The mesial root of MPEF-PV 2237 shows similar features to the distal root of the m1 specimen MPEF-PV 2317, except that the root canal in MPEF-PV 2337 is much more circular in cross section and labially placed below the lateral projection of the exodaenodont lobe. The distal surface of the mesial root has a wide, vertically oriented groove, the concavity of which is enclosed by medial and lateral expansions of the base of the root. The mesial surface of the mesial root is much less indented by a shallow vertical groove. The lingual surface of the mesial root is obliquely slanted ventrolabially, and is mesiodistally thinner than the labial surface of the mesial root, which is vertically directed. The lateral surface of the mesial root is smoothly convex in a horizontal plane, and is positioned under the lateral projection of the exodaenodont lobe.

Fig. 13 *Reigitherium* lower right m2 MPEF-PV 2237. **A** occlusal view; **B** ventral view of roots and interradicular crest; **C** dorsolabial view. Scale bar is 1 mm

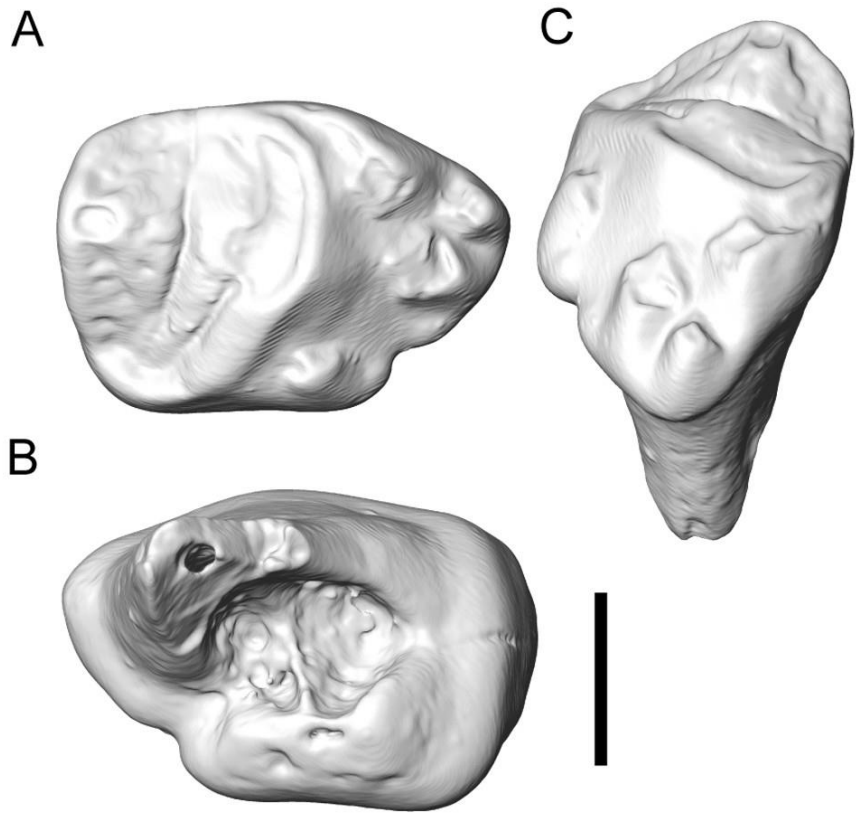

Upper Dentition

Upper Canine. The two specimens referred to this position, MPEF-PV 2375 and MPEF-PV 2349 (Figs. 9a,b,d,e), show a considerable amount of postmortem damage. The crown specimen MPEF-PV 2375 has avoided postmortem abrasion (although it is fragmentary), and better demonstrates original crown morphology to the extent that it is preserved. However, MPEF-PV 2349 preserves a larger fraction of the root structure of the upper canine, but is significantly rounded by postmortem abrasion and erosion. These specimens are inferred to represent the upper canine, because of the presence of a flattened premortem wear surface on the mesial aspect of MPEF-PV 2375, which would be produced against the distal face of the lower canine.

The two-rooted upper canine crown is mediolaterally compressed but still conical in general form. The apex is positioned over the distal root, giving the crown a recurved profile in lateral view, which is more gracile than in the lower canine. The apex of the canine extends approximately 2.36 mm above the interradicular arch.

The distal root forms a bulge, or heel, near its commencement on the crown surface. The commencement of the mesial root does not alter the convex curvature of the crown's mesial aspect. Unlike in the lower canine, both roots preserved in MPEF-PV 2349 are vertically oriented and cylindrical. An interradicular crest is visible running mesiodistally between the two roots; however, there is no laterally placed rootlet projecting from the interradicular crest as seen in the lower canine.

Upper Third Premolar. The putative penultimate upper premolar is only known in MPEF-PV 2339 (Fig.14), an isolated crown lacking any attached cervical or root structures. The

crown morphology is largely influenced by a single centrally placed central cusp (paracone), and a smaller parasitic stylocone. This morphology makes orientation of the P3 with respect to the major anatomical axes particularly challenging. However, based on the criteria described above, the inferred distolabial position of the stylocone allows the life position to be estimated. The P3 in *Reigitherium* shows several detailed similarities to the penultimate premolars known in *Peligrotherium* and *Coloniatherium*, such as its triangular occlusal outline formed by a small mesial cingulum and transversely wide distal cingulum. The enlarged distal cingulum is more extensive than in the other mesungulatoid taxa mentioned, commences lingually near the transverse midline of the crown, and is terminated labially by merging with the stylocone. The small mesial cingulum is also comparatively more transversely extensive in *Reigitherium*, and forms a hemispherical arc around the mesial half of the crown. This gives the penultimate premolar a maximal labiolingual width of approximately 2.0 mm, and a mesiodistal length of 2.64 mm.

The large central paracone is flanked by several linear corrugations descending linearly from its apex. Two more salient crests descend mesiolabially and distolabially from the apex as well, with the mesiolabial crest terminating indistinctly near the basal portion of the mesial aspect of the paracone. The distolabial crest descends along the distolabial flank of the paracone to meet a mesiolingually directed frenular crest projecting from the stylocone.

Fig. 14 *Reigitherium* upper right third premolar (reversed) MPEF-PV 2339. **A** labial view; **B** occlusal view. Mesial is towards the left. Scale bar is 1 mm, and is for A and B. Directional arrows for B only, L - Labial, D - Distal

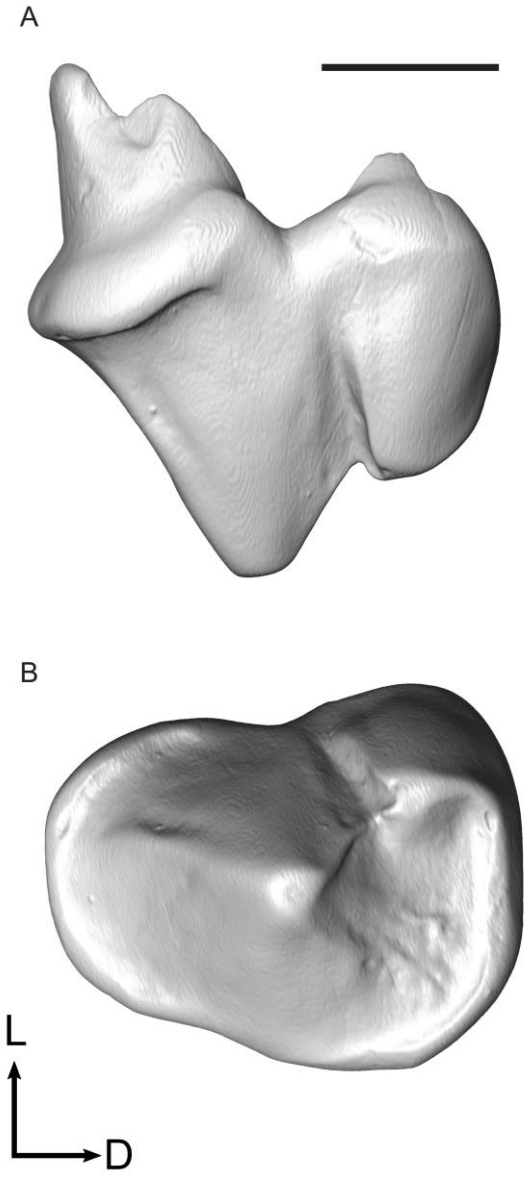

Upper Fourth Premolar. The morphology of the ultimate upper premolar in *Reigitherium* is known from three specimens (MPEF-PV 2341, MPEF-PV 2344 and MPEF-PV 2072; Fig. 15). Only one of these (MPEF-PV 2072) preserves enough of its original morphology to provide reliable measurements, being 1.89 mm mesiodistally and 3.01 mm labiolingually. While each of these specimens show a significant amount of rounding and fragmentation, the major features — an enlarged central cusp (paracone) and a distally placed stylocone — are consistent. Mediolateral elongation and the association of the stylocone with the distal cingulum are characteristics seen the molars and molariform premolars in mesungulatoid meridiolestidans, and these elements in particular are inferred to represent P4 based on the mesial deflection of the lingual lobe of the crown. This mesial deflection is also seen in the ultimate premolars of *Peligrotherium* and *Coloniatherium* (Fig. 1), as opposed to the direct mediolateral or distally deflected, conformation of the lingual lobe in the true molars. There is also a reasonable mechanical correspondence between MPEF-PV 2072 and the embrasure between p4 and m1 in specimen MPEF-PV 2338 (although these specimens represent different stages of wear).

In *Reigitherium* and other mesungulatoid taxa the ultimate premolar is the largest element of the upper tooth row. Specimen MPEF-PV 2072 shows that the P4 contains a large central cusp, similar to the preceding premolar position, and two labial cingular cusps. However, the fourth upper premolar shows much lower crenulations on its occlusal surface, and has a very indistinct and intermittent cingulum. The ultimate upper premolar also shows a small stylocone on the distolabial flank of the large central cusp, approximately halfway between the apex of the central cusp and the distal cingular cuspule.

The base of the paracone is generally ovoid, and wider labiolingually than mesiodistally, with a centrally placed apex. The centrifugal corrugations on this cusp are very

indistinct, partially resulting from taphonomic abrasion in all specimens; they are more apparent but still small in MPEF-PV 2344. The apex of the central cusp shows a distinct, indirect crest connecting with the apex of the stylocone. The stylocone also shows two subsidiary crests running along its mesiolabial and distolabial aspects. Damage to the basal crown in all specimens prevents identification of the number and orientation of roots at this tooth position.

Fig. 15 Figure comparing ultimate upper premolar morphology as preserved in three different isolated dental specimens. **A**,**D** MPEF-PV 2344 (reversed); **B**,**E** MPEF-PV 2072 (reversed); **C**,**F** MPEF-PV 2373 (reversed). These specimens demonstrate the variable extent of postmortem abrasion seen in La Colonia microfossils. **A**,**B**,**C** labial view. **D**,**E**,**F** occlusal view. Mesial is towards the left. Scale bar is 1 mm, and is applicable to all specimens. Directional arrows are for D,E,F only, L - Labial, M - Mesial

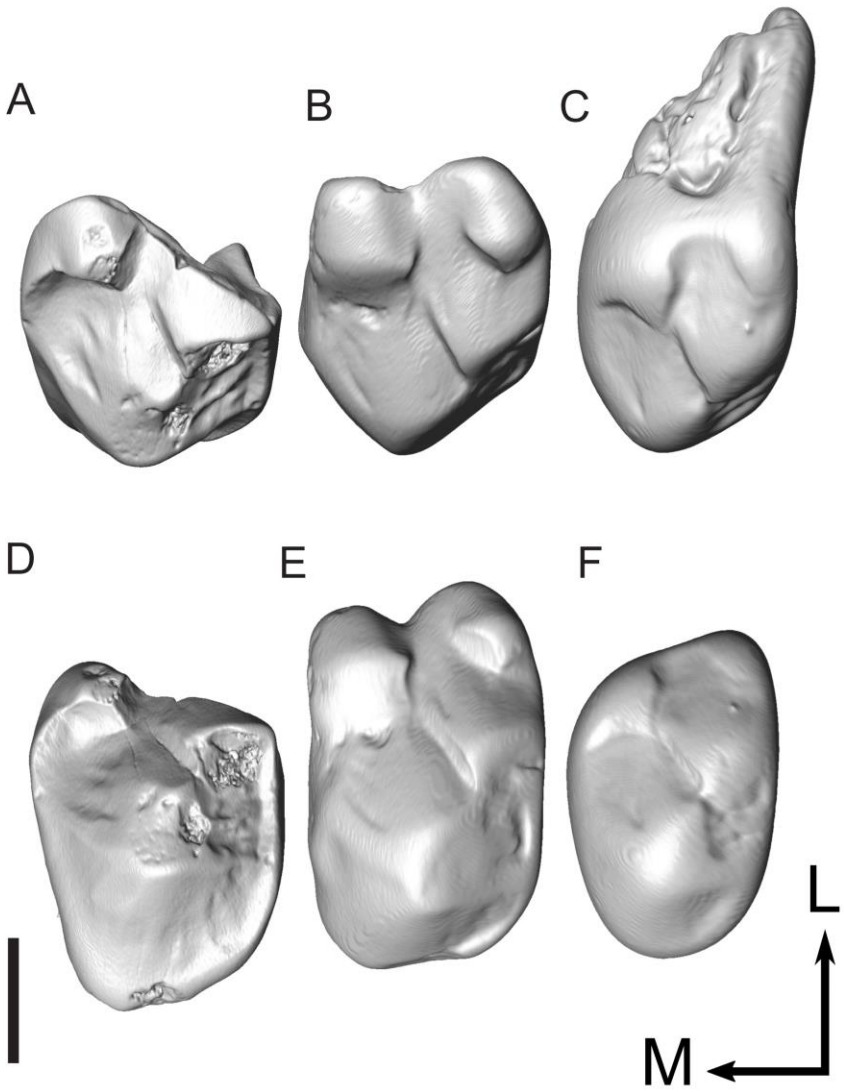

Upper First Molar. Because of the observable distal gradient of decreasing width in the upper molars of *Peligrotherium*, the specimen MPEF-PV 2238 (Fig. 16 a and d) is inferred to represent the upper first molar in *Reigitherium* because of its greater width (3.11 mm) than the specimen inferred to represent the M2 position. However, the morphology of MPEF-PV 2238 has been obscured because of heavy wear and the fact that much of its crown surface can only be inspected using photographs and cast specimens, with most of the primary trigon region having been sacrificed as part of the enamel microstuctural analysis reported by Wood and Rougier (2005: Fig. 5). While the photography and cast replicas obscure some of the finer features of the original crown surface, it is still apparent that the M1 is elongate labiolingually, with the lingual two-thirds of the crown composed of the primary trigon region. Root structure for this tooth position also cannot be described.

Fig. 16 Figure comparing upper molar morphology. **A**,**D** cast of MPEF-PV 2238 upper first molar; **B**,**E** MPEF-PV 2343 possible upper second molar (reversed); **C**,**F** MPEF-PV 2341 upper second molar (reversed). The close similarity between hypothesized first and second upper molars is apparent, as well as the variable preservation quality seen in the La Colonia material. **A**,**B**,**C** ventrolabial view; **D**,**E**,**F** occlusal view. Mesial is towards the left. Scale bar is 1 mm and is for all specimens. Directional arrows are for D,E,F only, L - Labial, M - Mesial

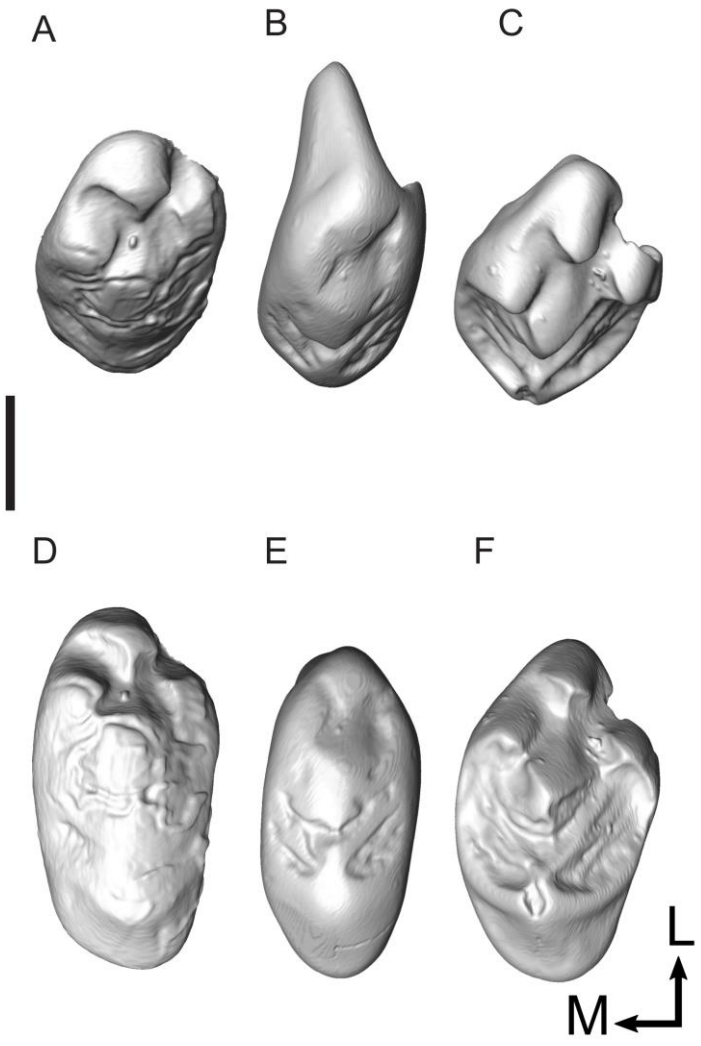

Upper Second Molar. Two specimens, MPEF-PV 2343 and MPEF-PV 2341 (Fig. 16b,c,e and f), are inferred to represent the M2 in *Reigitherium* based on their thinner mediolateral width (2.95 mm and 2.71 mm, respectively), compared with MPEF-PV 2238 (1.29 mm), the inferred M1. The distance in the occlusal plane between the apex of the paracone and stylocone is also smaller in MPEF-PV 2343 (0.89 mm) and MPEF-PV 2341 (1.06 mm), than in the M1 specimen (1.29 mm). While both M2 specimens described above are isolated teeth, the damaged basal region of MPEF-PV 2341, and postmortem rounding of MPEF-PV 2343 make each specimen an appropriate representative of different aspects of the M2 anatomy. As such, all features of crown morphology are based on MPEF-PV 2341, while cervical and root features are based on MPEF-PV 2343. Additionally, as much of the morphology of the known M1 specimen in *Reigitherium* is obscured, most of the characterizations of the M2 morphology described below are likely applicable to the M1 as well.

The buccal one-third of the molar crown is composed of the labially extended lateral slope of the stylocone, with three labial cusps partially connate with its surface. These labial cusps mirror the arrangement of the labial cuspulids on the lower molars, but are too low to have come into occlusal contact. The labial-most cusp is here termed the ectostyle (based on Hershkovitz 1971) and forms the buccal terminus of a small mesial cingulum, which is indistinct further lingually. A short, lingually direct frenular crest descends from the ectostyle to merge indistinctly into the lateral surface of the stylocone.

The mesial most cusp is a parastyle; the cusp is at the labial end of the preparacrista, and has a minute frenular crest that is partially obscured by wear. The distal most stylar cusp is the metastyle, and similar to the parastyle, forms the labial termination of the postparacrista. The frenular crest projecting from the metastyle is slightly longer and more

salient than the other frenular crests seen in M2. The metastyle itself is smaller and lower than the other stylar cusps, and blends with an indistinct distal cingulum on the lingual portion of the molar crown. The small mesial and distal cingula do not meet labially, and a small cleft is formed on the molar crown between the parastyle and metastyle.

The lingual two-thirds of the crown shows two subequally large cusps, the paracone lingually and stylocone labially. The paracone is the only cusp in MPEF-PV 2341 to show any degree of apical wear; however, this does not obscure the strong preparacrista and postparacrista, which extend from its apex (although, see below for an alternative interpretation of these crests). The preparacrista and postparacrista take a hemispherical course from their lingual origin on the paracone, and become confluent with the mesial and distal cingulae, respectively, along the middle one-third of their extent. The paracristae detach from the cingula to curve labially into the parastyle or metastyle, respectively.

Lingual to the paracristae the paracone forms a shallow but featureless lingual slope towards the indistinct lingual confluence of the mesial and distal cingulae. Labial to the paracristae the lateral slope of the paracone shows several crenulated linear corrugations running toward the base of the stylocone on both its mesial and distal aspects. The paracristae thus circumscribe a region of ornamented enamel within the primary trigon, which matches the enceinte structure formed from the trigonid on the lower molariform teeth. The apex of the stylocone does not have linear corrugations associated with it; however, two more salient crests can be seen to descend labially, terminating abruptly beneath the parastyle and metastyle, respectively.

The cervical region and roots corresponding to the M2 are only preserved in specimen MPEF-PV 2341. Three roots can be clearly identified for this tooth, each buttressed by a limb of a ``Y'' shaped compound interradicular crest. Each limb of the

tripartite interradicular crest is similar to the single mesiodistally oriented interradicular crests found on the lower molars. A mesiolabially directed branch of the interradicular crest contacts the mesial root along its lingual edge. While a lingually-oriented branch contacts the lingual root along the center of its labial surface, and a distolabialy-oriented branch contacts the distal root along the center of its mesial surface. The contact between all three branches is positioned under the space between the paracone and stylocone.

The mesial root of the M2 is approximately triangular in outline, with a vertical root canal located opposite the lateral preparacrista and parastyle on the crown surface. This root is flattened mesiolabially-distolingually, with a convex mesiolabial surface and concave distolingual surface. The distal root is mediolaterally elongate, and located centrally beneath the distal border of the crown surface. The lingual root has a concave labial surface and convex lingual surface, both vertically oriented.

An alternative hypothesis regarding the homology of what are here termed paracristae is that these structures represent the vertically extended and lingually coalesced mesial and distal cingula. In *Reigitherium* the paracone is labially thickened (Fig. 3A) and the morphology around it shows a convergence of corrugations. If the mesial and distal borders of the upper molars were to be interpreted as full height cingula that have essentially merged with the trigon, the subdued topology of the center of the crown should be seen as the homolog of the primitive dryolestoid upper molar. If this is the case, it would explain the lack of expression of cingula on the lingual surface of the paracone; and would be in greater agreement with the hypertrophied cingular morphology seen in the other known mesungulatoid meridiolestidans. Under this interpretation the paracristae would possibly be homologous to several of the more salient corrugations descending labially from the apex of the paracone, or have lost distinction altogether. A similar morphology is present,

although not as highly developed, in *Peligrotherium*, where the cingula approach the trigon level; however, both cingula and the primary trigon persist as distinct features of the upper molars. While this interpretation is plausible and compatible with the available evidence, it is not adopted in the following discussion because of the lack of vertically enlarged cingula in the known premolars of *Regitherium*, and the ambiguity and capriciousness in identifying trigon and cingular homologs in these highly derived upper molars. The scheme adopted here is simpler and does not vitiate the interpretation of *Reigitherium* as a close relative of *Peligrotherium*, which would only be strengthened if the alternative is adopted.

Upper Third Molar. This tooth position is only known from MPEF-PV 2369 (Fig. 17), a fragmented isolated tooth missing approximately the lingual one-third of its crown surface, but showing only minor abrasion. The mesiodistal length of the M3 is 1.67 mm, labially across the stylocone; and the apices of the paracone and stylocone were separated by approximately 1 mm. This specimen is inferred to be the ultimate upper molar because of the large and laterally projecting form of the parastyle, a condition that matches the ultimate upper molar morphology in both *Peligrotherium* and *Coloniatherium*. The contrast in mediolateral width between the (damaged) base of the mesial root and base of the distal root is also greater than in the M2, suggesting that MPEF-PV 2369 succeeded this position. There is no trace of a lingual root in MPEF-PV 2369, possibly because of damage or its absence at this position.

The crown surface shows similar features to the M2, such as linear corrugations descending from the paracone, which are circumscribed by strong pre-and postparacristae. The paracristae themselves are labially terminated by a large parastyle and a smaller metastyle, respectively. Both of these stylar cusps show frenular crests directed lingually

towards the paracone. The stylocone also shows two crests running mesially and distally towards the base of both of these stylar cusps, but lacks linear corrugations such as those present in the paracone. The M3 also lacks an ectostyle, unlike in the preceding two positions, and therefore has a steeper labial slope of the stylocone.

The mesial and distal roots are both damaged, but the shape of the compound interradicular crest and the roots' commencement from the cervical region are still clear. The mesial and distal roots are transversely wide at their base, and the lingual surface of these roots curves labially causing the roots to taper to a conical form underneath the stylar cusps. As in the preceding molar, a compound "Y" shaped interradicular crest can be seen between the mesial and distal roots. The two lateral branches of the interradicular crest are short, and both can be seen terminating into the mesial and distal root bases near the transverse midline of the tooth. A longer lingual branch of the compound interradicular crest runs towards the lingual edge of the fractured surface of MPEF-PV 2369. As mentioned above, it is not clear if there was a lingual root in this tooth position to form a lingual termination for the interradicular crest. The point of intersection of all three branches of the interradicular crest is located beneath the expression of the paracone on the crown surface.

Fig. 17 *Reigitherium* upper left third molar MPEF-PV 2369. **A** occlusal view; **B** ventral view of roots. Mesial is towards the top of page. Scale bar is 1 mm and is for A and B. Directional arrows are for B only, Li - Lingual, M - Mesial

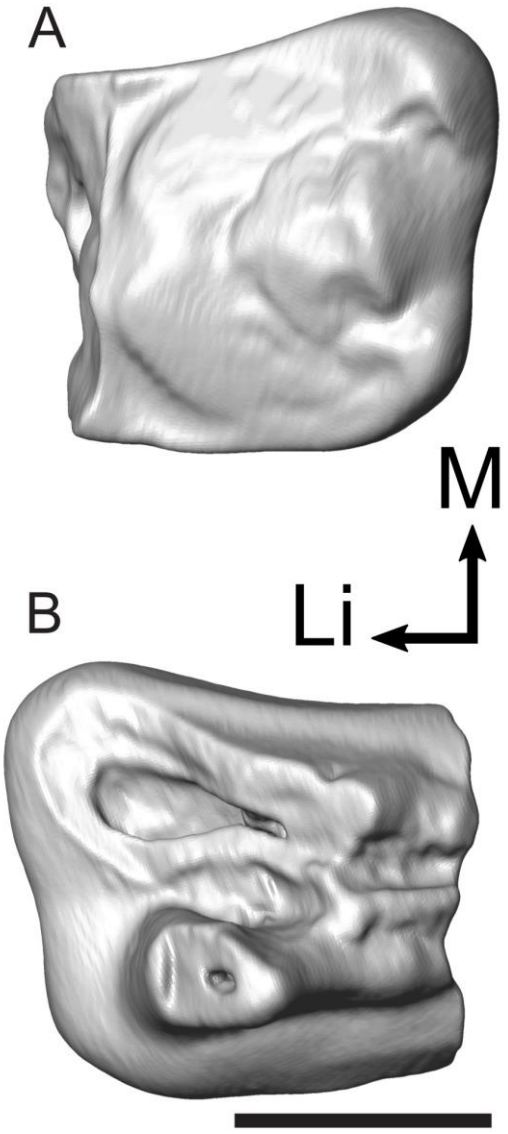

DISCUSSION

Systematics of *Reigitherium*. The type specimen of *Reigitherium bunodontum* (MACN-RN-173; Bonaparte 1990) is a fragmentary isolated molar with all of its root structure and much of its crown detail effaced by postmortem processes. In its initial description Bonaparte (1990) insightfully recognized the mediolaterally widened crown structure seen in this specimen as indicative of the capacity for ectental occlusion (i.e., unilateral mastication with mediolateral translation) developed apomorphically in cladotherian mammals (Moore 1981; Kielan-Jaworowska et al. 2004). Thus, because of its advanced stem therian but non-tribosphenic characteristics the type specimen of *Reigitherium* was referred by Bonaparte (1990) to a monotypic family, probably related to Mesungulatidae, within the cladotherian lineage Dryolestoidea. Additionally, the labial cuspulids at the lateral end of the mesial and distal cingulids were inaccurately regarded as homologues of the anterior and posterior cingular cusps present along the lingual margins of the cingula in *Mesungulatum* (Bonaparte 1986; Rougier et al. 2009b), and it was this conflation that was ultimately responsible for the description of the type specimen as an upper left molar.

An additional complication in the interpretation of the type specimen is the crater-like excavation of the apex of the protoconid ("paracone" in Bonaparte 1990), possibly reflecting an accumulation of apical wear (Janis 1990) through repeated puncture-crushing masticatory behaviors, or an exaggeration of it through postmortem erosion. Similar but less deeply excavated patterns of apical wear are also seen on the paraconids of first and second lower molar specimens from the La Colonia sample (MPEF-PV 2317 and MPEF-PV 2237). Interestingly, apical wear seen on the protoconid of the La Colonia m2 (MPEF-PV 2237) is

shallower but more laterally extensive than in the Los Alamitos holotype, stretching mesially onto the paracristid and with an additional apical pit on the apex of the metaconid.

The *Reigitherium* holotype also resembles the La Colonia m2 in unworn morphology, and most likely is attributable to this position. This was in effect posited by Pascual et al. (2000) by their suggestion that the holotype molar represented the next locus distal to the most posterior tooth preserved in their dentary specimen from the La Colonia Formation (MPEF-PV 606), and that at least one more tooth position must be placed distal to the holotype's locus. Surface data gathered from a cast of the *Reigitherum* holotype also support and qualify the identification of the Los Alamitos specimen as a right lower m2. Compared to the m1 morphology seen in MPEF-PV 606, MPEF-PV 2317, MPEF-PV 2020, and MPEF-PV 2338, both MPEF-PV 2337 and the *Reigitherium* holotype show a medially inflected margin of the enceinte distal to the protoconid. Additionally, the labial cuspulid at the lateral end of the mesial cingulid is labially offset to a greater extent relative to the transverse position of the labial cuspulid at the lateral end of the distal cingulid. Both of these cingular cuspulids are also more closely appressed to the lateral aspect of the protoconid with concomitantly weaker development of their frenular crests. The lack of two labial cuspulids near the lateral margin of the exodaenodont lobe in the holotype is most likely attributable to the fractured lateral surface of the specimen. Similarities between MACN-RN-173 and MPEF-PV 2337 are apparent and we feel confident in assigning the La Colonia material to the genus *Reigitherium*. Because of the limited extent of its hypodigm, however, there is no positive evidence for assigning the La Colonia material a conspecific status with *R. bunodontum* known from the (probably older) Los Alamitos Formation, but we keep here the specific epithet until better material from the type locality allows evaluation of intraspecific variability in *Reigitherium*.

Comparative Context. The presence of roughened, crenulated, or otherwise ornamented enamel in Mesozoic dental remains is seen almost exclusively in the non-therian mammaliaform clades Docodonta, and Allotheria (including Multituberculata), in addition to several exceptional taxa such as *Brachyzostrodon*. Among these taxa Butler (1997) pointed out that only the first three of these clades show a broadly appositional relationship between the upper and lower dentitions. The additional presence in most docodont species of intermolar basins formed by the flanks of adjacent molars provide strong reasons to suspect that any Mesozoic taxon showing this suite of traits should also be referable to Docodonta. This line of reasoning was presented and expanded on by Pascual et al. (2000) in their description of the first specimen of *Reigitherium* (MPEF-PV 606) from the La Colonia Formation, a dentary fragment with intact but worn p3-m1 (as in the newly recovered MPEF-PV 2338, Fig.6). These authors rightly emphasized the presence of horizontal (apical) wear facets on the neomorphic cuspulids as evidence for the presence of lingually extended upper molars, and characterize the protoconid as supporting mesially and distally directed crests. Additionally, what is referred to as the "main internal cingulum cusp" in Pascual et al. (2000) would correspond to cusp "c" under the schematic of docodont cusp homology provided by Butler (1997) and further elaborated by Luo and Martin (2007). Being the homolog of cusp "c," this would make the metaconid in *Reigitherium* a correctly identified but renamed structure in Pascual et al. (2000). However, the majority of the subsequent argumentation provided by these authors for the docodont affinities of *Reigitherium* is the result of compounded misinterpretations based on the anatomy presented by the heavily worn specimen MPEF-PV 606 (Rougier and Apesteguía 2004; Rougier et al. 2011, 2012).

The highly molarized p4 of *Reigitherium* was interpreted by Pascual et al. (2000) as

representing the first molar, and the Los Alamitos type specimen, correctly identified as the locus succeeding the posterior tooth in MPEF-PV 606, was misinterpreted to be an m3. Because the *Reigitherium* type specimen does not show an "ultimate molar" morphology (e.g., a distally extended and tapering posterior crown) this was used by the authors as support for the presence of at least four molars in the dental formula in *Reigitherium*, matching the condition seen in many docodontans. The elongate p3 in *Reigitherium* was concomitantly interpreted to be a p4, and the inferred presence of a third lingual root at this position was used as another docodontan apomorphy. Further investigation of the p3 position in the expanded La Colonia sample described here (specimens MPEF-PV 2338, MPEF-PV 2372, and MPEF-PV 2376) using high resolution CT imaging does not corroborate the presence of a third lingual root at this position, or a small interradicular alveolus capable of accommodating this structure (although an accessory alveolus is present at the m1 position in MPEF-PV 2337). Observation of a neomorphic structure at the p3 position by Pascual et al. (2000) is likely attributable to the variable appearance of the interradicular crest, which likely forms a lingual extension with a similar appearance to the labial extension of the interradicualr crest seen in the lower canine (MPEF-PV 2347, Fig. 9c). Finally, the crest of the enceinte as it crosses mesiodistally posterior to the protoconid was interpreted to represent the vestige of the "a-d crest" (or posteromain crest of Sigogneau-Russell 2003), another feature diagnostic of docodonts. These initial misinterpretations provided inertia for several hypotheses mentioned by Pascual et al. (2000) whereby the enceinte structure of *Reigitherium* was interpreted to be the product of a coalescence of several main cuspids (protoconid, paraconid, and "main internal cingulum cusp"/metaconid), cuspulids ("posterior cingulum cusp," "postero-internal cingulum cusp") and lingual cingulid. The new lower molar specimens from La Colonia allow the identification of both the protoconid and

metaconid as integral components of the enceinte; however, there is no evidence of any structure corresponding to the cuspulids and lingual cingulid theorized by Pascual et al. (2000). Additionally, the continuous circuit of the lower molar enceinte mesial to the metaconid was not reconstructed in *Reigitherium* by these authors, but can be confirmed with the better preserved specimens now available. The hypothesized morphological evolution of the lower molars of *Reigitherium* by "expansion of area of opposition by expansion of lingual sector" (p. 408) from a more typical docodont ancestor, and "shearing function between linear blades initiated in *Docodon* [that] was enhanced in *Reigitherium* by the enlargement of the occlusal surfaces of the molars, and its transformation, by thegosis, into flat blade-like facets" (p. 405) are fundamental misstatements based on the above mentioned inaccurate but logically supported arguments. Naturally, our reinterpretation of the crown structure of *Reigitherium* also vitiates the hypothesized sister relationship between *Reigitherium* and *Docodon*.

Certainly, some of the newly discovered *Reigitherium* material does present morphological similarities to several docodont taxa, such as the presence of an angular notch on the ventral contour of the mandible. However, these similarities are much more easily explained as the result of convergence or retention of generalized features; the angular notch in particular is associated with the ventral deflection of the dentary's angular process, either to accommodate a posterior facing angular articular facet in docodonts, or for muscular leverage in cladotherians (Kielan-Jaworowska et al. 2004).

Although the "pantotherian" similarities of docodonts, as originally mentioned by Simpson (1928, 1929), suggest that care should be taken in the taxonomic attribution of any new and apomorphic dental remains, the hypothesis of *Reigitherium* as the latest surviving and only known South American docodont has not been borne out by the weight of available evidence. However, later discoveries of Gondwannan docodonts from the early

Middle Jurassic (Prasad and Manhas 2001 and 2007) and near relatives from the Late Triassic (Datta 2005) have substantiated the suspicions of Pascual et al. (2000), and a preliminary report by Martin et al. (2013) suggested that docodonts may well have survived until the early Late Cretaceous of South America.

With the collection of these new and informative fossils the initial attribution of *Reigitherium* by Bonaparte (1990) to the South American radiation of dryolestoid mammals has once again become the most plausible phylogenetic hypothesis. This taxonomic stance is not a default interpretation due to the abundance of meridiolestidan species and lack of ordinal diversity in the Cretaceous mammals of South America (Rougier et al. 2010). In fact, many of the same features suggestive of a docodontan relationship equally support a "eupantotherian" ancestry for *Reigitherium*. In particular, the bunodont and brachydont nature of the posterior cheek teeth point to a close relationship with the mesungulatoid meridiolestidans, an omnivorous-herbivorous radiation of rat-sized to dog-sized species found in Upper Cretaceous and Paleocene formations in Argentina (Bonaparte 1986; Rougier et al. 2009a and 2009b; Forasiepi et al. 2012) and Bolivia (Gayet et al. 2001). A series of explicit comparisons between *Reigitherium* and a sequence of taxa representative of increasingly more inclusive clades within Cladotheria (the advanced mesungulatoid *Peligrotherium*, dryolestoids, and the extant cladotherian groups Eutheria and Metatheria) will therefore provide a useful and appropriate context in which to interpret the evolutionary significance of *Reigitherium*.

Comparison to *Peligrotherium*. Despite the enormous body mass differential between the shrew-sized *Reigitherium* and dog-sized *Peligrotherium*, there are several dental and gnathic features shared by both species suggestive of their exclusive relationship among the other

South American cladotheres. These shared derived characteristics, as mentioned by Paez-Arango (2008) and Rougier et al. (2011, 2012), involve the elevation of occlusally functional cingulids, the acquisition of labial accessory cusps/cuspulids, and the inflated and intermittent condition of the primary trigon/trigonid crests.

This list of similarities can be validated and expanded based on evidence from the new La Colonia *Reigitherium* specimens described above, particularly with regard to the form of the dentary and upper dentition. Both taxa share the position of the posterior-most mental foramen (the type specimen of *Peligrotherium* shows duplicate mental formanina on the right side only) posteroventral to the mesial root of the penultimate premolar. Additionally, the ventral contour of the dentary in both species reaches maximal convexity beneath the lower second molar. The upper molars also show a subrectangular to ovoid occlusal outline, with a complete loss of any kind of stylar lobes or projections.

While the apomorphies uniting *Reigitherium* and *Peligrotherium* are convincing, the morphological differences between these two species are also significant, and suggestive of the differing trajectories of trait evolution experienced by their lineages since their divergence from a more typical meridiolestidan common ancestor. These anatomical differences can be summarized by three major trends, possibly related to allometry and/or degree of herbivorous specialization: 1) the shortened and robust mandible of *Peligrotherium*, with its lateral deflection of the ascending ramus relative to the mandibular corpus; 2) the greater degree of molarization (i.e., characteristics shared with true molars) of the upper penultimate and ultimate premolars in *Peligrotherium*, and greater degree of ultimate lower premolar molarization in *Reigitherium*; and 3) the greater development of the trigonid relative to cingulids and cuspulids in the lower molars of *Peligrotherium*, and greater development of the trigon relative to the mesial and distal cingula in the upper molars of *Reigitherium*.

Features associated with the strengthened mandible of *Peligrotherium* are the extensive symphysis, which reaches the level of the penultimate premolar (and which only reaches the level of p2 in *Reigitherium*), and reduced premolar dental formula with only three loci. The slight lateral deflection of the ascending ramus relative to the mandibular corpus creates a narrow and parallel tooth row, and is associated with a shallower anterior border of the masseteric fossa, and a coronoid process placed more laterally to the line of the lower molar alveoli.

The posterior upper premolars of *Reigitherium* show fewer similarities to the upper molars than in corresponding positions in *Peligrotherium*. This is evidenced by the more continuous cingula on the upper penultimate premolar of *Reigitherium* compared with the separated mesial and distal cingula on the true molars. Conversely, *Peligrotherium* shows greater posterior upper premolar molarization because of the shorter mesial and distal cingula on the distal two premolars and the presence of a lateral accessory cuspule on the ultimate premolar (which does not form the labial terminus of either cingula). That being said, the distal two premolars of *Peligrotherium* do differ from the molar condition by consistently showing a wider distal cingulum relative to mesial cingulum, opposite to what is found in the true upper molars. The lower ultimate premolar of *Reigitherium* is actually more molarized relative to its counterpart in *Peligrotherium* because of its more labially extended mesial and distal cingulids, which are terminated labially by accessory cuspulids. In the lower ultimate premolar of *Peligrotherium* the labiolingual extent of the mesial and distal cingulids is narrower than the width of its trigonid region, and the size of this tooth position is also much greater than any of the true molars.

The lower molars of *Reigitherium* have departed from the plesiomorphic meridiolestidan condition to a greater degree than those of *Peligrotherium*, as shown by the

almost complete loss of the paraconid (remaining as a small cuspule only in unworn teeth), development of the enceinte structure on all lower molariforms, relatively smaller size of the trigonid compared to the cingulids, and greater number and development of accessory cuspulids. Conversely, the upper molars of *Peligrotherium* have more elaborate marginal structures, based on the relatively smaller trigon relative to the greatly enlarged mesial and distal cingula. Additionally, the distally directed gradient of decreasing molar size in *Peligrotherium* is much steeper, causing the third upper molar to take on a diminutive and sub-quadrate morphology. As mentioned above, it is unclear whether or not the structures identified here as paracristae in *Reigitherium* are actually vertically extended and lingually coalesced cingula. If this is indeed the case then the tall vertical extent of the upper molar cingula would be an additional apomorphic character uniting *Reigitherium* and *Peligrotherium*. However, under the interpretation followed here, the upper molars of *Reigitherium* are characterized by reduced cingula that are inconsequential for occlusion, opposite the condition seen in *Peligrotherium*. However, we feel this decision in the interpretation of the basic homologies of the upper molar is insufficiently supported. A definitive choice cannot be made without additional material or perhaps intermediate taxa filling the gaps between plesiomorphic mesungulatids and *Reigitherium*-like forms.

These differences between *Reigitherium* and *Peligrotherium* point to the diverging patterns of cheek tooth elaboration in these sister taxa. From an ancestral condition resembling *Coloniatherium*, the lower molariforms of *Reigitherium* have diverged to a greater degree and have widened considerably. Although the upper molars of both species are fairly derived, only in *Peligrotherium* is there an obvious tendency towards increased hypsodonty. Finally, probably the most apparent difference between *Reigitherium* and *Peligrotherium* is the intense but circumscribed crenulation of the primary trigon and enceinte regions of all

molariform cheek teeth in *Reigitherium*. This type of enamel ornamentation is not seen in *Peligrotherium* (or any other Cretaceous trechnotherian mammal). We hypothesize that this represents an adaptive response to selective pressures for increased herbivory unique to *Reigitherium* (outlined below).

Comparison to Other Dryolestoids. Analyses of 44 dental and dentary characters among ten dryolestoid species support a nested position of *Reigitherium* among other South American endemic pre-tribosphenic mammals (see Fig. 18). The data are based on 38 characters described in Rougier, et al. (2012) (updated based on the new *Regitherium* sample), with six additional dental characters included. The character data and analysis specifications used here are available in the supplementary materials associated with this report. Irrespective of optimality criterion, these results demonstrate that *Reigitherium* is best considered as a small and dentally sophisticated member of the Meridiolestida, and not a Late Cretaceous immigrant representative of a more basal mammaliaform lineage (as suggested by Pascual et al. 2000). These results corroborate the initial taxonomic assignment given by Bonaparte (1990), and further detailed by Bonaparte (1994), Bonaparte and Migale (2010), Rougier et al. (2011, 2012), and Wible and Rougier (2017).

Both Maximum Parsimony and Bayesian analyses treated all characters as equally weighted and unordered; however, four of the included characters are parsimony uninformative (autapomorphic) and therefore were not considered in the Maximum Parsimony analysis.

An exhaustive (branch and bound) Maximum Parsimony analysis, performed using PAUP* version 4.0 (Swofford 2002), using these observations and assumptions, produced a single optimal topology with a length of 74 steps (Fig. 18a). This corresponds to a

Consistency Index of 0.74 and Retention Index of 0.77. Randomization using ten thousand bootstrap replicates shows weak support for clades outside of Meridiolestida, particularly the node containing the North American *Laolestes* and all South American taxa. This provides only weak support for the dryolestoid relationships of the South American taxa, being supported by only one unambiguous synapomorphy (character 11, presence of a central crest in upper molariforms). Meridiolestidan relationships inter se are more reliably supported.

An uncalibrated Bayesian phylogenetic estimation based on the full 44 character matrix and a Mkv morphological likelihood model (Lewis 2001) integrated over gamma distributed rate variation produces the majority rule consensus and average branch lengths seen in Fig. 18b. These results are based on a Metropolis Coupled MCMC heuristic search implemented in the program MrBayes version 3.2 (Huelsenbeck 2001; Ronquist et al. 2012), using default parameters and a chain length of one million steps. Because the consensus topology produced does not resolve the exclusive relationship between *Laolestes* and the South American endemic clade, the dryolestoid affinities of the meridiolestidans are not supported. Aside from this polytomy at the root node, the topology and relative support values (posterior probabilities) within Meridiolestida correspond closely to the results found using Maximum Parsimony.

These results emphasize the apomorphic morphology diagnostic of Mesungulatoidea (which is well supported using either optimality criterion) discernable in *Reigitherium*. These characters include thickened enamel, tall cingulids, and mesiodistal compression of lower molar roots and the labial two upper molar roots. The trend towards increased bunodonty shown by mesungulatids and *Peligrotherium* is also apparent in *Reigitherium*, but is further accentuated by the localized crenulation seen only in this taxon.

The presence of alveoli corresponding to three lower molar positions, and inferred matching presence of three upper molar positions, is also characteristic of Meridiolestida as a whole. The inferred presence of four premolar positions in *Reigitherium* is, however, disruptive to a completely parsimonious model of evolution for the premolar formula within Meridiolestida, as four premolars are also seen only in the plesiomorphic taxon *Cronopio*. Additionally, a Coniacian edentulous dentary fragment referred to Mesungulatoidea by Forasiepi et al. (2012) clearly preserves six postcanine tooth positions, most likely belonging to three premolars and three molars. The homoplastic distribution of four premolar loci in both the most dentally plesiomorphic *Cronopio* and dentally derived *Reigitherium* suggests that a reduction to three premolars occurred in several separate lineages within Meridiolestida. However, for most meridiolestidans the dental formula cannot be accurately determined, and the optimization of this character may also be hindered because of the large amount of missing data.

Comparison with the dentition preserved in better known mesungulatoid taxa (See Figs. 1 and 2) suggests that the locus referred to as P1/p1 in *Reigitherium* contains the elements missing in the remaining species. The hypothesis that the first premolar in *Reigitherium* is a retained deciduous predecessor of the element referred to here as p2 is not supported by known aspects the morphology of the anterior dentition (i.e., simplified structure of the lower p1, without noticeably thinner enamel; Fig. 10). Conversely, the hypotheses that the p1 in *Reigitherium* could be a neomorphic acquisition, or that the element referred to as p2 in *Reigitherium* is actually a retained dp1 element can not be strictly ruled out, but are unlikely given the common modes of mammalian dental evolution and the relative size of the lower p2 (Luckett 1993). The appearance of a three-premolar mesungulatoid dental formula in the Coniacian therefore suggests that the lineage leading

towards *Reigitherium* and *Peligrotherium* had split from the lineage leading to the Mesungulatidae by at least the early Late Cretaceous.

As described by Crompton et al. (1994) and Wood et al. (2005), the enamel ultrastructure seen in the mesungulatids *Mesungulatum* and *Coloniatherium* (referred to as "La Colonia Dryolestoid" by the latter authors) also shows significant differences from the more derived pattern seen in *Reigitherium*. Specifically, the mesungulatid enamel contains a relatively large proportion of interprismatic, as opposed to prismatic, enamel crystallites. The distribution of enamel prisms and tubules is also highly polarized, with enamel tubules being restricted to the basal 25% of the total enamel thickness, and a consistently thick outer layer of aprismatic enamel near the outer enamel surface. In contrast, *Reigitherium* shows a complete loss of enamel seams, a regular and tightly packed distribution of enamel prisms nearly throughout the entire extent of its total enamel thickness, and a variably thick outer aprismatic layer near the outer enamel surface. This is a derived enamel microstructure pointing once again to the peculiar adaptation and long branch separating *Reigitherium* from other mesungulatoids. However, *Reigitherium* also displays several enamel ultrastructural synapomorphies with the mesungulatids and *Groebertherium*, such as the association of enamel tubules with the open side of enamel prism sheaths, and the orientation of interprismatic enamel crystallites perpendicular to the outer enamel surface, further supporting the meridiolestidan affinities of *Reigitherium*.

The mesiodistal compression of molar roots, and the presence of a larger mesial root with a labially emarginated lateral aveolar border in the lower molars, are also characters which have been suggested to represent a close affinity of the meridiolestidans as a whole with the holarctic Dryolestidae. However, the results of this summary analysis do not support the close relationship of these taxa to the exclusion of the more plesiomorphic

paurodontid species *Henkelotherium* used as an outgroup. What has been reported about the enamel ultrastructure in *Laolestes* (Wood et al. 1999) and a Jurassic dryolestoid from Portugal (Lester and Koenigswald 1989) does support the possible derivation of the South American Mesozoic cladotheres from mammals of this type, and this is reflected in the phylogeny produced by Maximum Parsimony by the sister relationship *Laolestes* with the South American endemic taxa. While the presence of incomplete enamel sheaths open toward the outer enamel surface, an abundance of interprismatic enamel material, and the presence of enamel seams are shared features seen in holartic dryolestoids and the mesungulatids, they are also apparent in the enamel of *Spalacotheridium*, as reported by Wood et al. (1999). This leaves open a possible relationship of these South American endemic taxa with the spalacothere symmetrodonts, as suggested by Averianov et al. (2013). However, the presence of a prominent and posteroventrally deflected angular process is an apomorphic characteristic of cladotheres, which is apparent in several meridiolestidan taxa (*Cronopio*, *Peligrotherium*, and an unidentified mesungulatoid; Rougier et al. 2011; Paez-Arango 2008; Forasiepi et al. 2012; contra Averianov et al. 2013), which strongly supports a cladotherian, if not dryolestidan, ancestry of Meridiolestida. The nested position of Meridiolestida and other South American taxa among the more typical dryolestoids is only recovered in our Maximum Parsimony phylogeny (Fig. 18a), which therefore provides only weak support for the proposed relationship between these two groups. However, it is unlikely that the highly modified and limited material referable to *Reigitherium* will be able to definitively resolve the problem of the origin of the meridiolestidans as a whole. Better material of basal meridiolestidans, and a focused phylogenetic analysis may be required to fully address this problem.

The relatively blunt cristids and thickened enamel along salient parts of the molar crowns in meridiolestidans, as compared to the dryolestid *Dryolestes*, is mentioned by Shultz and Martin (2011) as possible evidence for an alternative expression of the common utilization of the mesial and distal borders of the trigonid for masticatory grinding (sensu Kay and Hiiemae 1974). Ostensibly, the deep downward sloping exposed dentine surfaces in worn molars of *Dryolestes* acted as receptacles for the oblique compression of food particles during rhythmic chewing. In Dryolestidae this function would be facilitated by the thinned enamel coating, which would accelerate abrasional wear and the formation of prevallid and postvallid compression zones. This is supported by the lack of attritional wear (pits and striations) characteristically found on surfaces experiencing tooth-tooth contact. If the founding lineage of South American endemic cladotheres was derived directly from dryolestids (or as our results suggest from a nearby sister lineage with enamel of more typical thickness) the trajectory seen in Meridiolestida towards morphological and enamel ultrastructural adaptation for a more routinely compressed trigonid can be detected at an incipient stage in the Late Jurassic in Holarctic dryolestoids. This hypothesis would also help explain the otherwise confusing fact that *Groebertherium*, while showing the most plesiomorphic lower molar morphology among South American cladotheres, has accumulated more synapomorphic enamel features (greater proportion of prismatic to interprismatic crystallites, and loss of enamel seams) than even the mesungulatid taxa *Mesungulatum* and *Coloniatherium*. By extension, the dentition of *Reigitherium* could also be seen as representing the most sophisticated product of this trend, with molars showing highly modified crown morphology and apomorphic enamel containing an abundance of regularly spaced prisms and a loss of enamel seams. Under the assumption that the amplification of compressive force is prerequisite for mammalian herbivory (Lucas 2004), the South

American native cladotheres represent a greater expansion into the adaptive landscape of plant-based feeding than any northern symmetrodont, dryolestoid, or therian lineage in the Mesozoic.

Fig. 18 Phylogeny of dryolestoid taxa and South American endemic cladotheres. **A** results of Maximum Parsimony analysis of 40 parsimony informative morphological characters, showing 50% majority rule consensus tree found using an exhaustive search. Node values are proportional support values found in 10 thousand bootstrap replicates. **B** majority rule consensus from Bayesian estimation using a Mkv morphological likelihood model. Branch lengths and node heights are estimated from posterior sample averages, and are not time-scaled. Posterior support values are shown at their respective nodes

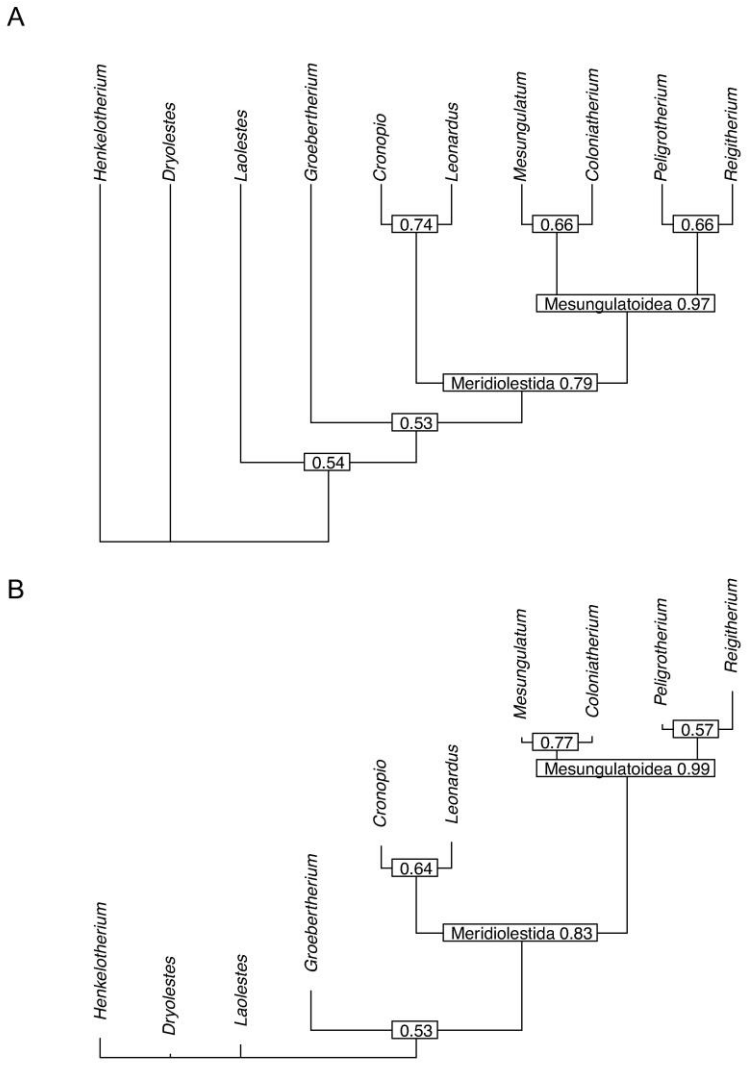

Comparison to Northern Tribosphenic mammals. The presence of a cingular protocone in the upper dentition has been heralded as one of the most consequential anatomical developments in the therian lineage (Patterson 1956; Crompton 1971; Crompton and Kielan-Jaworowska 1978; Davis 2011). The defining characteristic of this transformation is a shift from a bi-directionally convex lingual cingulum on upper molars (as seen in *Peramus*; Mills 1964; Davis 2012) into a radially convex lingual protocone (as seen in *Kielantherium*; Lopatin and Averianov 2007). The co-option of this feature has allowed for many Cenozoic tribosphenic mammals to specialize their posterior dentitions toward highly efficient "grinding" (sensu Rensberger 1973) types of mastication (Crompton 1971; Davis 2012). However, the functional importance of the protocone at the time of its first occurrence among aegialodontids and therians (the northern tribosphenic clade) is difficult to interpret. This is because of the apparent lack of increased abundance or diversity in northern tribosphenic fossils near their probable origin during the Late Jurassic; and also because of the manifest capacity of pre-tribosphenic stem therian lineages to develop complex and bunodont crown morphologies, without the benefit of a protocone or a basined talonid. This capacity for elaborate mastication in pre-tribosphenic stem therians is nowhere better demonstrated than in *Reigitherium* and the other mesungulatoid meridiolestidans, making these species an appropriate comparative sample with which to contrast the trajectory of tribosphenic and pseudotribosphenic cheek-tooth specialization.

While gestalt similarities of the molar morphology seen in mesungulatoids and omnivorous Paleogene therians have been noted by several authors (Bonaparte 1984; Paez-Arango 2008), the common assumption that the attainment of tribospheny presents a morphological gap too large to cross with traditional distance-based or landmark-based morphometric methods has precluded any formal quantitative comparison of pre-

tribosphenic and tribosphenic taxa. However, the recent development of "homology-free" dental metrics based on high-level features of crown topography provides an opportunity to compare functionally interpretable aspects of tooth shape across a wide variety of extinct and extant taxa (e.g., Wilson et al. 2012). As the acquisition of the tribosphenic condition is predicated on the punctuational appearance of a neomorphic feature of the upper dentition (the protocone), the analysis here is limited to the morphology of the lower second molar. Since the lower molars of stem therians show a more continuous pattern of shape change across the pre-tribosphenic/tribosphenic phylogenetic boundary, quantitative comparisons of lower molar shape are more likely to produce a continuous (as opposed to disjoint) distribution of measured dental topography metric values. As noted above, the three most popular dental topography metrics (Orientation Patch Count, OPC/OPCR; Relief Index, RFI; and Dirichlet Normal Energy, DNE) have been given a common implementation with the R package *MolaR* (Pampush et al. 2016), which is used in the Dental Topography Analysis reported below (see materials and methods).

These metrics have functional interpretations based on analogy to simple percussive tools. The value of OPCR can be analogized with the number of tools on a tooth's surface. Similarly, DNE can be thought of as the sharpness of the average tool, and RFI the average tool's height. Under this interpretation, the trend toward increased herbivory in tribosphenic mammals is represented by the increase in number of shorter tools on the lower second molar surface (as seen in Figs. 19-21).

Small-bodied marsupials are the tribosphenic mammals thought to competitively replace the latest Cretaceous mesungulatoids, particularly species within Paucituberculata and Polydolopimorphia (Goin et al. 2016). The earliest evidence for the radiation of these major subgroups of small-bodied marsupials is seen in the Cretaceous or Paleocene Peruvian

Chulpas locality (Sigé et al. 2004). They are, however, not found anywhere in sympatric association with meridiolestidan taxa.

The N = 8 marsupial specimens analyzed in this report are the early didelphimorph *Caroloameghinia*, polydolopomorphans *Roberthoffstetteria* (a Paleocene sillustaniid), *Epidolops ameghenoi* (a bonapartheriid), and the polydolopids *Polydolops rothi*, *Polydolops thomasi*, and *Eudolops tetragonus*(= *Eudolops caroliameghinoi*); the early Miocene caenolestoids analyzed include *Acdestis owenii* and *Palaeothentes lemoinei* (both palaeothentids) (Goin et al. 2016). These species show a range of trigonid and talonid morphologies, which are highly modified compared to the plesiomorphic tribosphenic condition, and therefore represent the most herbivorously adapted marsupials in the early Cenozoic of South America.

As a counterpoint to the extreme dental specialization seen in the South American mesungulatoids and marsupials, N = 13 stem eutherian specimens are analyzed as well. These taxa are Turonian (94-90 mya) stem eutherians, outside of the placental crown group, which have been recovered from the Bissekty Formation of western Uzbekistan (Archibald and Averianov 2003, 2012). The Bissekty Fauna represents the first fossil environment with a mammalian component dominated by eutherians (nine out of 12 species), and the two families studied for this analysis (zhelestids and zalambdalestids) represent the most herbivorously adapted tribosphenic taxa, not only in their fauna but also the entire Mesozoic until the latest Cretaceous. The zhelestids included in this project, in successively increasing body size, are *Aspanlestes aptap*, *Zhelestes temirkazyk*, *Eoungulatum* sp., and *Parazhelestes* sp. These taxa have low crowned, basally inflated lower molars, with well-developed talonid attritional wear surfaces, but they are still fairly close morphologically to the primitive therian condition. The only zalambdalestid taxon analyzed here is *Kulbeckia* sp., which, being the

most primitive member of the Zalambdalestidae, has a lower trigonid relative to the talonid, compared to later members of this family.

When the topographic metrics described above are applied to the lower second molars of stem eutherians, marsupials, *Reigitherium*, and *Peligrotherium*, it is clear that the pre-tribosphenic mesungulatoid taxa lie broadly within the range of values seen in both Cretaceous and Paleogene therians. Separate one-way ANOVAs, implemented using base functions in the R programming language with taxonomic category (eutherian, marsupial, or mesungulatoid) as a predictor and OPCR, RFI, and DNE as responses, further clarify the variation in dental topography between these taxa. The data used for these analyses are available in the supplementary materials associated with this report.

The insignificant ($p = 0.608$) result of the ANOVA with DNE as a response suggests that there is no systematic differentiation of molar sharpness between tribosphenic and pre-tribosphenic taxa, or between Cretaceous and Paleogene forms. This is surprising given the stereotypically insectivorous feeding strategy often assumed for Cretaceous eutherian taxa. However, this lack of significance may be attributed to the small sample sizes involved, and/or to the attainment of a degree of omnivory by all taxa considered, even the Cretaceous zhelestids and zalmbdalestids (see Fig. 20).

Both one-way ANOVA and Kruskal-Wallace omnibus tests of OPCR and RFI show that there are significant differences between the major clades considered. For each of these two dental topographic variables, three 2-sample T-tests (unadjusted for multiple comparisons) were subsequently used as post hoc tests to define the differentiation detected by each omnibus test (non-parametric post hoc Mann-Whitney-Wilcoxon tests show identical patterns of significance). For both OPCR and RFI post hoc analysis suggests that no significant differences exist between the South American marsupials and mesungulatoids

(*Reigitherium* and *Peligrotherium*). However, the OPCR and RFI for the South American mammals are significantly differentiated (OPCR higher and RFI lower, on average) from the corresponding metrics in the Cretaceous eutherians (see Fig. 21). Among the sampled marsupials OPCR in palaeothentids and the polydolopid *Eudolops* are closest to the advanced mesungulatoids. Interestingly members of these families are inferred by Goin et al. (2016: chapter 6) as being mixed feeders of high energy food products, with palaeothentids representing "insectivorous-frugivorous" and polydolopids representing "frugivorous-insectivorous" feeding strategies, respectively. The surprising fact that the bonapartheriid *Epidolops* and *Polydolops rothi* are closest in OPCR to stem eutherians is likely a byproduct of the advanced stage of premortem dental wear seen in these cast specimens. These taxa also show the lowest DNE values among the South American forms. Additionally, the plesiomorphic silustaniid polydolopiform *Roberthoffstetteria* and the "primate-like" didelphimorph *Caroloameghinia* both show values of OPCR and RFI intermediate to the sampled eutherians and mesungulatoids. This finding makes sense given the early-diverging phylogenetic and stratigraphic positions (from the early Paleocene and early Eocene, respectively) of these species, and suggests that they attained an incipient form of herbivory which is further developed in later marsupial groups. The caroloameghiniids are also estimated to be mixed "insectivorous-frugivorous" feeders by Goin et al. (2016).

These results demonstrate that the trends in dental topography seen across the K-Pg boundary in omnivorous therians, namely an increase in complexity and decrease in relative crown height, are seen precocially in the Cretaceous and early Paleocene South American taxa *Reigitherium* and *Peligrotherium*.

The crenulation of the trigonid in *Reigitherium* (and extensive cingulids seen in *Peligrotherium*) can be seen as an alternative approach to increasing OPCR without the aid of

a well-developed talonid, like those present in therians. Conversely, the mortar-and-pestle protocone-and-talonid relationship can therefore be considered just one more tool, or one more set of tools, in the tuberculosectorial molar. This points to the advanced degree of herbivory attained by the mesungulatoids, possibly in response to the earlier availability of angiosperm reproductive structures in gondwanan floras (Wilf et al. 2013; Goin et al. 2016). Alternatively, the acquisition of the protocone and the talonid grinding surface can be considered a relatively minor morphological modification, with the later convergent development of a hypocone in many tribosphenic lineages representing the adaptive breakthrough responsible for the modern success of many groups of therian mammals (Hunter and Jernvall 1995).

Regardless of how significant the early development of the protocone was to the first tribosphenidans, the fact that a major clade of pre-tribosphenic mammals can occupy a more herbivorous niche along the spectrum of omnivory-herbivory defined by a sample of tribosphenic mammals suggests that functional demands constrained the morphology of both types of molars in a similar fashion. This undermines explanations positing molar formula and morphology as unique determining factors for the Cenozoic adaptive radiation of therian mammals.

Fig. 19 Violin plots showing distribution of dental topographic values for marsupials (N =8), mesungulatoids (N=2), and eutherians (N=13), respectively. White circles show median values, black bars delimit lower 25th and 75th percentiles, and shaded boxes encompass full data range. This sample demonstrates the broad overlap of all taxa in DNE. Additionally, the significant differences in RFI and OPCR between the advanced mesungulatoids and marsupials on the one hand, and Cretaceous eutherians on the other, are also apparent. The mesungulatoid and marsupial groups do not significantly differ in any of the dental topography metrics analyzed

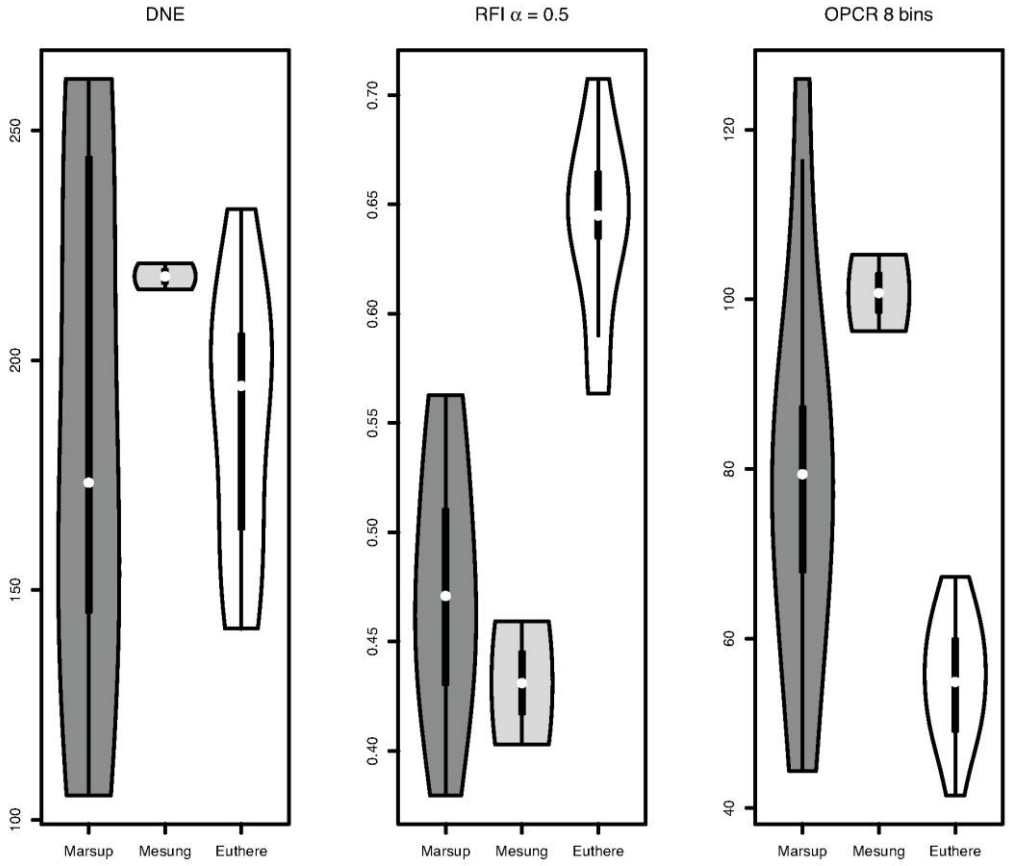

Fig. 20 Comparison of Dirichlet Normal Energy values in representative lower left second molars in oblique view. Mesial is toward the top-left, and lingual is towards the top-right of the page

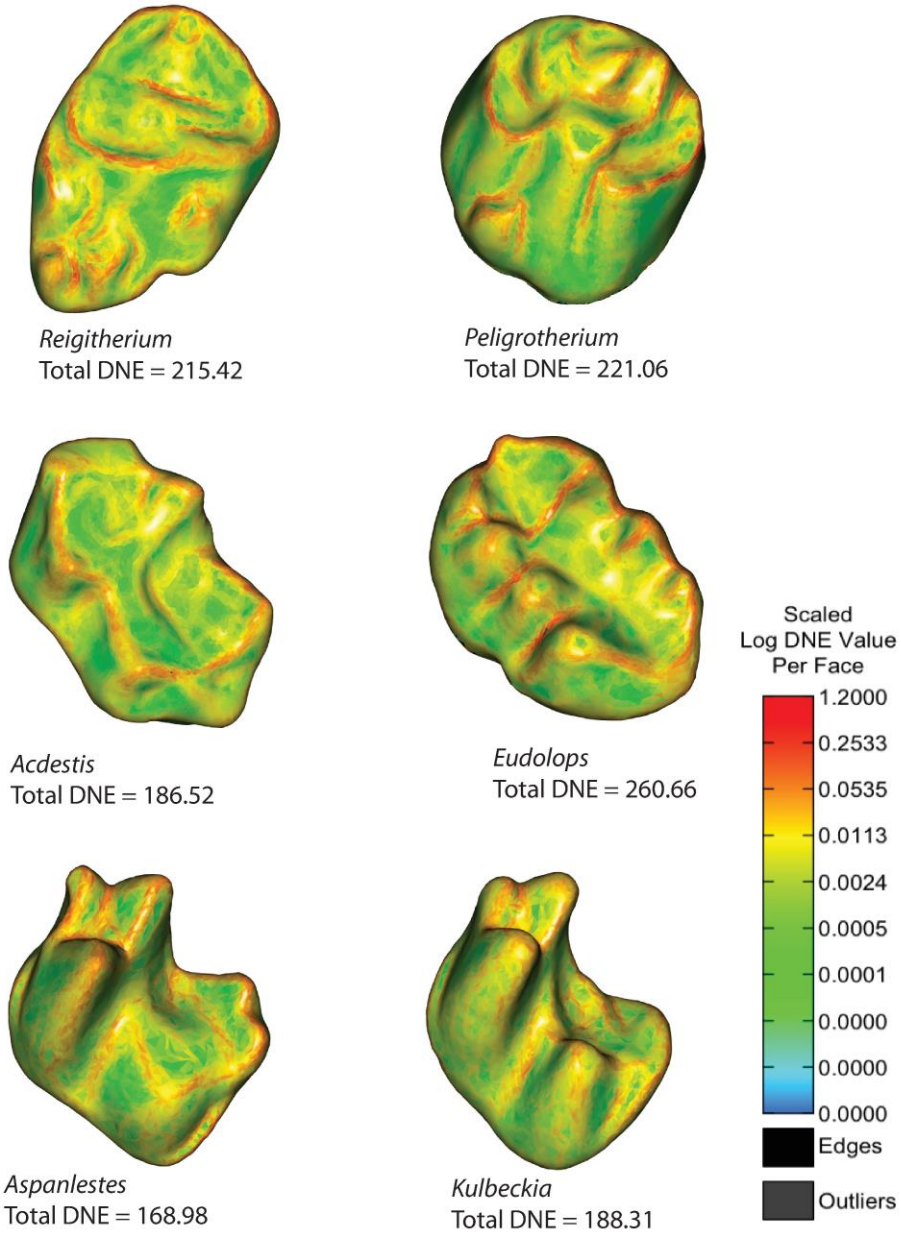

Fig. 21 Comparison of Orientation Patch Count values in representative lower left second molars. Mesial is toward the left, and lingual is towards the top of the page

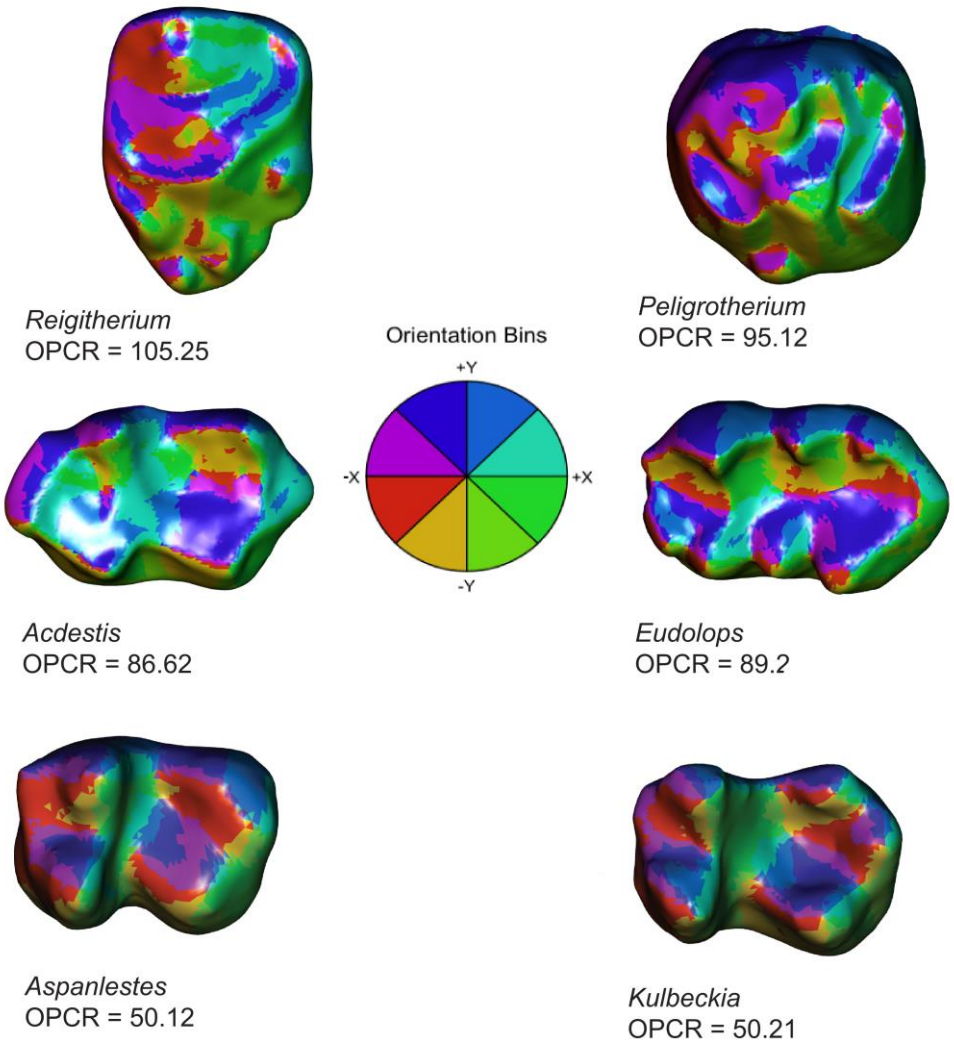

CONCLUSION

Aside from several Paleogene experiments such as *Bemalambda* and *Arsinoitherium* (Rose 2006), no therian clade has successfully adapted towards obligate herbivory with a reduced or absent protocone. This, combined with the presumed insectivory of Mesozoic stem therians, resulted in *Reigitherium* being overlooked as one of the first and most overt examples of ecological expansion into a plant-based feeding strategy (along with multituberculates and gondwanathereres). The new material presented here provides additional evidence of the uniquely derived and complex dentition developed in the genus *Reigitherium*, and summarizes the best current hypotheses for its phylogenetic location and feeding strategy. The newly described upper dentition provides abundant support for the pre-tribosphenic position of *Reigitherium* within the larger radiation of endemic South American cladotheres. Additionally, high-level analysis of the lower second molar demonstrates the advanced stage of herbivory attained by this taxon and its closest meridiolestidan relatives.

While the derived morphology of *Reigitherium* contributes little additional resolution on relationships of Meridiolestida among basal stem therians, the summary phylogenies reported here support the sister relationship of *Reigitherium* with the most derived meridiolesidans such as *Peligrotherium*, and the mesungulatids. Each member of this advanced mesungulatoid clade shows many dental characteristics traditionally associated with omnivory and herbivory in extant mammals, such as bunodonty, hypsodonty, exodaenodonty, neomorphic cusps/cuspulids, enlarged cingula/cingulids, deepening and connation of molar roots, molarization of premolars, and with *Reigitherium* enamel ornamentation. This is an impressive roster of apomorphies for any herbivorous mammalian

group, and the fact that these traits make their earliest appearance in the South American Cretaceous points toward a glaring deficit in the current narrative of the radiation of mammals near the K-Pg boundary. The Upper Cretaceous of South America offers a systematic and morphological landscape distinct from the benchmark communities of North America and Asia; and as such sets up a natural experiment of the influence of global trends (climate, floral expansion, etc.) on faunas with radically different heritage.

Acknowledgments. We would like to thank Dr. Rubén Cúneo, Leandro Canessa, and other personnel of the Museo Paleontológico Egidio Feruglio, Chubut, Argentina for years of support. We are additionally grateful to David Archibald and Ken Rose for their deep insight into mammalian evolution and access to the therian comparative specimens used here, and Patrick Luckett for helpful comments on dental homology and proofreading early drafts of the manuscript. Tim Phelps and the other faculty at Johns Hopkins University Department of Art as Applied to Medicine provided expert input and guidance to TH in the production of illustrations, and Justin Gladman and Doug Boyer at Duke University's Shared Materials and Instrumentation Facility (SMIF) graciously contributed access and assistance with the high quality imaging required for the description of small enigmatic mammalian fossils, for which we are also very grateful. We would also like to thank Dr. Alejandro Karmarz for access to the collections of Museo Argentino de Ciencias Naturales, Buenos Aires, Argentina, and intellectual and material support through the years. Finally, we thank Rosío B. Vera for her diligent assistance in picking through La Colonia sediments. This research was supported by NSF via the DEB 0946430 and DEB 1068089 grants (to GWR), USA, and by the RAICES program (PICT-2016-3682), Agencia de Investigación Cientifica, CONICET, Argentina.

Bibliography

Andreis RR (1987) The Late Cretaceous fauna of Los Alamitos, Patagonia Argentina. I. Stratigraphy and paleoenviroments. Revista del Museo Argentino de Ciencias Naturales Bernardino Rivadavia 3:103-110

Andreis RR, Bensel CA, Rial G (1989) La transgression marina del Cretácico Tardío en el borde SE de la Meseta de Somuncurá, Río Negro, Patagonia Septentrional, Argentina. In: Contribuciones de los Simposios sobre el Cretácico de América Latina, Parte A: Eventos y Registros Sedimentarios pp 165-194

Archibald JD, Deutschman DH (2001) Quantitative analysis of the timing of the origin and diversification of extant placental orders. J Mammal Evol 8:107-124

Archibald JD, Averianov AO (2003) The Late Cretaceous placental mammal *Kulbeckia*. J Vertebr Paleontol *23*:404-419

Archibald JD, Averianov AO (2012) Phylogenetic analysis, taxonomic revision, and dental ontogeny of the Cretaceous Zhelestidae (Mammalia: Eutheria). Zool Linn Soc 164:361-426

Ardolino, A, Delpino, D (1987) Senoniano (continental-marino) Comarca Nordpatagónica, Provincia del Chubut, Argentina. X Congreso Geológico Argentino (Tucumán) Actas 3: 193–196

Ardolino A, Franchi M (1996) Hoja geológica 4366 - I Telsen. Provincia del Chubut. Programa Nacional de Cartas Geológicas de la República Argentina, escala 1:250.000. Dirección Nacional del Servicio Geológico, Buenos Aires, Boletín 215, 110 pp

Averianov AO, Martin T, Lopatin AV (2013) A new phylogeny for the basal Trechnotheria and Cladotheria and affinities of the South American endemic Late Cretaceous mammals. Naturwissenschaften 100:311-326

Bonaparte JF (1986) Sobre *Mesungulatum houssayi* y nuevos mamíferos Cretácicos de Patagonia, Argentina. Actas IV Congreso Argentino de Paleontología y Bioestratigrafía 2:48-61

Bonaparte J (1990) New Late Cretaceous mammals from the Los Alamitos Formation, northern Patagonia. Geogr Res 6:63-93

Bonaparte JF (1994) Approach to the significance of the Late Cretaceous mammals of South America. Berliner geowissensch Abh 13:1-44

Bonaparte JF, Migale LA (2010) Protomamíferos y Mamíferos Mesozoicos de América del Sur. Museo de Ciencias Naturales Carlos Ameghino, Buenos Aires

Bonaparte JF, Van Valen LM, Kramartz A (1993) La fauna local de Punta Peligro, Paleoceno inferior, de la Provincia del Chubut, Patagonia, Argentina. Evol Monogr 14:1-61

Boyer DM (2008) Relief index of second mandibular molars is a correlate of diet among prosimian primates and other euarchontan mammals. J Hum Evol 55:1118-1137.

Bunn JM, Boyer DM, Lipman Y, St Clair EM, Jernvall J, Daubechies I (2011) Comparing Dirichlet normal surface energy of tooth crowns, a new technique of molar shape quantification for dietary inference, with previous methods in isolation and in combination. Am J of Phys Anthropol 145:247-261

Butler PM (1939) Studies of the mammalian dentition–differentiation of the post-canine dentition. J Zool 109:1-36

Butler PM (1948) On the evolution of the skull and teeth in the Erinaceidae, with special reference to fossil material in the British Museum. J Zool 118:446-500

Butler PM (1997) An alternative hypothesis on the origin of docodont molar teeth. J Vertebr Paleontol 17:435-439

Cúneo NR, Gandolfo MA, Zamaloa MC, Hermsen E (2014) Late Cretaceous Aquatic Plant World in Patagonia, Argentina. PLoS One 9:1-18

Crompton AW (1971) The origin of the tribosphenic molar. In: Kermack DM, Kermack, KA (eds) Early Mammals. Zool J Linn Soc 50: 65-87

Crompton AW, Kielan-Jaworowska Z (1978) Molar structure and occlusion in Cretaceous therian mammals. In: Butler PM, Joysey KA (eds) Development, Function and Evolution of Teeth. Academic Press, London, pp 249-287

Crompton AW, CB Wood, Stern DN (1994) Differential wear of enamel: a mechanism for maintaining sharp cutting edges. In: Bels VL, Chardon M, Vandewalle P (eds) Biomechanics of Feeding in Vertebrates. Springer, Berlin, pp 321-346

Datta PM (2005) Earliest mammal with transversely expanded upper molar from the Late Triassic (Carnian) Tiki Formation, South Rewa Gondwana Basin, India. J Vertebr Paleontol 25:200–207

Davis BM (2011) Evolution of the tribosphenic molar pattern in early mammals, with comments on the "dual-origin" hypothesis. J Mammal Evol, 18:227-244

Davis BM (2012) Micro-computed tomography reveals a diversity of Peramuran mammals from the Purbeck Group (Berriasian) of England. Paleontol 55:789-817

Drummond AJ, Bouckaert RR (2015) Bayesian Evolutionary Analysis with BEAST. Cambridge University Press, Cambridge

Evans AR, Wilson GP, Fortelius M, Jernvall J (2007) High-level similarity of dentitions in carnivorans and rodents. Nature 445:78-81

Forasiepi AM, Coria RA, Hurum J, Currie PJ (2012) First dryolestoid (Mammalia, Dryolestoidea, Meridiolestida) from the Coniacian of Patagonia and new evidence on their early radiation in South America. Ameghiniana 49:497-504

Gasparini Z, Sterli J, Parras A, O´Gorman JP, Salgado L, Varela J, Pol D (2015) Late Cretaceous reptilian biota of the La Colonia Formation, central Patagonia, Argentina: occurrences, preservation and paleoenvironments. Cret Res 54:154-168

Gayet M, Marshall LG, Sempere T, Meunier FJ, Cappetta H, Rage JC (2001). Middle Maastrichtian vertebrates (fishes, amphibians, dinosaurs and other reptiles, mammals) from Pajcha Pata (Bolivia). Biostratigraphic, palaeoecologic and palaeobiogeographic implications. Palaeogeogr, Palaeoclimatol, Palaeoecol 169:39-68

Gelfo JN, Pascual R (2001) *Peligrotherium tropicalis* (Mammalia, Dryolestida) from the early Paleocene of Patagonia, a survival from a Mesozoic Gondwanan radiation. Geodiversitas 23:369-379

Goin FJ, Woodburne MO, Zimicz AN, Martin GM, Chornogubsky L (2016) A Brief History of South American Metatherians. Springer, Heidelberg

Gould SJ (2002) The Structure of Evolutionary Theory. Harvard University Press, Cambridge

Guler MV, Borel CM, Brinkhuis H, Navarro E, Astini R (2014) Brackish to freshwater dinoflagellate cyst assemblages from the La Colonia Formation (Paleocene?), northeastern Patagonia, Argentina. Ameghiniana 51:141-153

Grossnickle DM, Polly PD (2013) Mammal disparity decreases during the Cretaceous angiosperm radiation. Proc R Soc of Lond B 280:20132110

Grossnickle DM, Newham E (2016). Therian mammals experience an ecomorphological radiation during the Late Cretaceous and selective extinction at the K–Pg boundary. Proc R Soc Lond B 283: 20160256

Halliday TJD, Goswami A (2016) Eutherian morphological disparity across the end-Cretaceous mass extinction. Biol J Linn Soc 118:152-168

Hershkovitz P (1971) Basic crown patterns and cusp homologies of mammalian teeth. In: Dahlberg AA (ed) Dental Morphology and Evolution. University of Chicago Press, Chicago, pp 95-150

Huelsenbeck JP, Ronquist F (2001) MRBAYES: Bayesian inference of phylogeny. Bioinformatics 17:754-755

Hugo CA, Leanza HA (2001) Hoja geológica 3969-IV, general roca. Provincias de Río Negro y Neuquén. Boletín Servicio Geológico Minero Argentino, Instituto de Geología y Recursos Minerales 308:1-65

Hunter JP, Jernvall J (1995) The hypocone as a key innovation in mammalian evolution. Proc Natl Acad Sci USA 92:10718-10722

Janis CM (1990) The correlation between diet and dental wear in herbivorous mammals, and its relationship to the determination of diets of extinct species. In: Boucot AJ (ed) Paleobiological Evidence for Rates of Coevolution and Behavioral Evolution. Elsevier, New York, pp 241-259

Jernvall J, Hunter JP, Fortelius M (1996) Molar tooth diversity, disparity, and ecology in Cenozoic ungulate radiations. Science 274:1489-1492

Kay RF, Hiiemae KM (1974) Jaw movement and tooth use in recent and fossil primates. Am J Phys Anthropol 40:227-256

Kielan-Jaworowska Z, Cifelli RL, Luo ZX (2004) Mammals from The Age of Dinosaurs: Origins, Evolution, and Structure. Columbia University Press, New York

Lester KS, Koenigswald W von (1989) Crystallite orientation discontinuities and the evolution of mammalian enamel--or, when is a prism? Scanning microscopy 3:645-662

Lewis PO (2001) A likelihood approach to estimating phylogeny from discrete morphological character data. Syst Biol 50:913-925.

Lopatin A, Averianov AO (2007) *Kielantherium*, a basal tribosphenic mammal from the Early Cretaceous of Mongolia, with new data on the aegialodontian dentition. Acta Palaeontol Pol 52:441-446

Lucas PW (2004) Dental Functional Morphology: How Teeth Work. Cambridge University Press, Cambridge

Luckett WP (1993) An ontogenetic assessment of dental homologies in therian mammals. In: Szalay FS, Novacek MJ, McKenna MC (eds) Mammal Phylogeny: Mesozoic Differentiation, Multituberculates, Monotremes, Early Therians, and Marsupials. Springer, New York, pp 182-204

Luo ZX, Martin T (2007) Analysis of molar structure and phylogeny of docodont genera. Bull Carnegie Mus Natural Hist 39:27-47

Malumián N, Caramés A (1995) El Daniano marino de Patagonia (Argentina): Paleobiogeografía de los foraminíferos bentónicos. In: Náñez C (ed) Paleógeno de América del Sur. Asociación Paleontológica Argentina, Publicación Especial 3, Buenos Aires, pp 83-105

Martin T, Goin, F, Chornogubsky L, Gelfo J, Shultz J (2013) Early Late Cretaceous (Cenomanian) Mammals and other vertebrates from the Mata Amarilla Formation of southern Patagonia (Argentina). Soc Vertebr Paleontol Annual Meeting Abstracts

McDowell SB (1958) The Greater Antillean insectivores. Bull Am Mus Nat Hist 115:113-214

McKenna MC (1975) Toward a phylogenetic classification of the Mammalia. In: Luckett, WP, Szalay FS (eds) Phylogeny of the Primates. Plenum Press, New York, pp 21-46

Mills JRE (1964) The dentitions of *Peramus* and *Amphitherium*. Proc Linn Soc Lond 175:117-133

Moore WJ (1981) The Mammalian Skull. Cambridge University Press, Cambridge

O´Gorman JP, Salgado L, Varela J, Parras A (2013) Elasmosaurs (Sauropterygia, Plesiosauria) from La Colonia Formation (Campanian-Maastrichtian), Argentina. Alcheringa 37:259-267

Paez-Arango N (2008) Dental and craniomandibular anatomy of *Peligrotherium tropicalis*: the evolutionary radiation of South American dryolestoid mammals. Dissertation, University of Louisville

Page R, Ardolino A, de Barrio RE, Franchi M, Lizuain A, Page S, Silva Nieto D (1999) Estratigrafía del Jurásico y Cretácico del Macizo de Somún Curá, provincias de Río Negro y Chubut. In: Caminos R (ed) Geología Argentina. Servicio Geológico Minero Argentino SEGEMAR Anales 29, Buenos Aires, pp 460–488

Pampush JD, Winchester JM, Morse PE, Vining AQ, Boyer DM, Kay RF (2016) Introducing molaR: a new R package for quantitative topographic analysis of teeth (and other topographic surfaces). J Mammal Evol 23:397-412

Pascual R, Goin FJ, González P, Ardolino A, Puerta PF (2000) A highly derived docodont from the Patagonian Late Cretaceous: evolutionary implications for Gondwanan mammals. Geodiversitas 22:395–414

Patterson B (1956) Early Cretaceous mammals and the evolution of mammalian molar teeth. Fieldiana Geol 13:1-105

Pesce AH (1979) Estratigrafía del arroyo Perdido en su tramo medio e inferior provincia del Chubut. VII Congreso Geológico Argentino (Neuquén, 1978), Actas 1:315–333

Prasad GVR, Manhas BK (2001) First docodont mammals of Laurasian affinities from India. Curr Sci 81:1235-1238

Prasad, GVR, Manhas BK (2007) A new docodont mammal from the Jurassic Kota Formation of India. Palaeontol Electronica 11:1-11

Prothero, DR (1981) New Jurassic mammals from Como Bluff, Wyoming, and the interrelationships of non-tribosphenic Theria. Bull Am Mus Nat Hist 167:277-326

Rensberger JM (1973) An occlusal model for mastication and dental wear in herbivorous mammals. J Paleontol 47:515-528

Riccardi AC (1987) Cretaceous paleogeography of southern South America. Palaeogeogr, Palaeoclimatol, Palaeocol 59:169-195

Ronquist F, Teslenko M, van der Mark P, Ayres D, Darling A, Höhna S, Larget B, Liu L, Suchard MA, Huelsenbeck JP (2012) MrBayes 3.2: efficient Bayesian phylogenetic inference and model choice across a large model space. Syst Biol 61:539-542

Rose KD (2006) The Beginning of The Age of Mammals. Johns Hopkins University Press, Baltimore

Rougier GW, S Apesteguía (2004) The Mesozoic radiation of dryolestoids in South America: dental and cranial evidence. J Vertebr Paleontol 24 (Suppl to No 3):106A

Rougier GW, Apesteguía S, Gaetano LC (2011) Highly specialized mammalian skulls from the Late Cretaceous of South America. Nature 479:98-102

Rougier GW, Chornogubsky L, Casadio S, Arango NP, Giallombardo A (2009a) Mammals from the Allen Formation, Late Cretaceous, Argentina. Cret Res 30:223-238

Rougier GW, Forasiepi AM, Hill RV, Novacek M (2009b) New mammalian remains from the Late Cretaceous La Colonia Formation, Patagonia, Argentina. Acta Palaeontol Pol 54:195-212

Rougier GW, Leandro G, Drury BR, Colella R, Gomez RO, Arango NP, Calvo J, Porri J, Gonzalez Riga B, Dos Santos D (2010) A review of the Mesozoic mammalian record of South America. In: Calvo J, Porri J, B. Gonzalez Riga B, Dos Santos D (eds) Paleontologia y dinosaurios desde America Latina. Universidad Nacional de Cuyo, Mendoza, pp 195-214

Rougier GW, Wible JR, Beck RM, Apesteguía S (2012) The Miocene mammal *Necrolestes* demonstrates the survival of a Mesozoic nontherian lineage into the late Cenozoic of South America. Proc Natl Acad Sci USA 109:20053-20058

Schultz JA, T Martin (2011) Wear pattern and functional morphology of dryolestoid molars (Mammalia, Cladotheria). Paläontol Z 85:269-285

Sigé B, Sempere T, Butler RF, Marshall LG, Crochet JY (2004) Age and stratigraphic reassessment of the fossil-bearing Laguna Umayo red mudstone unit, SE Peru, from regional stratigraphy, fossil record, and paleomagnetism. Geobios 37:771-794.

Sigogneau-Russell D (2003) Docodonts from the British Mesozoic. Acta Palaeontol Pol 48:357–374.

Simpson GG (1928) A Catalogue of the Mesozoic Mammalia in the Geological Department of the British Museum. Trustees of the British Museum, London, pp 1-215

Simpson GG (1929) American Mesozoic Mammalia. Mem Peabody Mus 3:1-235

Spradley JP, Pampush JD, Morse PE, Kay RF (2017) Smooth operator: the effects of different 3D mesh retriangulation protocols on the computation of Dirichlet normal energy. Am J Phys Anthropol 163:94-109

Suárez M, Márquez M, De La Cruz R, Navarrete C, Fanning M (2014) Cenomanian-?early Turonian minimum age of the Chubut Group, Argentina: SHRIMP U-Pb geochronology. J So Am Earth Sci 50:67-74

Swofford DL (2002) PAUP* Phylogenetic Analysis Using Parsimony (*and Other Methods) Version 4. Sinauer Associates, Sunderland

Wible JR, Rougier GW (2017) Craniomandibular anatomy of the subterranean meridiolestidan *Necrolestes patagonensis* Ameghino, 1891 (Mammalia, Cladotheria) from the Early Miocene of Patagonia. Ann Carnegie Mus, 84:183-252

Wilf P, NR Cúneo, IH Escapa, D Pol, MO Woodburne (2013) Splendid and seldom isolated: the paleobiogeography of Patagonia. Annu Rev Earth Planet Sci 41:561-603

Wilson GP, Evans AR, Corfe IJ, Smits PD, Fortelius M, Jernvall J (2012) Adaptive radiation of multituberculate mammals before the extinction of dinosaurs. Nature 483:457-460

Wood CB, Rougier GW (2005) Updating and recoding enamel microstructure in Mesozoic mammals: in search of discrete characters for phylogenetic reconstruction. J Mammal Evol 12:433-460

Wood CB, Dumont ER, Crompton AW (1999) New studies of enamel microstructure in Mesozoic mammals: a review of enamel prisms as a mammalian synapomorphy. J Mammal Evol 6:177-213

Woodburne MO, Goin FJ, Bond M, Carlini AA, Gelfo JN, López GM, Inglesias A, Zimicz, AN (2014) Paleogene land mammal faunas of South America; a response to global climatic changes and indigenous floral diversity. J Mammal Evol 21:1-73

Vandebroek G (1961) The comparative anatomy of the teeth of lower and non-specialized mammals. Kon Vlaamse Acad Wetensch Lett Sch Kunsten Belgie 1:1-215

Varela JA, Parras A (2013) Análisis tafonómico de una concentración de vertebrados en la Formación La Colonia (Cretácico Tardío), Chubut, Argentina. Reunión Anual de Comunicaciones de la APA (Córdoba). Ameghiniana 50:74-75

Yardeni J (1942) Facts and fancy in dental morphogenesis. Am J Orthodont Oral Surg 28:725-735

Supplementary Table 1. Listing of new La Colonia specimens described in text

Spec Number	Locality	Description
MPEF-PV 2014	El Uruguayo	Left posterior dentary fragment, with alveoli for m1-3
MPEF-PV 2020	El Uruguayo	Left dentary fragment with alveoli for p3 and p4-m1
MPEF-PV 2072	El Uruguayo	Right P4
MPEF-PV 2237	El Uruguayo	Right m2
MPEF-PV 2238	El Uruguayo	Left M1
MPEF-PV 2317	El Uruguayo	Right m1
MPEF-PV 2337	Anfiteatro 1	Left fragmentary dentary with alveoli for p3-m3
MPEF-PV 2338	Anfiteatro 1	Right dentary fragment with partial alveoli for c1-p2 and p3-m1
MPEF- PV 2339	El Uruguayo	Right P3
MPEF-PV 2341	El Uruguayo	Right M2
MPEF-PV 2343	El Uruguayo	Right M2 or M1
MPEF-PV 2344	El Uruguayo	Right P4
MPEF-PV 2347	Anfiteatro 1	Left lower canine, missing roots
MPEF-PV 2349	Anfiteatro 1	Right upper canine
MPEF-PV 2368	Anfiteatro 1	Right p1
MPEF-PV 2369	Anfiteatro 1	Left fragmentary M3
MPEF-PV 2372	Anfiteatro 1	Left anterior dentary fragment with alveoli for p1, and p2 and mesial half of p3
MPEF-PV 2373	Anfiteatro 1	Right P4

MPEF-PV 2375	Anfiteatro 1	Right upper canine tip
MPEF-PV 2376	Anfiteatro 1	Right p3

Supplementary Table 2. Data for Dental Topographic Analysis (DTA) presented in text. Methods and institutional abbreviations are listed in text. Column "Group" refers to major taxonomic grouping, e.g. Eu = Eutheria, Meta = Metatheria, Mes = Mesungulatoidea

Spec Number	Species	Family	Group	DNE[1]	RI[2]	OPCR[3]
URBAC 04-341	*Kulbeckia kulbecke*	Zalambdalestidae	Eu	205.61	0.66	47.75
URBAC 98-136	*Kulbeckia kulbecke*	Zalambdalestidae	Eu	194.42	0.65	53.75
CCMGE 8-12953	*Kulbeckia Sp.*	Zalambdalestidae	Eu	164.91	0.71	49.12
URBAC 97-004	*Aspanlestes aptap*	Zhelestidae	Eu	157.05	0.65	41.5
URBAC 04-185	*Aspanlestes aptap*	Zhelestidae	Eu	205.07	0.64	59.75
URBAC 03-086	*Aspanlestes aptap*	Zhelestidae	Eu	208.54	0.63	64.5
ZIN C 82582	*Aspanlestes aptap*	Zhelestidae	Eu	144.83	0.57	49.12
URBAC 00-046	*Eoungulatum kudukensis*	Zhelestidae	Eu	141.61	0.56	53
URBAC 98-014	*Parashelestes robustus*	Zhelestidae	Eu	163.43	0.59	54.88
URBAC 02-065	*Zhelestes temirkazyk*	Zhelestidae	Eu	192.27	0.67	57.38
URBAC 98-015	*Zhelestes temirkazyk*	Zhelestidae	Eu	218.21	0.64	59.88

URBAC 04-309	*Zhelestes temirkazyk*	Zhelestidae	Eu	232.91	0.64	67.25
URBAC 06-026	*Zhelestes temirkazyk*	Zhelestidae	Eu	196.03	0.69	61.38
MPEV-PV 2350	*Peligrotherium tropicalis*	Peligrotheriidae	Mes	221.06	0.46	96.25
MPEF-PV 2237	*Reigitherium Sp.*	Reigitheriidae	Mes	215.42	0.40	105.25
MNRJ 2492-v	*Epidolops ameghinoi*	Bonapartheriidae	Meta	105.36	0.46	58.25
MACN 10348	*Caroloameghinia Sp.*	Caroloameghiniidae	Meta	238.52	0.56	76.38
FMNH P13160	*Acdestis oweni*	Palaeothentidae	Meta	186.52	0.43	86.62
MACN 8293	*Palaeothentes*	Palaeothentidae	Meta	261.21	0.38	126
MACN 10334	*Eudolops caroliameghinoi*	Polydolopidae	Meta	260.66	0.50	89.25
MLP 11-122	*Polydolops rothi*	Polydolopidae	Meta	121.76	0.48	44.38
AMNH 28434	*Polydolops thomasi*	Polydolopidae	Meta	153.09	0.43	71.12
HNHNVIL 100	*Roberthoffstetteria nationalgeographica*	Sillustaniidae	Meta	160.23	0.54	82.38

1 DNE (Diriclet Normal Energy) values calculated with Boundary Values = "Vertex" as recommendd by Spradley et al. 2017

2 RI (Relief Index) calculated with parameter Alpha = 0.5

3 OPCR (Orientation Patch Count Rotated) calculated using 8 bins

#NEXUS

[Supplementary Tables for "New specimens of the enigmatic fossil mammal Reigitherium (Meridiolestida, Mesungulatoidea) from the Late Cretaceous of Patagonia, Argentina: morphology and natural history".

Characters 1-38 are taken from the specified character in the larger matrix of Rougier et al. 2012, with an asterix indicating that a character has been updated based on the new La Colonia Reigitherium sample. The following MrBayes block shows the commands used to produce the phylogeny shown in Figure 18b. The Maximum Parsimony analysis shown in Figure 18a was conducted using an exhaustive search.]

```
BEGIN TAXA;
        DIMENSIONS NTAX=10;
        TAXLABELS
                Henkelotherium Dryolestes Laolestes Groebertherium Cronopio
Leonardus Mesungulatum Coloniatherium Peligrotherium Reigitherium
        ;
END;
BEGIN CHARACTERS;
        DIMENSIONS  NCHAR=44;
        FORMAT DATATYPE = STANDARD GAP = - MISSING = ? SYMBOLS =
"  0 1 2 3";
        CHARSTATELABELS
                1 '40* - Total Number of Premolars: 0 two or fewer, 1 three, 2 four, 3
five or more', 2 '42 - Penultimate Lower Premolar size: 0 small and subequal to other
```

premolars, 1 Larger than any other premolar and/or longer, 2 Hypertrophied main tooth in series', 3 '48* - Last Lower Premolar outline: 0 laterally compressed Longer than wide, 1 Transversely wideened only sligltly longer than wide or wider than long ', 4 '49 - Last lower Premolar SIze: 0 small and subequal to other premolars, 1 Large aller or subequal to molars, 2 hypertrophied largest tooth', 5 '55* - Number of lower Molars: 0 two molars, 1 three molars, 2 four or five molars, 3 six or more', 6 '73 - Mesial Transverse Cingulid: 0 Absent, 1 present as a continous shelf below trigonid but without occlusal function, 2 present, having occlusal contace with uppers', 7 '75 - Postcingulid: 0 Absent, 1 Present oblique and connected to usp d, 2 Present horizontal above gum level', 8 '78* - Orientation of paracristid relative to longitudinal axis of molars: 0 Logitudinally oriented, 1 oblique, 2 Nearly transverse', 9 '79* Paraconid presence: 0 present, 1 absent', 10 '82 - Proximity between paraconid and metaconid: 0 bases widely separated, 1 Bases approximated or confluent, 2 single cusp (amphyconid)', 11 '106* - Central crest (Medianergrat) in upper molariformes: 0 absent, 1 present', 12 '108* - Crown length/width ratio in lower molariformes: 0 crown longer than wide, 1 lenth width subequal, 2 crown wider than long', 13 '120* - Metacristid(protocristid) orientation on molars: 0 paralell to tooth row, 1 oblique, 2 transverse', 14 '125 - Position of Stylocone in Molars: 0 along buccal margin, 1 separated', 15 '126 - Stylocone relationship in triangular teeth: 0 stylocone connected to preparacrista or mesial to its end, 1 stylocone distal to labial ending of preparacrista, 2 stylocone detached of preparacrista and occupying central position on crown', 16 '128 - Parastylar hook in upper molars: 0 absent or weak, 1 present', 17 '129* - Paracone orientation: 0 erect, 1 recumbent', 18 '130 - Metacone(or cusp C): 0 present, 1 absent', 19 '132 - Accessory cuspules on upper molars: 0 absent, 1 present',

20 '135 - Number of lower molariform roots: 0 one root, 1 two roots, 2 three or more', 21 '136* - Size of lower molar roots: 0 subequal, 1 posterior root smaller, 2 single root, 3 anterior root smaller', 22 '140* - trigonid major axis orientation: 0 labial, 1 mesial, 2 sharply distal', 23 '142 - Precngulum on molars: 0 absent, 1 present', 24 '143 - Postcingulum on upper molars: 0 absent, 1 present', 25 '144 - Cingula/id height: 0 absent or little differentiated, 1 Close to crown base, 2 Evevated reacing occlusal surace', 26 '146 - Number of upper molariform roots: 0 one root, 1 two roots, 2 three, 3 more than three', 27 '148 - Supernumerary roots on penultimate upper premolar: 0 absen, 1 present', 28 '149 - Supernumary roots on penultimate lower premolar: 0 absent , 1 present', 29 '150* - Supernumerary roots on ultimate lower premolar: 0 absent, 1 present', 30 '151* - Supernumerary roots on ultimate upper premolar: 0 absen, 1 present', 31 '152* - Penultimate lower premolar distal root: 0 subequal to mesial root, 1 elongate root', 32 '153* - Lower molar interdental contact: 0 lowers contact somewhere along mesial and distal margins, 1 lower molars separated by interdental spaces', 33 '154* - Upper molar contact: 0 upper molars extensively contact each other, 1 upper molars do not contact each other or barely do', 34 '5* - Meckles groove: 0 weak or vestigeal, 1 absent', 35 '12 - Coronoid bone or its attachment scar: 0 present, 1 absent', 36 '17* - Ventral border of masseteric fossa: 0 present as a low and broad crest, 1 present as a well-defined and thin crest', 37 '18* - Position of mandibual foramen: 0 near base of anterior border of coronoid process, 1 posterior to the anterior edge of coronoid process', 38 '28 - Retromolar space: 0 absent, 1 present', 39 'NEW Presence of labial cuspulids on lower molars: 0 absent, 1 present', 40 'NEW primary trigon and talonid crests: 0 sharp and continous, 1 low and intermittent', 41 'NEW Capacity for embrasure shearing during mastication in

molar dentition: 0 present, 1 none or vestigeal', 42 'NEW Precingulid: 0 absent, 1 small and lingually placed, 2 reaches labial margin of trigonid', 43 'NEW Postcingulid/Talonid: 0 trenchant unicuspid talonid, 1 labiolingually extenden almost as wide as trigonid', 44 'NEW Metastyle located on discrete projeting lobe in moars: 0 present, 1 metastyle not on discrete lobe' ;

MATRIX

Henkelotherium 1001300100002000100100001200000001010000000 0

Dryolestes 2001300100022010100110001200000001010000000 0

Laolestes 2001300100122111100111001200000001010000000 0

Groebertherium ?????11100(0 1)2202111011?0112????0???????000100

Cronopio 2101100201022000110021000000001112110100000 1

Leonardus (1 2)111(1 2)00201121120010(1 2)31000100001112????000??1

Mesungulatum ?2?21221011111201101001112???11002????000211

Coloniatherium 12121221011111201101001112 11?0?0021011000211

Peligrotherium 12121221011221201111001122111100021011111211

Reigitherium 2111122212(0 1)22120011110112 2?1??0??21?11111211

;

END;

begin mrbayes;

ctype unordered: all ;

lset parsmodel=no coding=variable rates=gamma ngammacat=4;

mcmcp ngen=1000000 printfreq=10000 samplefreq=1000 nchains=4 savebrlens=yes;

end;

Chapter 2: Petrosal morphology and cochlear function in Mesozoic stem therians

Abstract

Here we describe the bony anatomy of the inner ear and surrounding structures seen in three plesiomorphic crown mammalian petrosal specimens. Our study sample includes the triconodont *Priacodon fruitaensis* from the Upper Jurassic of North America, and two isolated stem therian petrosal specimens colloquially known as the Höövör petrosals, recovered from Aptian-Albian sediments in Mongolia. The second Höövör petrosal is here described at length for the first time. All three of these petrosals and a comparative sample of extant mammalian taxa have been imaged using micro-CT, allowing for detailed anatomical descriptions of the osteological correlates of functionally significant neurovascular features, especially along the abneural wall of the cochlear canal. The high resolution imaging provided here clarifies several hypotheses regarding the mosaic evolution of features of the cochlear endocast in early mammals. In particular, these images demonstrate that the membranous cochlear duct adhered to the bony cochlear canal abneurally to a secondary bony lamina before the appearance of an opposing primary bony lamina or tractus foraminosus. Additionally, while corroborating the general trend of reduction of venous sinuses and plexuses within the pars cochlearis seen in crownward mammaliaforms generally, the Höövör petrosals show the localized enlargement of a portion of the intrapetrosal venous plexus. This new vascular feature is here interpreted as the bony accommodation for the vein of cochlear aqueduct, a structure that is solely, or predominantly, responsible for the venous drainage of the cochlear apparatus in extant therians. Given that our fossil stem therian inner ear specimens appear to have very limited high-frequency capabilities, the development of these modern vascular features of the cochlear endocast suggest that neither the initiation or enlargement of the stria vascularis (a unique mammalian organ) was

originally associated with the capacity for high-frequency hearing or precise sound-source localization.

Introduction

Therian mammals (the last common ancestor of marsupials and placentals and its descendants [1]) today display an impressive variety of auditory characteristics facilitating the adept detection of airborne sound, making this group arguably the most acoustically sophisticated and diverse clade of terrestrial vertebrates [2]. The widespread capacity for high-acuity hearing (in terms of sensitivity, specificity, and highest detectable frequency) among the majority of extant therian mammals has reinforced the assumption among neontologists that the Mesozoic members of the therian stem linage were stereotypically nocturnal forms that leveraged their auditory faculties to locate small prey and escape gigantic predators (i.e. [3]). However, this supposition has not been supported by the known fossil record of stem therians, with prior descriptions [4-9] demonstrating that these forms lacked the level of petrosal organization characterizing plesiomorphic marsupials [10], afrotheres [11], eulipotyphlans, and primatomorphs [12]. Additionally, many of these older reports lacked CT imaging, reliying heavily on the description of the external morphology of the ear region. Therefore, much of the anatomical detail informing the performance and/or physiological evolution of the inner ear remained understandably inaccessible.

Conversely, several biomechanical/experimental studies on auditory anatomy and physiology across extant tetrapods [2, 13-16] highlight the unique nature of the therian cochlear apparatus (with its well-ordered acoustic hair-cell populations arrayed along the organ of Corti, high endolymphatic potential, and absence of the lagenar macula), as well as the plesiomorphic nature of the monotreme cochlea with respect to many modern and fossil

therians [17,18]. The complete loss of the lagenar macula in particular has been posited as an adaptive breakthrough that permitted later elongation and sophistication of the cochlear apparatus for non-linear amplification of high-frequency stimuli [19]. The plesiomorphic retention of a functional lagenar macula, along with its accompanying otoconial and neurovascular structures, in the monotreme and sauropsid lineages is also physiologically incompatible with several soft tissue adaptations seen in modern therians. These "therian" features include: 1) the exclusive reliance on the stria vascularis as the major endolymph producing organ, 2) the well-developed electromotility of prestins and other molecular components of the "cochlear amplifier", and 3) the radical elongation and geometrical reorganization of the cochlear sensory epithelium. The accumulation of these characteristics among therian ancestors points to a fundamental transformation of the cochlear apparatus somewhere near the origin of Theria [19].

The lack of detailed cochlear reconstructions for Mesozoic fossils is understandable given the general lack of high-fidelity bony correlates for key soft tissue structures such as the cochlear duct, lagenar macula, and stria vascularis. This report uses high-resolution micro-CT information to update descriptions of petrosal anatomy provided in the representative sample of stem therians focused on by [4] and [5], two large-scale studies characterizing the fossil record of early mammalian petrosal evolution (Fig 1). These images and reconstructions are framed within a broader comparative and functional setting of modern mammalian auditory physiology, and morphology with the hope of bridging both fields which, due to the steep learning curves involved, have had only limited cross-referencing. The new high-resolution images presented here allow the first descriptions of the labyrinthine anatomy in some of the most morphologically plesiomorphic petrosal regions known in the crown mammalian fossil record. The three specimens focused on here

include the relatively well-known triconodontid *Priacodon fruitaensis* and the two isolated petrosal specimens known as the Höövör petrosals. The second Höövör petrosal (Fig 1 a, b) has not been fully described or figured, and has only been cursorily referred to in [4] and briefly discussed in [5]. We regard this second petrosal as taxonomically distinct from that of the previously described petrosal in [4], and therefore provide here a complete description and assessment of this specimen.

Fig 1. Stem therian petrosal specimens described in this report. a, b Höövör Petrosal 2 (H2; PSS-MAE-119); c, d, Höövör Petrosal 1 (H1; PSS-MAE-104); e,f left petrosal of *Priacodon fruitaensis* (LACM 120451). a, c, e in ventral view; b, d, f in dorsomedial view. Scale bar is 1 mm.

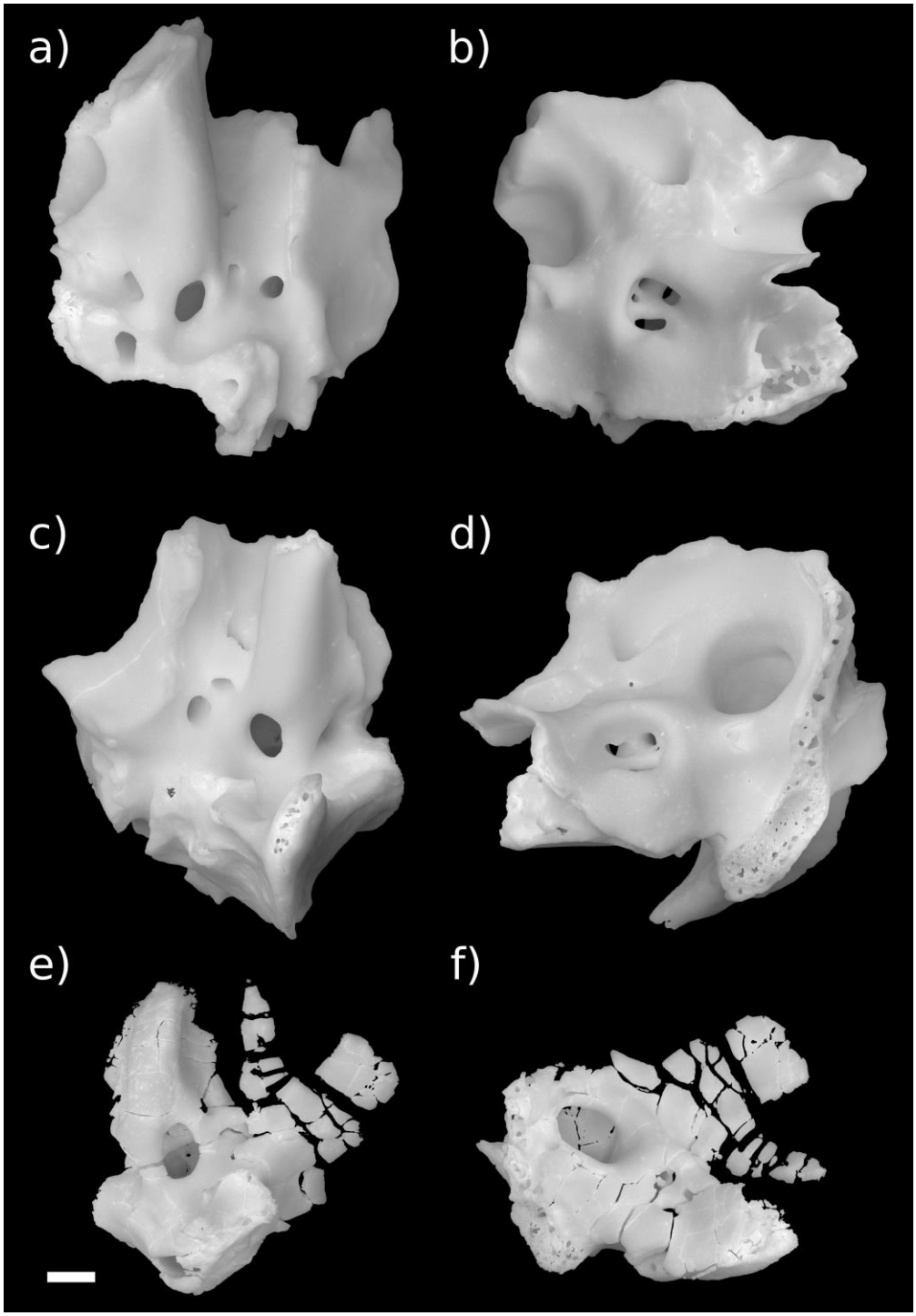

The novel information presented here does little to overturn previous taxonomic arrangements of these stem therians because they only slightly change their scorings in previous matrices [5]; and because most details of inner ear anatomy is yet to be distilled into characters/character states to be used in a phylogenetic estimation (Fig 2). However, the new anatomical representation provided by the images used here demonstrate the presence of a combination of plesiomorphic and derived character states of the cochlear canal that support their shared ancestry with crown therian mammals. In particular, the presence of a secondary lamina, and in the Höövör petrosals, the earliest reported appearance of the vein of the cochlear aqueduct (the main venous drainage for the cochlear apparatus in therian mammals today). For reasons outlined in the discussion section, these osteological features are most likely associated with the elaboration of the macromechanical form of tuning, a unique cochlear functionality that provides the majority of modern therian mammals ultrasonic frequency sensitivity. However, because of the plesiomorphic dimensions of the cochlear canal seen in our specimens, the ability to detect mid-range to high frequencies was likely at most only incipiently developed in these stem therians. The osteological evidence provided here therefore suggests that many of the unique features of therian cochlear blood supply, histology and physiology evolved gradually after their split from the lineage leading to monotremes, and that these features originally functioned in service of highly sensitive and selective low-frequency hearing.

Fig 2. Simplified Phylogeny of Mammalia. Example phylogeny showing phylogenetic locations of the stem therian petrosals described here. Toplogy simplified from Rescaled Consistency Index PAUP analysis presented in [5].

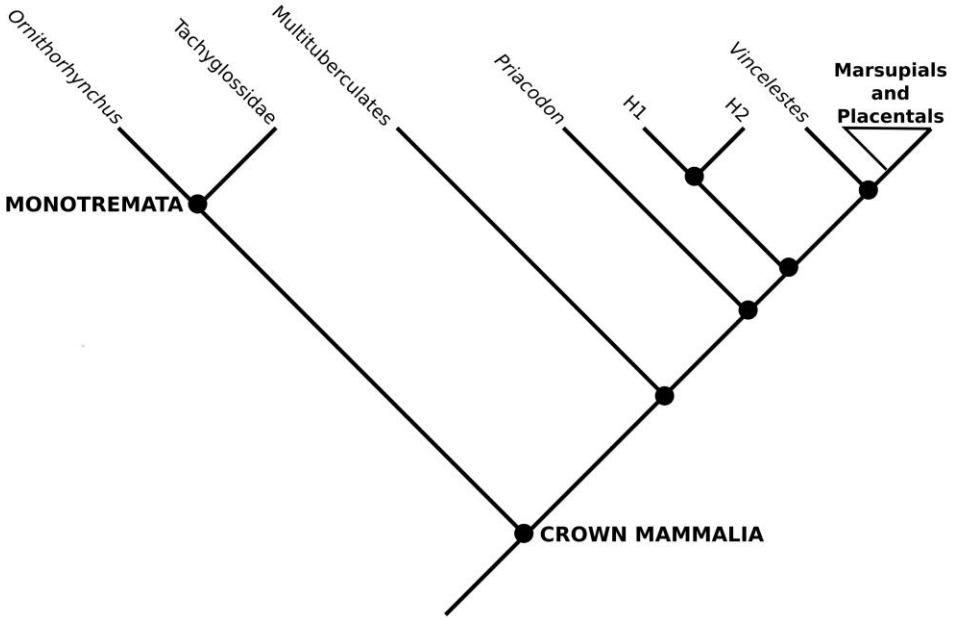

Materials and methods

Anatomical images produced for this report were generated from manual segmentations of high resolution (~9 μm voxel size) CT stacks shot using a Nikon XTH 225 ST Scanner housed at Duke University's Shared Materials Instrumentation Facility (SMIF). Labeled volumes of petrosal bones and their associated endocasts were converted into triangular mesh surfaces using the "Generate Surface" module in Amira. These surfaces were subsequently edited to contain 1-4 million topologically closed, manifold faces. Final images were rendered using these surfaces and the "cycles" shader in the free graphics program Blender.

In referring to *Priacodon fruitaensis*, the taxa represented by the Höövör petrosals, or other fossil taxa as stem therians, we are emphasizing their phylogenetic position as fossil taxa with more recent common ancestry to the extant clade Theria than any other living non-therian taxon (such as monotremes, and non-mammals). This matches the usage of the term "stem" seen in [5] and in phylogenetic discussions generally.

Osteological nomenclature used in the following descriptions of petrosal morphology are taken primarily from [20-22]. Terms specific to the description of labyrinthine endocasts are also taken from [23,24] for therian mammals; and [25] and [18] for non-mammals and monotremes, respectively. Nomenclature for cranial vasculature is taken from [12, 26-30].

Anatomical abbreviations used in figures and text:

ac – aqueductus cochleae (for perilymphatic duct)
acf – aperture of cochlear fossula (external to fenestra cochleae)
adm – arteria diploëtica magna
al – anterior lamina

amp-a – anterior semicircular canal ampulla
amp-h – horizontal semicircular canal ampulla
amp-p – posterior semicircular canal ampulla
av – aqueductus vestibuli (for endolymphatic duct)
bpsal – border of periosteal surface of anterior lamina
bs – basisphenoid sutural surface
cas – cavum supracochleare
cc-p – primary common crus
cc-s – secondary common crus
cdh – centripetal diverticulum of horizontal semicircular canal
ce – cavum epiptericum
ci – crista interfenestralis
cVIII – cochlear branch of vestibulocochlear nerve
coc – cochlear canal
dag – dorsal ascending groove
eapc – endocranial aperture of prootic canal
ect – ectotympanic bone
eps-p – posterior epicochlear sinus ("trans-cochlear sinus p" in [31])
fac – facial canal (aqueductus Fallopii in [32])
fc – fenestra cochleae (for secondary tympanic membrane)
fcn – foramen for cochlear nerve
fs – fenestra semilunaris
fv – fenestra vestibuli (fenestra ovalis)
gpn – greater petrosal nerve
hF – hiatus Fallopii (for greater petrosal nerve)
hfn – hyomandibular branch of facial nerve
hps – hypocochlear sinus
hs – half-pipe shaped sulcus
iam – internal acoustic meatus
ips – inferior petrosal sinus
ijv – internal jugular vein
ir – inferior ramus of stapedial artery
jn – jugular notch
lf – lateral flange
lhv – lateral head vein
li – lagenar inflation
mm – manubrium of malleus
ntr-a – notch for temporal ramus a
ntr-b – notch for temporal ramus b
pcs – sinus around prootic canal
pf – perilymphatic foramen
pfc – prefacial commissure (suprafacial commisure)
pop – paroccipital process
pos – paroccipital sinus
pov – prootic vein
pptc – petrosal contribution to post-temporal canal
?ptv – possible location of post-trigeminal vein
re – recessus ellipticus (for utricle)

rpm – rostral (anterior) process of malleus (= goniale/ prearticular)
rs – recessus sphericus (for saccule)
rso – ramus supraorbitalis
ssc-a – anterior semicircular canal
sa – stapedial artery
saf – subarcuate fossa
sas – subarcuate venous sinus
sl – secondary (abneural) bony lamina of cochlear canal
sf – stapedius fossa
sff – secondary facial foramen
sm – sulcus medial to promontorium
sr – superior ramus of stapedial artery
tapc – tympanic aperture of prootic canal
tf – tractus foraminosus
tph – tympanohyal
tr-a – anterior temporal ramus
tr-b – posterior temporal ramus
uaf – foramen for utriculoampullar branch of vestibular nerve
vag – ventral ascending groove
VII – facial nerve
vVIII – vestibular branch of vestibulocochlear nerve
vcaq - canal for vein of the cochlear aqueduct (Canal of Cotugno)

Other abbreviations taken from [33], and [16]:

H1 - Höövör petrosal specimen 1 (PSS-MAE-104)
H2 - Höövör petrosal specimen 2 (PSS-MAE-119)
IHC – inner hair cell
OHC – outer hair cell
SC – cochlear space constant (in octaves/ mm)
ILD – interaural level difference
ITD – interaural time difference
FHS – functional head size (in microseconds)

The Aptian or Albian Höövör locality ([34] following spelling conventions of [35-36], but also transliterated Khoobur, Khobur, Khoboor, Khovboor, with varying diacritical marks) in Guchin-Us District, Mongolia has yielded an abundant sample of mammalian dental specimens (e.g. [37-42]) and three isolated petrosal specimens: an early stem therian termed "Höövör petrosal 1" (Fig 1 c, d, PSS-MAE-104; [4]), a crown therian petrosal referred to the eutherian taxon *Prokennalestes trofimovi* (PSS-MAE-106; [37]), and an undescribed (but previously phylogenetically scored) specimen termed "Höövör petrosal 2" (Fig 1 a, b, PSS-

MAE-119) that is described below. Höövör petrosals 1 and 2 are referred to as Khoobur petrosals 1 and 2 in [4,5].

One of the most plesiomorphic mammals known from petrosal remains is *Priacodon fruitaensis* (Fig 1 e, f; [5, 43]) from the Upper Jurassic (Kimmeridgian) microfossil locality at Fruita Paleontological Area, Mesa County, Colorado [44-45]. The specimen of *Priacodon fruitaensis* figured and described here (LACM 120451) is the left periotic region figured in [5], that was found in association with a fragmentary left exoccipital and other cranial elements. To facilitate the following discussion, the generic term *Priacodon* will refer specifically only to *Priacodon fruitaensis*. Also, the contractions H1 and H2 will be used to signify PSS-MAE-104 and PSS-MAE-119, respectively.

All permits for collecting and export of the Höövör specimens temporarily stored at the Collections of the American Museum of Natural History (AMNH), New York, were obtained as part of the on-going collaborative project between the AMNH and The Mongolian Academy of Sciences. The petrosals and associated remains of *Priacodon* are accessioned at the Los Angeles County Museum of Natural History.

As mentioned in [46], the description of isolated petrosal fossils from taxa insufficiently known from cranial remains often precludes the use of precise global anatomical directional terms. This report attempts to describe petrosal remains using a "local" directional system, whereby "anterior" or "rostral" is used to signify the authors' best estimate of the direction corresponding to the anterior direction in a complete skull. In the petrosals described here, "anterior" therefore signifies the direction toward the lateral side of the tip of the petrosal promontorium furthest away from the fenestra ovalis, and toward the presumed location of the alisphenoid and entopterygoid bones. The term "posterior" or "caudal" is therefore used to refer to the opposite direction; whereas "medial" and "lateral"

are used to refer to the directions perpendicular to the anteroposterior axis, toward the internal and external surface of the skull, respectively. Since the dorsoventral axis is much less ambiguous in these remains, no special definition is needed. These directional terms are chosen to reflect our presumption that the long axis of the promontorium is oriented approximately 45° towards the midsagittal plane, as seen in many Mesozoic mammalian petrosals that have been preserved in situ [27, 47].

Finally, novel abbreviations are used here for large-scale middle-ear character states seen in early mammals. These are "Detached Middle Ear" (DME), "Partially Detached Middle Ear" (PDME), and "Mandibular Middle Ear" (MME), referring to the adult condition of having a completely independent auditory apparatus and mandible, a primarily cartilaginous connection between the malleus and dentary, and a completely integrated jaw and ossicular chain, respectively. This terminology is meant to substitute for the less descriptive terms used by ([48-50], inter alios) that were defined with implicit taxonomic content. These terms: "Definitive Mammalian Middle Ear" (DMME), "Partial Mammalian Middle Ear" (PMME), Transitional Mammalian Middle Ear (TMME), and "Mandibular Middle ear of Cynodonts" (MMEC), are undesirable for the following discussion because of their assumed (and likely incorrect) application to members of the clades mentioned in their name. For instance, the term Definitive Mammalian Middle Ear suggests that this character state can be shown to be apomorphic for the crown mammalian common ancestor, and therefore unites the sister lineages leading to modern monotremes and therians; however, the DMME is neither definitive (under most hypotheses of the relationships of early mammals), nor is it diagnostic of Mammalia as a clade, making it not only incorrect but pernicious. The terms DME, PDME, and MME have under most current phylogenetic hypotheses of Mesozoic mammal relationships a congruent distribution (i.e they are extensively identical)

as DMME, PMME, and MMEC (respectively), but are defined solely on observable anatomical features of the ear and jaw which will remain unaffected by changing tree topologies. This nomenclature allows the following text to more clearly differentiate the anatomical and phylogenetic composition of varying sets of synapsid taxa, especially in the discussion section and Supplementary Material 1.

Results

External anatomy of the second Höövör petrosal

The petrosal [21,27,51,52] can be envisaged as a generally tetrahedral structure with four major surfaces: tympanic (Fig 3 a, b), cerebellar (Fig 3 c, d), squamosal (Fig 4 a, b) and mastoid. The petrosal itself is composed of two conceptual components, the pars canalicularis (containing the utricle and semicircular ducts) dorsoposteriorly, and the pars cochlearis (containing the saccule and cochlear duct) anteroventrally [12,53]. The tympanic surface is most apparent in ventral view and contains structures associated with the suspension of the ossicular chain, the fenestra cochleae, and foramina supporting the distribution of neurovascular structures. The topography of this region is defined mainly by the promontorium and lateral trough anteriorly, and an expanded post-promontorial region posteriorly. The cerebellar surface of the petrosal has several excavations, that accommodate central and peripheral nervous structures and vasculature. These include the internal acoustic meatus anteromedially, the subarcuate fossa (only the anterior half having been preserved in H2) posteromedially, a depression for the trigeminal ganglion (=semilunar/gasserian

ganglion) anterolaterally, and the endocranial aperture of the prootic canal posteriolaterally running along the edge of the subarcuate fossa. The laterally facing squamosal surface, and the caudally facing mastoid surface (poorly preserved in H2) are both rugose because of their complex sutural interdigitations with surrounding bones (most probably the squamosal and exoccipital), and canals transmitting ramifications of the diploëtic and stapedial vessels. The anterior and medial margins of the petrosal are formed by exposed cancellous bone and the intramural inferior petrosal sinus which governs the topography here (Fig 4 c, d).

Fig 3. Renderings of Höövör 2 petrosal. a, b ventral view; c, d endocranial view. b, d showing partial labyrinthine endocast in teal and circumpromontorial venous plexus in blue. **A**, anterior; **L**, lateral. Numerical abbreviations: 1, primary facial foramen; 2, foramen for utriculoampullar branch of vestibular nerve; 3, foramen for sacculoampullar branch of vestibular nerve; 4, foramen for cochlear nerve. Scale bars are 1 mm. Asterisk marks location of small foramen which was interpreted by [4] as the tympanic aperture of the cochlear aqueduct. Refer to list of abbreviations in text for other abbreviations.

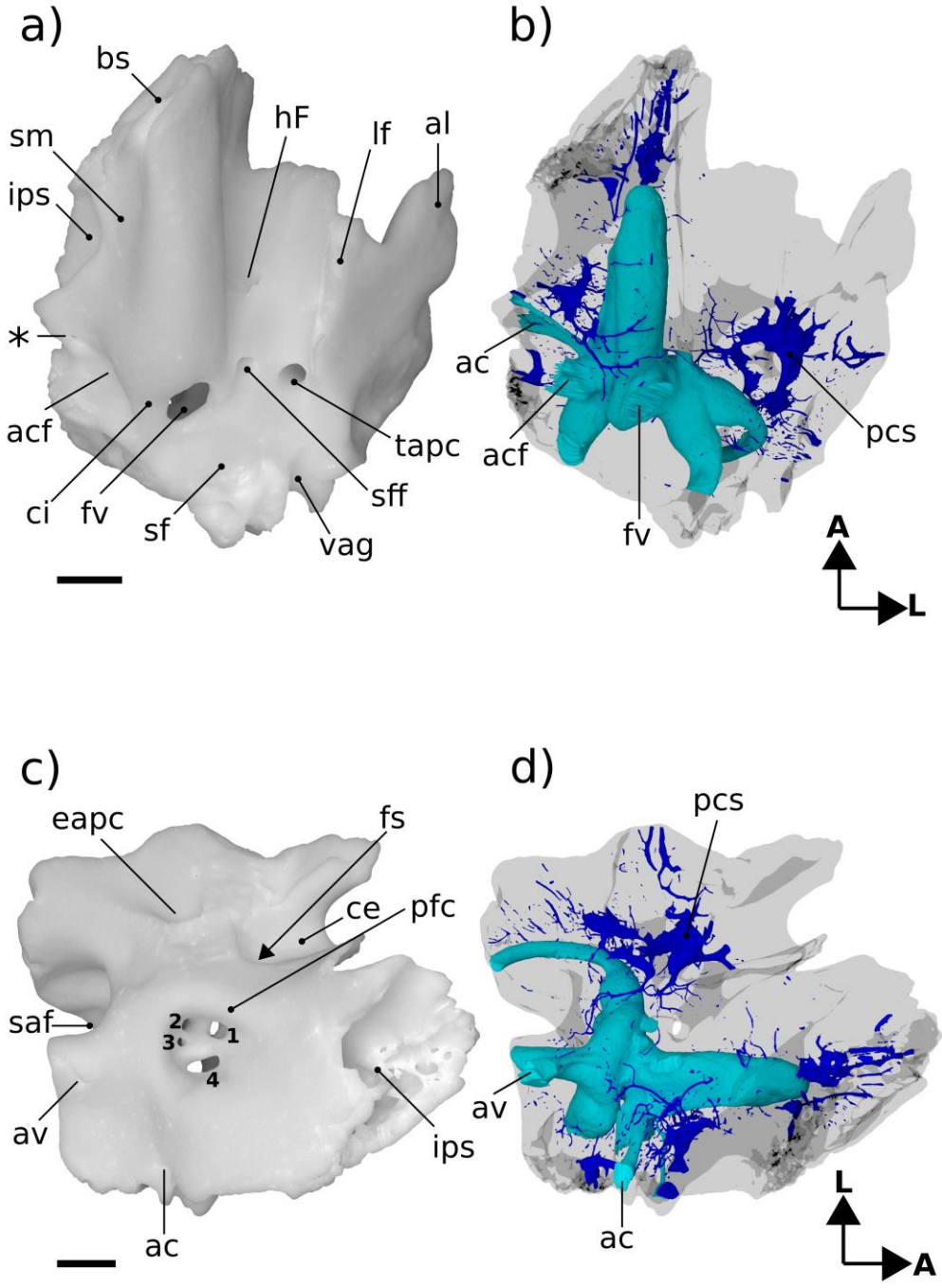
a)
bs
sm
ips
hF
lf
al
*
acf
ci
fv
sf
vag
sff
tapc
b)
ac
acf
fv
pcs
A
L
c)
eapc
fs
ce
pfc
saf
2
3
1
4
av
ac
ips
d)
pcs
av
ac
L
A

Figure 4. Renderings of Höövör 2 petrosal. a, b lateral view; c, d medial view. b, d showing partial labyrinthine endocast in teal and circumpromontorial venous plexus in blue. Scale bars are 1 mm. **A**, anterior; **D**, dorsal. Refer to list of abbreviations in text for other abbreviations.

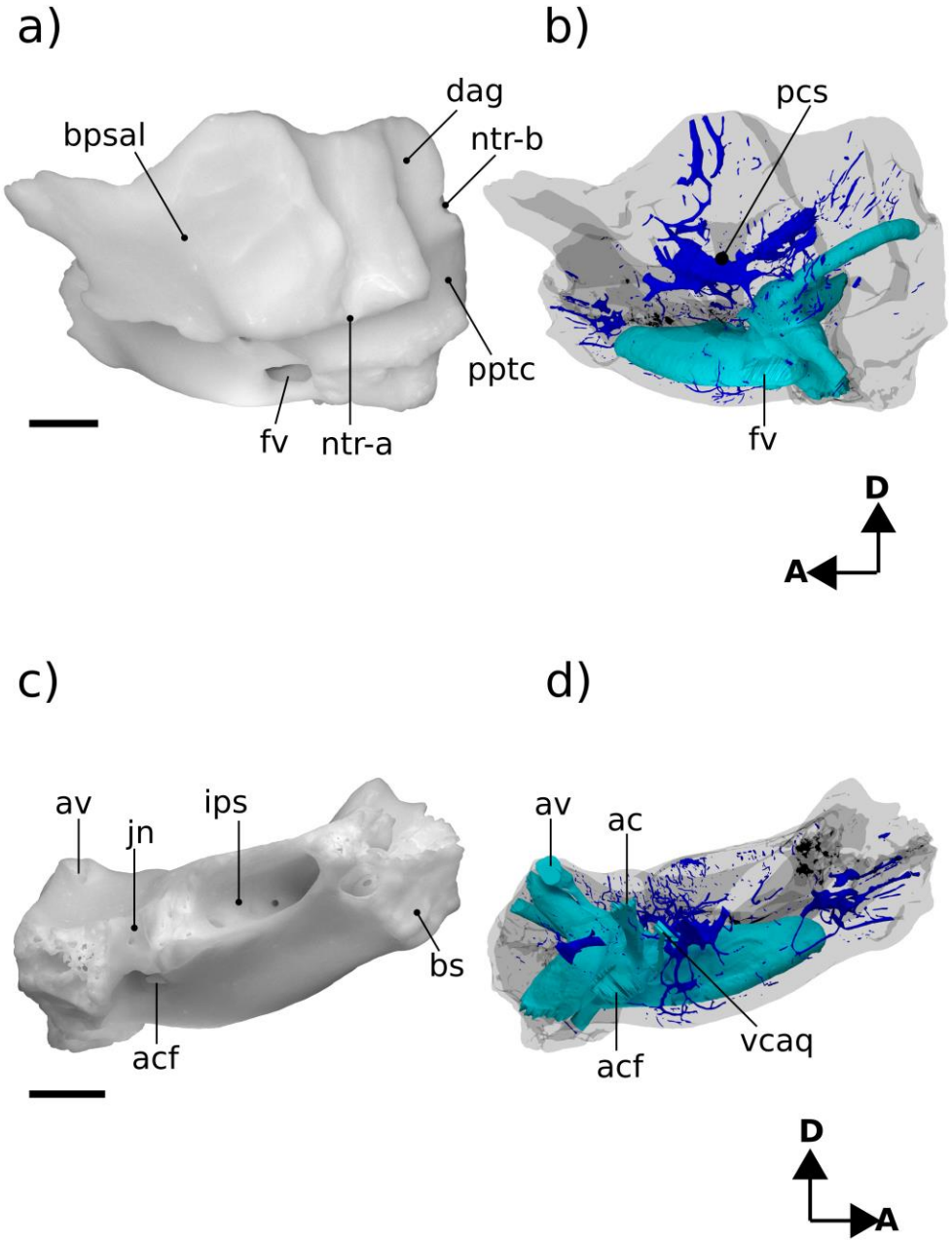

Lost structures in H2 presumably include, the full extent of the tympanohyal, crista parotica, paroccipital process, and caudal tympanic process; the posterior half of the subarcuate fossa and impression of the sigmoid sinus; and most of the post-temporal canal accommodating the arteria diploëtica magna. However, several phylogenetically informative structures are better preserved in H2 than in H1; in particular, the anterior extent of the promontoruim and the anterior lamina-lateral flange.

Tympanic surface

The ventral expression of the pars cochlearis is the elongate and laterally steep promontorium (Fig 3a). Almost the full extent of this structure is preserved, and as such it can be determined that the anterior limit of the promontorium abuts into an anteromedially facing planar suture, most likely with the basisphenoid ("bs" in Fig 3a). The dorsal extent of this sutural plane is obscured by damage exposing underlying venous sinuses and cancellous bone. Posteriorly, the promontorium is terminated by the posterolaterally facing fenestra vestibuli. The 0.92 mm horizontal width of the fenestra vestibuli occupies almost the full extent of the posterior aspect of the promontorium, with the posteriorly directed crista interfenestralis projecting from the posteromedial corner of the promontorium as well. In both H1 and H2 the stapedial ratio [24] is approximately 1.2 (not above 1.5, as originally scored by [4,5]); and the anterolateral margin of the fenestra vestibuli is grooved to accommodate the footplate of the stapes.

The crista interfenestralis is straight and despite a minor posterior slant it follows the same general horizontal plane as the body of the promontorium. The posterodorsal root of the crista interfenestralis (along with all other structures within the posterior one third of the petrosal) is incompletely preserved; however, the surface curvature in this region suggests

that the crista interfenestralis did not contact the posterior processes within the mastoid region, and that it blended subtly to lose distinction within the post-promontorial tympanic recess.

Between the anterior and posterior terminations of the promontorium there are no surface impressions of the promontorial artery, stapedial artery, or deep petrosal nerve (internal carotid nerve). The length of the promontorium is therefore shaped into a straight and smoothly rounded cylinder, with a sub triangular cross sectional profile. While the ventral edge of the promontorium is distinct (more so anteriorly) it does not show the level of salience seen in *Haldanodon* or *Megazostrodon* [5]. There is also no suggestion of a reduced rostral tympanic process (as in *Dasypus*; [22]) or impressions suggesting ventral contact of the promontorium with the lateral flange (as seen in multituberculates; [54]).

The lateral slope of the promontorium dips directly into the lateral trough, showing no distinct impression for the origin of the tensor tympani muscle anterior to the hiatus Fallopii ("hF" in Fig 3a), although the lateral trough is distinctly deeper in this region and it's a likely position for the muscle. Along the anterior two thirds of the promontorium, its medial slope dips shallowly towards the concave medial margin of the petrosal bone. This area also contributes to the intramural enclosure of the inferior petrosal sinus dorsally. The medial aspect of the posterior one third of the promontorium curves directly into the ventral margin of the medially facing aperture of the cochlear fossula ("acf" in Fig 3a) [21,22,55]. The aperture of the cochlear fossula lies external to the fenestra cochleae and is fully separated from the perilymphatic canal (aqueductus cochleae) by a thin, horizontally oriented bony strut (the processus recessus; [56,57]); and is approximately 0.59 mm wide anteroposteriorly, and 0.75 mm high dorsoventrally. The space defined by the aperture of the cochlear fossula medially and the processus recessus dorsally leads anteromedially to a

small anonymous venous canal (marked with an "*" in Fig 3a, and confluent with the inferior petrosal sinus and endocranial cavity) and to the jugular notch posteromedially (Fig 3a).

The bony perilymphatic canal in both H1 and H2 is approximately 1.3 mm in length, however H2 shows a greater degree of sophistication of the processus recessus structure because of the rounder, more ovoid, cross section of the perilymphatic canal it encloses. The perilymphatic canal in H1 in contrast is dorsoventrally flattened, and has much sharper anterior and posterior borders. Whether the morphology in H2 represents ontogenetic or phylogenetic development is uncertain, however, as variation in the compression of the cochlear aqueduct is commonly seen between individuals of *Dasypus novemcinctus* [22].

Because of its location posterior-dorsal-lateral to the pars cochlearis, the pars canalicularis and mastoid region is exposed ventrally as an "L"-shaped depression, dorsally offset from the promontorium. The perpendicular vertex of this "L" is posterolaterally offset approximately 1.5 mm from the center of the fenestra vestibuli. From this vertex, the mediolaterally oriented limb of the "L"-surface is damaged posteriorly, but the bases of four major topographic features are apparent. From lateral to medial these features are: 1) the ventral expression of the anterior lamina; 2) the open canal for the ventral ascending groove ("vag" in Fig 3a; for the proximal segment of the superior ramus of the stapedial artery); 3) the broken base of the paroccipital/mastoid region; and 4) the fossa for the stapedius muscle ("sf" Fig 3a) [32,58], placed directly posterior to the fenestra vestibuli. Major damage to the petrosal medial to the stapedius fossa precludes the recognition of other structures, such as the pocket medial to crista interfenestralis as seen in H1 [4].

The posteroventral extent of the anterior lamina is placed caudal to the line demarcating the periosteal surface of the anterior lamina anteriorly from its sutural surface

with the squamosal posteriorly. The lateral portion of the horizontal limb of the "L" is therefore interpreted as marking the zone of synostosis of the embryonic lamina obturans with the endochondral bone forming the bulk of the petrosal. Compared to the shape of this region in H1, the vertical line demarcating the periosteal and sutural surfaces of the anterior lamina in H2 is much less laterally offset from the rest of the petrosal. As suggested in [4] the petrosal's wide, solid, and laterally projecting sutural surface with the squamosal in H1 suggests that the glenoid fossa and other structures associated with the dentary-squamosal contact was relatively robust, a condition seen in many stem therians with large and transversely widened mandibular condyles.

Medial to the tympanic commencement of the ventral ascending groove (for the ramus superior of the stapedial artery) is the damaged base of the paroccipital/mastoid region. The anatomical landmarks commonly found in this region include a ventrally projecting paroccipital process, a rostrocaudally oriented crista parotica extending anterior to it, and possibly a caudal tympanic process of the petrosal running mediolaterally from the paroccipital process. All evidence of these features has been effaced from H2 due to the horizontal fracturing of their common base medial to the tympanic commencement of the ventral ascending groove. Therefore, while the presence and condition of the crista parotica, paroccipital process and most of caudal tympanic process of the petrosal cannot be commented on, the shape of this common base does demonstrate several significant contrasts with this region in H1. Most importantly, as mentioned in [4], the sutural surface of the squamosal bone's contact with the petrosal in H1 extends onto the lateral margin of the crista parotica, and therefore would have formed the bulk of the fossa incudis (the depression accommodating the crus brevis of the incus). In contrast, the intact lateral margin of the broken base of the paroccipital/mastoid region in H2 is vertically steep and

lacks a sutural surface with the squamosal. It is unclear what the phylogenetic polarity of these characteristics differentiating H1 and H2 would be; however, it is likely that these differences are a direct result of the more robust attachment of the squamosal to the lateral surface of the petrosal in H1, and the more ventral location of the ventral ascending groove (relative to the fenestra ovalis) in H2. The medial-most structure visible along the mediolateral limb of the "L" is the fossa for the stapedius muscle ("sf" in Fig 3a). The center of this depression in H2 is located further medially (closer to the crista interfenestralis) than in H1 (where it is located diametrically opposite the fenestra ovalis).

Anterior to the tympanic commencement of the ventral ascending groove ("vag" in Fig 3a), the anteroposteriorly oriented limb of the "L"- shaped exposure of the pars canalicularis is located between the lateral aspect of the promontorium medially, and the medial aspect of the lateral flange (ventral extension of the ossified lamina obturans; [27]) laterally. The tympanic surface of the anteroposteriorly oriented limb therefore forms an elongate and concave sulcus, termed the lateral trough [46]. The lateral trough is an anatomical crossroads for several important neurovascular structures (described below), and is perforated by three major foramina. Between the anterior margin of the fenestra vestibuli and the posterior base of the lateral flange, two of these foramina are aligned mediolaterally at the posterior end of the lateral trough. The lateral of the two is the tympanic aperture of the prootic canal (for the prootic vein = middle cerebral vein; [28]). The tympanic aperture of the prootic canal does not approximate or become confluent with the ventral commencement of the canal for the superior ramus of the stapedial artery, as is seen in *Ornithorhynchus* and many multituberculates [54,59]. There is also a small, anonymous, vascular foramen placed anterolateral to the tympanic aperture of the prootic canal, that

communicates with the circumpromontorial venous plexus, and has a small sulcus leading into it (not visible in figures).

Medial to the tympanic aperture of the prootic canal is the more posteriorly directed secondary facial foramen for the entrance of the hyomandibular branch of the facial nerve into the cavum tympani. Compared to H1 and the spalacotheroid *Zhangheotherium* [47] the tympanic aperture of the prootic canal and the secondary facial foramen in H1 appear much closer. The location of these foramina are however ambiguous in the zhangheotheriid *Maotherium* [60]. In H1 the center of the secondary facial foramen is located anteromedial to the prootic aperture.

Anterior to the secondary facial foramen, the anteriorly oriented hiatus Fallopii perforates the lateral trough near the lateral margin of the promontorium. The hiatus Fallopii admits the palatine branch of the facial nerve (= greater petrosal nerve) in to the lateral trough. Therefore, the (approximately 1.28 mm long) lamina of bone extending between the secondary facial foramen and the hiatus Fallopii represents the bony floor of the cavum supracochleare (the space containing the geniculate ganglion of the facial nerve) and the inferior margin of the hiatus Fallopii. Anterior to the hiatus Falopii the lateral trough is more deeply excavated and roughened, similar to the condition seen in H1. This surface may represent a relatively indistinct area for the attachment of the tensor tympani muscle.

Lateral Surface

The preserved squamosal surface of H2 is composed mainly of the anterior lamina anteriorly, with some exposure of the lateral surface of the pars canalicularis posteriorly (Fig 4a). Four grooves are apparent on this surface, that represent the petrosal's contribution to

arterial canals enclosed laterally by the squamosal. Commencing near the posterior margin of the anterior lamina, posterior to the tympanic aperture of the prootic canal, the approximately 1.74 mm long groove for the superior ramus of the stapedial artery (ventral ascending groove) curves posterodorsally in a smooth arc. Almost halfway along its length, this canal gives off a distributary branch to a groove for a minor temporal ramus (of the superior ramus) of the stapedial artery. The posterior termination of the groove for the superior ramus of the stapedial artery is its point of confluence with the groove for the arteria diploëtica magna and groove for the ramus supraorbitalis of the stapedial artery (dorsal ascending groove; [27]). The large size (0.70 mm diameter) of the canal for the arteria diploëtica magna suggests that this vessel was the major supplier of arterial blood to the cranial connective tissues in this region ([5]; see Fig 3a and Fig 5a and c). However, neither this groove nor the groove for the supraorbital ramus of the stapedial artery are preserved along their full extent or diameter, preventing the description of their precise distributions and possible ramifications. The visible extent of the groove of the supraorbital canal runs vertically along the lateral surface of the petrosal, directly lateral to the endocranial expression of the subarcuate fossa. A subsidiary groove for a possible second temporal ramus of the stapedial artery may be seen branching from the posterior wall of the dorsal ascending groove (for the supraorbital ramus of the stapedial artery). However, this feature may be the result of postmortem fragmentation and rounding.

Fig 5. Neurovascular reconstructions of Höövör 2 petrosal. a, ventral view; b, medial view; c, lateral view. Venous structures shown in dark gray; nervous structures shown in light gray; the stapedial artery and its ramifications are unshaded. Refer to list of abbreviations in text for other abbreviations.

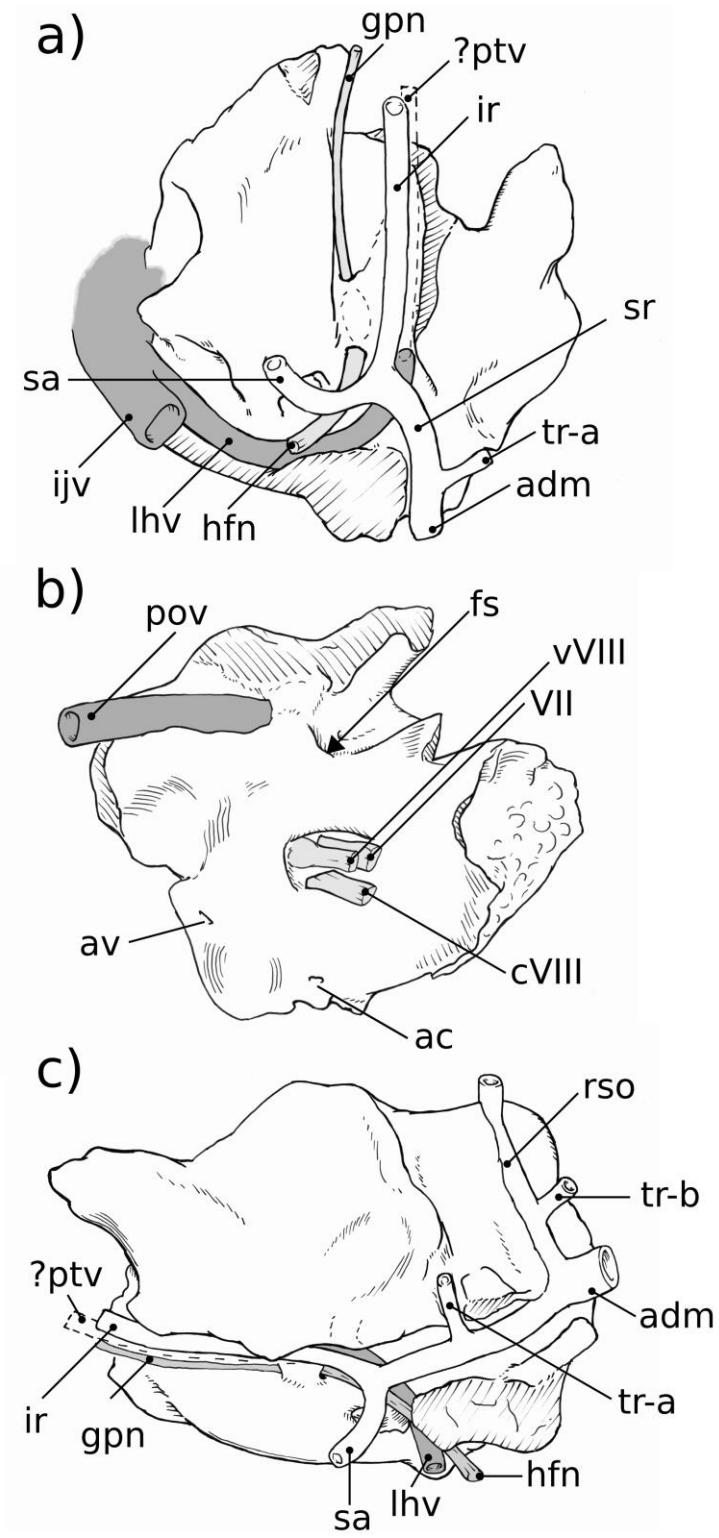

Ascending laterally from the lateral flange there is an extensive anterior lamina. The ventral projection of the lateral flange is damaged; however, it is probable that not much of its original surface has been lost, and judging from the shape of the breakage it is improbable that it could have supported a sutural contact with a large quadrate ramus of the alisphenoid.

The lateral aspect of the anterior lamina does not show the mediolaterally projecting and horizontally flattened area (termed the anterolateral recess) that is seen in H1 [4]. Instead the lateral surface of the anterior lamina in H2 shows a steeper vertical slope, and terminates anteroventrally at the lateral opening of the cavum epiptericum (described below). The posterior extent of the anterior lamina contains a small vertical crest of bone lateral to the tympanic aperture of the prootic canal separating the periosteal and sutural surfaces of the periotic ("bpsal" in Fig 4a).

Cerebellar surface

The preserved cerebellar surface of H1 (Fig 1b and Fig 3c) can be visualized as being composed of three endocranially exposed neural invaginations, anteriorly (the cavum epiptericum), medially (the internal acoustic meatus) and posteriorly (the subarcuate fossa) and a venous canal (the prootic canal) laterally; thus forming a "+" shaped pattern of topologically negative spaces in cerebellar view (Fig 3c). The intervening elevated surface between these four structures therefore forms a matching "x" shaped pattern, the center of which being composed of a massive elevation of bone. Lateral to this "x" is a large fragment of the vertically oriented anterior lamina, and most of the area medial to the "x" is formed by the pars cochlearis enclosing the cochlear canal. The posteromedial border of the "x"

however is formed by a thin sheet of bone near the jugular notch (i.e. the processus recessus, with some contribution from the petrosal bone proper). The endocranial aperture of the aqueductus cochleae ("ac" in Fig 3c; also termed the perilymphatic canal) can be seen at the anterior border of this sheet of bone.

The internal acoustic meatus in H1 is an approximately 1 mm deep invagination, terminated by four foramina distally (numbered "1-4" in Fig 3c). Because of its oblique angle of descent into the substance of the petrosal bone, the endocranial rim of the internal acoustic meatus is shaped differently in each of its four quadrants, providing a convenient pattern for the description of its contents.

The prefacial commissure ("pfc" in Fig 3c; also suprafacial commissure; [20,21]) is the name given to the portion of the anterior ossified wall of the internal acoustic meatus partially bounding the proximal bony conduit of the facial nerve ("1" in Fig 3c), and which is not first preformed developmentally in the chondrocranium [21]. In both H1 and H2 the prefacial commissure extends posterolaterally from the shallower curvature of the posterior cranial fossa, and terminates laterally at the lateral-most point of the proximal aperture of the internal acoustic meatus. The entire 90° arc of the anterolateral quadrant of the internal acoustic meatus in H2 can therefore be thought of as consisting of the prefacial comissure, which extends distally (beyond the internal acoustic meatus) to form the anterior wall of the approximately 0.5 mm diameter primary facial foramen ("1" in Fig 3c).

Directly lateral to, and contiguous with, the prefacial commissure the endocranial surface (outside the internal acoustic meatus) shows a blunt, anteroposteriorly oriented crista petrosal separating the bulk of the cerebellar surface of the petrosal from the petrosal's contribution to the bony floor of the cavum epiptericum (accommodating the trigeminal ganglion=semilunar ganglion=Gasserian ganglion; [21,61]). Being the anterior attachment of

the tentorium cerebelli in extant mammals, the location of the crista petrosa near the medial margin of the cavum epiptericum likely marks the point of dorsal enclosure of the trigeminal ganglion into the dural folds separating the middle and posterior cranial fossae in H2. In more plesiomorphic forms such as *Morganucodon* [32] and *Priacodon* [5], and in modern *Ornithorhynchus* [62], the prefacial comissure itself and the pila antotica form the medial margin of the cavum epiptericum. Specimens H1 and H2 show a much wider prefacial commissure. This morphology is likely an osteological byproduct of the mediolateral dilation of the endocranial space within the posterior cranial fossa.

The anteromedial quadrant of the internal acoustic meatus is a continuation of the wider curvature of the surrounding pars cochlearis, and so does not form a distinct lip for the meatus. However, in H1 and H2 the ventral surface of the internal acoustic meatus in this region contains a low ridge of bone running distally into its depths, the crista transversa [22]. This low ridge loses distinction before reaching the distal terminus of the meatus (and therefore should not be called a "falciform crest"), but forms a separation between the foramen for the cochlear nerve ("4" in Fig 3c; in the posteromedial quadrant) and the primary facial foramen ("1" in Fig 3c; in the anterolateral quadrant). The crista transversa is distinctly higher in H1 and longer in H2, but in neither does it reach the height or salience of the falciform crest seen in *Homo* [51] and other modern mammals. The foramen for the cochlear nerve is ovoid, approximately 0.74 mm long along the axis of the cochlear canal and 0.3 mm wide mediolaterally, and shows smooth margins with no development of a tractus foraminosus (or cribriform plate). Dorsal to the foramen for the cochlear nerve, the distal surface of the internal acoustic meatus contains the two circular foramina for the branches of the vestibular nerve ("2-3" in Fig 3c). Based on the orientation and location of these two foramina for the vestibular nerve it is likely that they are homologous to the

foramina for the utriculoampullar ("2" in Fig 3c) and sacculoampullar ("3" in Fig 3c) branches [18] seen in both extant therians and monotremes.

In both H1 and H2 the posterolateral and posteromedial quadrants of the internal acoustic meatus are formed by the raised wall of bone partitioning the internal acoustic meatus from the subarcuate fossa. The ventral floor of the internal acoustic meatus in this region contains the anteroposteriorly elongate foramen for the cochlear nerve medially, and the two smaller vestibular nerve foramina laterally or posterolaterally. These inferred homologies are supported by the trajectories of these foramina when viewed on the virtual endocast of the bony labyrinth; however, because these vestibular foramina do not form cylindrical canals leading directly to their peripheral targets, the precise targets of innervation of the nerves traversing the vestibular foramina cannot be determined conclusively.

Unlike the stem therians discussed here, fossil and extant cladotheres unanimously show the apomorphic distribution of peripheral axons within the vestibulocochlear nerve by the formation of osseous cribriform areas within preexisting foramina (the tractus foraminosus forming within the foramen transmitting the cochlear nerve being the most prominent example); although most of the contents of the foramen acusticum superius (area of the internal acoustic meatus dorsal to the crista transversa) remain free of trabeculated bony outgrowths in crown therians and all fossil cladotheres so far studied [7,8,63]. The foramen acousticum inferius on the other hand comprises the common depression for the foramen of the cochlear nerve and the foramina for nerves targeting the saccular macula (penetrating through the macula cribrosa media; [64]) and ampulla of the posterior semicircular canal (through the foramen singulare). The contents of the foramen acusticum inferius commonly recruit cribriform bony structures to secondarily infill these ancestral foramina in cladotheres. Additionally, because of its incorporation of a branch of

the vestibular nerve (the sacculoampullar branch, or inferior vestibular nerve in *Homo*) along with the cochlear nerve, the foramen acusticum inferius is typically at least twice as large in areal extent than the foramen acusticum superius in Cladotheria. This trait has been mentioned by [63] as showing the apomorphic condition of their cladotherian specimen relative to *Priacodon*. In contrast, the area likely homologous to the foramen acusticum inferius in *Priacodon,* H1 and H2 is subequal or smaller than the foramen acusticum superius, and completely lacking cribriform bony infilling.

Directly posterior to the internal acoustic meatus is a wall of bone that forms the medial margin of the subarcuate fossa, enclosing the primary common crus of the bony labyrinth, and supporting the endocranial aperture of the aquaductus vestibuli ("av" in Fig 3c; containing the membranous endolymphatic duct). The distal half of this medial wall has been lost in H2 due to postmortem fracturing; and features such as the impression of the sigmoid sinus and contact with the exoccipital bone cannot be confirmed. However, the preserved morphology of this wall provides a reliable estimate of the maximal diameter of the proximal entrance to the subarcuate fossa. The proximal aperture of the subarcuate fossa is the endocranial expression of the anterior semicircular canal, and its 1.86 mm diameter in H2 closely matches the same length measured in H1. However, in both specimens it is apparent that the distal extent of the subarcuate fossa has a significantly larger diameter because of its medial excavation of its medial wall, distal to the constriction formed by the anterior semicircular canal. The medial diversion of the subarcuate fossa projects into the loop of the posterior semicircular canal, similar to the way the proximal aperture of the subarcuate fossa itself projects into the the loop of the anterior semicircular canal. The state of preservation in H2 does not allow the maximal diameter of the distal subarcuate fossa to be confidently estimated.

Anterolateral to the subarcuate fossa, and medial to the posterior region of the anterior lamina, is the endocranial aperture of the prootic canal ("eapc" in Fig 3c). A groove leading into this aperture can be seen following the curvature of the anterolateral margin of the subarcuate fossa for a short distance before leaving the preserved edge of the petrosal. This structure is termed the groove for the middle cerebral vein in [32], and represents the approximate branching point of the transverse sinus from the middle cerebral vein. The enclosed prootic canal in H2 is substantially shorter (1.72 mm, versus 2.55 mm in H1) and less sigmoidal than the bony canal seen in H1. The diameter of the canal in both specimens is approximately 0.6 mm along its entire length (Fig 3c and Fig 6a).

Fig 6. Renderings of stem therians in endocranial view. a, b Höövör petrosal 1 (right-to-left reflected); c, d *Priacodon*. Showing labyrinthine endocast in teal and circumpromontorial venous plexus in blue. Scale bars are 1 mm. **A**, anterior; **L**, lateral. Numerical abbreviations: 1, primary facial foramen; 2, foramen for utriculoampular branch of vestibular nerve; 3, foramen for sacculoampular branch of vestibular nerve; 4, foramen for cochlear nerve. Refer to list of abbreviations in text for other abbreviations.

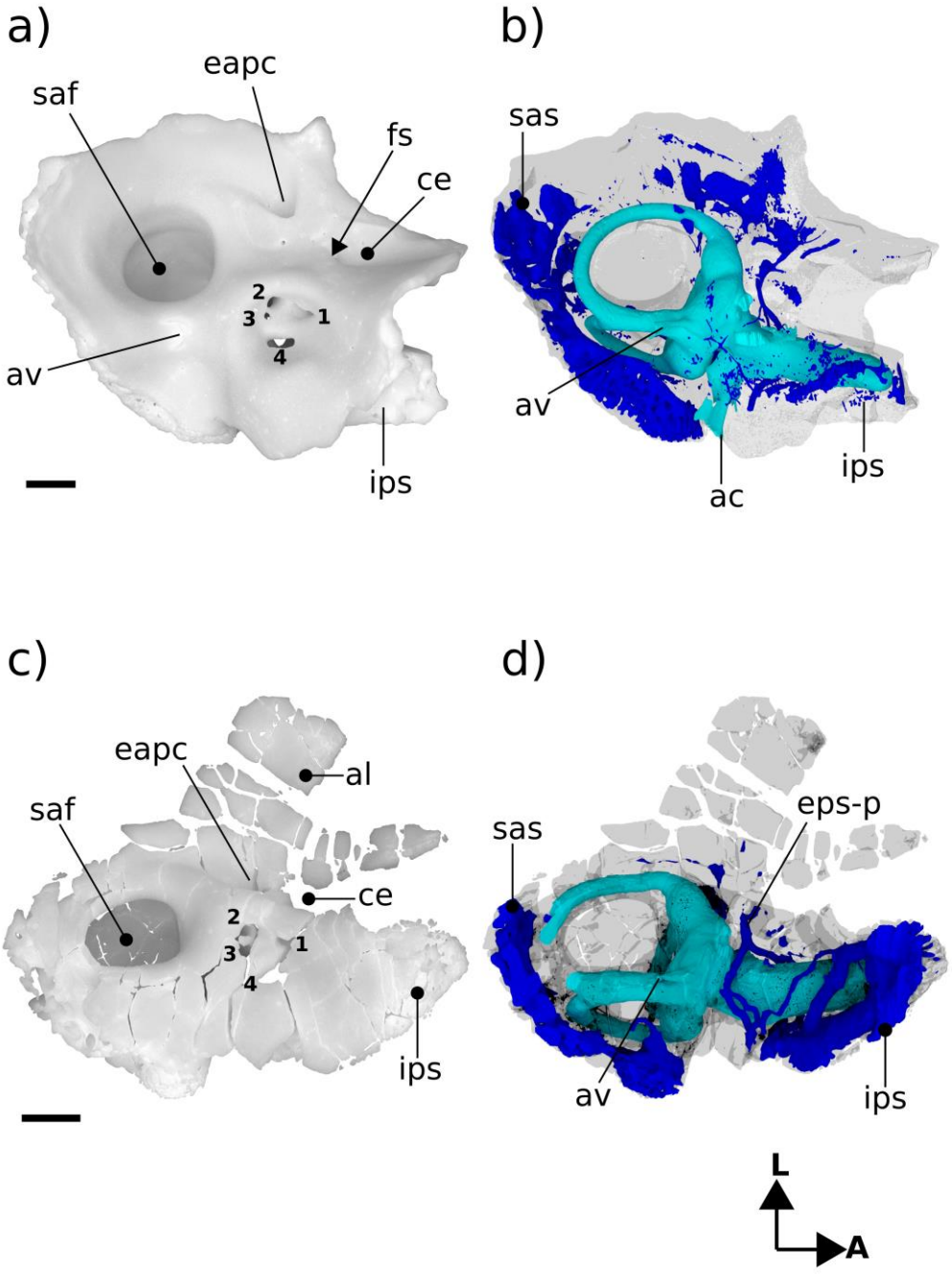

The petrosal bone's enclosure of the cavum epiptericum ("ce" in Fig 3c) is better preserved in H2 than in H1, allowing for a more precise characterization of this phyogenetically significant structure. As such, in H2 it can be determined that the impression for the cavum epiptericum on the petrosal is rectangular in general dimensions, with its posterior margin formed by an anteriorly facing border of bone placed anteromedial to the endocranial aperture of the prootic canal (this wall may represent the original anterolateral margin of the ossified otic capsule before its subsequent fusion with the ossified lamina obturans). Anterior to this posterior margin the bony floor of the cavum epiptericum extends approximately 1.64 mm anteriorly before terminating at the anterior margin of the petrosal. As mentioned above, the medial and lateral margins of the cavum epiptericum are formed by the crista petrosa and anterior lamina, respectively. These structures define the 1.19 mm width and 0.86 mm depth of the cavum epiptericum and contribute to two foramina communicating with this space. The posteriormedial corner of the cavum epiptericum contains the fenestra semilunaris ("fs" in Fig 3c) [27], that extends 0.5 mm medially within the crista petrosa to communicate with the cavum supracochleare. The anterolateral margin of the petrosal's contribution to the cavum epiptericum is formed by an emargination of the broken rostral margin of the anterior lamina. This emargination would have comprised the majority, or entirety, of the margin of the foramen for the mandibular branch of the trigeminal nerve, and hence would be termed the foramen ovale (or the foramen pseudoovale [65]). The preserved posterior margin of the foramen ovale is an approximately 1.19 mm diameter semicircular indentation. However, preservation prevents the determination of whether this foramen is entirely contained within the anterior lamina, and what its total anteroposterior length would have been.

Neurovascular Reconstruction

Figure 5 illustrates reconstructions of the major vascular ramifications on the external surface of the H2 petrosal. The vessels for which osteological correlates can be observed include tributary veins of the internal jugular circulation and distributary arteries of the stapedial/occipital circulation [66,67]. While not leaving a distinct impression on the fenestra vestibuli, the stapedial artery ("sa" in Fig 5a) likely ran laterally to a bifurcation point slightly posterior to the tympanic aperture of the prootic vein. Running posterior from this bifurcation the superior ramus of the stapedial artery occupies the ventral ascending groove, then forms an anastomosis with the wider arteria diplöetica magna, and also gives off a small temporal ramus near its anterior extent. Because of damage to the dorsolateral extent of the petrosal forming the dorsal ascending groove, the course of the ramus supraorbitalis ("rso" in Fig 5c) extending from the confluence of the arteria diplöetica magna and superior ramus of the stapedial artery cannot be reliably reconstructed. Likewise, the occipital artery, which likely contributed the majority of arterial blood to the cranial connective tissues through its confluence with the arteria diplöetica magna ("adm" in fig 5c) and elsewhere, has no osteological correlate within the preserved morphology of H2 except for the grooves that represent its distributary branches.

The two main tributaries of the internal jugular vein are the lateral head vein ("lhv" in Fig 5a) and inferior petrosal sinus [28,59]. As will be discussed below both the prootic vein ("pov" in Fig 5a; also termed prootic sinus or middle cerebral vein in extant therians), before its confluence with the lateral head vein, and the inferior petrosal sinus receive minor venous tributaries along their course through the body of the petrosal bone. Because there is

no anterior emargination of the tympanic aperture of the prootic canal ("tapc" in Fig 3a), H2 shows no osteological correlate of the post-trigeminal vein, leaving its existence in this taxon uncertain (it is therefore shown only with a dashed outline marked "?ptv" in Fig 5a and c). If, as in extant therians, H2 lacked a post-trigeminal vein the boundary between the prootic vein and lateral head vein would become completely arbitrary, and in this report it is taken to be at the point of emergence of the prootic vein onto the tympanic surface of the petrosal. A small venous foramen anterolateral to the tympanic aperture of the prootic sinus likely conducted a small tributary to the lateral head vein as well (not reconstructed in Fig 5).

In most respects the external vascular reconstruction of H2 is broadly similar to that provided by [4] for H1. The most salient contrasts being the relatively more ventral position of the ventral ascending groove (and therefore the superior ramus of the stapedial artery) relative to the foramen for the arteria diplöetica magna in H2 (Fig 5c). Given the uncertainty and variability in the presence and branching pattern seen in temporal rami ("tr-a" and "tr-b" in Fig 5c), the different reconstructed connectivity of the posterior temporal ramus in H1 (at the point of confluence of the arteria diplöetica magna and superior ramus of the stapedial artery) and H2 (from the ventral extent of the supraorbital ramus) should not be considered systematically significant.

Comparison of labyrinthine endocast morphology between *Priacodon*, the Höövör petrosals, and extant mammals

Endocast Preserved in Pars Cochlearis

The straight distance along the bony cochlear canal, measured from the anterior surface of the recessus sphericus (the caudal apex of the saccular expansion; [24]) to the distal terminus (anterior apex) of the cochlear canal, is approximately 0.8 mm shorter in *Priacodon* than in either of the Höövör petrosals. However, the differences in length of the cochlear canal in all three of these specimens closely match the intra-specific variation seen in cochlear canal length reported in *Ornithorhynchus* (CL-cp; [18]), although *Ornithorhynchus* is much larger bodied than any of these stem therians. Also, despite being shorter, the shape of the cochlear canal in *Priacodon* can be still be interpreted as more derived than the cochleae seen in the Höövör petrosals because of its slightly stronger lateral curvature (see Figs 3-10).

Fig 7. Renderings of stem therians in ventral view. a, b Höövör petrosal 1(right-to-left reflected); c, d *Priacodon*. Showing labyrinthine endocasts in teal and circumpromontorial venous plexuses in blue. Scale bars are 1 mm. **A**, anterior; **L**, lateral. Refer to list of abbreviations in text for other abbreviations.

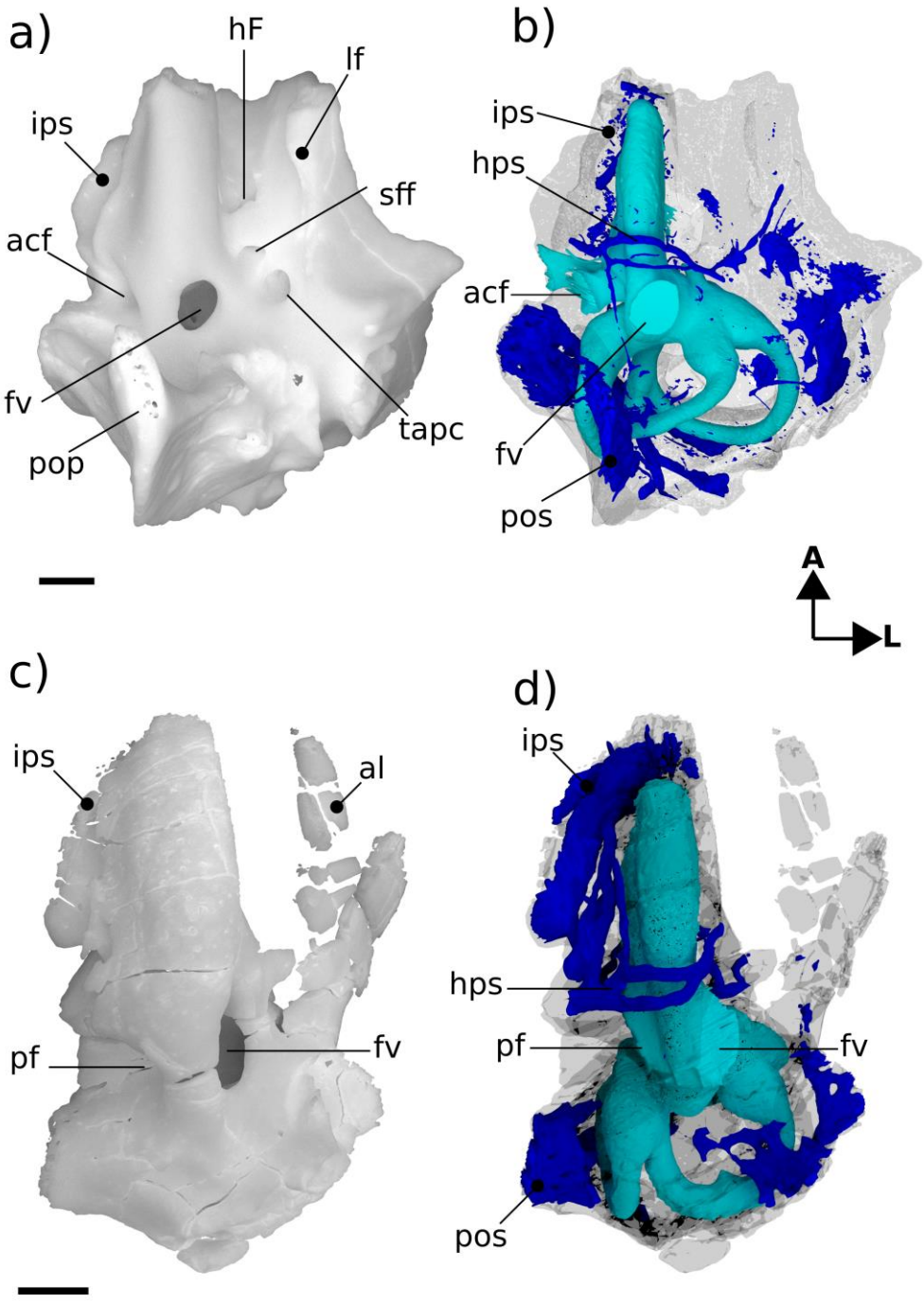

Fig 8. Resliced CT images of Höövör petrosals. a, c, e Höövör petrosal 1 (volume renderings are right-to-left reflected); b, d, f Höövör petrosal 2. a, b are oblique planes through both the cochlear aqueduct and canal for the vein of the cochlear aqueduct; c, d, e, f are coronal planes through the promontorium. Parts c, d are taken from a more posterior plane than e and f to show the hypocochlear sinus in H1. In all images left is lateral and dorsal is approximately toward the top of the page; all scale bars are 1 mm. Refer to list of abbreviations in text for other abbreviations.

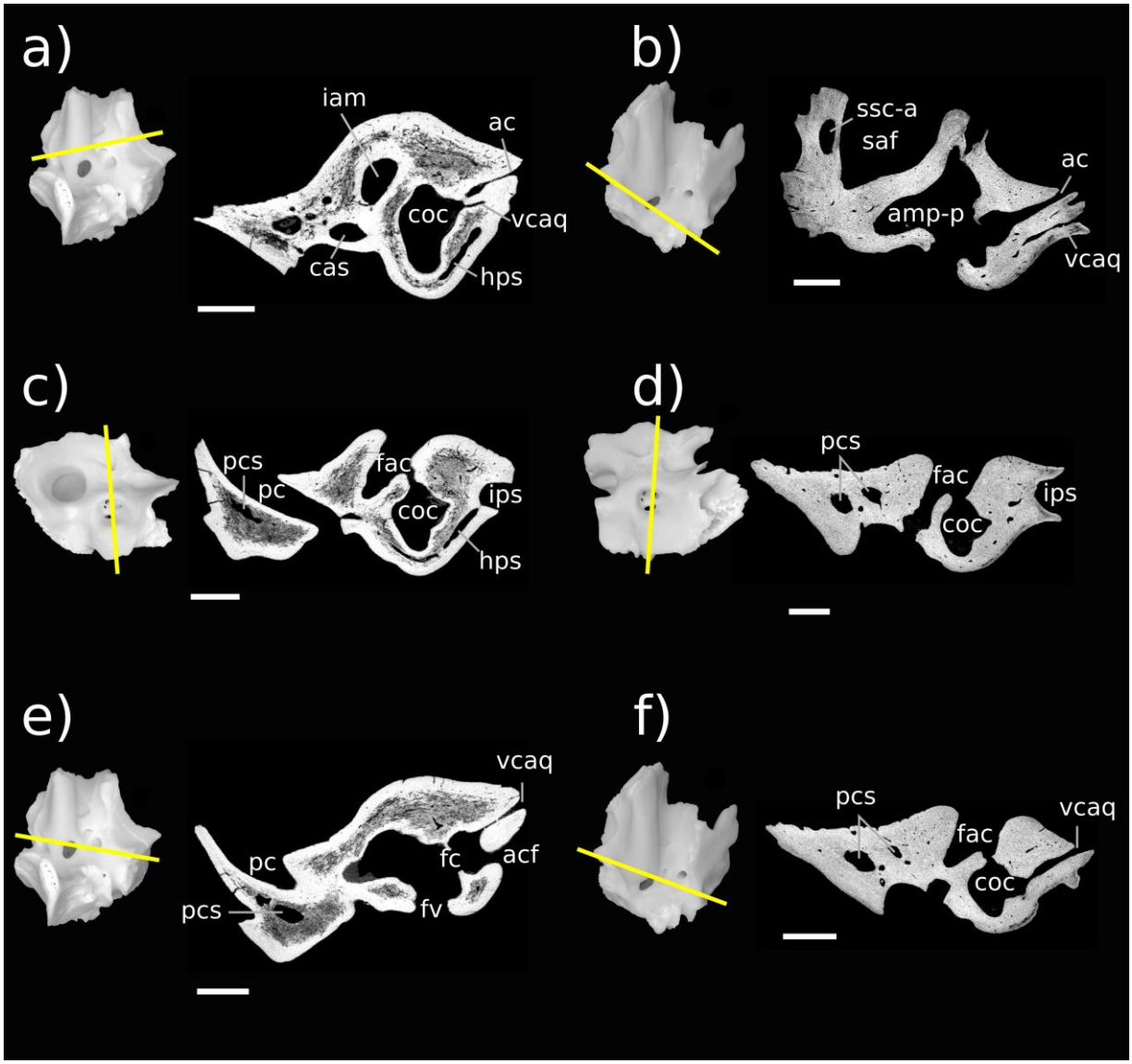

Fig 9. Resliced CT images showing *Priacodon* and several extant mammals. a, b, c images of *Priacodon*; d, coronal section through promontorium of *Ornithorhynchus*; e, coronal section through promontorium of *Didelphis*; f, coronal section through promontorium of *Dasypus*. a, b, are coronal sections through the promontorium of *Priacodon,* a is taken posterior to b to show the posterior epicochlear sinus; b, is taken rostral to the fenestra vestibuli and perilymphatic foramen to show the hypocochlear sinus. c, shows horizontal plane through the horizontal semicircular canal and its centripetal diverticulum. All scale bars are 1 mm; for 2D slices in a, b, d, e, and f lateral is toward the left of the page and dorsal is toward the top of the page; in c lateral is toward the right of the page and posterior is toward the top of the page. Asterisk shows location of damage to anterior wall of perilymphatic foramen in *Priacodon*. Refer to list of abbreviations in text for other abbreviations.

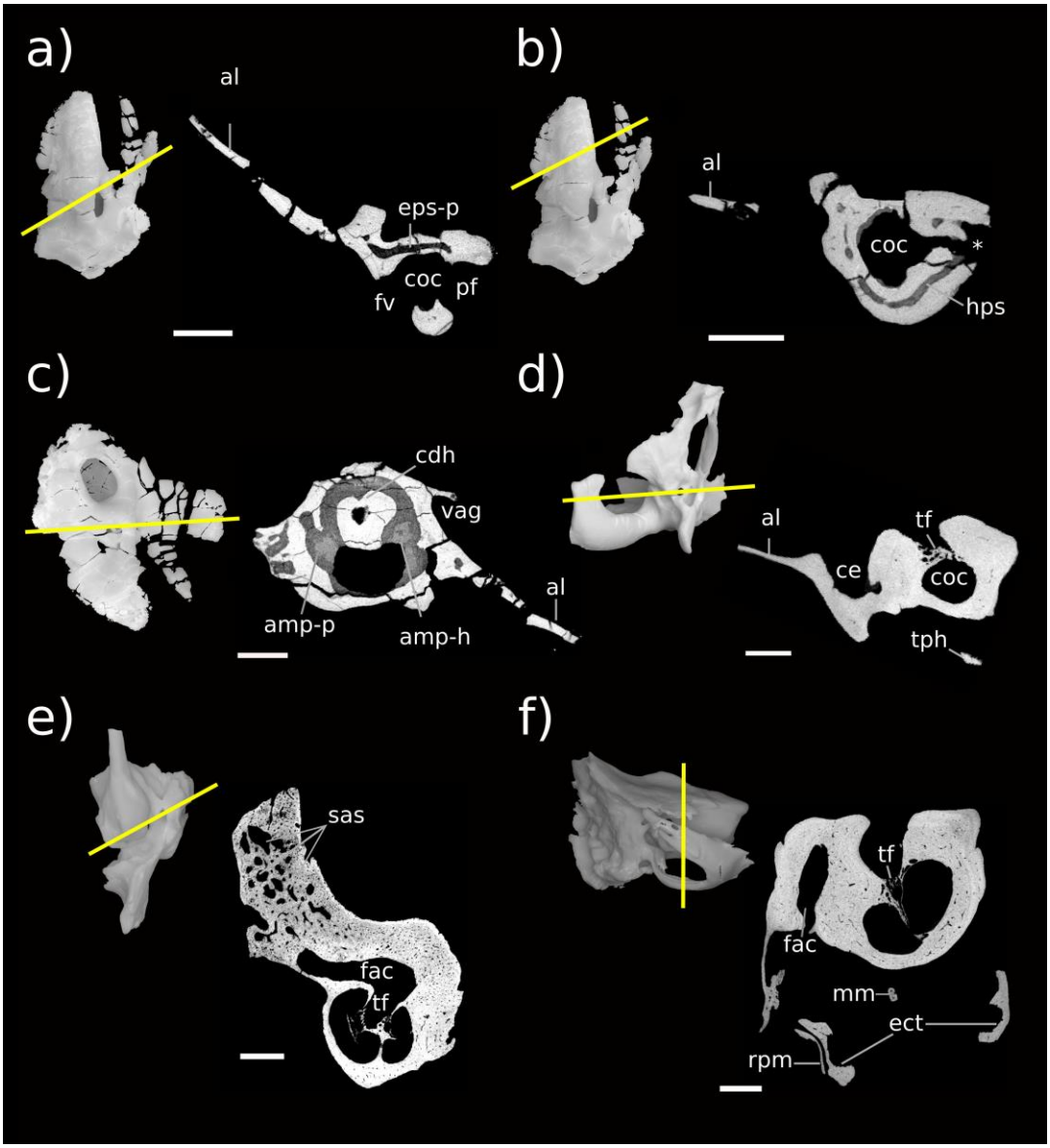

Fig 10. Renderings of labyrinthine endocasts in stem therians. a, b, Höövör petrosal 2; c, d Höövör petrosal 1 (right-to-left reflected); e, f *Priacodon*. All specimens shown as left-sided all scale bars are 1 mm. Refer to list of abbreviations in text for other abbreviations.

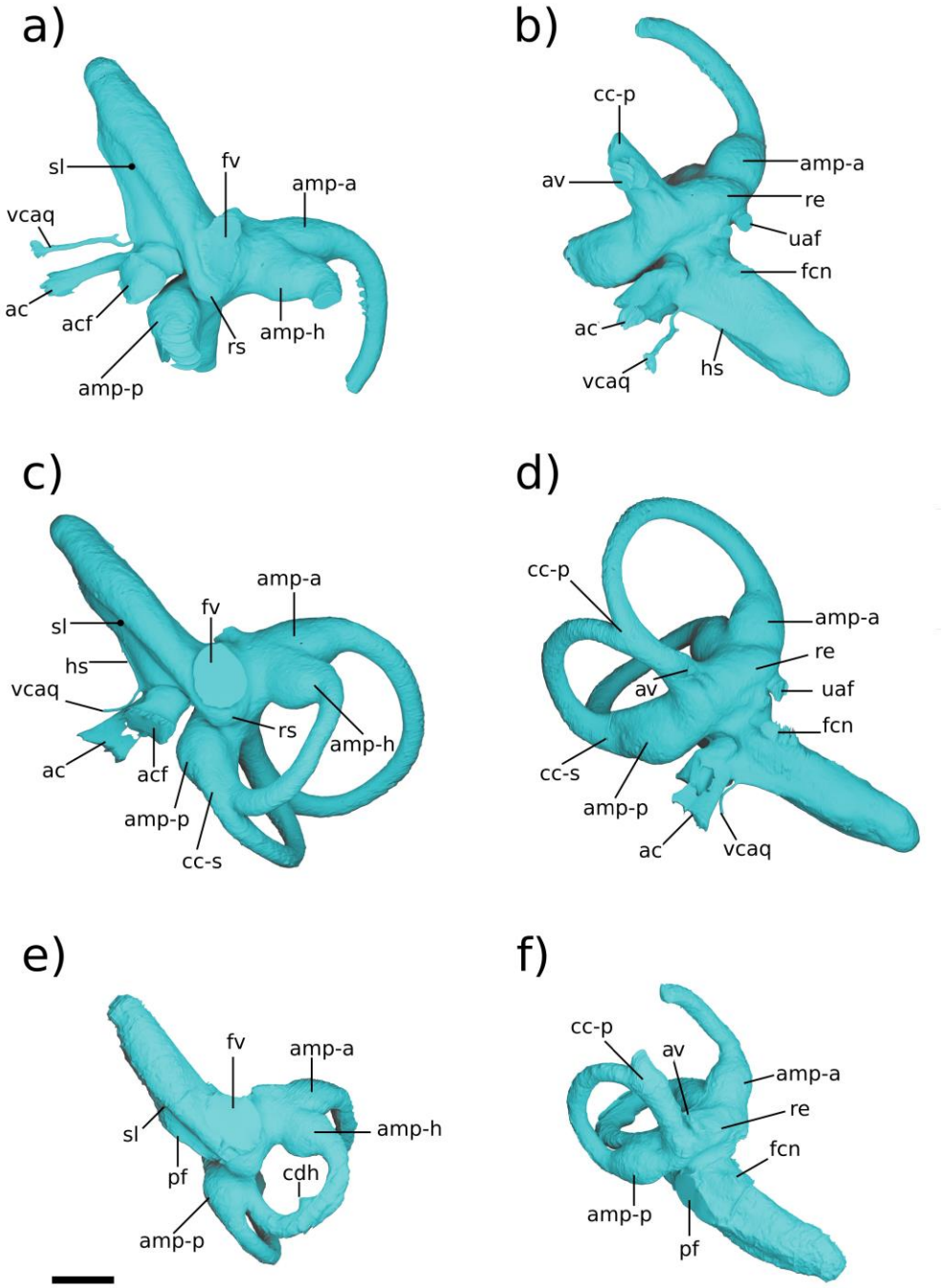

While being a particularly homoplastic character, lateral curvature of the cochlear canal is seen only in mammaliaforms (especially the most plesiomorphic forms), with other amniotes developing medial curvature (i.e. convex towards the insertion of the cochlear nerve) to accommodate cochlear elongation. However, the incipient cochlear curvature in *Priacodon* only shows lateral deflection near its base, and no dorsoventral coiling (Fig 10e,f). Additionally, the fact that similar, or stronger, degrees of cochlear curvature are reported for mammaliaforms outside the mammalian crown group [68] presents the possibility (dependent on the precise phylogenetic interrelationships hypothesized for the taxa involved) that loss of lateral cochlear curvature may actually be an apomorphic feature of the taxa represented by the Höövör petrosals and later stem therians.

All three of the stem therian endocasts (Fig 10) show that the cochlear canal tapered somewhat towards its distal terminus (much more so in the Höövör petrosals than in *Priacodon*). In particular, none of these endocasts show prominent inflations or emarginations of the cochlear canal capable of accommodating a lagenar macula larger in diameter than the more proximal portions of the cochlear endocast. While the loss of its osteological correlate does not logically implicate the absence of a functional lagenar macula in these taxa [15], the morphology of the cochlear canal in these cases at least presents the possibility that these taxa had attained a terminal helicotrema (as in modern therians). This contrasts with the large, terminally positioned lagena and related nervous structures that are apparent in the osseus morphology of monotremes, several multituberculates, and mammaliaforms outside of the mammalian crown group [68,69]. Significantly, none of these stem therian endocasts show any of the "lagena related osteological characters", as detailed by [70] for *Haldanodon*; such as a sulcus or canal for the lagenar branch of the cochlear nerve, a fossa for the lagenar macula, and/or canaliculi perforating a terminal portion of the cochlear canal for dendrites

innervating the lagenar sensory epithelium. The relative restriction of the apex of the cochlear canal suggests the progressive reduction of the lagena within progressively more crownward members of the stem therian lineage. Conversely, the bony accommodation of lagenar function would therefore be a retained symplesiomorphy within allotherians and modern monotremes [2 ,14-17].

All three stem therian endocasts also lack the "sunken" position of the fenestra ovalis (fenestra vestibuli) relative to the basal commencement of the cochlear canal, described by [63]. The sunken appearance of the fenestra ovalis was mentioned by these authors as being possibly apomorphic for the clade Cladotheria. However, given that this feature is also lacking in the South American cladothere *Vincelestes* [27], without a wider-scale phylogenetic analysis it seems at least equally plausible that an inset fenestra ovalis may be an apomorphic feature derived within dryolestoid cladotheres or some more exclusive group(s). A phylogenetic analysis informed by a large sample of cladotherian cochlear endocasts would be required to resolve the ancestral reconstruction of this feature.

One of the most marked features seen in the Höövör petrosals (Fig 8e and f) and not *Priacodon* (Fig 9a and b) and *Ornithorhynchus* (Fig 9d), is the complete segregation of the bony canal supporting the perilymphatic duct from the ossified aperture suspending the secondary tympanic membrane (the fenestra cochleae; "fc" in Fig 8e) and the aperture of the cochlear fossula ("acf" in Figs 3a,7a, and 8e). The secondary tympanic membrane is a thin epithelial bilayer found in many, if not most, amniotes [62], and segregates the fluid filled perilymphatic space from an air-filled intracranial space (such as a cavum tympani). The bony segregation of the secondary tympanic membrane from its confluent perilymphatic duct is, however, a characteristic seen only in advanced stem therians and variously in mature adult tachyglossids. The bony process of perichondral bone that completes the enclosure of

the fenestra cochleae and aqueductus cochleae in the cohclear endocast of therians is termed the processus recessus [12,22,55-57].

The performance implications of this partitioning of the proximal scala tympani are uncertain ([17]: chapter 10). For instance, the processus recessus may prevent the unconstrained flux of perilymph from the scala tympani into the subarachnoid space. Whatever its functional advantage, it is very likely that the homoplastic distribution of the processus recessus in stem therians and in older adult tachyglossids is due to convergence [18,54]. Additionally, the incipient expression of an incomplete "processus recessus" has also been recognized in *Priacodon* [5], where it forms a linear ridge associated with the reconstructed course of the perilymphatic duct. Similar ridges described in multituberculates [54,59] also form a variable recessed or enclosed groove for the perilymphatic duct.

Otherwise, the presence of a well-developed processus recessus, fenestra cochleae, and aquaductus cochleae is known among members of the clade Trechnotheria (including the spalacotheres, dryolestoids, and therians; [36]), and in the derived "triconodont" clade Gobiconodontidae (GWR Pers Obs). These structures are retained in almost all known trechnotherian mammals (Sirenia, Elephantomorpha, and Eschrichtiidae being the main exceptions, due to atavistic reversal [69]). The tympanic aperture of the scala tympani, (whether this is the perilymphatic foramen as in *Priacodon* - "pf" in Figs 7c,d and 9a; or aperture of the cochlear fossula as in the Höövör petrosals) is of similar length, width, and perimeter in all three stem therians described here.

The impression of the scala tympani on the cochlear endocast (Fig 10) is confluent with the fenestra cochleae and aquaductus cochleae. It is visible in the stem therian endocasts as a medial inflation of the cochlear canal, delimited ventrally by the base of the bony secondary lamina ("sl" in Fig 10). The posterior margin of this space is further inflated

as it meets the anterior margin of the cochlear fossula in the Höövör petrosals [56,57,62]. However, because of the lack of a tractus foraminosus, Rosenthal's canal (spiral ganglion canal), or primary bony lamina in these taxa, the scala tympani does not leave recognizable anterior and dorsal boundaries on the cochlear endocast. The choice of interpretation as to the presence or absence of a vestigial lagenar macula also greatly influences the inferred placement of the scala tympani in the apical areas of the cochlear endocast.

In these relatively short straight cochlear endocasts, the impression of the scala tympani has the profile of a right triangle when viewed ventrally, with the anterior rim of the fenestra cochleae/perilymphatic foramen and the secondary bony lamina forming the triangle's two perpendicular limbs. The hypotenuse of this triangle is formed by the medial contour of the cochlear endocast, which in the Höövör petrosals is also the location of a half-pipe shaped sulcus (i.e. a cylindrical prominence on the endocast; "hs" in Fig 10b,c), that originates immediately anterodorsal to the cochlear fossula. In *Priacodon*, damage to the rim of the perilymphatic foramen hinders the reconstruction of the endocast here ("*" in Fig 9b). However, it can be confirmed that there is no vascular sulcus along the medial margin of its cochlear canal (Fig 10e,f). Consequently, for *Priacodon* the medial hypotenuse of the triangle slopes anterolaterally more steeply than in the Höövör petrosals, causing the impression of the scala tympani to be limited to the proximal half of the cochlear canal (Fig 10e,f). In the Höövör petrosals the hypotenuse of the triangle has a much more gradual slope, causing the impression of the scala tympani to terminate more distally (approximately three quarters of the length along the cochlear canal). Distally, the impression of the scala tympani in the Höövör petrosals also shows a round secondary inflation, that interrupts the otherwise smooth lateral slant of the hypotenuse representing the medial contour of the cochlear canal. The half-pipe shaped medial sulcus is more distally extensive in H2 than H1,

and can be followed along the complete length of the impression of the scala tympani. In H1 the medial sulcus loses distinction approximately half way along the length of the impression of the scala tympani, proximal to its slight terminal inflation.

In both Höövör petrosals (Fig 10a-d) the proximal commencement of the half-pipe shaped medial sulcus within the impression of the scala tympani is confluent with the emergence of two tubular structures from the cochlear endocast. The anterior tubular structure is a small venous canal that, for reasons outlined below, is inferred to have contained the "Vein on the Cochlear Aqueduct" ("vcaq" in Figs 8a,b,e,f and 10a-d; [71] also see [55]), and is therefore homologized with the bony "Canal of Cotugno" [72]. In some therians this canal follows a tortuous mediolateral trajectory to contact the inferior petrosal sinus (Figs 11-13; [71]) which is likely to represent the plesiomorphic condition for therians. In the Höövör petrosals, given the observed medial connectivity of this canal with a lateral diverticulum of the intramural inferior petrosal sinus, and its lateral continuity with the half-pipe shaped sulcus on the impression of the scala tympani (Fig 10a-d), it is very likely that this medial sulcus transmitted venous components as well. In modern therians structures in this region represent the sole (or major; see [73]) outlet of venous blood from the pars cochlearis, and provide a subsidiary role in draining the pars canalicularis (Fig 13a, b and c). In the Höövör petrosals the half-pipe shaped medial sulcus on the impression of the scala tympani would then contain the homolog of what is the common cochlear vein (or one of its ramifications) in extant therian mammals.

Fig 11. Ventral view of comparative mammalian specimens. a, b *Erinaceus*; c, d *Didelphis;* e, f *Ornithorhynchus*. All specimens are left-sided, venous sinuses are not shown. In e, f a fragment of the exoccipital bone is synostosed to petrosal. Medial is toward the left, rostral is toward the top of the page. All scale bars are 1 mm. Refer to list of abbreviations in text for other abbreviations.

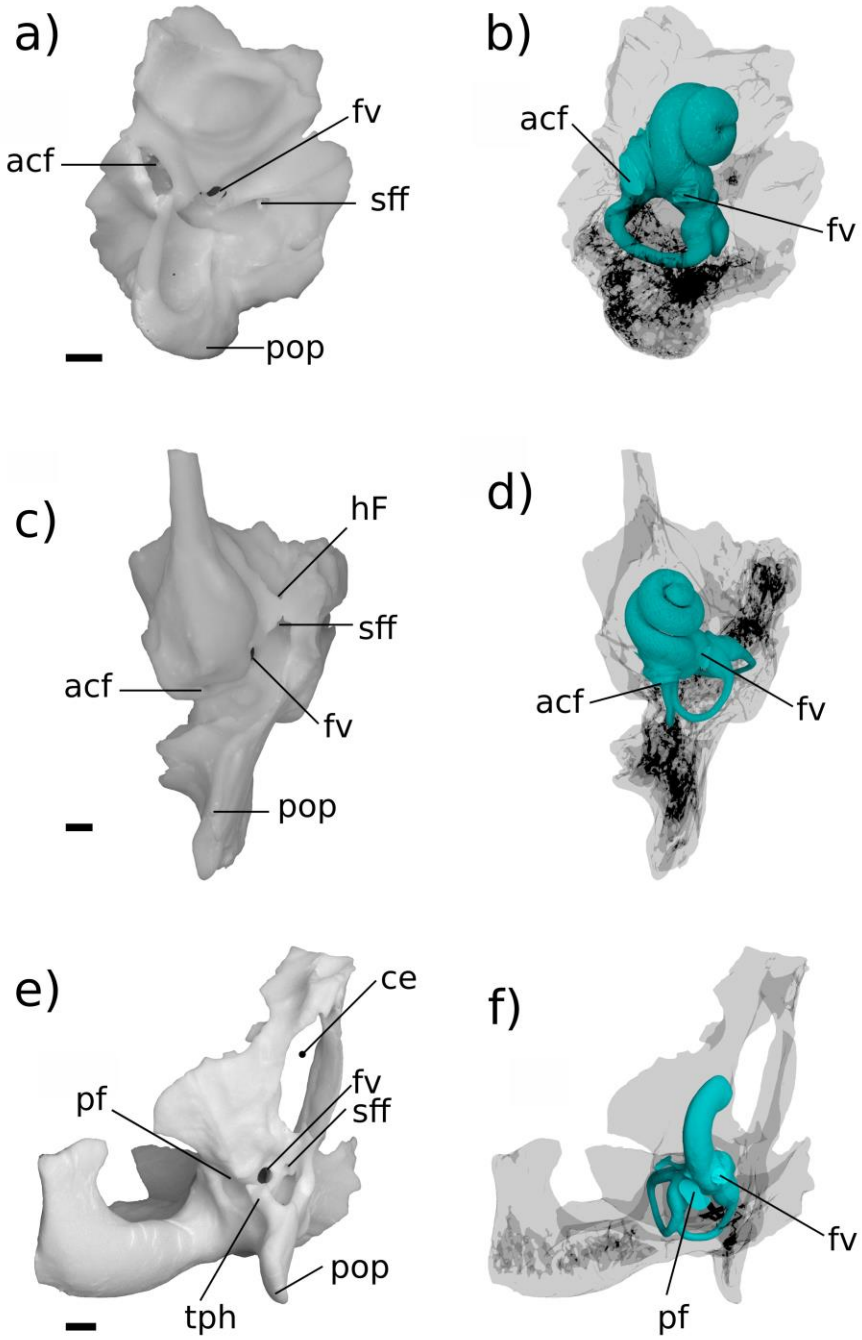

Fig 12. Medial view of comparative mammalian specimens. a, b *Erinaceus*; c, d *Didelphis*; e, f *Ornithorhynchus*. All specimens are left-sided, venous sinuses are not shown. In e, f a fragment of the exoccipital bone is synostosed to petrosal. Rostral is toward the right, dorsal is toward the top of the page. All scale bars are 1 mm. Refer to list of abbreviations in text for other abbreviations.

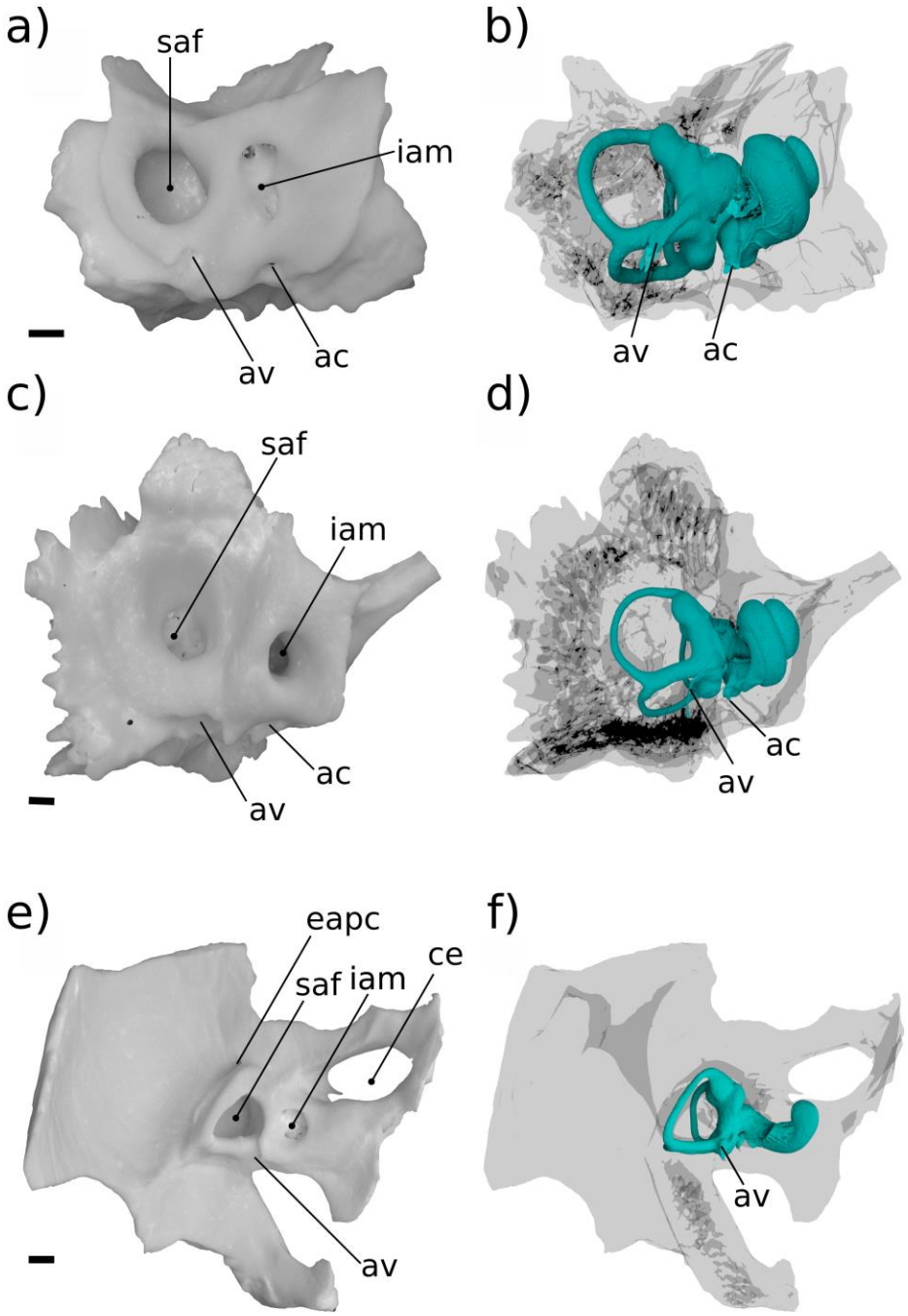

Fig 13. Medial view of cochlear endocast in crown mammals. All specimens are left-sided, vein of the cochlear aqueduct is shown in blue. a, *Dasypus*; b, *Erinaceus*; c, *Didelphis*; d, *Vincelestes*; e, Höövör petrosal 1; f, Höövör petrosal 2; g, *Ornithorhynchus*, h, *Priacodon*. All scale bars are 1 mm. Refer to list of abbreviations in text for other abbreviations.

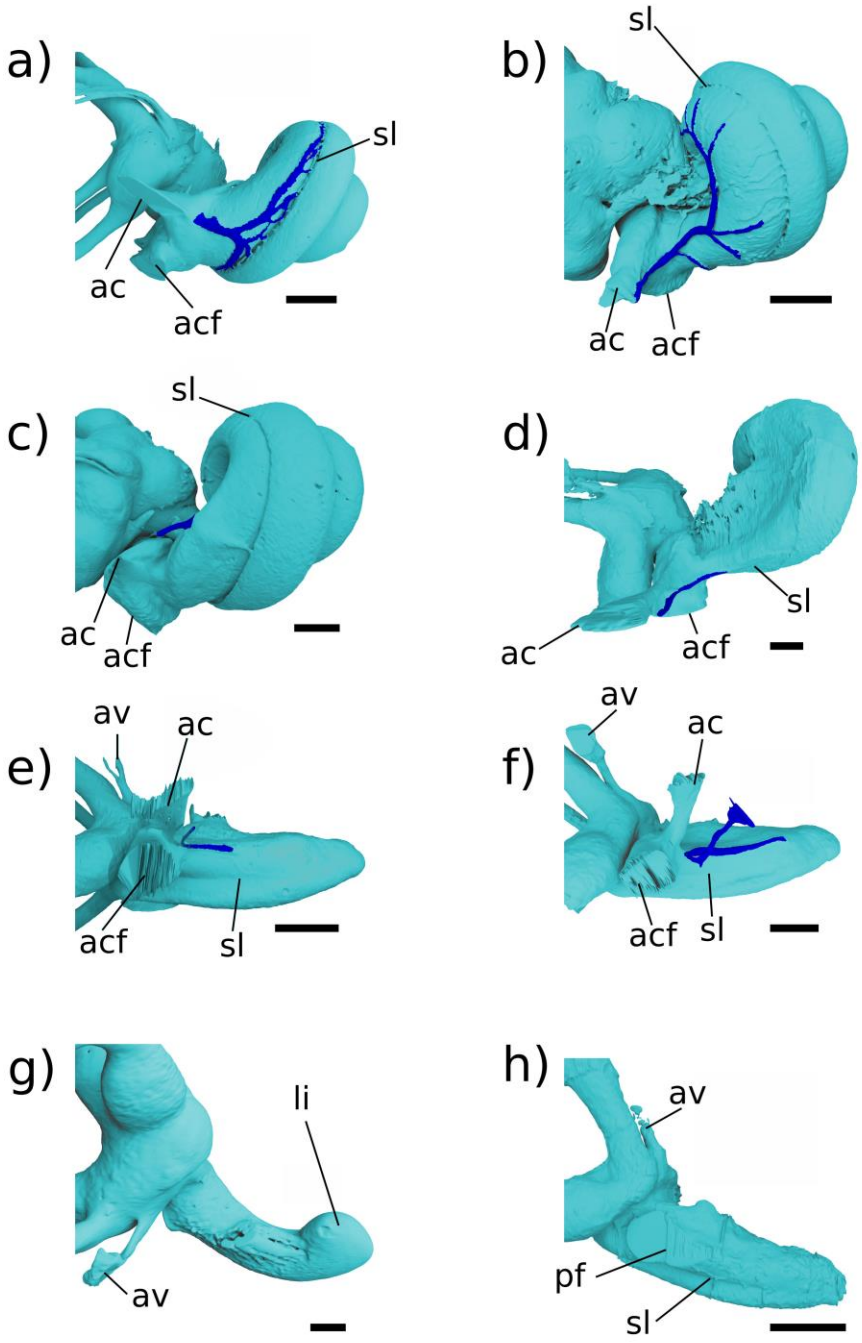

Assuming this inference of homology is correct, the fact that the impressions of these venous structures are so prominently expressed on the endocasts of the Höövör petrosals documents a localized increase in venous drainage along the abneural border of the cochlea. This localized increase of the intracochlear venous systems runs opposite to the general mammaliaform trend of reduction of the intrapetrosal venous system [54,74]. A sizable cochlear vein may be a response to the increasing metabolic demands of the cochlear apparatus itself. In particular, this neomorphic drainage may be an evolutionary reaction to the increasing energetic and electrolyte requirements of the enlarging stria vascularis. As summarized in the discussion section, the stria vascularis is responsible for generating and maintaining the highly positive endolymphatic potential in modern therians [2,75-77]. In the extant mammals in which it has been studied it is also an organ with a complex development, recruiting epithelial and connective tissue contributions from cranial ectomesenchyme and other neural crest cell populations [78].

Because the stria vascularis is a noted feature seen in all crown mammals including monotremes, the first appearance of bony correlates of venous structures servicing this organ in therian ancestors is likely a consequence of the closer impingement of the bony cochlear canal on to the stria vascularis and membranous cochlear duct generally (Fig 14). However, given the observations originally made by [79] of a probable endolymph-producing capillary plexus within the thickened Reissner's membrane of *Ornithorhynchus* (the plesiomorphic condition for amniotes), the impressions of neomorphic veins draining the pars cochlearis in the Höövör petrosals may represent a wider evolutionary reorganization of the vascular pattern of the cochlear apparatus. The "modern therian" form of cochlear endolymph production, is accomplished solely through secretion by a highly active stria vascularis (Fig 14b-e), with the arterial supply and venous return of blood servicing this

organ incorporated into the walls of the scala vestibuli and scala tympani of the cochlear canal, respectively [29,30]. Conversely, the vascular branching within Reissner's membrane seen in *Ornithorhynchus*, closely matches the position and morphology of a similar plexus in modern sauropsid amniotes [25]. In both monotremes and sauropsids the arteries and veins supplying the cochlear duct, Reissner's membrane, and in monotremes the stria vascularis, are embedded within the membrane of the cochlear duct [25,79]. These intrinsic vessels of the cochlear duct enter and leave the bony cochlear canal through the foramen for the cochlear nerve. This contrasts with the separate bony foramina in the therian cochlear duct for the entrance of the labyrinthine artery and exit of the vein of the cochlear aqueduct. Where studied, non-mammalian amniotes also lack a strong endolymphatic potential and the stria vascularis; it is possible that this is similar to the condition in monotremes, but the endolymphatic potential in these mammals is still unknown [80-84].

Fig 14. Schematic diagram showing hypothesized character states present in a cross section of the cochlear canal in early crown mammals and their fossil relatives. a, condition similar to that seen in sauropsid amniotes and hypothesized in eucynodonts; b, condition seen in modern monotremes; c, condition seen in *Priacodo*n and hypothesized in early stem therian mammals; d, more derived stem therian condition seen in the Höövör petrosals; e, condition seen in modern crown therians, e.g. *Homo*. At upper right is a medial view of the labyrinthine endocast of *Tachyglossus*, showing location of section diagrammed in b. **N**, neural; **AB**, abneural. Refer to list of abbreviations in text for other abbreviations.

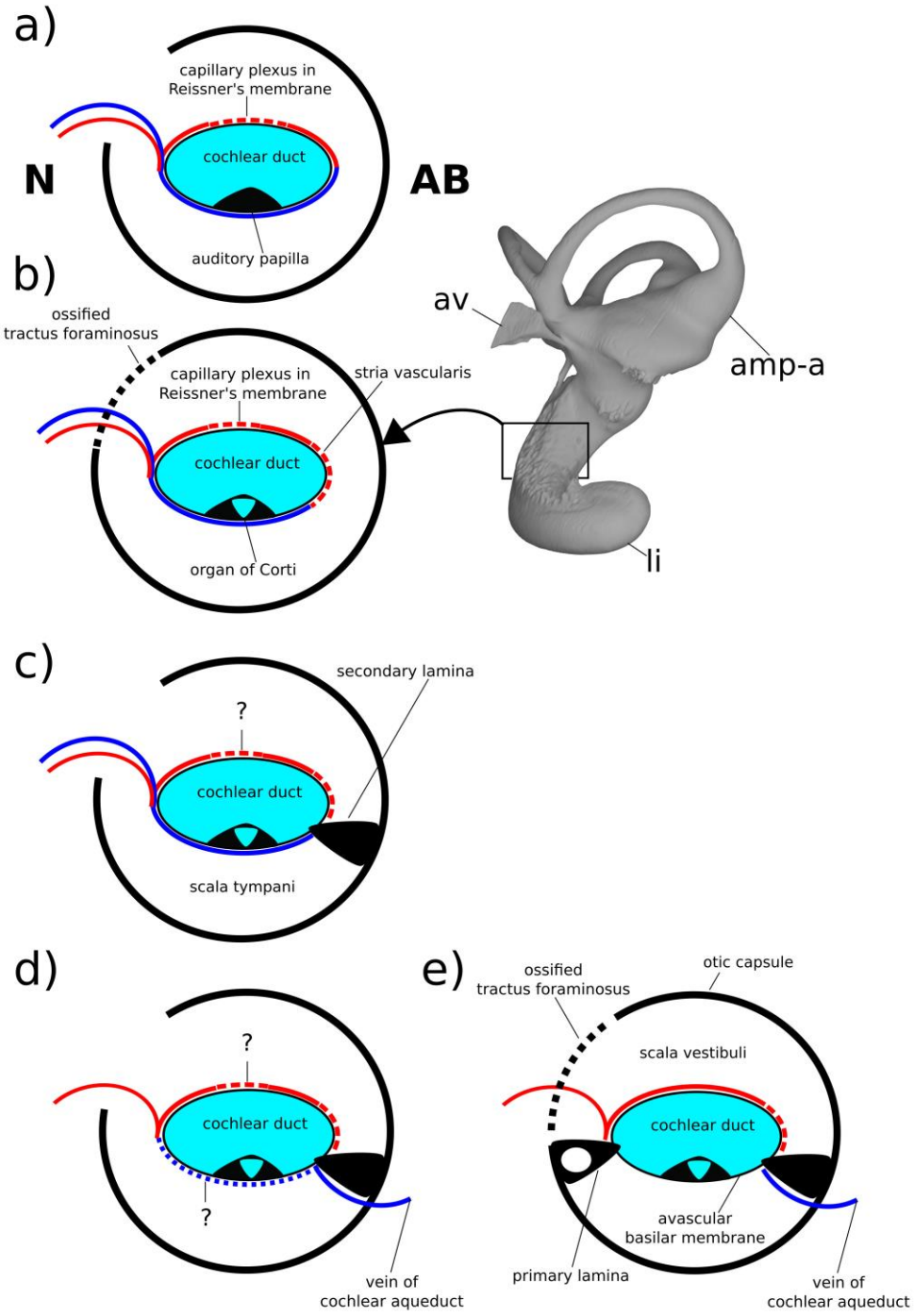
a)
capillary plexus in
Reissner's membrane
cochlear duct
N
AB
auditory papilla
b)
av
amp-a
ossified
tractus foraminosus
capillary plexus in
Reissner's membrane
stria vascularis
cochlear duct
organ of Corti
li
c)
secondary lamina
?
cochlear duct
scala tympani
d)
?
cochlear duct
?
vein of
cochlear aqueduct
e)
ossified
tractus foraminosus
otic capsule
scala vestibuli
cochlear duct
avascular
basilar membrane
primary lamina
vein of
cochlear aqueduct

The appearance of a clear intersection of the circumpromontorial venous plexus with the endocast of the cochlear canal in the stem therian lineage (Fig 10a-d), and the localized enlargement of venous structures solely along the abneural side of the cochlear canal (the location of the stria vascularis in modern therians; Figs 13-14) in fossils otherwise showing a reduced proliferation of circumpromontorial venous sinuses, suggests that the Höövör petrosals supported a cochlear apparatus that functioned more like those found in modern therians than modern monotremes or any other vertebrate taxon.

Many modern therian groups contain a prominent sulcus for the inferior petrosal sinus near the petrosal-basioccipital suture (also see [26,85] regarding the interpretation of petrosal sulci in general). In most crown therians the sulcus for the inferior petrosal sinus (sulcus sini petrosi inferior; [52]) is smoothly concave and exposed endocranially, and is floored ventrally by a medially sheet-like flange of bone (crista promontorii medioventralis) which usually meets the basioccipital at a sutural contact. In taxa with an intracranial inferior petrosal sinus (such as *Canis* or *Homo*; [29,86]), its exposure to the posterior cranial fossa is facilitated by the fact that the bony crest flooring the sulcus for the inferior petrosal sinus is much larger than the weaker ridge of bone dorsolateral to it. However, in the Mesozoic stem therians described here, and all known stem mammaliaforms, the two flanges of bone ventrally and dorsally enclosing the inferior petrosal sinus are subequally developed, and both likely contributed to the sutural contact with the basioccipital medially [54]. Additionally, in these Mesozoic forms the space accommodating the inferior petrosal sinus itself is not a smoothly and consistently surfaced sulcus, but is an elongate confluence of a highly ramified network of venous sinuses that form a substantial proportion of the total volume of the pars cochlearis.

The extent of venous excavation within the pars cochlearis has been remarked on in many prior descriptions of the petrosal morphology in Mesozoic mammalian and advanced cynodont fossils ([27,70,87,88] inter alios); and this anastomotic network together with the intramural inferior petrosal sinus has been conceptualized broadly as the circum-promontorial sinus plexus by [32]. However, only with the recent availability of high resolution micro-CT imaging (particularly [31]) has the morphology and connectivity of this venous network been sufficiently characterized so as to allow for the comparison of its discrete and homologous structures. The present report corroborates the existence of the discrete tubular "trans-cochlear sinuses" originally described by [31] ("eps-p" and "hps" in Figs 6d, 7b,d, 8a,c and 9a,b), and demonstrates their phylogenetic distribution outside of the clade Docodonta. The general reduction of the venous versus sensorineural contributions to the overall volume of the promontorium in successively more nested clades within Mammaliaformes has also been remarked on by [88] among other sources. However, despite the relatively prolific extent of venous excavation of the pars cochlearis in stem mammaliaforms, these forms show few if any clear intersections of the circumpromontorial venous plexus with the endocast of the cochlear canal (e.g. Fig 7d). Because of the imperfect preservation of the stem therian petrosal sample used here, the precise ratio of venous to labyrinthine space within these specimens cannot be quantified; however, it is still apparent that the anatomical extent of venous proliferation in *Priacodon* is greater than that seen in either of the Höövör petrosals, matching phylogenetic expectations.

Despite having the greatest proliferation of venous structures in the pars cochlearis, the *Priacodon* specimen shows no intersection of the circumpromontorial venous plexus with the cochlear endocast (Figs 7d and 14c). This absence may ostensibly be an artifact of preservation because of the highly fractured nature of the specimen, especially along the

medial surface of the petrosal where a structure such as the canal of Cotugno would be suspected ("*" in Fig 9b). However, since *Priacodon* shows consistently large-diameter distributary branches of the inferior petrosal sinus running tangentially to the cochlear canal near the perilymphatic foramen (Fig 9a,b), and lacks branches oriented radially towards the cochlear canal or a half-pipe shaped groove for venous structures on the cochlear endocast itself, it is reasonable to suspect that the venous reservoir within the petrosal of *Priacodon* had no direct confluence with the vessels servicing the interior of the cochlear canal. This pattern of connectivity is probably consistent with the lack of an additional drainage of venous blood seen in monotremes, suggesting that the veins draining the cochlea parallel the course of the labyrinthine artery and most likely empty endocranially into the basilar venous plexus (similar to sauropsids) [25,89].

In *Priacodon*, as in the docodont *Borealestes* described by [31], a large proportion of the circumpromontorial sinus plexus is formed by tubular "trans-cochlear" sinuses (Fig 15; I suggest a different terminology for these structures below). In this report, I choose to refer to these venous structures running dorsal to the cochlear canal as epicochlear sinuses, to emphasize their dorsal position. These sinuses show no anatomical association with the contents of the cochlear canal and likely form venous anastomoses between several of the larger veins that leave the ventral braincase. In *Borealestes* (Fig 15a) the two epicochlear sinuses both run mediolaterally within the pars cochlearis dorsal to the cochlear canal, and are termed the anterior epicochlear sinus ("trans-cochlear sinus a" in [31]) and posterior epicochlear sinus ("trans-cochlear sinus p" in [31]). The anterior epicochlear sinus in *Borealestes* connects the inferior perosal sinus medially to a large venous foramen within the cavum supracochleare laterally. In [31] it is hypothesized that because of the enlarged secondary facial foramen in *Borealestes* a neomorphic continuation of the anterior epicochlear

sinus may have left the ventral cranium with the hyomandibular branch of the facial nerve. In *Priacodon* (Fig 15b,c) there are several large tubular venous structures running laterally from their confluence with the inferior petrosal sinus. However, because none of these structures could have provided a conduit for a vein connecting the inferior petrosal sinus to the cavum supracochleare (in addition to the generally small space available for the geniculate ganglion), it is likely that a venous structure homologous to the anterior epicochlear sinus (as seen in [31]) did not exist (Fig 6d). However, the posterior epicochlear sinus, which in *Borealestes* forms a confluence between the inferior petrosal sinus and the prootic sinus, does have a clear anatomical homologue in *Priacodon* based both on its orientation and connectivity. The posterior epicochlear sinus in both of these taxa traverses the pars cochlearis dorsal to the cochlear canal, within the bone flooring the incipient internal acoustic meatus (Fig 15a,b). Specifically, the posterior epicochlear sinus runs within the bar of bone separating the foramen (*Borealestes*) or foramina (*Priacodon*) transmitting the branches of the vestibular nerve ("2-3" in Fig 6c) from the other contents of the internal acoustic meatus (the primary facial foramen and foramen for the cochlear nerve; "1" and "4" in Fig 6c, respectively).

Fig 15. Schematic showing morphology of internal acoustic meatus in stem therians. Illustrations and renderings of left-sided internal acoustic meatus from endocranial view. Anterior is toward the right dorsal is toward top of page. a, condition in the docodont *Borealestes* and hypothetically all early mammaliaforms; b, c condition in *Priacodon* and hypothetically many early stem therians; d, e condition in Höövör petrosal 1; f, g condition in Höövör petrosal 2; h, i condition in extant therian mammals (e.g. *Erinaceus*). Character states in d-i are more morphologically derived than in *Priacodon*.

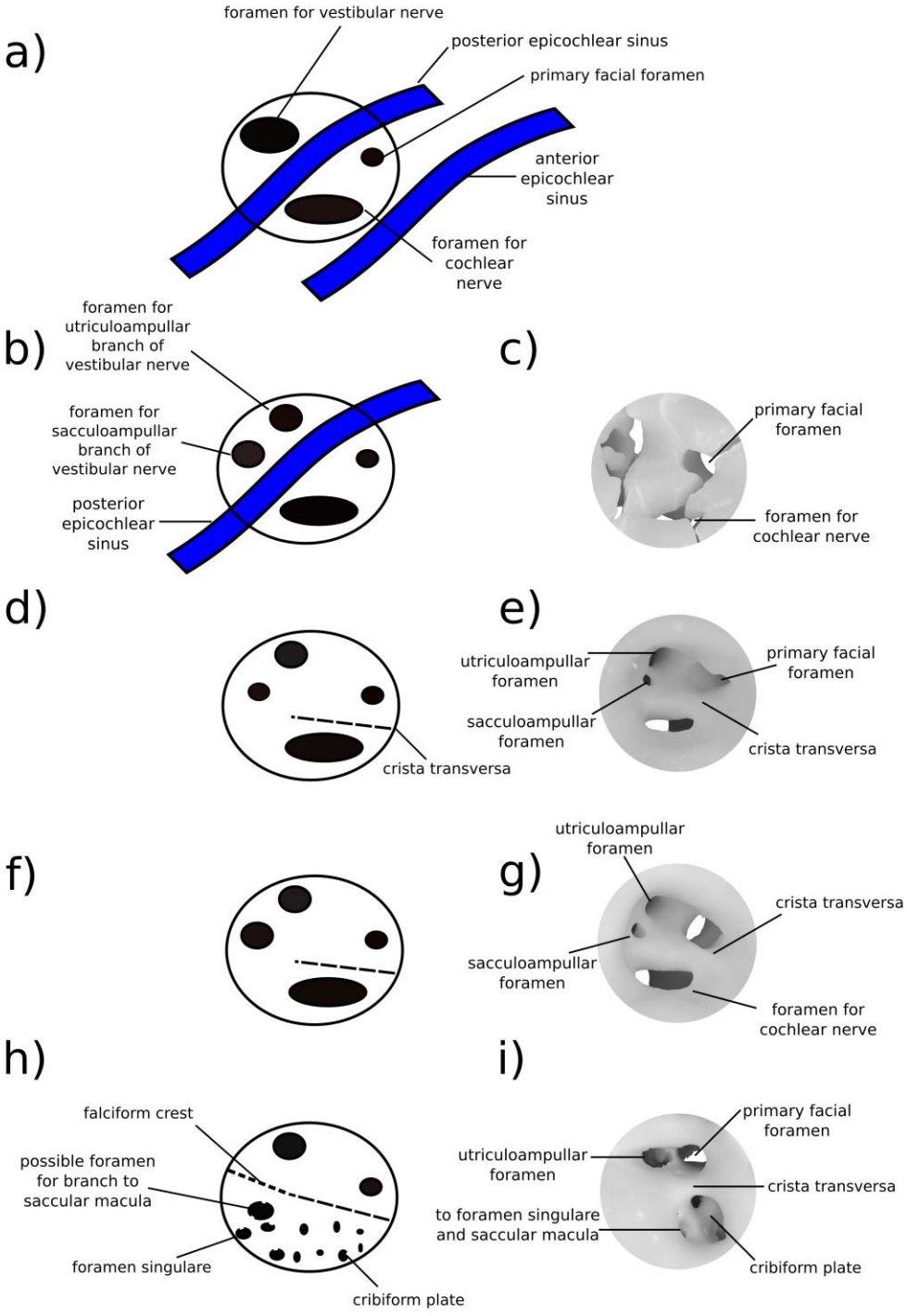

In *Priacodon* there is an additional "trans-cochlear sinus" running ventral to the cochlear canal, which is not seen in *Borealestes* ("hps" in Figs 7d and 9b). This sinus interconnects the inferior petrosal sinus with the same small aperture near the prootic canal as the posterior epicochlear sinus. While not present in *Borealestes*, this sinus is likely a plesiomorphic feature in many mammaliaforms given its presence in *Morganucodon* (as noted in an abstract by [90]) and in the first Höövör petrosal (Figs 7b and 8a,c), i.e. taxa both closer and more phylogenetically distant to crown therians than *Priacodon*. It is here termed the hypocochlear sinus (Figs 7b and 8a,c).

The hypocochlear sinus is the only "trans-cochlear" sinus shown by H1 (Fig 7b, and 8a,c), and there is noticeably less venous proliferation within this specimen compared with *Priacodon*. However, despite the overall reduction of venous sinuses in H1, as mentioned above, the localized hypertrophy of a neomorphic vessel (within the bony canal of Cotugno) connecting the inferior petrosal sinus with the abneural cochlear wall forms an intersection of the circumpromontorial plexus with the cochlear endocast. This kind of intersection is not seen in *Priacodon* (Fig 7c,d) or any known stem mammaliaform taxa. Additionally, because of the longer extent of the prootic canal in H1 compared with *Priacodon*, there are a greater number of discrete venous branches draining into (or connecting with) the prootic canal than seen in *Priacodon*, some of which form minor contacts with the cavum supracochleare and the hypocochlear sinus. Neither H1 or H2 show epicochlear sinuses dorsal to the cochlear canal (Figs 3d and 6b); the close approximation of the primary facial foramen and foramina for the utriculoampullar and sacculoampullar branches of the vestibular nerve leaves no space available for these venous structures (Fig 15d-g). Finally, H1 shows a possible smooth fracture connecting the medial border of the cavum supracochleare and

laterobasal extent of the cochlear canal. Whether this fracture was facilitated by a pre-existing region of highly vascularized bone is uncertain, but seems likely.

In H2 circumpromontorial venous proliferation is much less extensive than in that seen in H1 (Figs 3 and 4 versus Figs 6b and 7b), and there is no consistently wide tubular connection between the inferior petrosal sinus and prootic sinus within the pars cochlearis (Figs 3b and 4b,d). This causes a greater degree of separation to exist between the venous sinuses on the medial and lateral borders of the petrosal; even though, with higher resolution micro-CT imaging, a large number of very small anastomotic connections between the prootic canal and inferior petrosal sinus do exist. As in H1, there is a discrete sinus surrounding the prootic canal, that sends out a number of small (presumably venous) interconnections to the cavum supracochleare and area around the fenestra semilunaris (Fig 3b,d). There is also a separate dorsoventrally oriented foramen located near the cochlear fossula and jugular notch, that has apertures on both the endocranial and tympanic sides of the petrosal ("*" in Fig 3a and visible in 4c). This small canal is also confluent with the inferior petrosal sinus anteriorly, and most likely transmitted a small anonymous vein or small nervous branch; however, this foramen was incorrectly assumed to be the tympanic aperture of the perilymphatic canal in [5]. The posteromedial part of the cochlear fossula also shows several small (too small to be rendered in using the available micro-CT data) venous intersections with terminal tributary branches ventral to the cochlear canal. However, there are no "trans-cochlear" sinuses ([31]) anywhere within the pars cochlearis of H2, similar to the condition in modern therians and adult monotremes (e.g. Fig 9d-f; [54]).

Endocast Preserved in Pars Canalicularis

The portions of the labyrinthine endocast infilling the pars canalicularis in the stem therians reported here are broadly similar in morphology and most linear dimensions and angles (see Table 1; [91]). Of the morphological features differentiating these endocasts, especially those existing between the two Höövör petrosals, the majority are minor differences that do not rise above the level of what is commonly intraspecific variation. The remaining distinguishing features, generally support the more derived vestibular condition of the Höövör petrosals (Fig 10; [24]).

Table 1. Vestibule measurements of stem therian petrosals. All distance measurements are in millimeters, angle measurements are in degrees.

	Höövör 1	Höövör 2	*Priacodon*
Straight length of cochlear canal: from posterior saccule inflection behind fenestra vestibuli to tip of cochlea (mm)	4.357	4.38	3.66
Length of secondary bony lamina from saccular bulge behind fenestra vestibuli (mm)	2.57	2.69	NA
Anterior Semicircular Canal Height (ASCh SZ95)	2.48	NA	NA
Anterior Semicircular Canal Width (ASCw SZ95)	2.56	NA	NA
Length of primary common crus (mm)	1.95	NA	1.84
Posterior Semicircular Canal Height (PSCh SZ95)	1.73	NA	1.27
Posterior Semicircular Canal Width (PSCW SZ95)	1.62	NA	1.34

Horizontal Semicircular Canal Height (LSCh SZ95)	1.70	NA	1.12
Horizontal Semicircular Canal Length (LSCw SZ95)	1.79	NA	1.19
Length of impression of scala tympani: from front edge of the fenestra cochleae (or perilymphatic foramen) (mm)	2.15	1.96	NA
Angle Between Ant-Post SSC (degrees)	89.29	NA	100.47
Angle Between Ant-Hoz SSC (degrees)	73.30	NA	79.04
Angle Between Post-Hoz SSC (degrees)	95.26	NA	95.38

SZ95 – Measurement from [91]

This is apparent from the thinner diameter and more exaggerated loop of the semicircular canals, especially the anterior semicircular canal, which are both longer and wider in the first Höövör petrosal than in *Priacodon* (Fig 10c-f). The anterior semicircular canal in the Höövör petrosals seem to be extended relative to the other canals by the endocranial invagination of the subarcuate fossa into the endocranial space circumscribed by the anterior semicircular canal ("saf" in Figs 3c and 6a,c). In H2, it is also apparent that the subarcuate fossa forms a medial diversion that also projects within the circumference of the posterior semicircular canal as well. Because of damage to the posterodorsal portion of the pars canalicularis in the second Höövör petrosal (Figs 3c and 10a,b), it is not certain if the configuration of the semicircular canals is even more elongate than in H1, however it is still apparent that H2 is much more similar to H1 than *Priacodon* (Fig 10e,f). Both Höövör specimens also show a relatively more inflated bony recessus ellipticus [92] for the utricular

macula ("re" in Fig 10b,d,f). Conversely *Priacodon* shows greater similarity to H1 compared to H2, extant monotremes, and *Erinaceus,* by its greater projection of the posterior apex of the recessus sphericus (for the saccular macula) caudal to the posterior wall of vestibule ("rs" in Fig 10).

The canalicular endocast of H1 (and likely H2 as well) is unlike previously described Mesozoic dryolestoids [7,8,63] and more similar to *Priacodon* in that the arc of the horizontal semicircular canal is regularly circular, with their height and width being approximately equal. Strangely, the lateral (horizontal) semicircular canal in *Priacodon* is arguably apomophic compared to the condition seen in the Höövör specimens because of an anteriorly projecting (centripetally pointing) conical diverticulum in the horizontal semicircular canal placed within the inner contour of the canal ("cdh" in Figs 9c and 10e). Additionally, the lack of a secondary common crus ("cc-s" in fig 10c,d; a feature likely to be plesiomorphic for mammaliaforms generally; [63]) in *Priacodon* may also represent a derived trait in this taxon.

The height of the primary common crus ("cc-p" in Fig 10b,d,f; the bony confluence of the anterior and posterior semicircular canals) is also similar between *Priacodon* and H1. The aqueductus vestibuli ("av" in Fig 10b,d,f; the bony accommodation for the endolymphatic duct) is similar in size between H2 and *Priacodon* (~0.1 mm in diameter), even though it appears relatively larger compared to other tubular structures present in *Priacodon*. The paravestibular canaliculus (the bony accommodation for the vein of the vestibular aqueduct, the main veinous drainage for the pars canalicularis, contributing blood to the sigmoid sinus in humans and probably most other amniotes; [29,30]) joins the aqueductus vestibuli along its proximal half in H1 and H2, but remains separate along its entire length in *Priacodon* where it directly intersects the dorsal surface of the vestibular endocast (Fig 10).

While this is a salient difference visible in the high resolution images of stem therian endocasts used in this study, the polarity and distribution of this character are difficult to evaluate given the lack of sufficiently high resolution information for most Mesozoic petrosal specimens and the variable connectivity of the paravestibular canaliculus among extant mammals; i.e., the canaliculus can be seen to join the vestibular aqueduct proximally in *Ornithorhynchus*, *Tachyglossus*, and *Erinaceus*, but remains separate to the base of the vestibular labyrinth in *Dasypus and Didelphis*.

The angle formed by the intersection between the planes of the anterior and posterior semicircular canals is however significantly more plesiomorphic in *Priacodon* than in H1 (the only Höövör specimen for which this can be measured reliably). As reported by [92,93], a range of angles between 103°-157° between the planes of the anterior and posterior semicircular canals is typical of non-mammalian therapsids, and the ~100° angle measured in *Priacodon* is much closer to this range than it is to the range of values (~90° and smaller) typifying multituberculates and extant small mammals [92,93]. The ~89° angle seen in H1 is however within the range seen in extant therian mammals [92].

Two areas of the pars canalicularis in all three stem therians specimens show localized venous excavations (Figs 3, 4, 6 and 7). One of these sinuses, located in the posteroventral portion of the pars canalicularis and extending into the mastoid process, has been termed the paroccipital sinus by [31] ("pos" on Fig 7b,d). The greater extent of this structure in H1 than H2 is likely related to the better preservation in this specimen and the apomorphically large paroccipital process in this taxon (Fig 7b). A separate venous sinus arcs dorsal to the anterior semicircular canal, and is termed here the subarcuate sinus ("sas" in Figs 6b,d and 9e). I consider these regions of abundant, smooth-walled, interconnected cavities to be venous sinuses because 1) I do not see any confluence with the middle ear

airspace whereby these sinuses could be pneumatized; and 2) even though these sinuses are only localized enlargements of the wider cancellous bony fabric of the interior petrosal structure, venous blood (as opposed to oxygenated arterial blood) is the major constituent of the spaces between bony trabeculae generally. As with other venous structures in the pars cochlearis, these venous sinuses are least developed (and may be missing altogether) in H2.

Discussion

Estimating the neurosensory capabilities of any group of non-model organisms is necessarily more complex and error prone than research using humans or traditional animal models. These problems are compounded when analyzing fossil material, due to the obvious lack of relevant soft tissues and inability to work in an experimental paradigm. These complications do not decrease the unique value of fossil taxa in the study of mammalian nervous systems, however [94-96].

Because of the complexity and variety of evolutionary and neurobiological concepts involved, this discussion section begins with a summary of the auditory features of Mammalia and several consecutively nested subclades of therian relatives. Our hope is that this will provide a relevant paleontological, morphological, and neurobiological background to interpret the petrosals described above (see Fig 16). Supplementary Material 1 provides a longer review of prior research on the internal and external morphology of the periotic region in Mammalia and several more inclusive groups of terrestrial vertebrates, which may provide a useful introduction to the paleontological

Fig 16. Cladogram showing consecutively nested clades referred to in discussion.

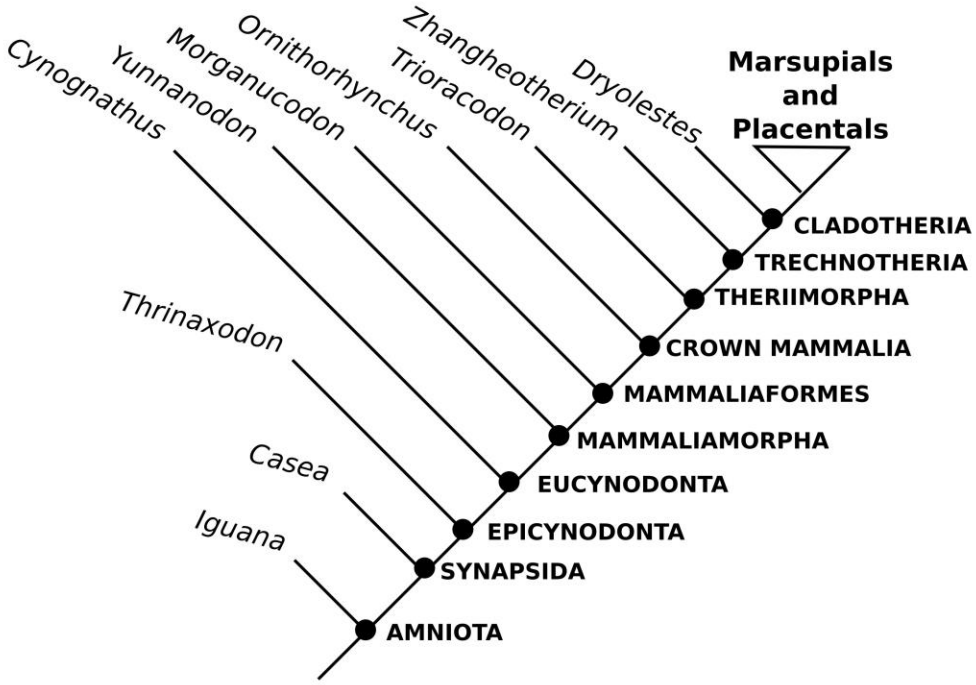

Mammalia

The characterization of the crown mammalian ear solely from the morphology of extant taxa would provide a markedly distorted reconstruction of the mammalian common ancestor compared to what is known from modern paleontological evidence. This is because of the over 150 million years of independent transformation seen in both living mammalian lineages (monotremes and therians), making extant mammals an unrepresentative sample of mammalian diversity as a whole; and because of the homoplasy seen in the evolution of petrosal structures [36,68]. Based on the distribution of characteristics within fully adult extant mammals only, one could reasonably conclude that the condition of the crown mammalian common ancestor consisted of 1) a Detached Middle Ear (DME), with auditory ossicles fully independent from the lower jaw apparatus, and 2) an osseus armature for the distribution of the cochlear nerve axons termed the tractus foraminosus ("tf" in Fig 9d,f; creating the perforated cribriform plate within the internal acoustic meatus). However, recent fossil discoveries strongly suggest the convergent acquisition of these traits ([68,97], also see [98]).

The base of the secondary bony lamina is variably present in monotremes [18] and now seen in a more elongate state in *Priacodon* (Fig 10e), suggesting that some development of this structure may have been a derived feature of mammals in general (Figs 13g,h and14b,c; although according to [18] in monotremes the base of the secondary lamina does not contact the basilar membrane). Of greater significance for the reconstruction of auditory capacities in early mammals are soft-tissue characteristics, many of which must be inferred based on their distribution in extant taxa. This heavy reliance on soft tissue for reconstructing past auditory ability highlights the importance of our models; i.e. it is difficult

to predict in extinct forms functional or physiological traits that are not readily available in living representatives. These considerations suggest that the mammalian ancestor contained a secondary tympanic membrane (a membrane interface between the airspace of the cavum tympani and liquid-filled subarachnoid space, [62]), that was not at this stage completely suspended by a bony frame (such as the round window that formed in later mammals; "fc" in Fig 8e). As such the secondary tympanic membrane is a symplesiomorphy in crown mammals, and its suspension within a round window is a derived condition only within more nested members of this group. Several other soft-tissue symplesiomorphies in the mammalian ancestor are the retention of the lagenar macula and a membranous endolymph producing vascular plexus (both seen in Reissner's membrane in monotremes today; [79]). These soft-tissue components of the cochlear duct were complemented by the presence of the stria vascularis, a specialized endolymph secreting organ (Fig 15b-e), that developed within the synapsid lineage sometime before the divergence of the modern mammalian clades.

Most importantly, the mammalian common ancestor can be reliably inferred to have attained a true organ of Corti, the morphologically distinctive homolog of the amniote basilar papilla. The organ of Corti is diagnosed by the functional differentiation and separation of two subgroups of auditory hair cells along an axis perpendicular to the axis of tonotopy [17,99]. This division of labor between the less derived and more afferently innervated Inner Hair Cells (IHCs) on the neural side of the basilar membrane, and more specialized and efferently innervated Outer Hair Cells (OHCs) on the abneural side of the basilar membrane, is a fundamental component of macromechanical tuning [100,101], the characteristic tuning present in mammals. In therian mammals the functional specialization of OHCs to amplify weak (i.e. quiet) or dampened pressure waves propagating along the

cochlear canal is implemented through the action of an apomorphic reverse transduction mechanism [2,101]. Possibly correlated with this adaptation is the lack of evidence for non-macromechanical forms of frequency resolution (the electrical or micromechanical forms of cochlear tuning; see Supplementary Material 1) in mammalian cochlear function ([14]; although for evidence of a possible minor role of a micromechanical active processes in some mammals see [102,103]).

The segregation of two sub-populations of auditory hair cells is delimited morphologically by a patent tunnel of Corti running longitudinally within the endorgan, and specialized populations of non-sensory supporting cells within the cochlear epithelium. Additionally, the mammalian common ancestor seems to have also defined the relative allometric size of the combined auditory hair cell population, with extant monotremes and similarly sized therian mammals (dogs, cats, etc.) having a similar total number of these cells [104]. However, the relatively much more elongate and organized organ of Corti seen in modern therians creates a thinner and longer distribution of the auditory hair cells, compared to monotremes.

It is unclear how innovative these soft tissue characteristics are to the mammalian clade itself, and the organ of Corti and stria vascularis in particular are likely to have appeared at an earlier point in synapsid phylogeny, within Mammaliaformes if not earlier. It is therefore also unclear if the petrosal of the earliest crown mammals would be diagnostically recognizable from the petrosals seen in other early mammaliaforms such as *Hadrocodium* and *Morganucodon* (see [105] for two examples of this frustrating ambiguity). Finally, it is also unknown if the uniquely mammalian external ear, with its characteristic pinna structure, would have appeared within the crown mammalian ancestor, within other advanced synapsid taxa, or at some later point solely within the stem therian lineage. The

soft-tissue evidence for an involuted cartilaginous pinna in *Tachyglossus* reported by [106] is a possible homolog to the external structures seen in extant therians. Otherwise the phylogenetically deepest evidence for the presence of external pinnae is provided by *Spinolestes*, an excellently preserved gobiconodontid [107], and member of the diverse stem therian clade Theriimorpha.

Theriimorphans

The monophyletic group containing the carnivorous eutriconodonts, the more derived "acute symmetrodonts," and therian mammals – Theriimorpha – is the most inclusive well-supported group within the therian stem lineage [1,5,68,108]. Despite the relative abundance of excellently preserved fossil remains referable to early members of this group (such as *Spinolestes* mentioned above [107]), several authors have mentioned the relative lack of knowledge on the internal petrosal morphology in most members of this clade (e.g. [69,81]). However, the prior descriptions of external petrosal morphology in eutriconodonts [5,46], combined with the observations of the internal petrosal anatomy of *Priacodon* outlined above, suggest that basal theriimorphans can be characterized by a similar but slightly straighter morphology of the cochlear canal than the earliest mammaliaforms. This is reflected by the steeper lateral aspect of the promontorium in ventral view, and lack of an apparent apical inflation for the lagenar macula within the labyrinthine endocast (although in *Priacodon* the cochlear canal remains relatively untapered and thick to its apex).

The cochlear endocast of *Priacodon* (Fig 10e,f) also shows the first appearance of a elongate and projecting secondary lamina in early theriimorphs. In extant therians the secondary lamina is associated with tonotopic locations of the cochlea dedicated to hearing

above 10 kHz [15,109]. However, at the time of its first definite appearance in the theriimorph taxa described here, its functional significance is much less clear. Given that the secondary lamina appears without an opposing primary bony lamina or even tractus foraminosus to provide an opposing attachment for the basilar membrane, it seems unlikely that significant tension would be able to be transmitted across the scala tympani side of the cochlear duct. Additionally, as the variably present "base of the secondary lamina" in extant monotremes has been observed to lack a direct connection (histological adherence) with the cochlear duct when present [18], it is conceivable that the (much longer and wider) secondary lamina seen in *Priacodon* and the Höövör petrosals similarly lacked an association with the cochlear duct. For reasons outlined in the next section, this seems like an improbable scenario, especially for the Höövör specimens. However, even in *Priacodon*, arguably the most plesiomorphic stem therian for which internal petrosal structure is known, it seems likely that the large secondary lamina is a true homolog of the secondary lamina seen in Mesozoic cladotherians and modern therians. For example, the secondary bony lamina in *Priacodon* runs longitudinally onto the crista interfenestralis, that separates the fenestra ovalis and perilymphatic foramen (Figs 7c and 10e,f). This is essentially the same positional relationship seen in later cladotherian petrosals [109], suggesting that some association of the abneural side wall of the cochlear canal and the cochlear duct had begun to form even at this early stage in the stem therian lineage. Thus, while its role in the generation and transmission of tension across the basilar membrane may not have been as functional as in modern therians, the appearance of the large secondary lamina may still have served as a mechanism to better match the stiffness between the middle and inner ear [15], or as a means of stabilizing the position of the cochlear duct with respect to the larger cochlear canal.

The status of the middle ear on the other hand can be relatively well characterized in the theriimorph common ancestor, and has been confidently reconstructed as having attained the PDME character state [68] in the earliest forms. Interestingly, many members of this clade show the further calcification of Meckel's element which forms the structural attachment between the malleus and dentary; a peramorphosis possibly related to the continued reliance on the detection of seismic sound sources through direct conduction even after the mediolateral separation of the postdentary bones from the medial surface of the lower jaw [68]. The fortunate conversion of Meckel's element into a fossilizable structure therefore provides some possible evidence for the use of non-tympanic low-frequency sound conduction even after the attainment of a true middle ear. However, [110] have advanced arguments for why this element may not be homologous with the embryonic Meckel's cartilage: if so some of our consideration here would need to be nuanced, but the evidence for non-tympanic conduction is still defensible.

Trechnotheres

The clade Trechnotheria includes crown therians, the "acute symmetrodonts" (spalacotheroids and amphidontids), various "pre-tribosphenic" taxa (such as *Vincelestes* seen in Fig 13d), and the dryolestoids [36]. While this group is known from a considerable diversity of dental and postcranial remains, the description of Höövör petrosal 1 provided by [4] represents the first tentative information on the external petrosal anatomy in either a basal trechnothere or a closely related stem theriimorphan. The descriptions of the second Höövör petrosal provided here demonstrate several more derived features of H2, making it slightly more likely (but still not certain) that this specimen is referable to Trechnotheria.

However, because of the limited amount of information on mammals with this kind of petrosal organization, and possible close relatives of Trechnotheria (especially gobiconodontids) showing broadly similar features, the following characterization of the trechnotherian common ancestor can only be tentative at best.

Probably the most salient feature (if not synapomorphy) seen in the Höövör petrosals and other more confidently referred trechnotherians, is the formation of a true fenestra cochleae (round window) by the bony subdivision of the ancestral perilymphatic foramen (Figs 3a and 7a). This character has uncertain mechanical implications for the isolation and function of the cochlear apparatus. This process is a neomorphic bony strut that bifurcates the ancestral perilymphatic foramen, forming the elongate cochlear aqueduct (containing the membranous perilymphatic duct) dorsomedially and fenestra cochleae ventrolaterally (i.e. Fig 8e; [56,57]). The enclosure of the perilymphatic duct in a bony canal is also seen in some multituberculates and late adult tachyglossids [54], in addition to several groups of squamates and archosaurs [111]. As such the perilymphatic foramen is likely present in the mammalian common ancestor [62,111-113]. Therefore, only about one quarter of the bony "frame" of the round window (the edge of the processus recessus) can be considered an apomorphy; but its significance, if any, is at present unclear. The lack of exposure of a relatively long perilymphatic duct into the middle ear cavity may be considered as significant a transformation as that of the true round window because of its facilitation of a direct connection of the perilymphatic duct with the inner ear.

The most plesiomorphic trechnotherians [4,47,60] also show features related to the increased ventral extension of the pars cochlearis relative to the surrounding pars canalicularis and other cranial elements. These include the more vertical orientation of the crista interfenestralis which, as in the Höövör petrosals described above, terminates caudal to

the promontorium without contacting the mastoid area or paroccipital process. The area immediately caudal to the promontorium within the tympanic aspect of the pars canalicularis also forms a post-promontorial tympanic sinus, that is broadly confluent laterally with the lateral trough [54]. In trechnotheres the post-promontorial tympanic sinus increases the volume of the cavum tympani, thereby reducing the effective rigidity of the (primary) tympanic membrane [21]. As also seen in monotremes, the earliest trechnotherians also reduce or lose a robust quadrate ramus of the alisphenoid (epipterygoid), while retaining a thin lateral flange of the petrosal (the ancestral attachment of the quadrate ramus); and similar to several eutriconodontans, one early spalacothere shows a calcified Meckel's element [114].

Cladotheres

Defined as the clade containing the common ancestor of therians and the diverse Mesozoic group Dryolestoidea [115,116], a significant characteristic of Cladotheria is the dorsoventral coiling of the cochlear canal, above and beyond the initial lateral (abneural) curvature of the cochlear canal developed in early mammaliaforms [49]. This reconfiguration of the cochlear apparatus is expressed on the ventral surface of the pars cochlearis as the projecting bulbous morphology of the tympanic surface of the promontorium. The cladotherian common ancestor likely also attained a transpromontorial course of the internal carotid artery, as is evidenced by the sulcus left by this vessel on the pars cochlearis.

Ventral bulging of the promontorium is likely not the result of volume restrictions within the pars cochlearis, due to the variably incomplete filling of the bony space available within the pars cochlearis by the cochlear canal [8,63]. However, limitations in the relative

dorsoventral linear distance available to the cochlear canal within the pars cochlearis may be responsible for the evolutionary timing of the dorsoventral coiling, as the images described above (Figs 3,6,7) demonstrate that the progressive reduction and loss of the epicochlear and hypocochlear sinuses is a trend taken to near completion in the stem therian circumpromontorial venous plexus before the initiation of dorsovental coiling in cladotheres. It is however clear that basal members of Mammaliaformes and non-therian mammals have substantially more petrosal bone surrounding the cochlear endocast; while therians, have a closer cochlea-pars cochlearis fit.

While all previously described stem cladotherian petrosals from northern continents (i.e., dryolestoids [7,8,49,63] and possibly [105]) and the pre-tribosphenic mammal *Vincelestes* (Fig 13d; [27]) show at most 270° of dorsoventral coiling, cladotherian petrosals from Argentina [6,117,118] demonstrate that complete (360° and beyond) cochlear coiling was attained by later Mesozoic and Cenozoic stem cladotherian lineages in parallel to crown therians.

In Northern Hemisphere dryolestoids, complete cochlear coiling is not known to occur; however, the cochlear endocasts of *Henkelotherium* [7] and *Dryloestes* [8] demonstrate that the suspension of the basilar membrane between a true bony primary lamina and secondary lamina may have developed in these forms, also possibly in parallel to crown therians. In dryolestoids and therians, this increased contact between the endolymphatic cochlear duct and perilymphatic cochlear canal is thought to provide better impedance matching between the middle and inner ears [81], that may have allowed for adaptive increases in maximal detectable frequency. However, theoretical concerns outlined in [84,119] suggest that the gain in selectivity and sensitivity by the cochlear apparatus from these osteological features would be mainly limited to frequencies less than 20 kHz in

Mesozoic taxa, where a complete primary lamina is only present basally. The variable extent of cochlear coiling, and presence/absence of bony laminae, and their extent, make the restructuring of the cochlear canal difficult to interpret. However, all cladotherian taxa invariably show the presence of a neomorphic bony armature, termed the tractus foraminosus, for the individual distribution of cochlear nerve fibers and supporting tissues through the foramen acusticum inferius ([63]; although the presence of a tractus foraminosus is ambiguous in the specimen described by these authors). The presence of the foramen acusticum inferius itself, composed of the foramina for the cochlear and sacculoampullar branches of the vestibulocochlear nerve and their derivative and supporting structures, may also be a neomorphic feature of Cladotheria, or cladotheres and their closest trechnotherian relatives (Fig 15f-i).

Theria

With the advent of the crown clade Theria, mammals attained the most sophisticated form of airborne sound detection known among terrestrial vertebrates. Members of this clade are typically characterized by the capacity for the detection of ultrasonic frequencies [15]. These capacities are facilitated by the coordinated development of many osteological characters that have been widely commented on in the paleontological literature [24,68,69,120]. Prominent among these are the attainment of a DME, and the completion of at least one full whorl by the dorsoventrally coiled cochlear canal. The level of cochlear coiling in therians is also more derived than that seen in most other cladotheres because of the presence of a modiolar structure (bony armature for the spiraled cochlear nerve) within the concavity defined by the coiled cochlear canal. This morphology causes the peripheral

processes of auditory afferent neurons to take on a radial, as opposed to parallel, distribution [120]. However, despite the diverse literature on these and other osteological apomorphies, displayed by all species or particular subsets of crown Theria, precise functional implications of the bony structures of the therian middle and inner ear remain ambiguous [15,23].

Because of their representation by the majority of extant mammals, soft-tissue characteristics within the earliest crown therians can also be reasonably estimated. For instance, unique vascular features that can be inferred to have been present in the petrosal of the therian common ancestor (but likely appearing in their much earlier ancestors) include the almost-completely intracranial course of the superior ramus of the stapedial artery [12], and the loss of the post-trigeminal vein [12,28]. The progressive reduction and loss of the bony canal for the prootic sinus, and reduction of the lateral head vein are also an apparent trend in plesiomorphic members of both major therian clades, Eutheria and Metatheria (Figs 11a-d and 12a-d; [12,28,69]). More pertinent for the reconstruction of auditory sensitivity in early therians is their exclusive reliance on the stria vascularis for the production of endolymph (Fig 14e), and their uniquely high-positive endocochlear potential [76,83]. A recent publication [19] hypothesizes that these and other distinguishing features of the therian cochlear apparatus are related to the evolutionary compensation required by the loss of the lagenar macula, yet another unique condition seen in the therian inner ear. The stem therian petrosals described here can be seen as broadly concordant with this hypothesis, and can ostensibly provide boundaries for the reconstruction of auditory performance in the first crown therians and their earlier ancestors.

Concurrent with the evolutionary development of the most sophisticated and high-frequency sensitive ear known among tetrapods, crown therians also sever the last potential

vibrational interconnections mediolaterally linking both ears (i.e. the middle ear airspaces on each side of the head are acoustically isolated and independent) by the elongation and stenosis of the lateral parts of the ancestral interaural canal [62,98,121], forming a muscular and facultatively patent eustachian tube. The implications of this increased separation for the reconstruction of sound localization and central processing capacities in early therians are discussed below; however, fossilizable evidence of this trend in interaural isolation is shown by the widespread and homoplastic development of ossified bullae within many crown therian lineages [61], which are lacking in non-therian mammals (for evidence of functionally analogous "pseudobullae" present in specialized multituberculates see [122]).

Significance of stem therian petrosals

Phylogenetic Placement of the Höövör Petrosals

As outlined in the above descriptions, the amount of morphological similarity between H1 and H2 is much greater than the similarity between either specimen and *Priacodon*, or any extant mammalian taxon. This similarity is in fact closer than originally appreciated by [5], because of the mistaken character scoring of the condition of the perilymphatic duct in H2 used in their phylogenetic analysis. As can be confirmed from the above descriptions, the membranous perilymphatic duct in both H1 and H2 had a direct confluence with the inner ear by way of its bony enclosure within the aqueductus cochleae (the bony perilymphatic canal; Fig 10a-d). As such, the close similarity between H1 and H2 in terms of size, morphology, and provenance supports the hypothesized sister-relationship [5] between the two taxa represented by these specimens (Fig 2). However, despite the close morphological

resemblance between H1 and H2, I treat these specimens as distinct at the species level, if not higher. This is because of the many instances of contrasting morphology between H1 and H2 outlined in the above descriptions (such as the presence of a hypocochlear sinus and relatively large fenestra semilunaris in H1, compared to H2), which I consider to be outside the plausible range of intraspecific variation. Additionally, I suggest that the above descriptions of the external anatomy of H2, and the internal features of both Höövör petrosals, also do not provide a decisive conclusion to the problem of the phylogenetic attribution of these specimens with respect to the mammalian taxa known from dental remains recovered from Höövör.

However, for the following reasons, the hypothesis that the Höövör petrosals represent both of the major stem therian lineages known from dental elements at this locality is still defensible as one of the two most probable hypotheses for the phylogenetic assignment of these specimens (the other, and equally probable, hypothesis is that they are both gobiconodontid taxa). First, irrespective of the relative relationship between the H1 and H2, the robust development of caudal and lateral structures on H1 (Fig 7a) strongly suggest its affinity as a gobiconodontid. For example an elongate and robust paroccipital process is also seen in *Repenomamus*, a close relative of the gobiconodontids [123]. While correlates of relative robustness have not previously been scored and used in phylogenetic analyses, these features are likely associated with the mediolaterally widened mandibular condyle seen in gobiconodontids and their nearest relatives (such as *Repenomamus*). Additionally, relative to H2, H1 shows a shorter rostrocaudal extent of the floor of the cavum supracochleare (measured as the length of the bony lamina flooring the space for the facial ganglion), and the tympanic aperture of the prootic canal positioned more posterolaterally to the secondary facial foramen ("tapc" in Figs 3a and 7a), both features also

seen in the "triconodonts" described by [46]. While the clear presence of a cochlear aqueduct, processus recessus, and true fenestra cochleae are characteristics which have not been reported in prior descriptions of gobiconodontid cranial remains, they have been observed in gobiconodntids (GWR Pers Obs) and are possibly present in other members of the likely non-monophyletic group Eutriconodonta (e.g. the evidence for a cochlear aqueduct is inconclusive in the amphilestid taxon *Juchilestes* [124]). If the evidence supporting the gobiconodontid affinities of H1, and the possible trechnothere affinities of H2 is reliable, then based on the known roster of dental remains recovered from Höövör, the most likely taxonomic attribution for H1 would be to the fossil species *Gobiconodon borissiaki*.

While the similarities and suggested sister relationship between H1 and H2 have been remarked on here and by [5] (making it inconclusive as to which if either of these taxa are referable to *G.borissaiki*), many of the advanced features of H1 suggest its more proximate relationship with trechnotherian mammals. These features are all detailed in the above descriptions, but include the general reduction of venous proliferation within the pars cochlearis and loss of the hypocochlear sinus (Fig 3b). Additionally, the greater development of the vein of the cochlear aqueduct and its confluent sulcus on the abneural wall of the scala tympani ("hs" in Fig 13f), and closer approximation of the foramen for the sacculoampullar branch of the vestibular nerve to the foramen for the cochlear nerve near to the level of the crista transversa (Fig 15f and g) are plausible apomorphies in H2. Additionally, aside from not displaying the above mentioned "gobiconodontid" characteristics seen in H1, H2 also does not display the apparently apomorphic lack of the fossa incudis on the petrosal (as seen in H1 [4]). Even though the fossa incudis is not a preserved structure in H2, the separation of the fragmentary base of the mastoid region from its sutural surface for the squamosal demonstrates that these two regions would not

have been in overlapping contact (as in H1 they are, causing the fossa incudis to be lost or relocated to the squamosal bone in this taxon) (Fig 7a). The advanced features seen in H2, combined with the gobiconodontid features seen in H1, support, among the taxa described from Höövör, a closer phylogenetic affiliation of H2 with "symmetrodontan" mammals within the clade Trechnotheria. Under this interpretation the most likely dentally sampled taxon to which the H2 petrosal could be referred to is the tinodontid genus *Gobiotheriodon* [125,126]; however, the rarity of these specimens makes specific assignment unreliable, and I prefer to suspend the family-level taxonomic attribution of both Höövör petrosals until more material and character information is available. The plesiomorphic trechnotherian status of H2 is also supported by the less laterally deflected margin of the tympanic surface (Fig 3a), suggesting that the glenoid fossa would have been located far posterolaterally, possibly distal to a pedicle-like concavity ("post-glenoid depression") on the posterior root of the zygomatic arch. This condition is seen in *Zhangheotherium* and *Maotherium* [47,64]. Unlike *Zhangheotherium*, however, the mediolateral extent of the medial margin of the pars cochlearis is considerably wider in both H1 and H2.

While the new information on the Höövör petrosals provided here does not definitively resolve the phylogenetic location of these specimens, their status as stem therians, somewhat more closely related to crown therians than *Priacodon*, is secure (as reported in [5]; see Fig 2). The following functional implications of the morphology seen in these specimens relies only on the status of these petrosals as stem therians.

Osteological Correlates of the Stria Vascularis

The current narrative of mammalian auditory evolution has been assembled predominantly from insights gained from morphological and developmental sources (e.g. [127,128]). Less accessible inner ear structures have been difficult to observe. Because most unique features of the therian auditory percept rely on apomorphic histological and physiological characteristics, such as the large and tortuous stria vascularis and the highly positive endocochlear potential located inside the inner ear, the relative silence on these aspects represent a deficit in our understanding [129].

One under-emphasized question that is apparent in the inner ear of all extant therians is the conflicting set of demands placed on the auditory hair cells, which are required to alternately transmit and resist transduction currents at unparalleled rates while simultaneously being forced to function at a far remove from the vasculature providing for their nutrition, waste removal, and oxygenation [30,75]. While the use of potassium as opposed to sodium is an adaptation for metabolic efficiency seen in the hair cells of all vertebrates [80,83], the demands for high performance in the therian auditory endorgan seems to place this group's auditory hair cells in a unique metabolic crisis. In response to this, the relatively large stria vascularis and uniquely formulated endolymphatic composition developed as a partial solution [2,19,130,131]. Because monotremes retain an ancestral endolymph-producing capillary plexus in Reissner's membrane (see Fig 14b and f; [17,18]) in addition to the stria vascularis, and a greater number of radially oriented vessels crossing the cochlear duct [79], they seem to be less liable to metabolic distress than therians. However, the lamentable lack of physiological research on the cochlear apparatus of extant monotremes makes it impossible to judge whether the less specialized anatomy of the cochlear apparatus and supporting vasculature is attributable to weaker cochlear

performance compared to therians, or because of some currently unrecognized requirement for increased cochlear vascularization developed in monotremes [75,84].

Because of the ease of misinterpreting bony anatomy in extinct animals at both anatomical and functional levels, caution must be used when attributing significance to any morphological novelty. However, when seen against the wider trend of reduction of the circumpromontorial venous plexus in mammaliaforms generally, the localized venous hypertrophy at the sole intersection of the circumpromontorial venous plexus and cochlear endocast strongly suggests an adaptive significance for the vein of the cochlear aqueduct (VCAQ) at its earliest known instantiation in the Höövör petrosals described here. Because the stria vascularis is the most prominent organ within the abneural cochlear duct in both mammalian lineages bracketing the phylogenetic location of the Höövör specimens, the most reasonable functional attribution for this neomorphic vein is that it alleviated congestion within the hypertrophied stria vascularis in stem therians as it became the predominant or sole endolymph producing organ (Figs 10a-d and 14d). It is reasonable that this morphological innovation is itself a response to the increasing demands on the stria vascularis for the production of the high endocochlear potential and the potassium recycling biochemistry seen in extant therians [75,131]. In extant therians, these functions of the stria vascularis make it one of the most metabolically demanding organs in the body, with specific requirements for arteriovenous and capillary ramifications within its parenchyma. The physiologically expensive nature of the stria vascularis is also reflected in extant mammals by its intricate and developmentally complex structure, which requires contribution from both cranial mesoderm (ectomesenchyme) and other specialized neural crest cell populations (e.g. the melanocyte-like strial intermediate cells), and in adults contains one of the only vascularized epithelial tissues known in mammalian anatomy [78]. While other vertebrate

groups do show contributions from several embryonic tissue sources in the membranous lining of the membranous labyrinth, nowhere outside of theria do these cell populations reach the level of organization seen in the therian stria vascularis [71,78]. It is therefore fortunate that this unique organ requires an enlarged and conspicuous vasculature detectable in the cochlear endocast of ancestral therians (Fig 13c-f).

The neomorphic appearance of the VCAQ in the Höövör petrosals may also reflect a more general reorganization of the vascular supply to the cochlear duct, allowing for the withdrawal of those blood vessels that radially span the unadhered membrane exposed toward the scala tympani and scala vestibuli sides of the cochlear duct (Fig 14d,e). Because the formation of the sulcus for the VCAQ seen in the Höövör petrosals ("hs" in Fig 10b,c) represent the first extensive bony integration of the vasculature of the cochlear duct into the cochlear canal seen in Mammaliaformes, it is probable that the tissues of the membranous abneural wall of the cochlear duct relied to some extent on vasculature reaching it through its area of adhesion to the spiral ligament and bony cochlear canal (Fig 14 a-f). This is the situation seen in extant therians (e.g. [132]) where the VCAQ and other vessels do not cross the free basilar and vestibular surfaces of the cochlear duct (Fig 14e). This removal of blood vessels radially spanning the basilar and especially vestibular membranes is an apomorphic feature of the cochlear duct seen only in extant therians, and allows for the acoustic isolation of low-frequency interference generated by hemodynamic pulsations, away from the highly sensitive cochlear endorgan and supporting structures. As mentioned above, in extant monotremes and sauropsids the membranous tissues of the cochlear duct do not adhere to the bony side walls of the cochlear canal, leaving this structure mechanically unsupported and requiring that all blood vessels supplying the auditory epithelia travel in radial and

longitudinal directions across the full length and circumference of the cochlear duct [18,25,79].

While the veins servicing the stria vascularis are the only soft-tissue component of the mammalian cochlear duct to leave a recognized osteological correlate, the high performance of the stria vascularis in modern therians is predicated on the presence and precise functioning of many unique molecular, cellular, and histological structures. The acquisition and localized hypertrophy of the vein of the cochlear aqueduct is therefore likely associated with the pre-existent or incipient presence of unfossilizable characteristics of the therian-style cochlear apparatus. Chief among these features is the reinforced compartmentalization of the endolymphatic and perilymphatic spaces, necessitated by the requirement to limit paracellular diffusion of potassium and calcium salts between these fluids (e.g. [133]). In extant therians, the stable attachment of the cochlear duct to the spiral ligament within the cochlear canal allows for the segregation and recycling of potassium and other ions through interconnected epithelial and connective tissue syncytia [130,133]. For therians, this fluid homeostasis is reliant on the efficient transfer of material through the slender and precariously located processes of root cells within the abneural cochlear duct [133], which could be liable to mechanical damage if left unsupported within the free membrane of the cochlear duct in monotremes and other non-therians. The single foramen and linear sulcus for the vein of the cochlear aqueduct within the cochlear canal endocasts of the Höövör petrosals, as opposed to a highly perforated and reticulating venous network present in non-therians, may also support the potassium recycling function of the stria vascularis and cochlear syncytia by allowing salts resorbed into the VCAQ an opportunity to diffuse back into the intrastrial space before being conducted into systemic venous circulation outside the otic capsule (e.g. see [130]).

Even though nothing has been reported on the composition or electrical potential of endoymph in extant monotremes, it has been observed that the effects of voltage changes in OHC membranes are not as dramatic as those seen in therian mammals, and that monotreme prestin has a peak non-linear capacitance voltage optimum which is far from the cellular resting potential of OHCs [134,135]. This makes the electromotile function of prestin inefficient in monototremes. The calcium concentration of monotreme endolymph is likely also much higher than the ~ 20 micromolar concentration seen in the cochlear duct of most therians, because of the continued existence of the lagenar otoconial mass in this group and the need to prevent uncontrolled dissolution of this mass [19].

Osteological Correlates of Macromechanical Tuning

The problem of transducing airborne sound into an electrical signal and its further decomposition into spectral components, are a sophisticated functionality endowed to the cranium of many terrestrial vertebrates. As summarized in [16] the convergent innovations for airborne sound perception present in extant anurans, archosaurs, squamates, and mammals all operate with comparable levels of sensitivity and selectivity for frequencies under approximately 8 kHz. At the level of the auditory endorgan, the strategies for frequency selectivity (tuning) seen in these groups are effected through a mixture of molecular, bony, and histological adaptations. The field of comparative hearing [136] therefore can invaluably inform hypotheses of auditory capacities in extinct amniotes through the ancestral reconstruction of symplesiomorphic character states [2,84]. Inferences about which of several non-mutually exclusive tuning mechanisms are present in early

mammals are necessarily based on the distribution of the several forms of tuning in extant mammals, or predicted for the last common ancestor of amniotes [101,137]. Because of this dependence on extant representatives, the almost complete lack of physiological studies on the living monotremes in particular imposes a major obstacle to our understanding of tuning mechanisms in the synapsid lineage [77,138].

What is currently known about the distribution of tuning mechanisms across tetrapods suggests a major dichotomy in strategy between ancestral electrical tuning (see Supplementary Material 1; [139]), and several forms of mechanical tuning [101]. The varieties of mechanical tuning can be conceptually decomposed into intrinsic (action at the level of the hair cell) versus extrinsic (action at the organ level or larger), and active (requiring cellular energy) versus passive (based on inert geometrical and material properties) mechanisms (creating a total of four discrete categories; [137]). All of these tuning mechanisms are characterized by some degree of tonotopy (the correlation of best frequency response with anatomical linear distance) within the auditory endorgan, and therefore a corresponding Space Constant (SC) expressed in units of millimeters per octave (an octave is a doubling of frequency). The extant amniotes that rely solely on the plesiomorphic mechanism of electrical tuning (*Sphenodon* and the chelonians), show some of the smallest SC values (0.3 mm per octave or smaller) because of the extremely short length of their auditory papilla. As such, these forms, and most likely all early amniotes, show only short and undifferentiated sacculocochlear recesses within their labyrinthine endocasts. Conversely, in all non-mammalian amniotes showing a differentiated middle ear, a form of mechanical tuning is emphasized that relies on tonotopic variation in the mass, stiffness and number of stereovilli of the hair cells within the auditory papilla (homolog of the mammalian organ of Corti). This mechanism is instantiated in active (molecularly driven

motion of stereovilli) and passive forms [101]. This category of tuning is dependent on organelle-level features present within the auditory hair cells themselves and so is termed micromechanical tuning; and it is associated with an intermediate range of SC values (less than 1 mm per octave up to several mm per octave; [16]). Because of the elongate but absolutely short cochlear canals seen in the earliest mammaliaforms (such as *Morganucodon*; [13,87,140]), it has been hypothesized that micromechanical tuning provided the initial impetus for the development of the bony cochlear canal within the synapsid lineage as well [19]. However, in all known extant mammals (monotremes and therians) no evidence for significant electrical or micromechanical tuning has been physiologically recorded ([129]; although see [102] for possible evidence of active micromechanical tuning). Where characterized best in advanced therians, the sole form of tuning is based on an apomorphic extrinsic mechanism termed macromechanical tuning. Evaluating the performance of this form of tuning among synapsids depends on the cochlear length and the SC. Fossils are often amenable to cochlear measurement, but the SC can only be approximated in general terms. However, it is not until mammaliaforms achieve cochlear canals long enough to accommodate at least several octaves (somewhere near the emergence of Crown Mammalia; Fig 16) that macromechanical tuning is likely to enable auditory capabilities similar to living mammals. That being said, therians with extremely low body mass may show extremely short cochlear canals, such as *Sorex* with a cochlear canal length of 2.54 mm [24]. I am unaware of studies reporting SC values for *Sorex* or other such diminutive therians, but likely these forms achieve SC values well below 1 mm per octave because of their observed use of broadband echolocation clicks in the range of 20 - 95 kHz [141]. If this is correct, at least some modern therians are able to achieve ultrasonic audition in conjunction with macromechanical tuning of very short cochleae.

Even though little is known about tuning modalities in extant monotremes, there are strong reasons to suspect that somewhere along the backbone of synapsid evolution, between earliest mammaliaforms and crown therians, a shift toward extrinsic macromechanical tuning and away from more plesiomorphic forms of tuning should be recognizable. The presumed reliance on macromechanical tuning in mammals is likely also reflected by the universal presence of a true organ of Corti, with its functional differentiation of Inner and Outer Hair Cells (described above) and characteristic arrangement of membranes within the cochlear duct [109].

While the presence of macromechanical tuning appears to be consistently present within Mammalia, there is an obvious spectrum in terms of its performance (e.g. sensitivity, selectivity, and highest detectable frequency) and its morphological/molecular accommodation across mammalian species; with the monotremes defining the lower end and eutherians the higher end of the spectrum [2]. This spectrum is also recognizable in both the active and passive mechanisms of macromechanical tuning [101]. For instance, wide scale comparative studies on the structure of the prestin protein [134] estimate that monotreme prestins are much less capable of useful electromotility at physiological voltages. Additionally, monotremes show a lower proportion of Outer Hair Cells (expressing prestin on their basolateral surface) to Inner Hair Cells [109] when compared to therians. These observations support the generally comparable level of sensory traffic, but weaker instantiation of the macromechanical active process in the monotremes.

The macromechanical passive process is effected by the gradient in compliance of the basilar membrane, and its monotonic increase in width and decrease in depth (thickness) as it runs apically beneath the organ of Corti [101,142]. Therefore, the passive process is present even in an inert and lifeless basilar membrane; and its capacity to tonotopically

propagate traveling waves is modulated by the geometry of the cochlear duct [143], and its lateral attachments to the cochlear canal, or lack thereof [144,145]. The concerted action of this mechanical arrangement filters the range of frequencies presented to each individual auditory hair cell, allowing each cell to specialize for the transduction of a filtered frequency bandwidth [101]. Morphological features suggesting a weaker commitment to the macromechanical passive process in monotremes include their large and relatively untapered basilar membrane (which is wider than most of the largest and lowest frequency basilar membranes in found in extant therians; [109]), and lack of any adherence of the basilar membrane (or any other part of the endolymphatic cochlear duct) to rigid supports within the bony cochlear canal [18].

The stem therian labyrinthine endocasts described here contain apparently synapomorphic osteological features which allow them to be placed along the spectrum of passive macromechanical adaptation present in extant monotremes and therians. In particular, *Priacodon* and both Höövör petrosals differ from early mammaliaforms and monotremes, and resemble the more derived cladotherians, in the presence of a well-developed secondary bony lamina (Fig 14c,d). When present in modern therians, the secondary bony lamina provides a rigid attachment for the abneural cochlear duct and contributes to the concentration and transmission of tensile forces across the basilar membrane (Fig 14e; [23]). The first appearance of a well-formed secondary bony lamina in these stem therian endocasts (Figs 10 and 14c, d) is therefore strong evidence for the abneural adhesion of the membranous cochlear duct with the bony cochlear canal, and may also signify the presence of the spiral ligament and its specialized populations of fibroblasts (e.g. tension fibroblasts; [146]). These soft-tissue specializations are known to be associated with the secondary lamina in extant therians and are critical for normal therian hearing

function. However, as mentioned above, lack of an opposing primary bony lamina in *Priacodon* and the Höövör petrosals, or even an ossified tractus foraminosus, makes it unlikely that tensile forces similar to those in therians could be transmitted across the basilar membrane through its attachment along the secondary bony lamina in these forms. The stem therians described here therefore show an intermediate level of passive macromechanical adaptation by showing some rigid mechanical support for the cochlear duct, but lack the diametrically opposing primary bony lamina required for the catenary suspension of the basilar membrane, which is associated with the tonotopic region of frequencies greater than 10 kHz in modern therians [15]. Macromechanical active and passive processes were likely also evolutionarily associated with each other [134]. As such, it is reasonable to hypothesize that taxa showing a bony secondary (or primary) lamina represent useful phylogenetic calibrations for the initiation of features supporting rapid electromotility in the prestin molecule [134], a capacity which is known to be present, but much more weakly instantiated in modern monotremes [135].

Finally, the formation of a true round window (fenestra cochleae) and perilymphatic canal (aqueductus cochleae), such as that seen in both Höövör specimens (Figs 3a and 7a), does not have a clear functional interpretation but has been hypothesized as improving the vibrational insulation of the inner ear, allowing for the synchronized, opposite-phase pulsations of the primary and secondary tympanic membranes [109]. Conversely, the first appearance of these features and the development of a process recessus may have been initiated as a structural byproduct of increasing braincase width and associated lateral displacement of the perilymphatic foramen relative to the jugular foramen.

This comparative and fossil evidence for macromechanical tuning in the earliest crown mammals, especially along the therian stem, strongly suggests that a cochlear space

constant within the range of values associated with macromechanical tuning in extant mammals would be applicable to these fossil members of crown Mammalia as well [14,15]. The lower limit of mammalian SC values in extremely small mammals is currently unknown, and the anecdotally suggested average SC value of 2.5 mm per octave (based on an unidentified sample of eutherians including rodents, bats and other small-medium sized forms [14,15,99]) is likely very approximate and not readily applicable to non-therians. This makes inferences regarding the frequency limitations of early mammals uncertain. Because of the highly nested position of shrews and other minute eutherians in mammalian phylogeny, and their highly derived acoustic behavioral characteristics [147], I consider that extremely small macromechanical SC values in these forms are equally problematic for representing the primitive condition for theria in general and for the earliest mammals in particular. When measured in a generalized therian (*Monodelphis domestica*; [148]), SC values varied along the auditory epithelium ranging from ~1.5 mm per octave along the basal 60% of the cochlea to 1.8 mm per octave maximally and 0.8 mm per octave in a limited region near the apex of the cochlear duct. The ~40 mm skull length seen in *M. domestica* makes it comparable to the estimated size of the taxon represented by H1 [4]. The larger marsupial *Didelphis*, and the placental *Tupaia* [24,149,150] show typical SC values above 1 as well. Living monotremes also appear to also show a SCs above 1; the ~3 octave effective frequency range reported for *Tachyglossus* by [151] corresponds to an estimated SC value of 2.3 mm per octave using the cochlear measurements provided in [18]; while *Ornithorhynchus* has an estimated SC above 1 [18,152]. Additionally, it is likely that early mammals were receptive to very narrow frequency bandwidths; e.g. monotremes show 3-5 octave range and 4 octave range is reported for the lesser hedgehog tenrec *Echinops* [153], and generalized marsupials have a range at, or below, ~5 octaves [154].

Given the ~4 mm length of the cochlear duct in the stem therian endocasts described here, and their position in the mammalian "phylogenetic bracket", a range of four or five octaves is a skeptically large estimate for the frequency bandwidth available to these forms. The relationship between the bandwidth of detectable frequencies and maximum detectable frequency is, however, also dependent on the lowest detectable frequency. Given a relatively high low-frequency limit for small amniotes of 500 Hz (many modern mammals, lizards and birds have even lower limits, ~ 50-200 Hz) and using a skeptical SC of 0.8 as seen in a small portion of the cochlea in *Monodelphis* [148], the upper frequency limit for these stem therians would be at ~ 8-16 kHz. If given a lower frequency limit of 100 Hz typical of plesiomorphic amniotes the corresponding upper limit would be much lower at ~ 3.2-6.4 kHz [25]. The generous 500 Hz estimate of a low-frequency limit is likely unrealistic, given that it requires the abandonment of the range of many important environmental sounds at low-frequencies in exchange for a relatively very low upper frequency limit (similar to the upper frequency limit seen in modern *Ornithorhynchus* [17,152]). The probable retention of a lagenar macula in *Priacodon* would also diminish the frequency band available to this taxon as well, by taking up ~ 1 mm of length of the cochlear canal (Fig 13h; [81]). The most realistic upper frequency limits for *Priacodon* and the Höövör specimens is therefore likely less than16 kHz, and therefore not within the ultrasonic range. The absence of ultrasonic capability in our fossil taxa is therefore supported even adopting highly skeptical values for the low frequency limit (500Hz, likely in the vicinity of 100Hz), SC value (0.8, likely above 1) and the cochlear length (utilizing the whole length of the endocast, and dismissing the possible presence or remnant of an apical lagena).

However, it is important to emphasize that even under the extreme assumption that macromechanical tuning was entirely absent in early mammals, and therefore space constants

within the macromechanical range would not be applicable to the stem therians described here, no form of micromechanical or electrical tuning would feasibly have allowed the upper frequency limit to extend above approximately 16 kHz either [2,16]. Therefore, despite the existence of several autapomorphic high-frequency non-mammalian tetrapods (e.g. [155,156]), and several therian species with very short cochlear canals [24], no combination of the phylogenetically widespread forms of auditory tuning would have allowed the stem therians described here to detect ultrasonic frequencies (~20 kHz or higher; [16]).

Many of the earliest fossil therians are very small [37, 157,158] and are either known to have, or predicted to have, cochlear canals within the same range of sizes as the stem therians described here, and smaller [24]. These extremely small fossil therians, many of which have petrosals just a few of millimeters long are also known to have the osteological correlates of macromechanical tuning seen in living therians (coiled cochleae, Rossenthal's canal, primary and secondary lamina, etc.) and in several instances cochlear lengths below 5mm [24,120]. Comparisons with modern minute therians with macromechanical tuning suggest that: either 1) these fossil therians were sensitive to very narrow frequency bandwidths because of their very short cochlear canals; and/or 2) the allometric relationship between body mass and SC values seen in extant minute therians, such as in some soricids, would have been present in these earliest fossil therians as well. Both of these hypotheses ultimately rest on the optimization of auditory features on a phylogenetic tree including modern taxa with known auditory bandwidth/SC and the relevant small fossil therians. At present we lack both the pertinent information on the smallest extant therians, and the proper phylogenetic context integrating fossil and recent taxa. I, therefore choose to refrain from speculating about the auditory capacities of fossil therians within this smallest body-size range.

Osteological Correlates of the Lagenar Endorgan (or lack thereof)

The hair cells comprising the lagenar macula are perhaps the most variable and least understood of the many epithelial cell types found around the heterogeneous endolymphatic lining of the pars inferior of the membranous labyrinth [138]. This is especially so in the case of extant mammals, where in the monotreme lineage this sensory epithelium is located between the scala medial and scala vestibuli within a specialized lagenar sac [18]; while extant therians are unanimous in their lack of any adult morphological expression of the lagena altogether. Still, several inducible genetic atavisms seen in rodent models suggest that the distal (low-frequency) extent of the therian organ of Corti persists as the syngenetic homolog of the lagenar macula [95,138].

Nonetheless, as a discrete organ, supporting an otolithic mass and recruiting the innervation of a dedicated lagenar nerve and ganglion, the absence of the lagena is one of the unique and important features of the therian inner ear. It has also been suggested that the loss of the lagenar macula acted as a proximal cause, or immediate correlate, of the development of several other synapomorphic features of therian cochlear physiology, such as the extremely low calcium concentration and high electrical potential of therian endolymph [19,75]. In sauropsids, and presumably also the earliest synapsid taxa, a high (several hundred micromolar up to 1 millimolar; [19]) calcium concentration of the cochlear fluids is required to support electrical tuning and protect the lagenar otolithic mass. A minimal ambient calcium concentration is also known to be required to prevent dissolution of vestibular gravistatic structures [159] which (where examined in the otoconia of modern rodents; [160]) show compositional turnover on a monthly timescale. The released obligation

to generate high-calcium endolymph within the cochlear duct likely allowed stem therians the adaptational leeway to reformulate several aspects of their cochlear biochemistry, resulting in the low (~20 micromolar) calcium concentration in cochlear endolymph, and the correspondingly sharp calcium gradient along the membranous labyrinth generally [161,162]. There is also some evidence that the capillary plexus in Reissner's membrane is specifically associated with the support of the lagenar otolithic mass because of the retention of localized Calcium ATPases at this membrane in extant rodent models [131]. The increasingly exclusive reliance on the mammalian stria vascularis for endolymph production occurring during the evolution of crown therian mammals may therefore be directly correlated with the lost capacity to support a functional lagenar endorgan [19].

The timing and functional significance of lagenar loss is complicated by the lack of pertinent comparative and paleontological evidence. In particular, the lack of experimental recordings of the normal functioning of the lagenar endorgan in sauropsids and monotremes, and conflicting hypotheses regarding the relative importance of its gravistatic versus auditory modalities [25,82,138], make the physiological implications of lagenar loss in stem therians difficult to interpret. The available fossil material is also ambiguous because of the loose osteological association seen between the lagena and the surrounding skeleton of the otic capsule. Bony structures such as an apical inflation of the cochlear canal, and sulci or canals for the lagenar nerve, are variably present among mammaliaforms; however, based on the wider distribution of the lagena among amniotes, a functional lagenar macula almost definitely existed in synapsid taxa lacking such osteological correlates, both preceding the early mammaliaforms, and succeeding them within the mammalian crown group. Therefore, absence of evidence for a functional lagenar endorgan is not evidence of its absence, and it is likely that early stem therians such as *Priacodon* that lack obvious osteological correlates of

a lagenar macula retained it nonetheless. This is supported by the presence of lagenar correlates in multituberculates, which branch near *Priacodon* in stem therian phylogeny (Fig 2; [68,163]); and the lack of bony features indicating a switch to the modern therian-style of cochlear physiology predicated on the lack of the lagenar macula [19,46,82]. The reference to the loss of the lagena as "the Cretaceous Cochlear Revolution" [19] may therefore be misleading in that it is currently unclear as to whether the morphological expression of the lagena was lost in an evolutionarily punctuated event or a gradual interval of decreasing usefulness. Based on the stratigraphic distribution of fossil therians, and most phylogenetic hypotheses of their relationships (i.e [36,164] inter alios), the loss of the lagena also certainly occurred within the Jurassic if not earlier, and likely several times.

The internal bony anatomy visible in the high-resolution scans of the Höövör petrosals provide the earliest indications of advanced features seen today only in therian mammals. As outlined above, several of the osteological features seen in these specimens suggest that the cochlear duct achieved at least some adhesion to the abneural margin of the cochlear canal (Fig 15c-e) and show increased (if not exclusive) reliance on the functioning of the stria vascularis as an endolymph producing organ [83]. These characteristics are unique to therian mammals among extant vertebrates, and (combined with the presence of a straight and distally tapering cochlear canal in the Höövör cochlear endocasts; Figs 10a-d, 13e,f) strongly suggest that these stem therians have greatly reduced or lost the lagenar macula altogether. These forms could therefore have attained other soft tissue characteristics seen in modern therians such as a terminal helicotrema [18].

The consistent presence of dorsoventral coiling to accommodate the lengthened cochlear canal seen in later cladotherian mammals may have then been enabled by the lagenar macula reorienting to a position where its sensory input was mostly or exclusively

responsive to vertical linear acceleration [17], and therefore completely redundant to stimulus from the saccule and utricle [19]. Another hypothesis based on the physical modeling presented in [143] suggests that cochlear coiling represents an adaptation for the conduction and concentration of low-frequency vibrations of the basilar membrane along the abneural margins of the apical cochlear canal, thereby increasing sensitivity to these frequencies relative to an uncoiled cochlear canal. Under this hypothesis, the extremely straight cochlear morphology as seen in H1 and H2 (compared to the condition in several stem mammaliaforms [13,31,90]) may actually be seen as a modification de-emphasizing the sensitive detection of lower-frequency sounds. Whatever the original selective pressure for dorsoventral coiling, the complete loss of the remnant hypocochlear sinus in therians may also be an effect of dorsoventral expansion of the cochlea within the pars cochlearis, or a combination of factors.

The high likelihood that the Höövör petrosals described here were beneficiaries of the "cochlear revolution" provides a useful perspective on the selective regime responsible for the loss of the lagena and the development of the unique therian cochlear physiology. Particularly, because of criteria outlined in the discussion of macromechanical tuning, there was almost no capacity for high-frequency (above ~ 20 kHz) hearing in these early stem therians. Therefore, whatever factors led to lagenar loss must not be related to the development of ultrasonic hearing capacities. This is complementary to hypotheses that stem therians relied to a substantial extent on substrate based (i.e. non-tympanic) sound conduction [68,165]; more importantly, this evidence is contradictory to the hypothesis that these unique features of the therian inner ear are related to the unique capacity of extant therians to detect and localize ultrasonic sound sources [13,77]. As with the innovation of the three ossicle middle ear found in mammaliamorphs, the unique inner ear mechanisms

developed in ancestral stem therians (advanced theriimorphans or early trechnotheres) developed in service of acoustic performance within an ancestral frequency range, and later proved capable of being extended into ever higher frequencies in their descendant therian taxa. The late Cretaceous meridiolestidan *Coloniatherium* [6], with a fully coiled cochlea and a centrally located modiolus, optimizes in most phylogenies as an independent acquisition of these features. A highly derived inner ear morphology (with complete coiling, and without a lagenar inflation) is also present in more the plesiomorphic taxon *Cronopio* [166], and terminal taxa such as *Peligrotherium* [118] and *Necrolestes* [9,117]. The detailed similarities between meridiolestidan and therian inner ears, with their potential auditory convergences, have yet to be fully explored.

Auditory Localization in Stem Therians

Aside from the difficulties related to the sustenance of greater mass-specific caloric requirements, within topographically more heterogenous habitats, small mammals are faced with novel challenges for the segregation and localization of sound sources. This "small mammal problem" has been a central focus in the traditional explanation for the advent of ultrasonic hearing in therian mammals, because of the requisite use of high frequencies for sound localization at small body sizes (e.g. [109]). Indeed, the abilities of even very "primitive" small mammalian insectivores to utilize broadband and high-frequency cues for auditory localization, even to the point of echolocation in many cases, is well recorded (e.g. [147]). Therefore, it is probable that ultrasonic capacities evolved in the earliest crown therians in response to selection for greater localization capabilities; however, the evidence reported here of the likely very low upper detectable frequency limits in stem therians, and the manifest capacity of small-bodied sauropsids to locate sound sources with frequencies

below 5 kHz, suggest that traditional narratives of the evolution of ultrasonic hearing require qualification [3,33,77,167,168].

The one-dimension waveform presented to each ear carries very limited, and difficult to extract, information on the spatial location of its source. These difficulties in localization are both physical and computational in nature. For instance, the physical coupling of sound frequencies in air ranging from 20 Hz – 20 kHz to corresponding wavelengths ranging from 17 m – 17 mm (respectively), require sensitivity to frequencies with corresponding wavelengths larger than the head size (interaural distance) of many low-frequency limited terrestrial vertebrates. The many sauropsid groups to have developed a tympanic middle ear have convergently solved this physical challenge by the coupling of both right and left tympanic membranes through the medial air mass comprising their interaural canal (i.e the cavum tympani and other contiguous cavities). This has the effect of increasing interaural delay times and allows the detection of interaural phase differences at the level of the auditory transducers themselves, alleviating the neurological requirement to develop a complex internal representation of binaural differences within the central nervous system [169,170]. This "pressure-gradient receiver" form of auditory localization is the only mechanism for the perception of low-frequency limited sound sources known in terrestrial vertebrates; and it possibly also evolved in early eucynodonts and later synapsid taxa with angular tympanic membranes [171,172].

Conversely, modern therian mammals have developed a predominantly computational strategy for the localization of sound sources, based on the isolated functioning of both ears as simultaneous and independent "pressure receivers". The adaptations providing this capacity are categorized into monaural and binaural mechanisms, each making specific minimal demands for broadband and high-frequency (near-ultrasonic)

hearing. They are also commonly specialized for vertical and azimuthal localization, respectively. All of these mechanisms also make substantial demands on the central nervous system, such as the required detection of binaural coincidence on submillisecond timescales, and novel processing in the lower auditory brainstem [168,173]. Because of the conflicting demands that the pressure-gradient receiver versus pressure receiver forms of auditory localization place on the specific structure of the external, middle, and inner ear, the synapsid lineage must have reduced and ultimately lost its pressure gradient receiver capacities before the advent of the modern form of therian sound localization (if pressure gradient receivers existed in early synapsid taxa at all). The sequential development of the MME, PDME, DME, and development of discrete bullae in the therian crown group, may therefore represent the progressive reduction and eventual loss of the ancestral mechanisms for sound localization. Likewise, the presence of a broadly open interaural canal in some extant therians [174] could plausibly be interpreted as atavisms to a pre-mammalian condition. The platypus *Ornithorhynchus* [62] also shows a patent interaural communication which in fact narrows substantially before merging with the proximal segment of the pharynx. Depending on how the primitive condition for the last common ancestor of amniotes is reconstructed the condition of *Ornithorhynchus* could be primitive, or that of the echidnas with a recognizable eustachian tube would be symplesiomorphic for Mammalia. At present I consider this question unresolved and the primitive mammalian condition equivocal [172].

Binaural sound localization. The stem therian taxa described here most likely attained a PDME state of the middle ear [68], and therefore would have attenuated or lost the tentatively ancestral pressure-gradient capacity for sound localization if indeed it had

previously existed. However, regardless of whether or not the pressure-gradient receiver mechanism operated in earlier members of the synapsid lineage, the functional limitations imposed by the short length and macromechanical adaptations seen in the stem therian cochlear canals described above would also have precluded the useful functioning of the modern sound localization strategies seen in extant therians. The two strategies seen in extant therians most useful for azimuthal localization are based on the comparison of stereo binaural input, and are termed the Interaural Time Difference (ITD) and Interaural Level Difference (ILD) mechanisms [3]. These two mechanisms are based on the capacity to contrast the time of arrival of distinctive spectral features (ITD) or the instantaneous amplitude of the stimulus (ILD), respectively. However, the ability to precisely contrast arrival times of spectral features is contingent on a sufficiently large binaural time delay, which itself is a function of the Functional Head Size (FHS a metric of interaural distance measured in microseconds; [33]) of an animal. Therefore, ITD based localization is emphasized to the exclusion of ILD in modern therians with large FHS values (e.g. domesticated ungulates). Conversely, modern small mammals (with smaller than 200 microseconds FHS) emphasize ILD, and small mammals using only one binaural cue use ILD. Many of the known modern small therians that use both ITD and ILD are low-frequency specialist rodents [33,127,175]. As such, even with a possibly convoluted interaural canal extending the binaural time delays somewhat [120], the estimated FHS of very approximately 50 microseconds or less in the crown mammalian common ancestor [3, 176, 177] would place the earliest mammals within the predominantly ILD size range. This inference is also supported by the purportedly more plesiomorphic construction of the ILD circuitry within the lateral surperior olive in the therian Superior Olivary Complex [173].

However, while it is very unlikely that the first stem therians were able to use ITD as a localizing mechanism, the low estimated upper frequency limit of the stem therian cochlear endocasts presented here also suggests that the ILD mechanism would also have been inoperative or inefficient in these animals as well. While the exact frequency requirements for ILD functioning are somewhat variable across extant therian species, because the attenuation of sound amplitude is produced by cranial "shadowing" of the stimulus as it propagates across the tissues of the head, ILD requires frequencies with corresponding wavelengths shorter than the interaural distance of that particular taxon [178]. In the case of the small stem therians presented here, and with a very generous estimate of interaural distance of ~1 inch, the corresponding minimal ILD frequencies of ~13 kHz would likely be just marginally within or above the upper frequency limits of these small taxa. However, while it is likely that the lowest frequencies required for ILD were perceptible by the stem therians described here, the proper functioning of the ILD mechanism (and the other localization mechanisms) in extant small therians relies on the availability of a wide band of frequencies beginning with the lowest usable frequency. In the case of stem therians, the ILD mechanism would therefore have been poorly functional relative to its performance in modern therians if it had been present at all [168]. This is also complementary with what has been suggested as the most likely evolutionary trajectory for the assembly of the modern neural circuitry supporting ILD, where the hypothesized incipient stages of binaural processing was likely only sufficient for the segregation of discrete simultaneous sound sources, and possibly their relative localization [173].

Monaural Sound Localization. Therefore, while the capacity for sound localization based on the physical interconnection of both ears, or the simultaneous comparison of the

electronically encoded input from both ears, would be inoperative or poorly functional at best in stem therians, the final method of auditory localization known in extant tetrapods does actually have some empirical support from the fossil record of Mesozoic mammals. This final form of auditory localization is based on the spectral alteration of monaural input (termed Head-Related Transfer Functions; [173]) by the presence of a specialized external pinna. In extant therians this pinna-based form of auditory localization is most important in front-back discrimination of sound sources, and in specialized species allows the vertical localization of sound sources, such as along a mid-sagittal plane. Where tested in llamas, frequencies ~ 3 kHz and higher allow for consistent resolution of the front versus back location of a sound source [33]. In cats tested with frequencies greater than ~ 10 kHz, the vertical location of sounds is resolvable, as is the precise location of a sound source within each ear's "cone of confusion" [179]. As summarized above, the anatomical evidence of an involuted pinna in *Tachyglossus* [106] and the excellent soft tissue preservation in the gobiconodontid *Spinolestes*, suggest that an elaboration of the external ear may have been present in crown mammals (and was likely present in early theriimorphs; [107]). The mammalian pinna may have initially appeared as an inefficient but sufficient method to monaurally localize sound sources, possibly only for front-back discrimination (there is also a significant amplification effect provided by the pinna as well; [21]). The more sophisticated capacities for monaural vertical localization, predicated on minimal frequencies higher than approximately 10 kHz, likely only developed in crown therians and their close relatives as near-ultrasonic frequencies became detectable within the therian lineage. While the observation, provided in [2], that the dimensions of the soft tissue impression of the external pinna in *Spinolestes* would most efficiently provide localizing information (such as spectral cues) at frequencies above 20 kHz, for the reasons outlined above is appears unlikely

that these types of advanced localization mechanisms were present in early theriimorphs such as *Spinolestes* and the Höövör specimens.

This hypothesis regarding the acoustic capacities in Jurassic and Early Cretaceous stem therians, synthesized from both paleontological and physiological evidence, presents an unimpressive picture of the ancestors of modern therian mammals as poorly equipped, possibly nocturnal, insectivores compared to modern standards. While many extant small mammals show sophisticated sound localization capacities, even with frequencies below 20 kHz, it seems that early stem therians would not have attained a sufficient bandwidth of frequencies, and/or a high enough upper frequency limit to have been able to usefully localize short duration sounds faster than visual localization alone [33]. This may reflect the less competitive nature of the small insectivore niche within Mesozoic terrestrial ecosystems, but could equally support the presence of non-tympanic forms of conduction such as the hypothesized direct conduction of sound through Meckel's element as suggested by [68]. The combination of poor auditory localization abilities with adaptations suggesting increased sensitivity and selectivity at low frequencies in stem therians may therefore be a compromise between the low-frequency requirements for seismic sound conduction and the increasingly specialized capabilities for airborne sound localization.

It is currently ambiguous what behavioral and autecological implications the transitional morphology of these stem therian petrosals have for the reconstruction of Mesozoic mammals. However, it is important to reiterate that the inference of poor sound localization capabilities within the early stem therians is not based on any single ancestral reconstruction of the cochlear tuning mechanism or auditory physiology within the crown mammalian ancestor or first stem therians. All phylogenetically common cochlear tuning mechanisms typical of modern amniotes, working individually or in combination, would be

equally incapable of extending the upper frequency limit in the fossil taxa described here to frequencies above ~ 16 kHz. If, as seems most likely, macromechanical tuning was present within the early theriimorphans and trechnotheres, the relatively large SC values associated with this type of tuning commonly seen in extant therians would prevent the short cochleae in these fossil forms from extending into frequency ranges much higher than 16 kHz.

Even if a more ancient form of intrinsic tuning (electrical or micromechanical) was present in the earliest stem therian mammals, the low upper frequency limits associated with these forms of tuning in modern tetrapods would also cut-off the maximal detectable frequencies in stem therians to under ~ 10 kHz (as described above exceptions to this frequency limit are seen only in very specialized and phylogenetically restricted taxa among sauropsids and amphibians, e.g. [155,156]).

Conclusions

The descriptions and discussion provided here highlight the phylogenetically heterogeneous nature of stem therian petrosal evolution throughout the Mesozoic. The minimal age for the the successive nodes formed by *Priacodon*, the Höövör petrosals, and therians is currently dated as Early and Middle Jurassic, respectively (determined by the eutriconodontan *Argentoconodon* [180] and the therian *Juramaia* [181]); despite major differences in morphology, the internodal age difference is only on the order of 10-15 MY. The approximately 50 million year duration separating the stratigraphic provenance of the Upper Jurassic Priacodon and Lower Cretaceous Höövör specimens focused on here is simply the result of taxon sampling, illustrating the first known acquisitions of several derived internal labyrinthine features along the backbone of therian evolution. Even before the advent of the dorsoventral cochlear coiling characteristic of modern crown therians and their

cladotherian relatives, both *Priacodon* and the Höövör petrosals show morphologies suggestive of greater acoustic performance (in terms of selectivity and sensitivity) unique to this lineage within Mammalia.

Osteologically, these specimens demonstrate that several of the internal labyrinthine features appearing in the earliest mammaliaforms (e.g. lateral curvature of the cochlear endocast and lagenar inflation) were lost before most of the advanced cladotherian morphological features related to cochlear coiling and the bony support of the cochlear nerve appeared (Fig 10). Interestingly, this evolutionary loss of lateral curvature of the cochlear canal before the advent of its dorsoventral coiling is not matched by the developmental trajectory of the membranous cochlear duct; as seen in rodent models [128,182,183], lateral curvature and subsequent dorsoventral coiling form two discrete stages in the development of the membranous labyrinth [184]. Additionally, the ontogenetic initiation of hearing in humans and a variety of model organisms seems to parallel the hypothesized evolutionary transformation of the cochlea, with the hair cells responding to low-frequencies changing from basal to apical regions during normal development [185]. Dorsoventral coiling may then ultimately be evolutionarily associated with a rudimentary adaptation of the mammalian cochlea for the preservation of frequency sensitivity in the ancestral (low-frequency) range [143].

For reasons outlined above, it also seems likely that the perceptual capacity for sound source localization was undeveloped or rudimentary in early mammaliaforms. The hypothetical pressure gradient receiver form of auditory localization was either reduced or absent before the capacity to use advanced ILD and ITD forms of localization developed in the immediate ancestors of crown therians. The localization mechanism most likely to be present in the forms described here would have been based on monaural pinna-based

signals, for which the preservation of an external pinna in one exceptionally preserved theriimorph specimen can be considered evidence [107]. However, even using these pinna-based cues, this form of localization in the stem therians described here would mostly be competent for front-back localization of sound sources.

This is not to suggest that early stem therians displayed poor hearing capacities generally, and the presence of a salient secondary bony lamina within the cochlear endocasts described here ("sl" in Fig 10a,c,e) suggests some amount of adhesion between the cochlear duct and spiral ligament with the abneural cochlear canal (Fig 15c,d). This is an advanced level of structural organization beyond the state seen in even modern monotremes, and is likely associated with a greater commitment to macromechanical tuning than that seen in extant monotremes. The attachment of the basilar membrane to the newly evolved secondary lamina before the advent of the primary bony lamina also suggests that the basilar membrane in these forms was less tense and stabilized than is typical of modern therians. However, it is also likely that the low-frequency limitations of the stem therians described here would not have precluded these forms from relying on an insect-based diet, which has been predicted as the mainstay of most generalized Mesozoic lineages including those represented by the fossils described here [186-190]. One study [191] estimates that at least one Middle Jurassic katydid species produced frequencies (~6.4 kHz) which would very plausibly be detectable by these stem therians.

This report details the bony features pertinent for the phylogenetic and soft tissue reconstruction of *Priacodon*, Höövör petrosal 1 and especially the newly described Höövör petrosal 2 (Figs 1-10). However, perhaps the most significant aspect of cochlear morphology presented by these specimens is what they entail regarding the rate of high-frequency adaptation near the therian crown group. If the uniquely derived and phylogenetically

unstable clades Gondwanatheria and Multituberculata are excluded, the theriimorph specimens used here provide a phylogenetic bracket around the advanced clade Cladotheria. To date the majority of previously described Mesozoic mammalian petrosal specimens belong to Cladotheria, and several convergent derivations of the fully coiled cochlear canal, tractus foraminosus (convergent with monotremes; Fig 15b,e), and primary bony lamina are likely within this group. The petrosals described here corroborate the slow rate of upper frequency limit increase in the synapsid lineage up to the advent of Cladotheria; and that cladotheres may therefore be thought of as an evolutionary radiation into a high-frequency world [192]. Within the Cretaceous, both crown therians and South American dryolestoids both achieve a structurally "modern" fully-coiled form of the cochlear canal [6,85]. This may have been a response to selection for sound-source localization, particularly the capacity to locate brief environmental cues faster than visual inspection alone [3,33]. However, our hypothesis that this capacity was lacking, or poorly developed, in the immediate stem therian ancestors of the cladotheres suggests that the central or peripheral processing of sound in these early forms was either incapable of modern therian performance parameters, or an appropriate selective pressure for high frequency hearing was absent in earlier Mesozoic environments. The lack of clear selective advantage may in turn be attributable to evolutionary compromises between high-frequency requirements for sound localization and possible behavioral requirements for low-frequency perception (such as non-tympanic sound conduction); or the uncompetitive nature of the small insectivore niche in the Mesozoic. Whatever the original impetus for the development of ultrasonic frequency sensitivity, the segregation of terrestrial vertebrate faunas into a high-frequency therian component and low-frequency sauropsid component has persisted from the Jurassic to the present day.

Acknowledgments

I would like to sincerely thank Michael J. Novacek, Curator of Paleontology at the American Museum of Natural History, for access to the Höövör specimens; and Geoffrey Manley at the University of Oldenburg for generously lending the authors his time and expertise in the conceptualization and editing of this manuscript. Additionally, TH is grateful to Timothy Phelps at the Johns Hopkins Art as Applied to Medicine Program for his guidance in the production of the line art figures used in this report; and Gabriel Bever (Johns Hopkins University); Simone Hoffmann (NYIT College of Osteopathic Medicine); Julia Schultz (Universität Bonn); John R. Wible (Carnegie Museum of Natural History), and Brian Davis and Nobuyuki Kuwabara (both at University of Louisville) for their insight and assistance in understanding the complex literature on the anatomy and physiology of the inner ear.

This work was performed in part at the Duke University Shared Materials Instrumentation Facility (SMIF), a member of the North Carolina Research Triangle Nanotechnology Network (RTNN), which is supported by the National Science Foundation (Grant ECCS-1542015) as part of the National Nanotechnology Coordinated Infrastructure (NNCI). The CT lab, Austin Texas produced images of some specimens and provided technical and instructional support to GWR. Specimen collecting and data analysis was funded in part by PICT-2016-3682 from CONICET-Agencia de Promoción Científica y Técnica, Argentina; and NSF grants DEB 0946430, and DEB 1068089 to GWR and the Department of Anatomical Sciences and Neurobiology, University of Louisville. Finally, I thank Jin Meng, Eric Ekdale, and Alistair Evans for their attention and insightful comments during the review of this manuscript at PLOS One.

References

1. Rowe TB. Definition, diagnosis, and the origin of Mammalia. J Vertebr Paleontol. 1988;8: 241-264.

2. Köppl C, Manley GA. A functional perspective on the evolution of the cochlea. Cold Spring Harb Perspect Med. 2018; doi: 10.1101/cshperspect.a033241

3. Grothe B, Pecka M, McAlpine D. Mechanisms of sound localization in mammals. Physiol Rev. 2010;90: 983-1012.

4. Wible JR, Rougier GW, Novacek MJ, McKenna MC, Dashzeveg D. A mammalian petrosal from the Early Cretaceous of Mongolia: Implications for the evolution of the ear region and mamaliamorph interrelationships. Am Mus Novit. 1995;3149: 1-19.

5. Rougier GW, Wible JR, Hopson JA. Basicranial anatomy of *Priacodon fruitaensis* (Triconodontidae, Mammalia) from the Late Jurassic of Colorado, and a reappraisal of mammaliaform interrelationships. Am Mus Novit. 1996;3183: 1-38.

6. Rougier GW, Forasiepe AM, Hill RV, Novacek M. New mammalian remains from the Late Cretaceous La Colonia Formation, Patagonia, Argentina. Acta Paleontol Pol. 2009;54: 195-212

7. Ruf I, Luo ZX, Wible JR, Martin T. Petrosal anatomy and inner ear structures of the Late Jurassic *Henkelotherium* (Mammalia, Cladotheria, Dryolestoidea): insight into the early evolution of the ear region in cladotherian mammals. J Anat. 2009;214: 679-693.

8. Luo ZX, Ruf I, Martin T. The petrosal and inner ear of the Late Jurassic cladotherian mammal *Dryolestes leiriensis* and implications for ear evolution in therian mammals. Zool J Linn Soc. 2012;166: 433-463.

9. Wible JR, Rougier GW. Craniomandibular anatomy of the subterranean meridiolestidan *Necrolestes patagonensis* Ameghino, 1891 (Mammalia, Cladotheria) from the early Miocene of Patagonia. Ann Carnegie Mus. 2017;84: 183-252.

10. Archer M. The basicranial region of marsupicarnivores (Marsupialia), interrelationships of carnivorous marsupials, and affinities of the insectivorous marsupial peramelids. Zool J Linn Soc. 1976; 59: 217-322.

11. Asher RJ, Novacek MJ, Geisler JH. Relationships of endemic African mammals and their fossil relatives based on morphological and molecular evidence. J Mammal Evol. 2003;10: 131-194.

12. MacPhee RD. Auditory reigions of primates and eutherian insectivores. Basel: S. Karger; 1981.

13. Rosowski JJ, Graybeal A. What did *Morganucodon* hear?. Zool J Linn Soc. 1991;101: 131-168.

14. Manley GA. Cochlear mechanisms from a phylogenetic viewpoint. Proc Natl Acad Sci. 2000;97: 11736-11734.

15. Manley GA. The foundations of high-frequency hearing in early mammals. J Mammal Evol. 2016;25: 155-163.

16. Manley GA. Comparative auditory neuroscience: Understanding the evolution and function of ears. J Assoc Res Otolaryngol. 2017;18: 1-24.

17. Ashwell KW. Auditory and vestibular systems. In: Ashwell K, editor. Neurobiology of monotremes. Collingwood: CSIRO Publishing; 2013. pp. 219-233.

18. Schultz JA, Zeller U, Luo ZX. Inner ear labyrinth anatomy of monotremes and implications for mammalian inner ear evolution. J Morphol. 2017;278: 236-263.

19. Manley GA. The mammalian Cretaceous cochlear revolution. Hearing Res. 2017;352: 23-29.

20. DeBeer GR. The development of the vertebrate skull. Oxford: Clarendon Press.; 1937.

21. Moore WJ. The mammalian skull. Cambridge: Cambridge University Press; 1981.

22. Wible JR. Petrosal anatomy of the nine-banded armadillo, *Dasypus novemcinctus* Linnaeus, 1758 (Mammalia, Xenarthra, Dasypodidae). Ann Carnegie Mus. 2010;79: 1-28.

23. Meng J, Fox RC. Osseus inner ear structures and hearing in early marsupials and placentals. Zool J Linn Soc. 1995;115: 47-71.

24. Ekdale EG. Comparative anatomy of the bony labyrinth (inner ear) of placental mammals. PLOS One. 2013;8: 1-100.

25. Wever EG. The reptile ear: Its structure and function. Princeton: Princeton University Press; 1978.

26. Wible JR. Transformations in the extracranial course of the internal carotid artery in mammalian phylogeny. J Vertebr Paleontol. 1986;6: 313-325.

27. Rougier GW, Wible JR, Hopson JA. Reconstruction of the cranial vessels in the Early Cretaceous mammal *Vincelestes neuquenianus*: Implications for the evolution of the mammalian cranial vascular system. J Vertebr Paleontol. 1992;12: 188-216.

28. Wible JR, Hopson JA. Homologies of the prootic canal in mammals and non-mammalian cynodonts. J Vertebr Paleontol. 1995;15: 331-356.

29. Janfaza P, Nadol Jr JB, Galla R, Fabian RL, Montgomery WW. Surgical anatomy of the head and neck. Cambridge: Harvard University Press; 2011.

30. Nomura Y. Morphological aspects of inner ear disease. Tokyo: Springer Japan; 2014.

31. Panciroli E, Schultz JA, Luo Z. Morphology of the petrosal and stapes of *Borealestes* (Mammaliaformes, Docodonta) from the Middle Jurassic of Skye, Scotland. Papers in Paleontol. 2018; doi: 10.1002/spp2.1753

32. Kermack KA, Musset F, Rigney HW. The skull of *Morganucodon*. Zool J Linn Soc. 1981;71: 1-158.

33. Heffner HE, Heffner RS. The evolution of mammalian sound localization. Acoustics Today. 2016;12: 20-27.

34. Belyaeva EI, Trofimov BA, Reshetov VY. General stages in the evolution of late Mesozoic and early Tertiary mammalian faunas in central Asia. Trudy Sovmestnoi Sovetsko Mongol'skoi Paleontologicheskoi Ekspeditsii. 1974;1: 19-45.

35. Benton MJ. Conventions in Russian and Mongolian palaeontological literature. In: Benton MJ, Shishkin MA, Unwin DM, Kurochkin EN, editors. The age of dinosaurs in Russia and Mongolia. Cambridge: Cambridge University Press: 2000. pp. xvi-xxxix.

36. Kielan-Jaworowska Z, Cifelli RL, Luo ZX. Mammals from the age of dinosaurs: Origins, evolution, and structure. New York: University of Colombia Press; 2004.

37. Wible JR, Rougier GW, Novacek MJ, McKenna MC. Earliest eutherian ear region: a petrosal referred to *Prokennalestes* from the Early Cretaceous of Mongolia. Am Mus Novit. 2001;3322: 1-44.

38. Dashzeveg D. *Kielantherium gobiensis*, a primitive therian from the Early Cretaceous of Mongolia. Nat. 1975;227: 402-403.

39. Dashzeveg D. *Arguimus khosbajari* gen. n., sp. n., (Peramuridae, Eupantotheria) from the Lower Cretaceous of Mongolia. Acta Palaeontol Pol. 1979;24: 199-204.

40. Lopatin AV, Averianov AO. *Kielantherium*, a basal tribosphenic mammal from the Early Cretaceous of Mongolia, with new data on the aegialodontian dentition. Acta Palaeontol Pol. 2007;52: 441-446.

41. Lopatin AV, Averianov AO. The stem placental mammal *Prokennalestes* from the Early Cretaceous of Mongolia. Paleontol J. 2017;51: 1293-1374.

42. Lopatin AV, Averianov AO. A new stem placental mammal from the Early Cretaceous on Mongolia. Doklady Biol Sci. 2018;478: 8-11.

43. Rasmussen TE, Callison G. A new species of triconodont mammal from the Upper Jurassic of Colorado. J Paleontol. 1981;55: 628-634.

44. Callison G. Fruita: A place for wee fossils. In: Averett W editor. Paleontology and geology of the dinosaur triangle. Grand Junction: Grand Junction Geological Society: 1987. pp. 91-96.

45. Engelmann GF, Callison G. Mammalian faunas of the Morrison Formation. Mod Geol. 1998;23: 343-379.

46. Kermack KA. The cranial structure of the triconodonts. Phil Trans R Soc Lond B. 1963;246: 83-103.

47. Hu Y, Wang Y, Luo Z, Li C. A new symmetrodont mammal from China and its implications for mammalian evolution. Nature. 1997;390: 137-142.

48. Allin EF, Hopson JA. Evolution of the auditory system in Synapsida ("mammal-like reptiles" and primitive mammals" as seen in the fossil record. In: Webster DB, Fay RR, Popper AN, editors. The evolutionary biology of hearing. Heidelberg: Springer-Verlag: 1992. pp. 587-614.

49. Luo Z, Ruf I, Schultz JA, Martin T. Fossil evidence on evolution of inner ear cochlea in Jurassic mammals. Proc R Soc Lond B. 2011;278: 28-34.

50. Han G, Mao F, Bi S, Wang Y, Meng J. A Jurassic gliding euharamiyidan mammal with an ear of five auditory bones. Nature. 2017;551: 451-546.

51. Flower WH. An introduction to the osteology of Mammalia, 3rd ed. London: Macmillan; 1885.

52. MacIntyre GT. The trisulcate petrosal pattern of mammals. In: Dobshansky T, Hecht M, Steere WC, editors. Evolutionary Biology, Vol. 6. New York: Appleton-Century-Crofts: 1972. pp. 275-303.

53. DeBeer GR. The development of the skull of the shrew. Phil Trans. R Soc Lond B. 1929;217: 411-480.

54. Rougier GW, Wible JR. Major changes in the ear region and basicranium of early mammals. In: Carrano MT, Gaudin TJ, Blob RW, Wible JR, editors. Amniote paleobiology: Perspectives on the evolution of mammals, birds, and reptiles. Chicago: Chicago University Press; 2006. pp. 269-311.

55. Orliac MJ, O'Leary MA. The inner ear of *Protungulatum* (pan-Euungulatum, Mammalia). J Mam Evol. 2016;23: 337-352.

56. Bast TH. Development of the aquaeductus cochleae and its contained periotic duct and cochlear vein in human embryos. Ann Otol Rhinol Laryngol. 1946;55: 278-297.

57. Bast TH, Anson BJ. The development of the cochlear fenestra, fossula and secondary tympanic membrane. Ann Otol Rhinol Laryngol. 1954;62: 1083-1116.

58. Diogo R, Abdala V, Lonergan N, Wood BA. From fish to modern humans – comparative anatomy, homologies and evolution of the head and neck musculature. J Anat. 2008;213: 391-424.

59. Kielan-Jaworowska Z, Presley R, Poplin C. The cranial vasculature system in taeniolabidoid multituberculate mammals. Phil Trans R Soc Lond. 1986;313: 525-602.

60. Rougier GW, Ji Q, Novacek MJ. A new symmetrodont mammal with fur impressions from the Mesozoic of China. 2003;77: 7-14.

61. Novacek MJ. Patterns of diversity in the mammalian skull. In: Hanken J, Hall BK, editors. The skull, volume 2: Patterns of structural and systematic diversity. Chicago: University of Chicago Press; 1993. pp. 438-545.

62. Zeller U. Ontogenetic evidence for the cranial homologies in monotremes and therians, with special reference to *Ornithorhynchus*. In: Szalay FS, Novacek MJ, McKenna MC, editors. Mammal phylogeny: Mesozoic differentiation, multituberculates, monotremes, early therians, and marsupials. New York: Springer; 1993. pp. 95-107.

63. Hughes EM, Wible JR, Spaulding M, Luo ZX. Mammalian petrosal from the Upper Jurassic Morrison Formation of Fruita, Colorado. Ann Carnegie Mus. 2015;83: 1-17.

64. Turkewitsch BG. Comparative anatomical investigation of the osseous labyrinth (vestibule) in mammals. Am J Anat. 1935;57: 503-543.

65. MacIntyre GT. Foramen pesudovale and quasi-mammals. Evol. 1966;21: 834-841.

66. McDowell SB. The Greater Antillean insectivores. Bull Am Mus Nat Hist. 1958;115: 113-214.

67. Wible JR. The eutherian stapedial artery: character analysis and implications for superordinal relationships. Zool J Linn Soc. 1987;91: 107-135.

68. Luo ZX, Schultz JA, Ekdale EG. Evolution of the middle and inner ears of mammaliaformes: the approach to mammals. In: Clack JA, Fay RR, Popper AN, editors. Evolution of the vertebrate ear: Evidence from the fossil record. Cham: Springer; 2016. pp. 139-174.

69. Ekdale EG. The ear of mammals: From monotremes to humans. In: Clack JA, Fay RR, Popper AN, editors. Evolution of the vertebrate ear: Evidence from the fossil record. Cham: Springer; 2016. pp. 175-206.

70. Ruf I, Luo ZX, Martin T. Reinvestigation of the basicranium of *Haldanodon expectatus* (Mammaliaformes, Docodonta). J Vertebr Paleontol. 2013;33: 382-400.

71. Axelsson A. Comparative anatomy of cochlear blood vessels. Am J Otolaryngol. 1988;9: 278-290.

72. Lempert J, Meltzer PE, Wever EG, Lawrence M, Rambo JHT. Structure and function of the cochlear aqueduct. AMA Archives of otolaryngol. 1952;55: 134-145.

73. Perlman HB. Experimental occlusion of the inferior cochlear vein. Ann Otol Rhinol Laryngol. 1952;61: 33-44.

74. Forasiepi AM, Rougier GW. Additional data on early Paleocene metatherians (Mammalia) from Punta Peligro (Salamanca Formation, Argentina): comments based on petrosal morphology. J Zool Syst Evol Res. 2009;47: 391-398.

75. Nin F, Yoshida T, Sawamura S, Ogata G, Ota T, Higuchi T, et al. The unique electrical properties in an extracellular fluid of the mammalian cochlea; their functional roles, homeostatic processes, and pathological significance. Pflugers Arch Eur J Physiol. 2016;468: 1637-1649.

76. Wilms V, Köppl C, Söffgen C, Hartmann AM, Nothwang HG. Molecular bases of K+ secretory cells in the inner ear: Shared and distinct features between birds and mammals. Sci Rep. 2016;6: 1-13.

77. Manley GA. The cochlea: What it is, where it came from, and what is special about it. In: Manley GA, Grummer AW, Popper AN, Fay RR, editors. Understanding the cochlea. Cham: Springer; 2017. pp. 17-32.

78. Kikuchi K, Hilding DA. The development of the stria vascularis in the mouse. Acta otolaryngologica. 1966;62: 277-291.

79. Pritchard U. The cochlea of the *Ornithorhynchus platypus* compared with that of ordinary mammals and of birds. Phil Trans R Soc Lond. 1881;172: 267-282.

80. Schmidt RS, Fernández C. Labyrinthine DC potentials in representative vertebrates. J Cell Phys. 1962;59: 311-322.

81. Manley GA. A review of some current concepts of the functional evolution of the ear in terrestrial vertebrates. Evol. 1972;26: 608-621.

82. Manley GA, Haeseler C, Brix J. Innervation patterns and spontaneous activity of afferent fibres to the lagenar macula and apical basilar papilla if the chicken's cochlea. Hear Res. 1991;56: 211-226.

83. Köppl C, Wilms V, Russell IJ, Nothwang HG. Evolution of endolymph secretion and endolymph potential generation in the vertebrate inner ear. Brain Behav Evol. 2018; DOI: 10.1159/000494050

84. Manley GA. Evolutionary paths to mammalian cochleae. J Assoc Res Otolaryngol. 2012;13: 733-743.

85. Wible JR. Petrosals of Late Cretaceous marsupials from North America, and a cladistic analysis of the petrosal in therian mammals. 1990;10: 183-205.

86. Evans HE, De Lahunta A. Miller's anatomy of the dog. St Louis: Elsevier health sciences; 2013.

87. Graybeal A, Rosowski JJ, Ketten DR, Crompton AW. Inner-ear structure in *Morganucodon*, and early Jurassic mammal. Zool J Linn Soc. 1989; 96: 107-117.

88. Luo Z, Crompton AW, Lucas SG. Evolutionary origins of the mammalian promontorium and cochlea. J Vertebr Paleontol. 1995;15: 113-121.

89. Hossler FE, Olson KR, Musil G, McKamey MI. Ultrastructure and blood supply of the tegmentum vasculosum in the cochlea of the duckling. Hearing Res. 2002;164: 155-165.

90. Shahid R, Gil GG, Hoffmann S. Inner ear morphology of basal-most mammaliaform *Morganucodon*. The FASEB Journal, No 1 Supplement. 2018; 32: 780. Available from https://www.fasebj.org/doi/abs/10.1096/fasebj.2018.32.1_supplement.780.9

91. Spoor F, Zonnefeld F. Morphometry of the primate bony labyrinth: A new method based on high-resolution computed tomography. J Anat. 1995;186: 271-286.

92. Rodrigues PG, Ruf I, Schultz CL. Digital reconstruction of the otic region and inner ear of the non-mammalian cynodont *Brasilitherium riograndensis* (Late Triassic, Brazil) and its relevance to the evolution of the mammalian ear. J Mammal Evol. 2013;20: 291-307.

93. Olson EC. Origin of mammals based upon cranial morphology of the therapsid suborders. Spec Pap Geol Soc Am. 1944;55: 1-136.

94. MacLean PD. Neurobehavioral significance of the mammal-like reptiles (theriapsids). In: MacLean PD, Roth JJ, Roth EC, editors. The ecology and biology of mammal-like reptiles. Washington: Smithsonian Institution Press: 1986. pp. 1-21.

95. Butler AB, Hodos W. Comparative vertebrate neuroanatomy: Evolution and adaptation. 2nd ed. Hoboken: John Wiley and Sons Inc.; 2005.

96 Rowe TB. The emergence of mammals. In: Kaas JH, editor. Evolution of nervous systems, second edition, volume 2. Oxford: Elsevier; 2017. pp. 1-52.

97. Rich TH, Hopson JA, Musser AM, Flannery TF, Vickers-Rich P. Independent origins of middle ear bones in monotremes and therians. Science. 2005;307: 910-914.

98. Urban DJ, Anthwal N, Luo Z, Maier JA, Sadier A, Tucker AS. A new developmental mechanism for the separation of the mammalian middle ear ossicles from the jaw. Proc R Soc B. 2017;284: 1-8.

99. Vater M, Kössl M. Comparative aspects of cochlear functional organization in mammals. Hearing Res. 2011;273: 89-99.

100. Manley GA, Köppl C. Phylogenetic development of the cochlea and its innervation. Curr Opin Neurobiol. 1998;8: 468-474.

101. Fettiplace R, Fuchs PA. Mechanisms of hair cell tuning. Ann Rev Physiol. 1999;61: 809-834.

102. Chan DK, Hudspeth AJ. Ca 2+ current-driven nonlinear amplification by the mammalian cochlea in vitro. Nature Neurosci. 2005;8: 149-155.

103. Peng AW, Ricci AJ. Somatic motility and hair bundle mechanics, are both necessary for cochlear amplification. Hear Res. 2011;273: 109-122.

104 Ladhams A, Pickles JO. Morphology of the monotreme orgen of Corti and macula lagena. J Comp Neurol. 1996;366: 335-347.

105. Prothero DR. The oldest mammalian petrosals from North America. J Paleontol. 1983;57: 1040-1046.

106. Augee ML, Gooden B, Musser A. Echidna: Extraordinary egg-laying mammal. CSIRO Publishing; 2006.

107. Martin T, Marugán-Lobón J, Vullo R, Martín-Abad H, Luo ZX, Buscalioni AD. A Cretaceous eutriconodont and integument evolution in early mammals. Nature. 2015;526: 380-384.

108. Wible JR, Hopson JA. Basicranial evidence for early mammal phylogeny. In: Szalay FS, Novacek MJ, McKenna MC, editors. Mammal phylogeny: Mesozoic differentiation, multituberculates, monotremes, early therians, and marsupials. New York: Springer; 1993. pp. 45-62.

109. Vater M, Meng J, Fox RC. Hearing organ evolution and specialization: Early and later mammals. In: Manley GA, Popper AN, Fay RR, editors. Evolution of the vertebrate auditory system. New York: Springer; 2004. pp. 256-288.

110. Maier W, Ruf I. Evolution of the mammalian middle ear: A historical review. J Anat. 2016;228: 270-283.

111. Gauthier J, Kluge AG, Rowe T. Amniote phylogeny and the importance of fossils. Cladistics. 1988;4: 105-209.

112. Zeller U. The morphogenesis of the fenestra rotunda in mammals. In: Duncker HR, Fleischer G, editors. Functional morphology in vertebrates. Stuttgart: Fisher; 1985. pp. 153-157.

113. Zeller U. Die ontogenese und morphologie der fenestra rotunda und des aqueductus cochleae von *Tupaia* und anderen säugern. Gegenbaurs morphol jahrb. 1985;131: 179-204.

114. Ji Q, Luo ZX, Zhang X, Yuan CX, Xu L. Evolutionary development of the middle ear in Mesozoic therian mammals. Science. 2009;326: 278-281.

115. McKenna MC. Toward a phylogenetic classification of the Mammalia. In: Luckett WP, Szalay FS, editors. Phylogeny of the primates: a multidisciplinary approach. New York: Plenum Press; 1975. pp. 21-46.

116. Prothero DR. New Jurassic mammals from Como Bluff, Wyoming, and the interrelationships of non-tribosphenic Theria. Bull Am Mus Nat Hist. 1981;167: 281-317.

117. Ladevèze S, Asher RJ, Sánchez-Villagra MR. Petrosal anatomy in the fossil mammal *Necrolestes*: Evidence for metatherian affinities and comparisons with the extant marsupial mole. J Anat. 2008;213: 686-697.

118. Paez-Arango N. Dental and craniomandibular anatomy of *Peligrotherium tropicalis*: the evolutionary radiation of South American dryolestoid mammals. M.Sc Thesis, University of Louisville. 2008.

119. Ravicz ME, Slama MC, Rosowski JJ. Middle-ear pressure gain and cochlear partition differential pressure in chinchilla. Hearing Res. 2010;263: 16-25.

120. Meng J, Fox RC. Therian petrosals from the Oldman and Milk River Formations (Late Cretaceous), Alberta, Canada. J Vertebr Paleontol. 1995;15: 122-130.

121. Allin EF. The auditory apparatus of advanced mammal-like reptiles and early mammals. In: MacLean PD, Roth JJ, Roth EC, editors. The ecology and biology of mammal-like reptiles. Washington: Smithsonian Institution Press: 1986. pp. 283-294.

122. Rougier GW, Sheth AS, Spurlin BK, Bolortsetseg M, Novacek MJ. Craniodental anatomy of a new Late Cretaceous multituberculate mammal from Udan Sayr, Mongolia. Acta Paleont Polonica. 2016;67: 197-248.

123. Wang Y, Hu Y, Meng J, Li C. an ossified Meckel's cartilage in two Cretaceous mammals and origin of the mammalian middle ear. Science. 2001;294: 357-361

124. Gao CL, Wilson GP, Luo ZX, Maga AM, Meng Q, Wang X. A new mammal skull from the Lower Cretaceous of China with implications for the evolution of obtuse-angled molars and 'amphilestid' eutriconodonts. Proc R Soc B. 2009; rspb20091014

125. Trofimov BA. A new generic name *Gobiotheriodon* for a symmetrodontan mammal *Gobiodon* Trofimov, 1980. Acta Paleontol Pol. 1997;42: 496-496.

126. Averianov AO. Early Cretaceous "symmetrodont" mammal *Gobiotheriodon* from Mongolia and the classification of "Symmetrodonta". Acta Paleont Polonica. 2002;47: 705-716.

127. Mason MJ. Structure and function of the mammalian middle ear II: inferring structure from function. J Anat. 2016;228: 300-312.

128. Basch ML, Brown RM, Jen H, Groves AK. Where hearing starts: the development of the mammalian cochlea. J Anat. 2016;228: 233-254.

129. Manley GA. Evidence for an active process and a cochlear amplifier in nonmammals. J Neurophys. 2001;86: 541-549.

130. Wangemann P. K+ cycling and the endocochlear potential. Hearing Res. 2002;165: 1-9.

131. Wangemann P. Supporting sensory transduction: cochlear fluid homeostasis and the endocochlear potential. J Phys. 2006;576: 11-21.

132. Wantanabe Y, Nakashima T, Yanagita N. Venous communications of the cochlea after acute occlusion of the vein of the cochlear aqueduct. Arch Otorhinolaryngol. 1988;245: 340-343.

133. Shodo R, Hayatsu M, Koga D, Horii A, Ushiki T. Three-dimensional reconstruction of root cells and interdental cells in the inner ear by serial section scanning electron microscopy. Biomed Res. 2017;38: 239-248.

134. Tan X, Pecka JL, Tang J, Okoruwa OE, Zhang Q, Beisel KW, et al. From zebrafish to mammal: Functional evolution of prestin, the motor protein of cochlear outer hair cells. J Neurophys. 2010;105: 36-44.

135. Liu Z, Li GH, Huang JF, Murpohy RW, Shi P. Hearing aid for vertebrates via multiple episodic adaptive events on prestin genes. Molec Biol and Evol. 2012;29: 2187-2198.

136. Manley GA, Fuchs PA. Recent advances in comparative hearing. Hearing Res. 2011;273: 1-6.

137. Patuzzi, R. Cochlear micromechanics and macromechanics. In: Dallos P, Popper AN, Fay RR, editors. The Cochlea. New York: Springer; 1996. pp. 186-257.

138. Fritzsch B, Pan N, Jahan I, Ducan JS, Kopecky BJ, Elliot KL, et al. Evolution and development of the tetrapod auditory system: An organ of Corti centric perspective. Evol and Dev. 2013;15: 63-79.

139. Ramanathan K, Michael TH, Jiang GJ, Hiel H, Fuchs PA. A molecular mechanism for electrical tuning of cochlear hair cells. Science. 1999;283: 215-217.

140. Crompton AW, Luo ZX. Relationships of the Liassic mammals *Sinoconodon*, *Morganucodon oehleri*, and *Dinnetherium*. In: Szalay FS, Novacek MJ, McKenna MC, editors. Mammal phylogeny: Mesozoic differentiation, multituberculates, monotremes, early therians, and marsupials. New York: Springer; 1993. pp.30-44.

141. Forsman KA, Malmquist MG. Evidence for echolocation in the common shrew, *Sorex araneus*. J Zool. 1988;216: 655-662.

142. Fettiplace R. Hair cell transduction, tuning, and synaptic transmission in the mammalian cochlea. Comp Physiol. 2017;7: 1197-1227.

143. Manoussaki D, Chadwick RS, Ketten DR, Arruda J, Dimitriadis EK, O'Malley JT. The influence of cochlear shape on low-frequency hearing. Proc Nat Acad Sci. 2008;105: 6162-6166.

144. Sellick PM, Patuzzi R, Johnstone BM. Measurement of basilar membrane motion in the guinea pig using the Mössbauer technique. J Acoust Soc Am. 1982;72: 131-141.

145. Ruggero MA. Responses to sound of the basilar membrane of the mammalian cochlea. Curr Opin Neurobiol. 1992;2: 449-456.

146. Henson MM, Henson OW Jr. Tension fibroblasts and the connective tissue matrix of the spiral ligament. Hearing Res. 1988;35: 237-258.

147. Thomas JA, Jalili MS. Echolocation in insectivores and rodents. In: Thomas JA, Moss CF, Vater M, editors. Echolocation in bats and dolphins. Chicago: University of Chicago Press; 2004. pp. 547-564.

148. Müller MW, Wess FP, Bruns V. Cochlear place-frequency map in the marsupial *Monodelphis domestica*. Hear Res. 1993;67: 198-202.

149. Ravizza RJ, Heffner HE, Masterson B. Hearing in primitive mammals: I. Opossum (*Didelphis virginianus*). J Audit Res. 1969;9: 1-7.

150. Heffner HE, Ravizza RJ, Masterson B. hearing in primitive mammals III. Tree shrew (*Tupaia glis*). J Audit Res. 1969;9: 12-18.

151. Mills DM, Shepherd RK. Distortion product otoacoustic emission and auditory brainstem responses in the echidna (*Tachyglossus aculeatus*). J Ass Res Otolaryngol. 2001;2: 130-146.

152. Gates RG, Saunders JC, Bock GR. Peripheral auditory function in the platypus, *Ornithorhynchus anatinus*. J Acoustic Soc Am. 1974;56: 152-156.

153. Drexl M, Faulstich M, von Stebut B, Radtke-Schuller S, Kössl M. Distortion product otoacoustic emissions and auditory evoked potentials in the hedgehog tenrec, *Echinops telfairi*. J Ass Re Otolaryngol. 2003;4: 555-564.

154. Aitkin L. The auditory neurobiology of marsupials: a review. Hear Res. 1995;82: 257-266.

155. Köppl C. Phase locking to high frequencies in the auditory nerve and cochlear nucleus magnocellularis of the barn owl, *Tyto alba*. J Neurosci. 1997;17: 3312-3321.

156. Arch VS, Grafe TU, Gridi-Papp M, Narins PM. Pure ultrasonic communication in an endemic Bornean frog. PLOS One. 2009; DOI: 10.1371/journal.pone.0005413

157. McKenna MC, Kielan-Jaworowska, Meng J. Earliest eutherian mammal skull from the Late Cretaceous [Coniacian] of Uzbekistan. Acta Palaeontol Pol. 2000;45: 1-54.

158. O'Leary MA, Bloch JI, Flynn JJ, Gaudin TJ, Giallombardo A, Giannini NP, et al. The placental mammal ancestor and the post-K-Pg radiation of placentals. Sci. 2013;339: 662-667.

159. Payan P, Borelli G, Priouzeau F, De Pontual H, Boeuf G, Mayer-Gostan N. Otolith growth in trout Oncorhynchus mykiss: supply of Ca^{2+} and Sr^{2+} to the saccular endolymph. J exp Biol. 2002;202: 2687-2695.

160. Preston RE, Johnsson LG, Hill JH, Schacht J. Incorporation of radioactive calcium into otolithic membranes and middle ear ossicles of the gerbil. Acta Otolaryngologica. 1975;80: 269-275.

161. Salt AN, Mleichar I, Thalmann R. Mechanisms of endocochlear potential generation by stria vascularis. The Laryngoscope. 1987;97: 984-991.

162. Salt AN, Inamura N, Thalmann R, Vora A. Calcium gradients in inner ear endolymph. Am J Otolaryngol. 1989;10: 371-375.

163. Fox RC, Meng J. An x-radiographic and SEM study of the osseus inner ear of multituberculates and monotremes (Mammalia): Implications for mammalian phylogeny and evolution of hearing. Zool J Linn Soc. 1997;121: 249-291.

164. Bi S, Zheng X, Wang X, Cignetti NE, Yang S, Wible JR. An Early Cretaceous eutherian and the placental-marsupial dichotomy. Nature. 2018;558: 390-395.

165. Allin EF, Hopson JA. Evolution of the auditory system in Synapsida ("mammal-like reptiles" and primitive mammals) as seen in the fossil record. In: Webster DB, Popper AN, Fay RR, editors. The evolutionary biology of hearing. New York: Springer: 1992. pp. 587-614.

166. Rougier GW, Apesteguía S, Gaetano LC. Highly specialized skulls from the Late Cretaceous of South America. Nature. 2011;479: 98-102.

167. Christensen-Dalsgaard J, Manley GA. Directionality of the lizard ear. J Exp Biol. 2005;208: 1209-1217.

168. Nothwang HG. Evolution of mammalian sound localization circuits: a developmental perspective. Prog Neurobiol. 2016;141: 1-24.

169. Christensen-Dalsgaard J, Manley GA. Acoustical coupling of lizard eardrums. J Ass Res Otolaryngol. 2008;9: 407-416.

170. Köppl C. Evolution of sound localisation in land vertebrates. Curr Biol. 2009;19: 635-639.

171. Kemp TS. Non-mammalian synapsids: the beginning of the mammal line. In: Clack JA, Fay RR, Popper AN, editors. Evolution of the vertebrate ear: Evidence from the fossil record. Cham: Springer; 2016. pp. 107-137.

172. Mason MJ. Internally coupled ears in living mammals. Biol Cybern. 2016;110: 345-358.

173. Grothe B, Pecka M. The natural history of sound localization in mammals-a story of neuronal inhibition. Frontiers in neural circuits. 2014;8: 1-19.

174. Segall W. Morphological parallelisms of the bulla and auditory ossicles in some insectivores and marsupials. Fieldiana Zool. 1970;51: 169-206.

175. Mason MJ. Structure and function of the mammalian middle ear I: Large middle ears in small desert mammals. J Anat. 2016;228: 284-299.

176. Christensen-Dalsgaard J. Vertebrate pressure-gradient receivers. Hearing Res. 2011;273: 37-45.

177. Grothe B. The evolution of temporal processing in the medial superior olive, an auditory brainstem structure. Progress in neurobiology. 2000;61: 581-610.

178. Brown CH, May BJ. Comparative mammalian sound localization. In: Popper AN, Fay RR, editors. Sound source localization. New York: Springer: 2005. pp.124-178.

179. Rice JJ, May BJ, Spirou GA, Young ED. Pinna-based spectral cues for sound localization in cat. Hearing Res. 1992;58: 132-152.

180. Gaetano LC, Rougier GW. New materials of *Argentoconodon fariasorum* (Mammaliaformes, Triconodontidae) from the Jurassic of Argentina and its bearing on triconodont phylogeny. J Vertebr Paleontol. 2011;31: 829-843.

181. Luo ZX, Yuan CX, Meng QJ, Ji Q. A Jurassic eutherian mammal and divergence of marsupials and placentals. Nature. 2011;476: 442-445.

182. Cantos R, Cole LK, Acampora D, Simeone A, Wu DK. Patterning of the mammalian cochlea. Proc Natl Acad Sci. 2000;97: 707-711.

183. Bok J, Chang W, Wu DK. Patterning and morphogenesis of the vertebrae inner ear. Int J Dev Biol. 2007;51: 521-533.

184. Luo Z. Developmental patterns in Mesozoic evolution of mammal ears. Annu Rev Ecol Evol Syst. 2011;42: 355-380.

185. Polley DB, Seidl AH, Wang Y, Sanchez JT. Chapter 2 - Functional circuit development in the auditory system. In: Rubenstein JLR, Rakic P, editors. Neural circuit development and function in the brain. Oxford: Academic Press; 2013. pp 21-39.

186. Crompton AW. The origin of the tribosphenic molar. Zool J Linn Soc. 1971;50: 65-81.

187. Wilson GP. Mammals across the K/Pg boundary in northeastern Montana, USA: dental morphology and body-size pattens reveal extinction selectivity and immigrant-fueled ecospace filling. Paleobiol. 2013;39: 429-469.

188. Schultz JA, Martin T. Function of pretribosphenic and tribosphenic mammalian molars inferred from 3D animation. Naturwissenschaften. 2014;101: 771-781.

189. Grossnickle DM, Newham E. Therian mammals experience an ecomorphological radiation during the Late Cretaceous and selective extinction at the K-Pg boundary. Proc R Soc B. 2016;283: 1-8.

190. Grossnickle DM. The evolutionary origin of jaw yaw in mammals. Sci Rep. 2017;7: 1-13.

191. Gu JJ, Montealegre-Z F, Robert D, Engel MS, Qiao GX, Ren D. Wing stridulation in a Jurassic katydid (Insecta, Orthoptera) produced low-pitched musical calls to attract females. Proc Natl Acad Sci. 2012;109: 3868-3873.

192. Close RA, Friedman M, Graeme TL, Benson RBJ. Evidence for a Mid-Jurassic adaptive radiation in mammals. Curr Biol. 2015;25: 2137-2142.

Supplementary Information:

Evolution of the Synapsid Ear

Synapsid fossils have a unique significance for the study of the nervous system [1-3]. In particular, skeletal structures such as the mammalian petrosal and middle ear show an especially close relationship with the central and peripheral nervous tissues that utilize them. The fossil record also provides otherwise unattainable information on the sequence and timing of the evolution of these tissues. As emphasize in [3], the modern mammalian nervous system is the product of many consecutive episodes of reorganization, many of which are best studied in the cranial remains of fossil synapsids. This synopsis of the stem-based clade Pan-Mammalia (inclusive of all taxa more closely related to mammals than any other living organism), by the characterization of successively more exclusive clades based around the therian crown group therefore provides a useful focus and phylogenetic context for understanding neurosensory evolution within this lineage, and the significance of stem therian petrosal structure within it.

From the earliest stretch of stem therian evolution, several extinct but derived groups appear to have diverged [4,5]. These groups include the questionably paraphyletic eutriconodonts [6-9], the multituberculates ([10-14]; along with their probable sister taxon Gondwannatheria [15]), and the spalacotheroid symmetrodonts [16,17]. The high-resolution micro-CT images used in this report represent the first observations of the internal structure of the otic capsule in eutriconodonts and possibly "symmetrodont" mammals. Because of the highly derived apomorphies seen in even the earliest representatives of the multituberculate lineage, such as the presence of multiple "foramina ovale" (apertures for

the mandibular branch of the trigeminal nerve; [11]), and even more morphologically unique features found in later members of this lineage [10], the diversity of mutituberculate petrosal morphology is considered a specialized side branch of early mammals and is not discussed further here.

Aside from contributing to the body of anatomical detail known for these obscure stem therian groups, petrosal descriptions allow for the broad reconstruction of auditory sensitivity, selectivity, and range in the members of the stem therian lineage. These reconstructions require a wide perspective on petrosal diversity, however, and input from several independent research programs; particularly 1) biomechanical analyses of earlier synapsid fossils [18,19]; 2) comparative and developmental studies of therian and cladotherian anatomy [20,21]; and 3) physiological research on modern mammals and non-mammalian amniotes [22,23]. As outlined below, the reconstruction of which of three non-mutually-exclusive forms of cochlear tuning, or which of four forms of sound localization, were likely present in the stem therians described here will critically depend on the findings of prior analyses of auditory physiology and vascular anatomy in non-mammalian amniotes and the construction and distribution of middle ears and their anatomically precedent structures [24-27]. The following discussion therefore parallels [3] in tracing a series of sequentially more recent nodes along the backbone of synapsid phylogeny, beginning with the characterization of the amniote common ancestor and ending with the mammalian crown group (which is picked up in the main text; see SI Fig 1).

Fig S1. Example cladogram showing consecutively nested clades referred to in text.

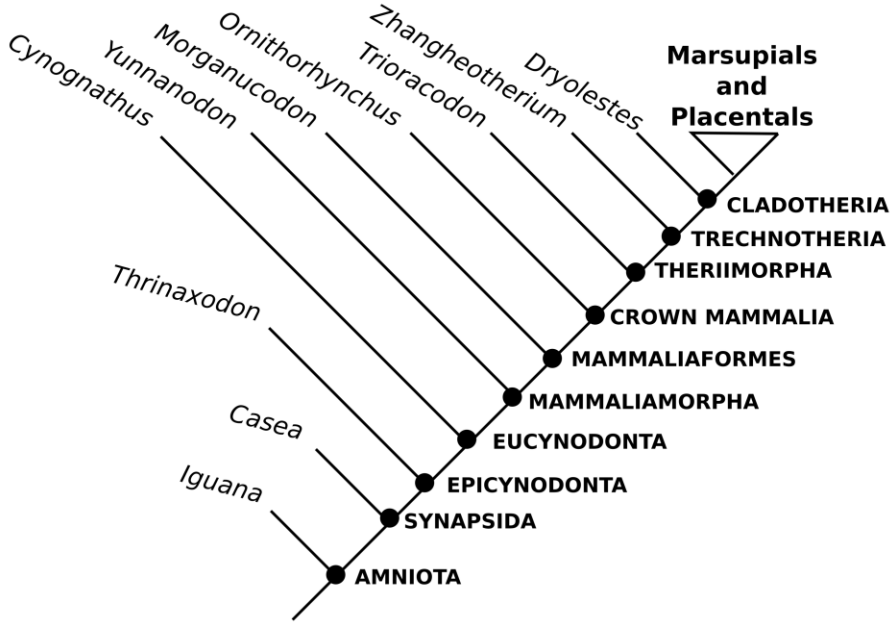

Amniotes

The late Paleozoic ancestors of the modern amniote lineages (Sauropsida and Synapsida) are reconstructed as petite "reptiles" with an estimated nine-inch snout-vent length [28]. The anteroventral subdivision of the endolymphatic labyrinth in these forms is termed the pars inferior, initially a minor diverticulum accommodating three specialized sensory epithelia [29,30]. These sensory epithelia include the incipiently subdivided saccular and lagenar maculae, and the basilar papilla (an even more recently acquired extension of the saccule; [2]). While the sensory modalities and performance parameters within which these epithelia operate are considerably more complex in fishes and amphibians, for extant and fossil members of the amniote lineage it is most likely that the saccular macula took on a dedicated role in equilibrium and proprioception, the basilar papilla an increasingly specialized role in sound perception, and the lagenar macula some combination of the two roles which became progressively more redundant thought out synapsid history [2]. The sensory epithelia contained within the pars inferior were in turn accommodated by a matching concavity within the bony labyrinth termed the sacculocochlear recess (i.e. the lagenar recess [29,31], inter alios). This configuration allowed the membrane supporting the basilar papilla to oscillate in response to vibrations induced within the bony labyrinth [32]. The reconstructed lack of a coherent gradient in width, thickness, and material properties in the early amniotic basilar membrane (a condition retained in most extant sauropsids) constrained the entire basilar membrane to oscillate homogeneously in response to the frequency content of external stimuli. In early amniotes (including early synapsids) the fenestra vestibuli was also located at the lateral or ventrolateral margin of the sacculocochlear recess.

The approximately 1 mm long basilar papilla (homolog to the mammalian organ of Corti) in the amniote common ancestor is estimated to have been competent for only a 3 or 4 octave interval of detectable frequencies; corresponding to an equally diminutive acoustic Space Constant (SC, or Space Per Octave) of ~0.3 mm per octave [33-37]. This short theoretical SC, together with the reconstructed consignment of these animals to the low-frequency range, is based on physiological observations of extant sauropsids (*Sphenodon* and turtles), many of which retain the most plesiomorphic form of frequency selectivity, termed electrical tuning [38].

Electrical tuning involves the active and intrinsic calibration of each individual auditory hair cell by the modulation of the density and kinetics of voltage-gated calcium channels in the basolateral cell membrane [39,40]. Calcium is critical for allowing the release of cytosolic potassium in a depolarized hair cell, and therefore its subsequent hyperpolarization. Because of the considerable refractory period in which an individual hair cell is required to import potassium from the endolymph, depolarize, import calcium from the basolateral membrane, export potassium through the basolateral membrane and thus repolarize - the intrinsic tuning of these auditory hair cells can only correspond to a dynamic range of frequencies starting from less than 100 Hz to around 1 kHz maximally in most ectotherms [34]. At the heightened body temperatures of endotherms, theoretical considerations suggest that electrical tuning would be functional up to approximately 4 kHz [41,42].

The likely electrically tuned basilar papilla within the first amniotes was metabolically supported by both vascular and epithelial tissues running throughout the pars inferior, especially the basilar membrane (the "bottom" of the reptilian cochlear duct) and Reissner's membrane (also termed the vestibular membrane; which forms the "top" of the cochlear

duct). The tortuous capillary plexus within Reissner's membrane in particular is homologous to the original and sole endolymph-producing organ in the ancestral amniotes, and is today retained in all extant sauropsids as well as monotremes (Fig 14a,b ;[43]). The initial configuration of blood vessels supporting the auditory apparatus therefore encircled the pars inferior with little to no integration of these vessels with the surrounding skeleton of the otic capsule. Indeed, one of the main observations made during resections of the auditory apparatus of non-mammalian amniotes is that the cochlear duct can be "scooped" cleanly with dissecting tools from its cartilaginous or bony housing in the otic capsule [44,22]. This lack of bony integration is most dramatically apparent in birds, where the hypertrophied capillary plexus in the vestibular membrane is termed the tegmentum vasculosum (e.g. in [44] fig 5 section 1; this reference also shows the source of this vasculature to be endocranial, penetrating the otic capsule in proximity with the cochlear nerve). The vascularized membrane, separating the endolymphatic labyrinth from the perilymphatic space, also supports the lagenar macula and its attached otoconial mass in extant sauropsids and monotremes [43,30]. Thus, it can be inferred that the production and composition of endolymph in modern sauropsids, with its characteristically high (~ 30 micromolar to over 1 millimolar; [45]) concentration of free calcium cations and low electrical potential, was initiated in the earliest amniote ancestors possibly as a means of facilitating the electrical tuning of the basilar papilla and stabilizing the lagena and other otoconial masses [46].

Synapsids

There is a consensus that forms in the early burst of synapsid evolution lacked any form of tympanic membrane or acoustically relevant cranial air-spaces [22,47]. Additionally, the co-

option of the hypertrophied stapes (a second arch viscerocranial element) as a firm structural interconnection between the posterior neurocranial and dermatocranial components of the skull, acted as a mechanism for reinforcing the ancestral jaw apparatus against structural deflections during biting. This probably also limited its auditory sensitivity [48,49,22].

What acoustic receptivity these forms achieved was likely mediated through a mixture of indirect conduction (where the majority of the dermatocranium acted as a vibrational antenna, possibly in service of a semiaquatic lifestyle in many taxa) and direct conduction (where seismic/airborne vibrations are transmitted through the lower jaw [19,50]). Waves of pressure were therefore transmitted into the otic capsule through the skull's out-of-phase motion with respect to the massive and inertially stabilized stapes [47,51]. These conduction mechanisms are most appropriate for low-frequency and high-amplitude vibrations and electrical tuning would have been more than capable of processing these signals.

Opposite to the condition of its lateral border, the endocranial wall of the otic capsule is poorly ossified in pelycosaurs and most other non-mammaliaform synapsids. This is reflected by the absence of an invaginated internal acoustic meatus and lack of ossified partitions separating the perilymphatic foramen and cranial nerves VII-XII along the medial aspect of the braincase [52]. What can be determined about the structure of the otic capsule shows that the pars cochlearis is absent in the earliest synapsids; however, the corresponding pars inferior of the endolymphatic labyrinth would have been accommodated by a shallow sacculocochlear recess that itself did not emarginate the wider contour of the bony labyrinth [32]. The lack of a pars cochlearis within the early synapsid otic capsule does not imply a more or less monolithic composition of the periotic skeleton, however; and the adult otic

capsule in early synapsids is a composite structure mainly formed by the prootic and opisthotic bones, with variable minor contributions from other cranial elements [47].

By the Middle Permian a diverse group of therapsids had evolved from the carnivorous sphenacodontan pelycosaurs. These animals display a trend of progressive loosening of the quadrojugal and quadrate from the squamosal, possibly resulting in some combination of incipient streptostyly and whole-bone sound conduction. Additionally, the increased development of the reflected lamina of the angular bone (homolog of the mammalian ectotympanic) and formation of the recessus mandibularis as a mandibular resonating chamber, suggest that direct conduction of low-frequency, possibly airborne, sound was possible. The relatively voluminous recessus mandibularis in some of the larger therapsids point to its possible dual function as a resonator for both the reception and production of airborne vocal signals [49]. With the increased development of the recessus mandibularis, a trend of decreasing reliance on sound conduction via intra-bone vibrations and greater reliance on conduction through whole-bone vibration is also likely [47]. However, the low transformation ratios between the area of the reflected lamina of the angular and the fenestra vestibuli would have provided little compensation for the energy lost due to impedance mismatch between the surrounding air and fluids inside the otic capsule [53,18,49].

Epicynodonts

Near the Permo-Triassic boundary the epicynodonts, along with other therapsid groups, show the complete subdivision of the oronasal cavity into dedicated oral and nasal cavities by the completion of an osseous secondary palate [54,55]. The resultant caudal aperture of

the nasal cavity, the internal choanae, created a new communication to the rostral pharynx (nasopharynx). The nasopharynx itself became a hub for gaseous communication to the larynx caudally, and its lateral apertures are also reconstructed as having communicated with the recessus mandibularis [56]. If this is the case, it constitutes the first well-delimited connection between the nasopharynx and the ear region.

The epicynodonts also show the subdivision of the sacculocochlear recess of the bony labyrinth into a dedicated saccular recess (recessus sphericus) and a separate bony cul-de-sac termed the cochlear recess [32]. This morphology of the bony labyrinth suggests that the corresponding pars inferior of the membranous labyrinth was also at least incipiently subdivided into a discrete saccule (confluent at one end to the endolymphatic duct and utricle, and the cochlear duct at the opposite end) and cochlear duct. In this transitional cochlear organization (as demonstrated by *Thrinaxodon*; [57]) the rostral border of the ventromedially pointing cochlear recess within the prootic bone does not extend anterior to the rostral border of the fenestra ovalis. As such, these forms lack a true pars cochlearis of the prootic bone [32].

Eucynodonts

Eucynodonts show a progressive trend of increasing relative size and differentiation of the jaw adductor musculature, while simultaneously reducing the size, strength, and cranial integration of the bony jaw apparatus itself. This counter-intuitive development was permitted by the reorientation of adductor leverage to minimize the reaction force experienced by the quadrate-articular joint and postdentary elements [58]. Other morphological features seen in basal forms of this taxon include the change from a plate-like

reflected lamina to a rod-like reflected lamina of the angular bone, creating a laterally facing gap between the reflected lamina and main body of the angular, that was almost certainly spanned in life by an incipient tympanic membrane [54]. The remaining postdentary bones were synostosed into a gracile but rigid postdentary rod that remained attached to the angular. As the postdentary rod, the postdentary bones lost their sutural connections with the dentary bone but remained appressed to the dentary within a smoothly concave postdentary trough [59]. The rostrocaudal orientation of the postdentary rod, with its flexible posterior connection to the squamosal, and lack of strong rostral attachments to the dentary, allowed the postdentary rod to function as a first-class lever with a longitudinally oriented fulcral axis. This provided a mechanical linkage for transmitting airborne vibrations impinging on the angular tympanic membrane onto the quadrate and stapes medially [47]. The air-filled space medial to the tympanic membrane (likely a vestige of the recessus mandibularis), combined with the approximately 1/30 area ratio between the fenestra ovalis and angular tympanic membrane [19], would create a precursory condition to the middle ear seen in the later and most advanced cynodonts. However, the existence of a true cavum tympani medial to the angular tympanic membrane and the usefulness of this apparatus for frequencies above 2 kHz is doubtful [19]. The eucynodonts also show the first appearance of a true pars cochlearis. This neomorphic region is defined in [60] (also see [61,32]) as the portion of the otic capsule accommodating the saccule and cochlear duct, that were likely present as discrete structures in epicynodonts. The weight of morphological evidence suggests that while not within crown mammalian performance levels, the auditory capacities of the early eucynodonts were heightened beyond anything preceding them in synapsid history [47].

Mammaliamorphs

Mammaliamorphs include the true mammaliaforms and several clades showing incredible morphological convergences with them [62]. This group also includes the only synapsid taxa to survive beyond the Early Cretaceous. These forms show many significant apomorphies related to the function of their inner ear and newly acquired middle ear - including the consolidation of the prootic and opisthotic into the true petrosal bone [54,32], the division of the common jugular fossa into a perilymphatic foramen and a jugular foramen, and separation of the foramina for the cochlear and vestibular branches of the vestibulocochlear nerve [63]. However, far and away the most lauded morphological characteristics seen in this group are the articulations between the dentary and squamosal bone, and development of a true cavum tympani [51,64]. The development of a tympanic middle ear in synapsid ancestry is an important event with functional implications regarding the sensitivity and maximal frequency attained by these and later forms; however, the accurate interpretation of these features, especially the contents of the otic capsule, rely on comparative inferences derived from the study of the tympanic middle ears in fossils and extant non-mammalian amniotes. It should therefore be reiterated here that, (for anatomical and developmental criteria skillfully outlined in [65,66,27] inter alios) the best interpretation of the available evidence suggests that the acoustically significant intracranial air spaces developed in advanced synapsids are not homologous with tympanic cavities developed in many other tetrapod lineages [22]. The initial form of the synapsid cavum tympani likely displayed a broadly confluent relationship with the nasopharynx. The medial (proximal) subdivision of the cavum tympani was therefore not separated from the nasopharynx by an extended auditory tube and likely allowed bulk motion of air between the lateral portion of the tympanic cavity

to the nasopharynx and onward across to the contralateral cavum tympani. Modern *Ornithorhynchus* also shows this condition [67].

An unconstricted (if tortuous) air-filled passageway connecting both ears is hypothesized as a mechanism for sound localization in advanced cynodonts and other, more plesiomorphic synapsids [68]. In the majority of extant sauropsids the sole method of sound localization in the horizontal (azimuthal) plane is by the simultaneous use of the ipsilateral and contralateral ears, and the air-mass medially connecting both, as a pressure-gradient receiver [22,69-72]. The successive medial-posterior-ventral relocation of the articular and quadrate relative to the newly formed dentary squamosal contact, likely made the contact between both ears progressively more constricted in the advanced cynodonts.

The degree of ossification of the otic capsule in Mammaliamorpha is also significantly greater than in other known cynodonts, with two discrete foramina for the vestibular and cochlear branches of the vestibulocochlear nerve, respectively. These are recognizable in the medial wall of the petrosal even in early forms [73,64], and in the most plesiomorphic condition they are of subequal diameter. These forms are also the first to show an appreciable amount of "waisting" between the components of the vestibular endocast contributed by the pars cochlearis and pars canalicularis. The development of a more or less prominent crista vestibuli also separates the areas of attachment for the utricular and saccular maculae, forming discrete vestibular recesses to accommodate these structures (the recessus ellipticus and recessus sphericus, respectively; [20,64]).

Mammaliaformes

Mammaliaformes includes Mammalia and their common ancestor with the Triassic-Jurassic *Morganucodon*, plus all of its descendants. Having inherited a mandibular middle-ear from advanced mammaliamorph cynodonts, the Mammaliaformes reinforce the dentary-squamosal jaw articulation by developing a true mandibular condyle on the dentary, matching an equally developed glenoid fossa on the squamosal [62,4]. However, with the progressive reduction of the crista parotica on the petrosal and redistribution of masticatory musculature onto the dentary bone, the placement and size of the ancestral jaw articulation became more directly under the influence of the auditory mechanism, while the dentary and squamosal became increasingly specialized for masticatory purposes [74,48, 58,4].

Along with the increasing specialization of the articular and quadrate for acoustic purposes, a wider reorganization of external and internal aspects of the petrosal can also be seen in early mammaliaform fossils. Externally, the enlargement of the pars cochlearis at the expense of the basisphenoid and other midline structures and loss of a thickened rim around the fenestra ovalis, and the separation of the hypoglossal and jugular foramina [74, 33] can be seen in early members of the clade. These features are possibly related to the insulation and stabilization of structures surrounding the otic capsule, or in the case of the reduced rim of the fenestra vestibuli to facilitate a greater range of motion between the stapes and petrosal (i.e. a "rocking"-type motion between the stapes and petrosal, in addition to a piston like motion; [65]). More significantly, these mammaliaforms also show the allometric enlargement and ventral inflation of the pars cochlearis of the petrosal relative to other advanced cynodonts, forming a variably flattened or convex promontorium on its newly exposed ventral surface. A promontorial structure has also been observed in juvenile non-mammaliaform probainognathians [75], and as [52] observed, at the time of its initial appearance the majority of the increased volume in the pars cochlearis is not immediately

utilized by the elongated but relatively small cochlear canal. Instead, the persistence of the promontorium into adult stages in mammaliaforms and other mammalimorph taxa may solely be a product of paedomorphosis, as in these early forms most of the volume of the promontorium is taken up by a complex network of venous canals and sinuses termed the circumpromontorial sinus plexus [76-78].

In some mammaliaformes the circumpromontorial sinus plexus includes two sets of venous canals dorsal and ventral to the cochlear canal accommodating the epicochlear and hypocochlear sinuses, that communicate with the inferior petrosal sinus. The inferior petrosal sinus is also located in an intramural location between the petrosal and basisphenoid in these early taxa [79]. The ventral bulging of the pars cochlearis relative to the cranial base also variably impressed onto the stapedial artery, forming an indentation along the margins of the fenestra ovalis in *Morganucodon* and more advanced forms [63]. Endocranially, the earliest mammalaiforms still lacked an excavated internal acoustic meatus, with the small prefacial commissure showing little association with the course of the vestibulocochlear nerve [76]. As mentioned in the descriptions of the Höövör petrosals in the main text, it is also very likely that a posterior epicochlear sinus, running between the inferior petrosal sinus and prootic sinus, was present within the bone separating the primary facial foramen and the foramen for the vestibular branch of the vestibulocochlear nerve. Other significant features of the pars cochlearis are internal, such as the initiation of the abneural curvature (concave toward the side of insertion of the cochlear nerve) of the cochlear canal and, as seen in *Morganucodon* and more derived stem mammaliaforms, the relative inflation of the apical cochlear canal for the accommodation of the lagenar macula [80].

References for Supplementary Material

1. MacLean PD. Neurobehavioral significance of the mammal-like reptiles (therapsids). In: MacLean PD, Roth JJ, Roth EC, editors. The ecology and biology of mammal-like reptiles. Washington: Smithsonian Institution Press: 1986. pp. 1-21.

2. Butler AB, Hodos W. Comparative vertebrate neuroanatomy: Evolution and adaptation. 2nd ed. Hoboken: John Wiley and Sons Inc.; 2005.

3. Rowe TB. The emergence of mammals. In: Kaas JH, editor. Evolution of nervous systems, second edition, volume 2. Oxford: Elsevier; 2017. pp. 1-52.

4. Kielan-Jaworowska Z, Cifelli RL, Luo ZX. Mammals from the age of dinosaurs: Origins, evolution, and structure. New York: University of Colombia Press; 2004.

5. Kielan-Jaworowska, Z. In pursuit of early mammals. Bloomington: Indiana University Press; 2013.

6. Kermack KA. The cranial structure of the triconodonts. Phil Trans R Soc Lond B. 1963;246: 83-103.

7. Meng J, Hu Y, Wang Y, Li C. The ossified Meckel's cartilage and internal groove in Mesozoic mammaliaformes: implications to origin of the definitive mammalian middle ear. Zool J Linn Soc. 2003;138: 431-448.

8. Gaetano LC, Rougier GW. New materials of Argentoconodon fariasorum (Mammaliaformes, Triconodontidae) from the Jurassic of Argentina and its bearing on triconodont phylogeny. J Vertebr Paleontol. 2011;31: 829-843.

9. Gaetano LC, Rougier GW. First amphilestid from South America: a molariform from the Jurassic Cañadón Asfalto Formation, Patagonia, Argentina. J Mammal Evol. 2012;19: 235-248.

10. Kielan-Jaworowska Z, Presley R, Poplin C. The cranial vasculature system in taeniolabidoid multituberculate mammals. Phil Trans R Soc Lond. 1986;313: 525-602.

11. Hahn G. Die ohr-region der Paulchoffatiidae (Multituberculata, Ober-Jura). Palaeovertebrata. 1988;18: 155-185.

12. Luo Z, Ketten DR. CT scanning and computerized reconstructions of the inner ear of multituberculate mammals. J Vertebr Paleontol. 1991;11: 220-228.

13. Meng J, Wyss AR. Monotreme affinities and low-frequency hearing suggested by multituberculate ear. Nature. 1995;377: 141-144.

14. Fox RC, Meng J. An x-radiographic and SEM study of the osseus inner ear of multituberculates and monotremes (Mammalia): Implications for mammalian phylogeny and evolution of hearing. Zool J Linn Soc. 1997;121: 249-291.

15. Hoffmann S, O'Connor PM, Kirk EC, Wible JR, Krause DW. Endocranial and inner ear morphology of *Vintana sertichi* (Mammalia, Gondwanatheria) from the Late Cretaceous of Madagascar. J Vetebr Paleontol. 2014;34: 110-136.

16. Hu Y, Wang Y, Luo Z, Li C. A new symmetrodont mammal from China and its implications for mammalian evolution. Nature. 1997;390: 137-142.

17. Rougier GW, Ji Q, Novacek MJ. A new symmetrodont mammal with fur impressions from the Mesozoic of China. 2003;77: 7-14.

18. Fleischer G. Evolutionary principals of the mammalian middle ear. Adv Anat Embryol Cell Biol. 1978;55: 1-70.

19. Kemp TS. Acoustic transformer function of the postdentary bones and quadrate of a nonmammalian cynodont. J Vetebr Paleontol. 2007;27: 431-441.

20. Meng J, Fox RC. Osseus inner ear structures and hearing in early marsupials and placentals. Zool J Linn Soc. 1995;115: 47-71.

21. Basch ML, Brown RM, Jen H, Groves AK. Where hearing starts: the development of the mammalian cochlea. J Anat. 2016;228: 233-254.

22. Manley GA. An evolutionary perspective on middle ears. Hearing Res.2010;263: 3-8.

23. Manley GA. The foundations of high-frequency hearing in early mammals. J Mammal Evol. 2016;25: 155-163.

24. Anthwal N, Joshi L, Tucker AS. Evolution of the mammalian middle ear and jaw: adaptations and novel structures. J Anat. 2013;222: 147-160.

25. Mason MJ. Of mice moles and guinea pigs: functional morphology of the middle ear in lining mammals. Hearing Res. 2013;301: 4-18.

26. Mason MJ. Structure and function of the mammalian middle ear II: inferring structure from function. J Anat. 2016;228: 300-312.

27. Maier W, Ruf I. Evolution of the mammalian middle ear: A historical review. J Anat. 2016;228: 270-283.

28. Laurin M. The evolution of body size, Cope's rule and the origin of amniotes. Sys Biol. 2004;53: 594-622.

29. Fritzsch B, Pan N, Jahan I, Ducan JS, Kopecky BJ, Elliot KL, et al. Evolution and development of the tetrapod auditory system: An organ of Corti centric perspective. Evol and Dev. 2013;15: 63-79.

30. Schultz JA, Zeller U, Luo ZX. Inner ear labyrinth anatomy of monotremes and implications for mammalian inner ear evolution. J Morphol. 2017;278: 236-263.

31. Sigogneau D. The inner ear of *Gorgonops* (Reptilia, Therapsida, Gorgonopsia). Ann S Afr Mus. 1974;64: 53-69.

32. Luo Z. The inner ear and its bony housing in tritylodontids and implications for evolution of the mammalian ear. Bull Mus Comp Zool Harvd. 2001;156: 81-97.

33. Clack JA. The evolution of tetrapod ears and the fossil record. Brain Behav Evol. 1997;50: 198-212.

34. Manley GA, Köppl C. Phylogenetic development of the cochlea and its innervation. Curr Opin Neurobiol. 1998;8: 468-474.

35. Manley GA. Travelling waves and tonotopicity in the inner ear: a historical and comparative perspective. J Comp Physiol A. 2018;204: 773-781.

36. Manley GA. Cochlear mechanisms from a phylogenetic viewpoint. Proc Natl Acad Sci. 2000;97: 11736-11734.

37. Manley GA. The foundations of high-frequency hearing in early mammals. J Mammal Evol. 2016;25: 155-163.

38. Ramanathan K, Michael TH, Jiang GJ, Hiel H, Fuchs PA. A molecular mechanism for electrical tuning of cochlear hair cells. Science. 1999;283: 215-217.

39. Fettiplace R, Fuchs PA. Mechanisms of hair cell tuning. Ann Rev Physiol. 1999;61: 809-834.

40. Fettiplace R. Hair cell transduction, tuning, and synaptic transmission in the mammalian cochlea. Comp Physiol. 2017;7: 1197-1227.

41. Wu YC, Art JJ, Goodman MB, Fettiplace R. A kinetic description of the calcium-activated potassium channel and its application to electrical tuning of hair cells. Prog Biophys Mol Biol. 1995;63: 131-158.

42. Manley GA. Comparative auditory neuroscience: Understanding the evolution and function of ears. J Assoc Res Otolaryngol. 2017;18: 1-24.

43. Wever EG. The reptile ear: Its structure and function. Princeton: Princeton University Press; 1978.

44. Hossler FE, Olson KR, Musil G, McKamey MI. Ultrastructure and blood supply of the tegmentum vasculosum in the cochlea of the duckling. Hearing Res. 2002;164: 155- 165.

45. Köppl C, Wilms V, Russell IJ, Nothwang HG. Evolution of endolymph secretion and endolymph potential generation in the vertebrate inner ear. Brain Behav Evol. 2018; DOI: 10.1159/000494050

46. Manley GA. The mammalian Cretaceous cochlear revolution. Hearing Res. 2017;352: 23-29.

47. Kemp TS. Non-mammalian synapsids: the beginning of the mammal line. In: Clack JA, Fay RR, Popper AN, editors. Evolution of the vertebrate ear: Evidence from the fossil record. Cham: Springer; 2016. pp. 107-137.

48. Kermack KA, Musset F, Rigney HW. The lower jaw of *Morganucodon*. Zool J Linn Soc. 1973;53: 87-175.

49. Allin EF. The auditory apparatus of advanced mammal-like reptiles and early mammals. In: MacLean PD, Roth JJ, Roth EC, editors. The ecology and biology of mammal-like reptiles. Washington: Smithsonian Institution Press: 1986. pp. 283-294.

50. Laaß M. The origins of the cochlea and impedance matching hearing in synapsids. Acta Paleontol Pol 2015;61: 267-281.

51. Luo ZX, Schultz JA, Ekdale EG. Evolution of the middle and inner ears of mammaliaformes: the approach to mammals. In: Clack JA, Fay RR, Popper AN, editors. Evolution of the vertebrate ear: Evidence from the fossil record. Cham: Springer; 2016. pp. 139-174.

52. Luo Z, Crompton AW, Lucas SG. Evolutionary origins of the mammalian promontorium and cochlea. J Vertebr Paleontol. 1995;15: 113-121.

53. Benoit J, Manger PR, Fernandez V, Rubidge BS. The bony labyrinth of late Permian Biarmosuchia: palaeobiology and diversity of non-mammalian Therapsida. Palaeont Afr. 2017;52: 58-77.

54. Olson EC. Relationships and ecology of the early therapsids and their predecessors. In: MacLean PD, Roth JJ, Roth EC, editors. The ecology and biology of mammal-like reptiles. Washington: Smithsonian Institution Press: 1986. pp. 47-60.

55. Ruta M, Botha-Brink J, Mitchell SA, Benton MJ. The radiation of cynodonts and the ground plan of mammalian morphological diversity. Proc R Soc B. 2013;280: 1-10.

56. Barghusen HR. On the evolutionary origin of the therian tensor veli palantini and tensor tympani muscles. In: MacLean PD, Roth JJ, Roth EC, editors. The ecology and biology of mammal-like reptiles. Washington: Smithsonian Institution Press: 1986. pp. 253-262.

57. Fourie S. The cranial morphology of *Thrinaxodon liorhinus* Seeley. Ann S Afr Mus. 1974;56: 337-400.

58. Crompton AW, Hylander WL. Changes in mandibular function following the acquisition of a dentary-squamosal jaw articulation. In: MacLean PD, Roth JJ, Roth EC, editors. The ecology and biology of mammal-like reptiles. Washington: Smithsonian Institution Press: 1986. pp. 175-282.

59. Allin EF, Hopson JA. Evolution of the auditory system in Synapsida ("mammal-like reptiles" and primitive mammals" as seen in the fossil record. In: Webster DB, Fay RR, Popper AN, editors. The evolutionary biology of hearing. Heidelberg: Springer-Verlag: 1992. pp. 587-614.

60. DeBeer GR. The development of the vertebrate skull. Oxford: Clarendon Press.; 1937

61. MacPhee RD. Auditory reigions of primates and eutherian insectivores. Basel: S. Karger; 1981.

62. Rowe TB. Definition, diagnosis, and the origin of Mammalia. J Vetebr Paleontol. 1988;8: 241-264.

63. Wible JR, Hopson JA. Basicranial evidence for early mammal phylogeny. In: Szalay FS, Novacek MJ, McKenna MC, editors. Mammal phylogeny: Mesozoic differentiation, multituberculates, monotremes, early therians, and marsupials. New York: Springer; 1993. pp. 45-62.

64. Rodrigues PG, Ruf I, Schultz CL. Digital reconstruction of the otic region and inner ear of the non-mammalian cynodont *Brasilitherium riograndensis* (Late Triassic, Brazil) and its relevance to the evolution of the mammalian ear. J Mammal Evol. 2013;20: 291-307.

65. Moore WJ. The mammalian skull. Cambridge: Cambridge University Press; 1981.

66. Presley R. Development and the phylogenetic features of the middle ear region. In: Szalay FS, Novacek MJ, McKenna MC, editors. Mammal phylogeny: Mesozoic differentiation, multituberculates, monotremes, early therians, and marsupials. New York: Springer; 1993. pp. 21-29.

67. Zeller U. Ontogenetic evidence for the cranial homologies in monotremes and therians, with special reference to *Ornithorhynchus*. In: Szalay FS, Novacek MJ, McKenna MC, editors. Mammal phylogeny: Mesozoic differentiation, multituberculates, monotremes, early therians, and marsupials. New York: Springer; 1993. pp. 95-107.

68. Christensen-Dalsgaard J. Vertebrate pressure-gradient receivers. Hearing Res. 2011;273: 37-45.

69. Christensen-Dalsgaard J, Manley GA. Acoustical coupling of lizard eardrums. J Assoc Res Otolaryngol. 2008;9: 407-416.

70. Köppl C. Evolution of sound localisation in land vertebrates. Curr Biol. 2009;19: 635-639.

71. Heffner HE, Heffner RS. The evolution of mammalian sound localization. Acoustics Today. 2016;12: 20-27.

72. Nothwang HG. Evolution of mammalian sound localization circuits: a developmental perspective. Prog Neurobiol. 2016;141: 1-24.

73. Olson EC. Origin of mammals based upon cranial morphology of the therapsid suborders. Spec Pap Geol Soc Am. 1944;55: 1-136.

74. Luo Z, Crompton AW. Transformation of the quadrate (incus) through the transition from non-mammalian cynodonts to mammals. J Vetebr Paleontol. 1994;14:341-374.

75. Bonaparte JF, Crompton AW. A juvenile probainognathid cynodont skull from the Ischigualasto Formation and the origin of mammals. Rev Mus Arg Cien Nat Bernardino Rivadavia Inst Nac Invest Cienc Nat. 1994;1: 1-12.

76. Kermack KA, Musset F, Rigney HW. The skull of *Morganucodon*. Zool J Linn Soc. 1981;71: 1-158.

77. Rougier GW, Wible JR, Hopson JA. Reconstruction of the cranial vessels in the Early Cretaceous mammal *Vincelestes neuquenianus*: Implications for the evolution of the mammalian cranial vascular system. J Vertebr Paleontol. 1992;12: 188-216.

78.. Forasiepi AM, Rougier GW. Additional data on early Paleocene metatherians (Mammalia) from Punta Peligro (Salamanca Formation, Argentina): comments based on petrosal morphology. J Zool Syst Evol Res. 2009;47: 391-398.

79. Rougier GW, Wible JR, Hopson JA. Basicranial anatomy of *Priacodon fruitaensis* (Triconodontidae, Mammalia) from the Late Jurassic of Colorado, and a reappraisal of mammaliaform interrelationships. Am Mus Novit. 1996;3183: 1-38.

80. Luo Z, Ruf I, Schultz JA, Martin T. Fossil evidence on evolution of inner ear cochlea in Jurassic mammals. Proc R Soc Lond B. 2011;278: 28-34.

Chapter 3: Models of craniodental transformation in early mammals

ABSTRACT— The disparity of shapes seen in early mammalian teeth represent one of the biggest challenges for morphologists interested in quantifying this variation in a unified coordinate system. The macroevolutionary analyses presented here utilize spherical harmonic registration (SPHARM) to accommodate the wide range of variation seen in a sample of representative lower molariforms, taken from several major Mesozoic mammaliaform lineages. Protocols for generating closed (genus-zero) surfaces from these sampled molariforms are outlined, and the effectiveness of this "homology-free" method for the analysis of crown shape is demonstrated. The principal components of the resulting wave-space shape specifiers are then fit to several diffusionary multivariate Brownian Motion (BMM) models evolving over an updated hypothesis of mammaliaform interrelationships. With these methods, and the increased character sampling of early mammalian petrosal characters used in these phylogenetic estimations, no support for a unique process of molariform shape change is found to correspond to the clade of northern tribosphenic mammals. This suggests that the evolutionary process influencing lower molariform shape in all extant toothed mammals began earlier in time, and in a more inclusive group, than just the crown therian mammals.

INTRODUCTION

The mineralized tissues of the skull and dentition have historically provided the bulk of material evidence for past mammalian biodiversity (Wible, 1991; Kielan-Jaworowska et al., 2004; Rose, 2006). Because the majority of mammalian lineages are extinct, fossil remains (particularly skulls and teeth) have had an exaggerated influence on characterizations and reconstructions of the earliest mammals and their ancestors. While this emphasis is understandable given the preservational limitations involved with fossil material, it is important that mammalogists also conduct analyses capable of detecting and correcting possible biases in their paradigm of mammalian evolution caused by an over-reliance on one particular anatomical region (McKenna, 1976). This report explicitly attempts to test traditional explanations of the evolutionary transformation of the mammalian inner ear and lower dentition – two character complexes which have contributed many classical case-studies in reviews of mammalian evolution (e.g. Simpson, 1944; Olson, 1944, Allin, 1975). The phylogenetic and macroevolutionary analyses performed here utilize probabilistic cladistic protocols (Felsenstein, 2004) for phylogenetic inference and comparison. These models, while not being strictly "objective," because of their partial reliance on Bayesian subjective probabilities, bypass many potential biases in the interpretation of morphological transformation caused by the unrepresentative sampling of mammalian anatomy and biodiversity (see Tarver and Donoghue, 2011; Mitchell, 2015). Additionally, the morphometric registration methods used for our analysis of tooth shape minimize the amount of assumed a priori homologous correspondence required for the generation of shape statistics in a widely disparate sample of early mammalian taxa. Our subsequent use of multivariate Brownian Motion models (Polly, 2004; Clavel et al., 2015) and Fourier "wave-

space," as opposed to object-space, morphometric specifiers (Shen et al., 2009) also allows for more realistic scenarios of molariform shape evolution to be contrasted using standard statistical model comparison metrics (AIC and corrected-AIC value; Cavanaugh, 1997).

The main phylogenetic context for this report is the constrained posterior sample generated by my updating and reanalysis of the taxon-character matrix used by (Rougier et al., (2011, 2012), and O'Meara et al., (2014); a taxonomically inclusive (58 early and generalized probainognathian OTUs) and intensively sampled (including 317 hard tissue characteristics from the dentition, cranium and postcrania) source of information on the earliest mammals and their close relatives. The Bayesian reanalysis of this matrix utilizes a constrained version of the Fossilized Birth-Death process (Ronquist et al., 2012; Zheng et al., 2016; Gavryushkina et al., 2016), and is modified to incorporate the Mka model of morphological transformation (Lewis, 2001; Wright et al., 2016; Pyron, 2016) implemented with the Bayesian phylogenetics program MrBayes (Ronquist et al., 2012). These phylogenetic results therefore present an opportunity for the investigation of the timing and character of early mammalian evolutionary radiations. Reasons why Mesozoic mammaliaforms are particularly amenable to this type of macroevolutionary analyses include the facts that: (1) irrespective of theoretical framing (Archibald, 2011), there is consensus that a radiation did in fact occur among some or all mammaliaforms (Archibald and Deuschman, 2001; Archibald, 2011; Close et al., 2015); and (2) the presence of several derived extinct lineages in the Mesozoic which show remarkable morphological convergences with modern species, suggesting that the accumulation of morphological disparity seen in early mammals has, in general terms, kept pace with the dynamics of lineage splitting and survival, and has proceeded largely independent of these processes (i.e., derived

groups do not appear more diverse or successful than generalized ones and vice versa; Luo, 2007).

Despite the logistical difficulties involved with the translation of complex morphology into either subjectively coded phylogenetic characters (Wiley et al., 1991), or continuous quantitative variables (and their subsequent analysis within a cladistic paradigm; Hunt and Carrano, 2010; Paradis, 2014), I present a macroevolutionary analysis of representative lower molariform shape seen in a sub-sample of the OTUs included in our Bayesian phylogenetic analysis. Difficulties of how best to define and register shape in the most natural way possibly, and allow for evolutionary co-variation between geometrically-independent shape specifiers (Polly, 2004), are also accommodated through the use of several computational methods described below.

The major result of this analytical series gives some support for the crown mammalian subclade Theriimorpha (Rowe, 1993) as the phylogenetic locus of a switch in evolutionary covariance structure in lower molariform shape change (Polly, 2004; Clavel et al., 2015). Being a more inclusive clade than the more extensively studied northern tribosphenic mammals (clade Tribosphenida), this finding supports the hypothesis that morphological responses to elaborate mastication appeared among therian ancestors earlier in time, and in more forms, than traditionally appreciated.

MATERIALS AND METHODS

Abbreviations

Institutional Abbreviations— **AMF**, Fossil collections of the Australian Museum, Sydney; **BMNH**, British Natural History Museum, London, UK; **DUEA**, Duke University Evolutionary Anthropology Collections (downloaded from morphosource.org), Durham; **LACM**, Los Angeles County Museum of Natural History Vertebrate Paleontology Collections, Los Angeles; **MACN**, Museo Argentino de Ciencias Naturales, Buenos Aires, Argentina; **MEF-PV**, Museo Paleontológico Egidio Feruglio, Trelew, Argentina; **NMVP**, Museum Victoria Palaeontological Collection; Melbourne, Australia; **OMNH**, Sam Noble Oklahoma Museum of Natural History, Norman; **PSS-MAE**, Collections of The Joint Paleontological Expeditions of the Mongolian Academy of Sciences and the American Museum of Natural History and cataloged in the Geological Institute, Ulaan Baatar, Mongolia; **SAMP**, palaeontological collections of the South Australian Museum, Adelaide, Australia; **URBAC**, Uzbek/Russian/British/American/Canadian joint paleontological expedition specimens, now housed in the National Museum of Natural History, Washington, D.C; **USNM**, Smithsonian National Museum of Natural History, Washington D.C.; **YPM**, Yale Peabody Museum, New Haven; **Z.Pal.**, Palaeozoological Institute of the Polish Academy of Sciences, Warsaw, Poland.

Anatomical Abbreviations Used in Figures—**ac**, aqueductus cochleae (perilymphatic canal); **av**, aqueductus vestibuli (endolymphatic canal); **cc-p**, primary common crus; **cc-s**, secondary common crus; **coc**, cochlear canal; **fc**, fenestra cochleae (round window); **fv**, fenestra vestibuli (oval window); **mtd**, metaconid; **pad**, paraconid; **pf,** perilymphatic foramen; **prd**, protoconid; **sl**, secondary bony lamina; **ssc-a,** anterior

semicircular canal; **ssc-h**, horizontal semicircular canal; **ssc-p**, posterior semicircular canal; **vcaq**; canal for vein of cochlear aqueduct (canal of Contugno).

A large proportion of the advanced synapdid paleontological literature is dedicated towards the reconstruction of direct and indirect connections between the lower jaw and ear (e.g. Crompton and Parker, 1978; Kermack and Musset, 1983; Meng et al., 2003; Laaß, M. 2015; Luo et al., 2016). The well -illustrated anatomical and functional linkages between these two character complexes (e.g. Allin 1975) suggest that the morphological transformation seen in the mechanical endpoints of each apparatus (the lower dentition and cochlea) may also have strongly associated patterns of trait evolution, or at least should be mutually informative. In effort to produce the most informed "morphological clock" phylogenetic inference and comparative results possible (Polly, 2004; Wagner and Marcot, 2010; Hunt and Carrano, 2010; Larsson et al., 2012), this paper utilizes the discrete morphological characterizations of early mammals and closely related probianognathian cynodonts included in the taxon-character matrix produced by Rougier et al., (2011, 2012; particular character ordering is taken from O'Meara and Thompson, 2014), with modifications of several characters and cells based on recently published morphological descriptions (e.g., Rodrigues et al., 2013; Harper et al., 2018, Panciroli et al., 2019) and my own observations of the internal structure of a sample of mammalian petrosal specimens (Figs. 1-2). This data set was updated to include 14 new characters based on internal features of the petrosal bone and labyrinthine endocast. Additionally, two additional OTUs representing the phylogenetically enigmatic Höövör petrosals 1 and 2 were added to this matrix (Wible et al., 1995; Rougier et al., 1996; Harper and Rougier, 2019). The updated taxon-character matrix used here contains 60 taxa and 329 parsimony informative

morphological characters (223 binary characters, 92, three state, 10 four state, 5 five state, and 1 six-state character.

In an effort to update the inner ear character scoring in this matrix, high-resolution micro-CT images were generated for six of the included fossil terminal taxa. The newly scanned fossil endocasts (Figs. 1 and 2) include the South American "dryolestoids" *Cronopio* (Rougier et al., 2011), *Coloniatherium* (Rougier et al., 2009), and *Peligrotherium* (Paez-Arango, 2008); the South American cladotherian mammal *Vincelestes* (Rougier et al., 1992); the Mongolian Höövör petrosals 1 and 2 (Wible et al., 1995; Rougier et al., 1996; Harper and Rougier, 2019); and the North American triconodontid *Priacodon fruitaensis* (Rougier et al., 1996). All these taxa diverge from Mesozoic nodes within crown mammals (Kielan-Jaworowska et al., 2004), and the addition of the Höövör petrosals as terminal taxa may help break up longer branches in the resulting topology. However, in addition to this new fossil character scoring, all petrosal information pertinent to *Reigitherium* (Harper et al., 2018) in the Rougier et al., (2012) matrix was removed. This is necessary because all petrosal character scoring for *Reigitherium* was based on a single isolated petrosal recovered from the La Colonia Formation, which was attributed to this taxon based solely on its small size and similarity to the larger *Coloniatherium* and *Peligrotherium* (Fig. 2). Subsequent sampling of La Colonia sediments recovered other small-bodied dryolestoids which could also correspond with the taxon represented by the isolated petrosal, and so the attribution of any petrosal characteristics to *Reigitherium* is suspect (Rougier et al., 2009). High-resolution micro-CT images for an additional three extant mammals (*Ornthorhynchus*, *Didelphis* and *Erinaceus*; Figs. 1a-d and 2i-j) represented as OTUs in Rougier et al., (2012), were also generated to update inner ear character scoring. Access to the high-resolution imaging equipment required for these images was provided by Duke University Shared Materials Instrumentation Facility

(SMIF) and the University of Texas High-resolution X-ray Computed Tomography Facility (UTCT).

Finally, a collection of triangular mesh surfaces of lower molariform elements (preferentially from lower second molariforms, but from differing positions where m2 was unavailable or impossible to clearly segment) was collected from taxa representing a sub-sample of 29 of the 60 OTUs used in this updated taxon-character matrix (see Fig. 3, Table 1). The uncontrolled variation in lower molariform position is not ideal; however, given the uncertainties involved with inferences of serial homology of molar position in even extant therian mammals (Novacek, 1986; Luckett, 1993; Martin, 1997; Luo et al., 2004; Juuri et al., 2013) and the wide variation in Mesozoic mammalian dental formula (up to nine molars in some dryolestid species), this preservation and availability based sampling is considered the best strategy available.

These surfaces (Fig. 3) were also generated using a mixture of fossil and plastic cast specimens, and micro-CT and surface scanning (white light surface scanner) imaging modalities. As all lower molariform surfaces are sub-sampled to contain 10,000 manifold triangular faces, no apparent systematic differences between different visualization modalities, or between surfaces generated from plastic casts or original fossils, are apparent. Additionally, in order to make each molariform surface a topologically closed ("genus zero") triangular mesh, the free edges marking the dentin-enamel junction for each molariform were closed off using hole filling algorithms in the 3D modeling programs Meshmixer and Blender (Sutton et al., 2014; Rowe et al., 2016). The underside of molariform surfaces were then manually rounded and each completed surface file was simplified to have exactly 10,000 faces and 5002 vertices, causing the closed-off region to conform to the surrounding curvature of the tooth-crown. Given the small absolute variation of lower molariform

shapes corresponding to different species (on the order of 10^{-3}, see below) the variation in tooth surface shape introduced by this arbitrary surface-closing method is assumed to be negligible. This assumption is supported by our sensitivity analysis described below.

In addition to the 29 representative lower molariform surfaces used as comparative data for the analyses described below, the dentitions of three mandibles corresponding to cast specimens of YPM 11826 (type specimen of *Docodon victor*), USNM 2722 (*Dryolestes priscus*) and YPM 13719 (*Laolestes eminens*) were segmented from CT scans and exported as closed triangular meshes, similar to the other dental specimens. These mandibles were used as test specimens for the sensitivity analysis of the morphometric protocols used here.

FIGURE 1. Anatomical renderings of labyrinthine endocasts in biogeographically "Northern" mammalian taxa. **A**, **B**, *Erinaceus sp.*; **C**, **D**, *Didelphis sp.*; **E**, **F**, Höövör Petrosal 2, PSS-MAE-119; **G**, **H**, Höövör Petrosal 1, PSS-MAE-104; **I**, **J**, *Priacodon fruitaensis*, LACM 120451. All endocasts are reflected to be left-sided and all scale bars are 1 mm. **A**, **C**, **E**, **G**, and **I** are oblique medial views; **B**, **D**, **F**, **H**, and **J** are ventral views. See list of abbreviations for anatomical structures.

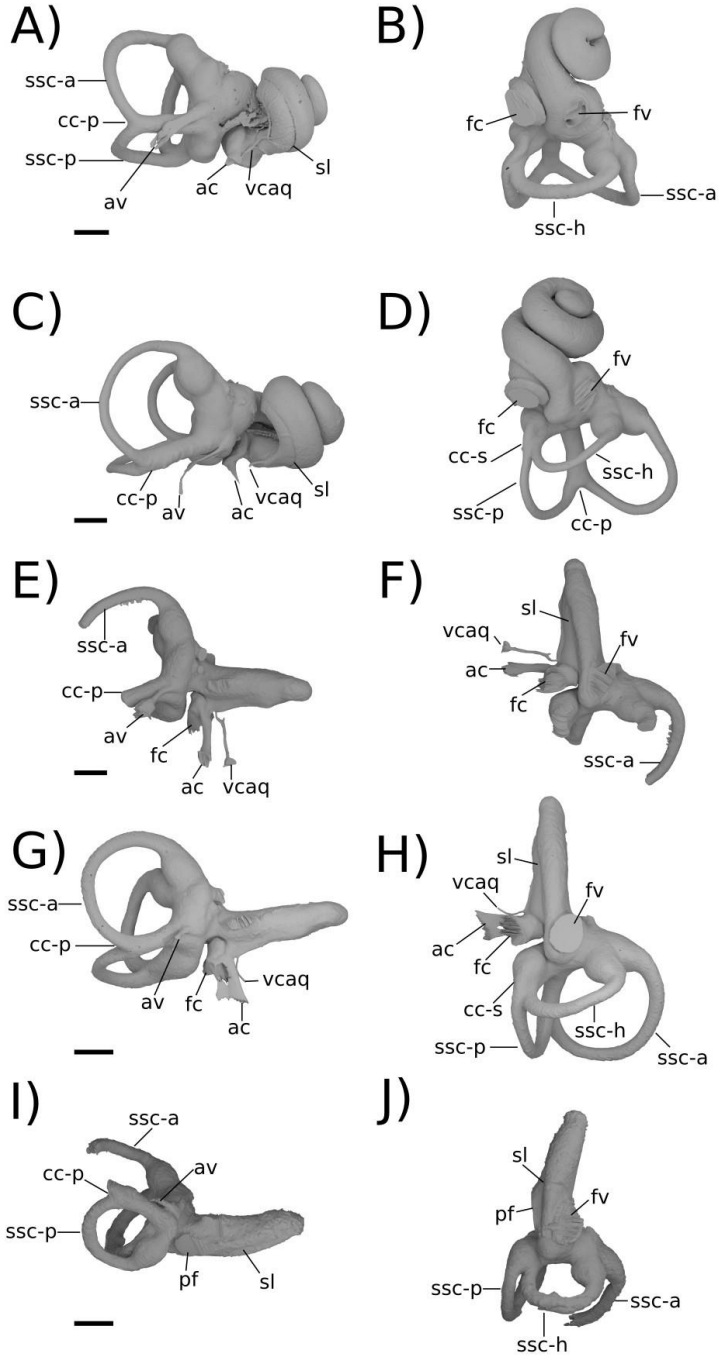

FIGURE 2. Anatomical renderings of labyrinthine endocasts in biogeographically "Southern" mammalian taxa. A, B, *Vincelestes* neuquenianus, MACN-N 16; C, D, *Coloniatherium cilinskii*, MEF-PV 600; E, F, *Peligrotherium tropicalis*, MEF-PV 2351; G, H, *Cronopio sp.* unaccessioned specimen; I, J, *Ornithorhynchus anatinus*. All endocasts are reflected to be left-sided and all scale bars are 1 mm. **A**, **C**, **E**, **G**, and **I** are oblique medial views; **B**, **D**, **F**, **H**, and **J** are ventral views. See list of abbreviations for anatomical structures. See list of abbreviations for anatomical structures. Damage to *Cronopio* (**G**, **H**), *Coloniatherium* (**C**, **D**) and *Peligrotherium* (**E**, **F**) prevents complete endocast reconstruction in some areas.

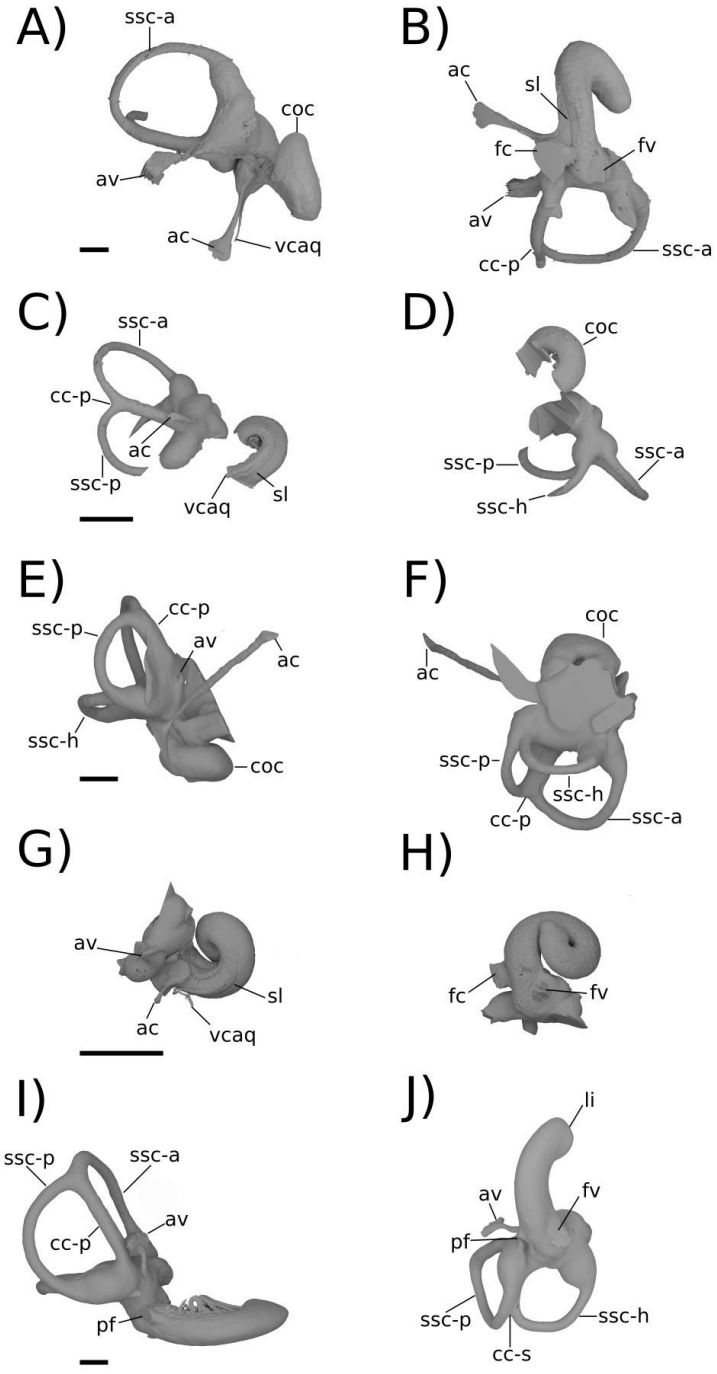

FIGURE 3. Representative lower molariforms for 29 terminal taxa used in comparative analyses. Labial view of the lower left molariforms used in SPHARM analyses described here. Upper rows show molariform surfaces approximated using the full set of 18 degree spherical harmonic coefficients, lower row for each taxon is the approximation of the 18 degree surface using only the first five principal components of molariform shape variation.

TABLE 1. List of lower molariform specimens used for morphometric analyses.

Taxon	Specimen number	Element	Type	OTU represented
Amphitherium rixoni	BMNH 36822	m3	cast	Amphitheriids
Aspanlestes aptap	URBAC 03-086	m2	fossil	*Erinaceus*
Ausktribosphenos nyktos	NVMP208090	m1	cast	*Ausktribosphenos*
Bishops whitmorei	NVMP210075	m1	cast	*Bishops*
Coloniatherium cilinskii	MEF-PV 2011	m2	cast	*Coloniatherium*
Cronopio sp.	Unaccessioned	m1	cast	*Cronopio*
Deltatheridium pretrituberculare	PSS-MAE 132	m1	cast	*Deltatheridium*
Didelphis sp.	DUEA 204	m3	tissue	*Didelphis*
Docodon victor	YPM 11826	m5	cast	Docodonts
Dryolestes priscus	USNM 2722	m5	cast	*Dryolestes*
Gobiconodon borissiaki	unaccessioned	m?	fossil	*Gobiconodon*
Groebertherium stipanicici	MACN 18	m2	cast	*Groebertherium*
Henosferus sp.	unaccessioned	m1	fossil	*Henosferus*
Kennalestes gobiensis	Z Pal No MgM-I/5	m3	cast	*Asioryctes*
Kokopellia juddi	OMNH 26361	m3	cast	*Kokopellia*
Laolestes eminens	YPM 13719	m5	cast	*Laolestes*
Mesungulatum houssayi	MACN 6	m3?	cast	*Mesungulatum*
Morganucodon sp.	UCMP 82743	m?	cast	*Morganucodon*
Obdurodon insignis	SAMP 18087	m1	cast	*Obdurodon*
Paurodon valens	USNM 2143	m4	cast	*Paurodon*
Peligrotherium tropicalis	MEF-PV 2351	m2	fossil	*Peligrotherium*
Peramus tenuirostris	BMNH 47739	m1	cast	*Peramus*
Prokennalestes trofimovi	unaccessioned	m1	fossil	*Prokennalestes*
Reigitherium sp.	MEF-PV 2237	m2	fossil	*Reigitherium*
Spalacolestes cretulablatta	OMNH 27421	m5	cast	*Spalacotherium*
Steropodon galmani	AMF 66763	m1	cast	*Steropodon*
Tinodon bellus	YPM 13644	m2	cast	*Tinodon*
Trioracodon bisulcus	YPM 10344	m2	cast	*Trioracodon*
Vincelestes neuquenianus	MACN 1	m2	Cast	*Vincelestes*

Phylogenetic Protocols and Stance

With the advent of numerical taxonomy, explicit and algorithmic protocols to conceptually decompose and parameterize rates, dates, and durations of morphological transformation in fossil taxa have become available to evolutionary biologists (Felsenstein, 2004; Wagner and Marcot, 2010; Larsson et al., 2012). These phylogenetic models have historically been defined in a probabilistic (likelihood based) framework, originally as generalizations of earlier methods designed for molecular sequence data. As such, morphological models have many of the same conceptual and practical problems as those applied to molecular sequences, with added complications arising from: ascertainment bias (Lewis, 2001); generally smaller data sets and inability to characterize anatomical structures exhaustively; and no commutative definition of character state "exchangabilities" across characters (as opposed to the nucleotide states "atcg"; Wagner and Marcot, 2010; Heath and Moore, 2014). These difficulties, in addition to the anatomical background required to evaluate many standard characters, make phenotypic information harder to generate, curate, and analyze relative to the sequence evolution of macromolecular polymers (Hunt and Carrano, 2010). The advent of large public repositories for phenotypic information such as Morphobank.org (O'Leary and Kaufman, 2012) has helped to minimize the logistical difficulties involved with modern morphological projects.

The recent development of total-evidence models has made available methods specifically tailored for the inclusion of non-contemporaneous (e.g., fossil) taxa as time-calibrated ("tip-dated") terminals for phylogenetic inference (Wagner and Marcot, 2010; Gavryushkina et al., 2016). The Fossilized Birth-Death (FBD) process is a particularly suitable model (prior distribution over tree parameters) for the inference of relationships among mostly extinct taxa, because of its explicit parameterization of extant taxon and fossil

taxon sampling probability, in addition to population-level properties such as speciation (birth) rate and extinction (death) rate (Zhang et al., 2016). The cost of generality in statistical modeling is complexity, however, and the rich parameterizations of FBD and most other total-evidence models necessitate the use of computationally intensive numerical methods for likelihood calculation and Monte Carlo approximation of their corresponding posterior distributions. The expensive nature of these analyses in terms of computational resources and time require the analyst to embrace High Performance Computing (HPC) and larger error variances (versus systematic variances) compared to more traditional approaches (Hoff, 2009). However, in those analyses that sample relatively inclusive and ancient clades such as Mammalia, the underlying biology of terminal taxa are liable to vary widely inter se, and the greatest proportion of these taxa are liable to be extinct. For these groups, idealized (or simplistic) models of evolution are likely to be violated, because of their lack of compensation for varying rates of transformation (between character-state transitions within a single character, between characters, and among branches in a single topology) and inability to model the temporal distribution of non-contemporaneous taxa (e.g. "relaxed-clock" methods for non-ultrametric trees; Felsenstein, 2004; Wagner and Marcot, 2010; Heath and Moore, 2014). For early mammals and their close relatives these problems are compounded because of the likely evolutionary modification of diversification rates associated with the transition from oviparous to viviparous modes of gestation (Helmstetter et al., 2016), and the likely reduction of generation times in smaller-bodied cynodont ancestors and early crown mammals (Evans et al., 2012; Slater, 2013).

No-common-mechanism phylogenetic models, such as those implemented with the Maximum Parsimony (MP) optimality criterion, would also be amenable to the likely wide variation in life-history characteristics among early mammals and closely related cynodonts

(see Gillooly et al., 2005). While the output of such an unconstrained MP analysis is presented below for comparison with prior analyses (Rougier et al., 2011, 2012), these results cannot serve as input for the subsequent macroevolutionary comparative analyses described below. The use of phylogenetic estimates to mitigate the effects of phylogenetic autocorrelation in morphometric observations (i.e., the non-independence of measured variables due to varying degrees of common ancestry among the taxa sampled) requires the reification and parameterization of the concept of a "morphological clock" (Polly, 2004; Hunt and Carrano, 2010; Larsson et al., 2012). The precise representation of this concept as a machine-compatible abstraction requires that internode distances (branch lengths) in phylogenetic estimates be quantified in a way proportional to "potential for character transformation," and in a time-calibrated phylogeny internode distances should represent durations in real time (millions of years; Wagner and Marcot, 2010). Because MP methods do not "share" information about potential for character transformation along internodes (i.e., the "length" for a given internode and ensemble of characters is the simple additive sum of expected transformations for all characters independently) the representation of branch lengths in parsimony methods do not inform character transformations across datasets other than those originally used to estimate the phylogeny (Felsenstein, 2004). Because my goal is to quantify aspects of the morphological transformation in anatomical characteristics generally (and the transformation of lower molariform shape in particular), I use constrained Bayesian probabilistic phylogeny estimation, which is capable of producing results usable by the macroevolutionary comparative methods and model comparisons described below (Hunt and Carrano, 2010; Babst, 2014).

Tip dates for all included fossil taxa were given uniform distributions between the boundary dates (rounded to the nearest million years) listed by the 2018 ICS

chronostratigraphic calendar for the first appearance datum of each OTU (i.e., the age corresponding to the first appearance of fossil representatives of that OTU; Cohen et al., 2013). The ages themselves were taken from Kielan-Jaworokska et al., (2004) and Paleobiodb.org.

Speciation (birth) rate was given an exponential distribution prior with λ (the reciprocal of mean) rate 10, giving a vague distribution, as used in Sterli et al., (2018). Extinction (death) rate and probability of fossilization were both given a flat, beta(1,1) distribution. The sampling probability for extant taxa (ϱ) was set to a constant value of 0.00006, based on the inclusion of only three out of approximately 5,000 living mammalian species (*Erinaceus*, *Didelphis* and *Ornithorhynchus*), with corresponding "sampling strategy" set to "diversity" because of the intentionally wide phylogenetic distances separating these taxa (Zhang et al., 2016; Sterli et al., 2018).

Origin time prior (tree age prior) for clade probainognathia (containing all included OTUs) was given a uniform distribution between 200–250 million years ago, corresponding to most of the Triassic Period. The overall clock rate parameter was given a lognormal prior corresponding to one expected change per character within 250 million years (Thorne and Kishino, 2002). Internode specific rate variation was given an inverse gamma rate prior with a corresponding alpha value distributed according to a vague exponential distribution with a rate of 10, thereby defining a relaxed clock model for tree proposals (Heath and Moore, 2014).

Nine strict topology priors were used to enforce the resolution of the historically recognized clades within Mammaliaformes (McKenna and Bell, 1997; Rowe, 1993; Kielan-Jaworokska et al., 2004). These constraints were deemed necessary to ensure the applicability of the resultant phylogenies for the reconstruction of ancestral PC scores corresponding to

clades recognized in the majority of current mammalian literature. However, while these constraints guarantee the applicability of the following comparative results to most of the traditionally defined Mesozoic mammalian clades, this precludes the Bayesian analysis described here from being a full phylogenetic estimation procedure. As such, questions regarding the alternative topological relationships for major groups (for example, the proposed sister relationship of spalacotheres and South American Late Cretaceous and Cenozoic "dryolestoids"; Averianov et al., 2013) cannot be reasonably addressed by this analysis. The clades given strict enforcement through the topology prior include: Eutheria, Metatheria, Theria (including Eutheria, Metatheria, and the ambiguous OTU *Pappotherium*), Dryolestoidea, Trechnotheria, Theriimorpha, Australosphenida, *Hadrocodium* + Crown Mammalia, and Mammaliaformes. Only the clade constraint for Theria was additionally given a temporal offset exponential distribution, parameterized to have 95% of its prior density within the Late Jurassic for the unsampled therian taxon *Juramaia* (Luo et al., 2011). Other constrained nodes were not given calibrations so as to allow internode lengths to be as informed by the morphological clock model as possible.

Morphological evolution of all characters was parameterized using Mkv likelihood models of standard character transformation (Lewis, 2001), which compensate for acquisition bias caused by the scoring of only variable morphological characters. For all binary characters a generalized version of this model (the Mka model, for asymmetric transition rates; Pyron, 2016; Wright et al., 2016) was used to accommodate differing rates of evolution away from a plesiomorphic state (coded as State 0) and atavistic reversal away from a derived state (coded as State 1). This model was instantiated in MrBayes following protocols recommended by Pyron (2016). Between-character variation in transformation rate

(i.e. among-site rate variation) was modeled for all characters using discretized (four bins) gamma distribution.

Morphometric and Phylogenetic Comparative Methods

This report attempts to demonstrate the usefulness of several statistical methods originally formalized for the analysis of physical phenomena (spectral decomposition and thermodynamics) for the characterization and reconstruction of the evolutionary transformation of lower molariform shape.

The chosen anatomical focus on the lower molariform dentition is based on practical considerations, such as the relative abundance and quality of preservation of these elements within the mammalian fossil record. These elements are also a particularly appropriate subject for modern morphometric analysis because of the possible over-reliance on qualitative specifiers for crown shape variation in many prior studies of mammalian dental evolution (Pattterson, 1956; Vanderbroek, 1961; Hershkovitz, 1971; Thenius 1989), and the possible biases these artificial categories tend to promote in the wider literature (see Harper et al., 2018). The differences-in-kind between triconodont, symmetrodont and tribosphenic/tuberculosectorial molars have in many cases limited the quantification of the continuous variation of tooth shape from one category to another in large scale morphometric studies (Polly, 2004; Polly et al., 2005; Wood et al., 2007; Grossnickle and Newham, 2016; also see Harper et al., 2018). In the case of lower molar variation this is particularly egregious because the "tribosphenic" molar condition is based on the presence of a functional grinding protocone in the upper molar dentition (Crompton and Sita-Lumsden, 1970; Crompton, 1971; Davis, 2011). The lack of a qualitative difference between the anatomy of "pre-tribosphenic" versus "tribosphenic" lower molars, and the continuous

functional gradation between the "triconodont" and "oblique symmetrodont" categories (Gill et al., 2014; Corinth et al., 2016), suggest that a large-scale quantitative analysis of lower molariform shape would be particularly valuable.

Morphometric Methods—The phylogenetic and autecological signal present in the relief, curvature, and complexity of mammalian molars has provided some of the best evidence for the natural history of many extinct lineages (e.g., Thenius, 1989; Lucas, 2004; Evans, 2013). The abundance of ancestral, developmental, and functional influences on molar shape also causes a great deal of uncertainty regarding the underlying homology of ostensibly corresponding features on a crown's surface (Patterson, 1956). This has been a particular problem for geometric morphometrics where assumptions of homology are based on the correspondence of single points (landmarks) as opposed to wider composite "structures" within the crown surface. In the case of point-wise homology of cusps and crests, landmarks available for analysis are generally less informative (type-2 or type-3; Zelditch et al., 2012), and sensitive to inter-observer error during digitization (Rizk et al., 2013).

Previous studies have made molar morphology more tractable for Geometric Morphometric (GM) analysis through the use of sliding-semilandmarks (Gunz et al., 2005; Wood et al., 2007) and by the location of corresponding points on the interior of the dentin-enamel junction surface, as opposed to the outer surface of the molar crown (Skinner et al., 2008). The approach taken in this report is an alternative to traditional GM techniques which are based upon an "elastic analogy" (Oxnard and O'Higgins, 2009). The morphometric analysis used here use a method originally derived for the study of gravity and physical rotors (MacRobert, 1967). This method models crown shape by numerical analogy with the

modes of vibration of an ideal unit sphere (Atkinson and Han, 2012), and it is hoped that this registration technique will better leverage more of the information inherent in the curvature of organic forms compared with the limited sampling of discrete sets of registration points (McPeek et al., 2009). Spherical Harmonic Registration (SPHARM) is a Fourier Series-based method relying on the superimposition of waveform functions, similar to elliptical Fourier analysis and other 2-dimensional outline techniques. The analysis used here is a generalized method applicable to triangular mesh surfaces developed by Shen et al. (2009) and McPeek et al. (2009) and implemented as a group of scripts and pre-compiled executables in the programming development environment MATLAB (release 2018b).

For use in this analysis, lower molariform surfaces were subsampled to 10,000 triangular faces and exported as stereolithography (STL) files using the imaging program Avizo. The landmark editor module of Avizo was also used to place six registration points on each tooth surface required for the object-space alignment of "preshape" tooth information to an initial target shape. These six landmarks were chosen as local and global extrema of curvature consistently identifiable across all lower molariforms used in the sample. Specifically, the six alignment landmarks were: 1) apex of protoconid or cusp "a"; 2) apex of metaconid or cusp "c"; 3) apex of cusp "d" or hypoconulid or apical-distal extent of crown surface; 4) mesial-ventro-labial extent of anterolabial lobe, or half, of crown; 5) disto-ventro-labial extent of posterolabial lobe, or half, of crown; and 6) lingual base of protoconid slope, on lingual surface or trigonid basin. Because of the variable presence of the paraconid among the taxa sampled, the apex of this cusp could not be used for object-space orientation. It should be emphasized that the use of these six registration points for initial object-space alignment of sampled tooth surfaces requires weaker assumptions of biological "sameness" among points than landmark-based analyses (Palci and Yee, 2018), and

that for SPHARM, correspondence of tooth surfaces is established by spherical parameter-space alignment, not landmark placement or object-space orientation (Shen et al., 2009).

Before alignment all molariform surfaces were parameterized using the CALD (Control for Area and Length Distortion) numerical optimization method (Shen et al., 2009) for spherical parameterization. Being periodic functions, these optimal spherical parameterizations are amenable to least-squares fitting using Fourier series (as opposed to more complex Fourier transform) based methods (Langton and Levin, 2017). The set of spherical harmonic functions is a generalization of Fourier series applicable to a longitudinal and colatitudinal domain; and this set of functions was fitted up to L=18 degrees to the estimated tooth surface parameterizations, generating a total of $(L + 1)^2 = 361$ spherical harmonic coefficients in the x, y, and z dimensions. The degree of a spherical harmonic expansion is loosely proportional to the maximum attainable "complexity" of shape information usable for down-stream principal component analysis and phylogenetic comparative methods. As can be seen in Figure 3, the 18 degree spherical harmonic expansion of molariform surfaces recreates almost all aspects of the original crown shape; higher degrees were therefore not considered because they would begin to over-fit artificial noise in input crown surface morphology and would entail much longer processing times.

Finally, reconstruction of view-able triangular mesh files (STLs) from arbitrary PC scores was performed using customized scripts in MATLAB (see Supplementary Data), which utilized linear combinations of the 15 degree fvec (spherical harmonic coefficient) matrices corresponding to the sample average specimen and the "eigenmodes" of the first five principal components.

Phylogenetic Comparative Methods—Having imposed a frequency-space representation for the domain of possible shape variation in lower molariforms, it could reasonably be asked if a similar (but continuous) frequency-space representation for the range of possible evolutionary transformations of these shape specifiers would also be appropriate. Surprisingly, a large amount of prior research is dedicated to the formalization and application of just such a family of stochastic processes over the frequency-space of possible evolutionary and environmental histories, in which the probability of a particular path of "trait" change is inversely proportional to the square of its frequency content (e.g. Halley, 1996; Vasseur and Yodzis, 2004). The corresponding object-space representation of this process models the fractal trajectory of a particle as an undirected "random-walk," in which slower sweeping trends are proportionally more important than short, jerky movements. This process is better known as Brownian Motion (BM; Einstein, 1905) or pedesis, a physical model originally formulated to explain the apparently spontaneous agitation of microscopic particles in liquids at thermal equilibrium (i.e., characterized by a certain temperature; Frey and Kroy, 2005). Within evolutionary biology, BM has been valuable as a (implicit or explicit) model of quantitative trait change (e.g., Felsenstein, 1985; Hunt and Carrano, 2010), and as a skeptical "null model" in comparison with more parameterized evolutionary scenarios. The properties which make BM so tractable as a probabilistic model for so many fields of inquiry include: (1) the instantaneous normality, homogeneity of variance and independence of trait changes during the process; (2) the expected value of a trait after some elapsed duration being equal to the initial (ancestral) value of that trait at the beginning of the duration; and (3) the variance of a (descendant) trait from its expected value being directly proportional to the amount of time separating it from its (ancestral) initial value. These properties are also criticized as oversimplifications in

many cases (Hansen, 2014), such as when single selective regimes persist over a large portion of a phylogeny. However, in macroevolutionary analysis BM has emerged as one of the canonical models for continuous quantitative trait evolution (e.g., Lande, 1976; Lynch, 1990; Harvey and Purvis, 1991; Harvey and Rambaut, 2000; Polly, 2004; Hunt and Carrano, 2010; Hunt, 2012).

This report utilizes the BM process to simultaneously quantify maroevolutionary trait variance and covariance in the five most important lower molariform Principal Component (PC) scores recovered from the SPHARM analysis described above, using the labeled history ("SIMMAP-like" summary phylogeny) of trait change generated from the constrained posterior sample from the MrBayes analysis. These models were fairly criticized (Hansen, 2014) because of their limitations that: (1) trait selective optima are not realistically modeled, leading to a situation termed "inherited maladaptation" if such optima exist; and (2) trait values corresponding to ancestral nodes are necessarily weighted averages of the values seen at descendant nodes. While being fairly rigid, these limitations are justifiable in the case of mammalian lower molariform evolution (see Polly, 2004), and the unsolicited incorporation of optima or deterministic trend parameters would unnecessarily over-fit the currently available data. Additional criticisms that BM processes have no way of modeling directional changes, or ability to decrease discrepancy in trait values through time, are only applicable to the use of this model based on ultrametric trees (Babst, 2014). Our use of a summary phylogeny with tip-dated fossil taxa allows for a range of possible trait trajectories to be estimated in which lineage extinction can prevent the continuous "radiation" of trait disparity over time. This is not to suggest that the trajectory of lower molariform evolution could not be best represented as a "radiation" of shape specifiers either, as has been depicted in many summaries of dental evolution (Vandebroek, 1961; Hershkovitz, 1971;

Jernvall et al., 1996). Macroevolutionary trait analyses implemented using my tip-dated summary phylogeny and the BM process are consitered flexible enough to estimate accurate parameterizations of molariform shape evolution under the full range of plausible evolutionary trajectories, and that more richly parameterized and general models of molariform shape change would be inappropriate for the limited (N=29) sample of molariform surfaces used here.

Finally, it should be emphasized that while the shape specifiers generated using the SPHARM registration protocols described above are geometrically independent (i.e., the real and imaginary components of the PC scores are orthogonal to each other and to all other PCs), these components of lower molariform shape likely show correlated changes throughout their history of evolutionary transformation across mammalian phylogeny (Polly, 2004). In order to accommodate the likely evolutionary covariance between shape PCs within a model of macroevolutionary trait evolution, and model possible punctuations in evolutionary mode within defined mammalian subgroups, the BM process as implemented with the maximum-likelihood based R statistical package mvMORPH (Clavel et al., 2015) was used to fit and compare the several candidate evolutionary models described in the results section below. Other tools used in this analysis come from the R phylogenetic packages ape (Paradis et al., 2004), phytools (particularly the function paintSubTree; Revell, 2012), and STRAP (Bell and Lloyd, 2015). The particular evolutionary models tested in this report are based on the undirected mutivariate Browian Motion models implemented using the mvBM function and model comparison tools provided by mvMORPH. The model comparison and ancestral state estimation functions in mvMORPH ("aicw" and "estim") were also used to contrast the relative support of these models.

RESULTS

Scoring of Inner Ear Characters

The evolutionary transformation of the mammalian ear is often summarized simplistically as a single linear series of alterations from primitive extinct synapsids to "modern" extant forms (Luo 2011; Laaß, 2015, Manley, 2017). This may cause misconception among non-specialists that the specialization of the modern (therian) ear is a uniquely sophisticated evolutionary breakthrough characteristic of the mammalian lineage. While it is true that no mammalian taxon is known to have lost its ancestral auditory percept completely, many extant non-mammalian taxa show comparable levels of auditory sensitivity and selectivity (tuning) to that seen in even the most highly derived therians (Manley, 2000). Additionally, many of the most derived anatomical characteristics seen solely in therian mammals today also appear homoplastically in extinct Mesozoic non-therian taxa (Luo et al., 2016).

The additional character scoring of 14 inner ear features/cochlear endocast features provided here emphasizes many of the most variable features of the mammalian inner ear (Luo et al., 2016), and therefore likely includes many instances of homoplasy. The inclusion of these features is considered important because of the heuristic value that character-rich anatomical regions have for informing transition rates and branch lengths in likelihood-based phylogenetic estimation, especially for extinct groups and "sagebrush" terminal taxa (McKenna, 1976) where limitations in character sampling may exclude the rarer, more quickly evolving, characteristics (Harrison and Larson, 2015). The additional characters used here are likely related to the increased sensitivity and selectivity of the cochlear apparatus (Harper and Rougier, 2019); however, it is unclear if these features are directly related to the

extremely high upper frequency limit attained by the modern therian taxa (Manley 2017, 2018).

The following headings list the 14 new labyrinthine characters generated for the phylogenetic analyses described below. Because of the importance that the numbering of binary character states has for the estimation of transition rates in the "asymmetric" Mka model of morphological transformation (Pyron, 2016) used in our Bayesian analysis, justifications are also given for our particular ordering of these character states.

Character 233: Presence of primary lamina in cochlear endocast—Scoring of the binary presence/absence of a primary bony lamina along the neural margin of the cochlear endocast is essentially the same as used as Character 233 of Rougier et al. (2012). The interpretation of the state of this character requires some additional nuance in order to score several non-therian taxa where there appears to be a structure homologous to the primary bony lamina as seen in therians (Meng and Fox, 1995), but a bony spiral ganglion canal (Rosenthal's canal) either can not be confirmed because of incomplete preservation (the case in *Vincelestes*, *Coloniatherium* and *Peligrotherium*; Fig. 2) or seems to be lacking (the case in *Henkelotherium*; Ruf et al., 2009). Therefore, in lieu of creating a third state for "the presence of a primary bony lamina but without being associated with a canal for the cochlear ganglion," which can only be unambigously scored in one case, we choose to score all taxa showing at least some development of a projecting, linear attachment for the cochlear apparatus along the neural side of the cochlear canal as having the "present" state of the primary bony lamina.

Character 234: Presence of secondary lamina in cochlear endocast—Similar to the condition of the primary bony lamina, a potential third intermediate state of the abneural secondary bony lamina could be defined. As above, the character matrix used here follows the binary scoring of the presence/absence of the secondary lamina as in Character 234 in Rougier et al 2012. In cases where a rudimentary "base of the secondary lamina" may be present (such as in Monotremes and possibly *Morganucdon*; Schultz et al., 2017; Shahid et al., 2018) this is scored here as the absence of a true secondary lamina. This is the most conservative treatment for forms with a low "base of the secondary lamina" because of its reported variable presence intraspecifically and lack of adherence to the cochlear duct where observed in living monotremes (Schultz et al., 2017).

Character 318: Subdivision of foramina for vestibulococchlear nerve in internal acoustic meatus—State 0, one foramen each for the vestibular and cochlear branches respectively; State 1, three or more foramina - one each for utriculoampullar, sacculoampullar, and cochlear nerve/tractus foraminosus. Many mammaliamorphs show the division of single foramen for the vestibulocochlear nerve into separate foramina for its vestibular and cochlear branches (Olson, 1944; Rodrigues et al 2013), and this condition is reconstructed to be plesiomorphic (State 0) for the taxa sampled in this analysis. The further subdivision of the foramen for the vestibular branch into two (utriculoampullar and sacculoampullar) or more subdivisions is inferred to represent the derived state (State 1). I scored the plesiomorphic state in tritheldontids (based on the closely related *Brasilitherium*; Rodrigues et al., 2013), tritylodontids (Luo, 2001), *Sinoconodon* (Crompton and Luo, 1993), *Morganucodon* (Kermack et al., 1981), and docodonts (Ruf et al 2013; Panciroli et al., 2018). The derived state is scored from the relevant literature in *Ornithorhynchus* (Schultz et al.,

2017), *Priacodon* (Rougier et al., 1996), *Henkelotherium* (Ruf et al., 2009), *Dryolestes* (Luo et al., 2012), *Coloniatherium* (Rougier et al., 2009), *Peligrotherium* (Paez-Arango, 2008); and scored based on our observations in *Cronopio*, *Vincelestes*, *Didelphis*, *Erinaceus*, and the Höövör petrosals.

Character 319: Presence of Crista transversa—State 0, not present; State 1, present, either as an incomplete crista transversa or well-formed falciform crest crossing entire internal meatus. The bony strut separating the foramen acusticum superius (area within the internal acoustic meatus for the primary facial foramen and utriculoampullar foramen) from the foramen acusticum inferius (area within the internal acoustic meatus for the foramen for the cochlear nerve and sacculoampullar foramen/foramina) in many mammals shows a raised linear crest of bone termed the crista transversa (Hughes et al., 2015). This crest can be limited to the rostral border of the floor of the internal acoustic meatus (as it is in the Höövör petrosals) or may completely span the floor of the internal acoustic meatus, attaching to its rostral and caudal borders (as in *Homo*, where it is termed the falciform crest). Both of these states are here scored as the derived (State 1) condition representing the presence of the crista transversa, as seen in *Ornithorhynchus* (Schultz et al., 2017), *Vincelestes*, *Didelphis*, *Erinaceus*, *Henkelotherium* (Ruf et al., 2009), *Dryolestes* (Luo et al., 2012) *Coloniatherium*, *Peligrotherium*, *Cronopio* and the Höövör petrosals. Conversely, lack of this structure is considered plesiomorphic (State 0) as is seen in tritheledontids (Rodrigues et al., 2013), tritylodontids (Luo, 2001), *Morganucodon* (Kermack et al., 1981), docodonts (Ruf et al 2013; Panciroli et al., 2018) and *Priacodon* (Rougier et al., 1996).

Character 320: Presence of lagenar inflation—State 0, tapering or blunt apex of cochlear canal/recess; State 1, distinct apical bulb for lagenar macula. While the presence or absence of a functional lagenar endorgan does not leave a reliable osteological correlate within the cochlear endocast (i.e., absence of a groove or sulcus for the lagenar nerve or terminal inflation of the cochlear canal does not indicate absence of a lagenar macula), in several cases an enlarged terminal inflation of the cochlear endocast is apparent. Whether this may represent a relative enlargement of the lagenar endorgan and surrounding structures, or the relative constriction of the more proximal space available to the cochlear apparatus, is unclear. However, this relative inflation is absent in non-mammaliaform synapsids and many other amniotes, and the absence of this inflation is considered plesiomorphic (State 0); as scored in tritheledontids (Rodrigues et al., 2013), tritylodontids (Luo, 2001). The lack of a lagenar inflation is apparent in *Priacodon*, *Vincelestes*, *Didelphis*, *Henkelotherium* (Ruf et al., 2009), *Dryolestes* (Luo et al 2012), *Coloniatherium* (Rougier et al, 2009), *Peligrotherium* (Paez-Arango, 2008). I also interpret *Cronopio* and the Höövör petrosals as lacking a terminal lagenar inflation, although a slight, sub-terminal, inflation of the cochlear canal is visible in these forms. A distinct terminal lagenar inflation (State 1) is present in *Morganucodon* (see abstract by Shahid et al., 2018), docodonts (Ruf et al 2013; Panciroli et al., 2018) and *Ornithorhynchus* (Schultz et al., 2017).

Character 321: Presence of tractus foraminosus—State 0, not present; State 1, present. While a cancellous bony infilling of the foramina seen within the region of proximal nervous ramification is common in several areas of the internal acoustic meatus in mammals (MacPhee, 1981), the presence of the tractus foraminosus specifically refers to the spongy infilling of the foramen for the cochlear nerve within the foramen acusticum inferius. This

forms an identifiable cribriform plate within the floor of the internal acoustic meatus, distributing the fibers of the cochlear nerve in a ribbon-like or radial manner. The plesiomorphic condition (State 0) is a lack of this bony infilling, and is therefore predicated on the presence of a discrete foramen for the cochlear nerve. The absence of the tractus foraminosus is scored for tritheledontids (Rodrigues et al., 2013), tritylodontids (Luo, 2001), *Sinoconodon* (Crompton and Luo, 1993), *Morganucodon* (Kermack et al., 1981), docodonts (Ruf et al 2013; Panciroli et al., 2018), *Priacodon* (Rougier et al 1996), *Trioracodon* (Kermack 1963), and the Höövör petrosals (Wible et al., 1995; Rougier et al., 1996). The tractus foraminosus is scored as present in *Ornithorhynchus* (Schultz et al 2017), *Vincelestes* (Rougier et al 1992), *Didelphis*, *Erinaceus*, *Prokennalestes* (Wible et al 2001), *Henkelotherium* (Ruf et al., 2009), *Dryolestes* (Luo et al 2012), *Coloniatherium* (Rougier et al, 2009), *Peligrotherium* (Paez-Arango, 2008), *Necrolestes* (Wible and Rougier 2017), and *Cronopio*.

Character 322: "Sunken" fenestra ovalis (fossula fenestra ovalis)—State 0, absent; State1, present. The "sunken" or "impressed" appearance of the fenestra vestibuli was mentioned by Hughes et al. (2015) as an advanced feature of the cochlear endocast seen in many cladotherian mammals. This impression is possibly the expression of to the fossula fenestra vestibuli onto the cochlear endocast. However, given the absence of the "sunken" fenestra vestibuli in both rootward and crownward synapsids such as tritheledontids (Rodrigues et al., 2013), tritylodontids (Luo, 2001), *Morganucodon* (Kermack et al., 1981), docodonts (Ruf et al 2013; Panciroli et al., 2018), *Priacodon* (Rougier et al 1996), *Ornithorhynchus* (Schultz et al 2017), *Vincelestes* (Rougier et al 1992), and the Höövör petrosals, the plesiomorphic condition (State 0) is considered to be the absence of the "sunken"

fenestra vestibuli. The derived state of the fenestra vestibuli is seen in *Didelphis*, *Erinaceus*, *Henkelotherium* (Ruf et al., 2009), *Dryolestes* (Luo et al 2012), and *Cronopio*.

Character 323: Vein of cochlear aqueduct—State 0, absent; State 1, present (opens intracranial or intramural). In extant therians the drainage of veinous blood from the pars cochlearis (portion of the petrosal containing the cochlear apparatus) is solely, or at least predominantly, directed through the vein of the cochlear aqueduct (VCAQ) before entering the inferior petrosal sinus and other tributaries of the internal jugular vein. In the cochlear endocast the VCAQ is accommodated by a discrete bony canal (termed the canal of Cotugno; Lempert et al., 1952) and linear sulci on the wall of the cochlear canal radiating from the intersection of the canal of Cotugno with the cochlear endocast. Based on reasoning presented in Harper and Rougier, (2019), we regard the presence of the VCAQ and its osteological correlates as the derived condition (State 1) in this report. Taxa with this condition include: the Höövör petrosals, *Vincelestes*, *Didelphis*, *Erinaceus*, *Coloniatherium* (see Fig. 2C for an image of damaged base of VCAQ), and *Cronopio*. Conversely, in several taxa known from CT imaging, the absence of the osteological correlated of the VCAQ (and presumably the vein itself) can be confirmed: tritheledontids (using Rodrigues et al., 2013), tritylodontids (Luo, 2001), *Morganucodon* (see abstract in Shahid et al., 2018), docodonts (Ruf et al 2013; Panciroli et al., 2018), *Priacodon* (Harper and Rougier, 2019), and *Ornithorhynchus* (Schultz et al, 2017).

Character 324: Shape of tip of cochlear canal—State 0, tapered; State 1, blunt or inflated by lagena. Aside from size and orientation, the shape of the apical termination of the cochlear canal/cochlear recess varies among the sampled taxa. The apex of the cochlear

canal can be categorized into generally conical and tapered forms, or forms with a club-shaped or blunt termination (or lagenar inflation). Because of the generally blunt shape of the cochlear recess (lagenar recess) in several non-mammaliaform cynodonts (Olson 1944, Luo 2001, Benoit et al 2017), the blunt/widned state of the cochlar canal/recess is considered plesiomorphic (State 0). This is the condition in tritheledontids (Rodrigues et al., 2013), tritylodontids (Luo, 2001), *Priacodon* (Harper and Rougier 2019), *Henkelotherium* (Ruf et al., 2009), *Dryolestes* (Luo et al 2012), and *Vincelestes*; additionally, taxa showing a distinct lagenar inflation of the cochlear canal are also classified as State 0, including *Morganucodon* (see abstract in Shahid et al., 2018), docodonts (Ruf et al 2013; Panciroli et al., 2018) and *Ornithorhynchus* (Schultz et al, 2017). Taxa showing the derived state (State 1) include the Höövör petrosals and *Cronopio*.

Character 325: Curvature of cochlear canal—State 0, straight; State 1, only mediolateral curvature; State 2, dorsoventral curvature (complete coil or not). The overall shape of the cochlear endocast can be categorized as being generally straight (or linear) as in tritheledontids (Rodrigues et al., 2013), tritylodontids (Luo, 2001), and the Höövör petrosals. While taxa showing only lateral curvature (concave toward the insertion of the cochlear nerve) include *Morganucodon* (see abstract in Shahid et al., 2018), docodonts (Ruf et al 2013; Panciroli et al., 2018), *Priacodon* (Harper and Rougier 2019), and *Ornithorhynchus* (Schultz et al, 2017). Dorsoventral coiling (in addition to lateral curvature) is seen in *Vincelestes* (Rougier et al 1992), *Henkelotherium* (Ruf et al., 2009), *Dryolestes* (Luo et al 2012), *Cronopio*, *Coloniatherium* (Rougier et al 2009), *Peligrotherium* (Paez-Arango, 2008), *Prokennalestes* (Wible et al 2001), *Didelphis* and *Erinaceus*. Being a multistate character, we do not model transition rates away-from and toward the plesiomorphic state asymmetrically with the Mka likelihood (Pyron

2016, Wright 2016). Additionally, unlike the similarly defined character 231 describing relative curvature of the cochlear canal (in any direction), I refrain from modeling the shape of the cochlear canal as an ordered character in our Bayesian analysis (as done in Rougier et al 2011). Therefore, assumptions regarding which of the three states in this character correspond to the most plesiomorphic condition are unnecessary.

Character 326: epicochlear sinus(es)—State 0, present; State 1, absent. Originally described as "trans-cochlear sinuses a and p" (Panciroli et al., 2018), the epicochlear sinus(es) are mediolaterally running canals that connect the intramural inferior petrosal sinus to either the prootic canal (posterior epicochlear sinus) or to the cavum supracochlearis (anterior epicochlear sinus; Harper and Rougier, 2019). The anterior epicochlear sinus runs anterior to the contents of the internal acoustic meatus, whereas the posterior epicochlear sinus courses through the bony strut separating the foramen/foramina for the vestibular nerve from the primary facial foramen and foramen for the cochlear nerve. Because of the highly venous nature of the pars cochlearis in early mammaliamorphs (Luo et al., 1995, Luo et al., 2001) and the identification of epicochlear sinuses in stem mammaliaforms such as *Morganucodon* (see abstract in Shahid et al., 2018) and the docodont *Borealestes* (Panciroli et al., 2018), I consider the presence of any number of these canals to be the plesiomorphic condition (State 0). In addition to the above mentioned stem mammaliaforms an epicochlear sinus is also visible in *Priacodon* (Harper and Rougier, 2019). Taxa known from sufficiently high resolution internal images to confirm the derived lack of epicochlear sinuses (State 1) include: *Ornithorhynchus*, *Vincelestes*, *Didelphis*, *Erinaceus*, *Coloniatherium*, *Peligrotherium*, *Cronopio* and the Höövör petrosals.

Character 327: Hypocochlear sinus—State 0, present; State 1 absent. In contrast to the epicochlear sinuses, the hypocochlear sinus (Harper and Rougier, 2019) is a venous canal coursing mediolaterally within the substance of the promontorium ventral to the cochlear canal. Following similar reasoning to that outlined above for the epicochlear sinuses, we consider the presence of a hypocochlear sinus to be the plesiomorphic condition (State 0). Taxa within our sample known to have a hypocochlear sinus include *Morganucodon* (Shahid et al., 2018), *Priacodon*, and Höövör petrosal 1 (Harper and Rougier, 2019). Conversely, taxa known from sufficiently high-resolution images to confirm the absence of a hypocochlear sinus (State 1) include the docodont *Borealestes* (Panciroli et al., 2018; used as a representative of docodonts generally), *Ornithorhynchus*, *Vincelestes*, *Didelphis*, *Erinaceus*, *Coloniatherium*, *Peligrotherium*, *Cronopio*, and Höövör petrosal 2.

Character 328: Relative proportion of pars cochlearis filled by cochlear canal—State 0, less than ~50%; State 1, more than ~50%. As observed by Luo et al., (1995), the cochlear endocast in earliest mammaliamorphs fills a relatively small proportion of the total volume (less than 50%, chosen as an approximate and arbitrary cutoff) of the pars cochlearis (as defined by Luo, 2001). The remainder of space available within the bony pars cochlearis is predominantly occupied by venous excavations (including the epicochlear and hypocochlear sinuses discussed above) surrounding the cochlear canal. Because of the likely highly venous nature of the pars cochlearis, the condition of having less than ~50% of the pars cochlearis filled by the cochlear canal is considered plesiomorphic (State 0); this condition can be determined from the literature for tritheledontids (as inferred from the closely related *Brasilitherium*, Rodrigues et al., 2013), tritylodontids (Luo et al 1995, Luo et al 2001), *Sinoconodon* (Crompton and Luo, 1993), *Morganucodon* (Kermack et al., 1981; Graybeal

et al., 1989; Shahid et al., 2018), docodonts (Ruf et al 2013; Panciroli et al., 2018), and *Priacodon* (Rougier et al., 1996; Harper and Rougier, 2019). The relatively greater (approximately greater than 50% of the volume of pars cochlearis) volume of the cochlear endocast (State 1) can be determined in *Ornithorhynchus*, *Vincelestes*, *Didelphis*, *Erinaceus*, *Coloniatherium*, *Cronopio* and the Höövör petrosals.

Character 329: Relative length of secondary lamina (starting from crista interfenestralis) to length of cochlear canal—State 0, approximately less than 0.5; State 1, approximately more than 0.5. As defined, this character is solely applicable to taxa with a "present" secondary bony lamina (character 234), and is inapplicable to other OTUs (therefore scored as an "?"). The relative length of the secondary bony lamina is a rough ratio of the length of the secondary lamina (starting from its basal initiation on the crista interfenestralis, and running toward its apical termination; Meng and Fox, 1995) to the length of the cochlear canal, (starting basally at the rostral margin of the fenestra vestibuli). We consider a relatively short secondary lamina (arbitrarily chosen to be less than 50% of cochlear canal length) to be the plesiomorphic condition (State 0), although in the earliest known stem therians it is a relatively long structure compared to the total length of the (absolutely short) cochlear canal. Taxa showing the relatively short secondary lamina include *Henkelotherium* (Ruf et al., 2009), *Dryolestes* (Luo et al 2012), and *Vincelestes* (Rougier et al., 1992). Taxa known to show a relatively long secondary lamina (State 1) include *Priacodon* and the Höövör petrosals (Harper and Rougier 2019), *Didelphis*, *Erinaceus* and *Cronopio*.

Character 330: Relative length of cochlear canal (in multiples of widest distance across fenestra vestibuli)—State 0, four or less; State 1, five or more. This

character describes a rough estimate of the relative length of the cochlear canal/recess, in multiples of the longest length across the fenestra vestibuli. Given that many early mammaliamorphs show a relatively large fenestra vestibuli and a relatively short cochlear canal/recess (Luo et al., 2016), we consider values below 5 to be the plesiomorphic condition (State 0). Taxa showing this condition include tritheledontids (see Rodrigues et al., 2013), tritylodontids (Luo, 2001), *Morganucodon (*Graybeal et al 1989), docodonts (Ruf et al 2013; Panciroli et al., 2018), *Priacodon* (Rougier et al 1996) and the Höövör petrosals (Harper and Rougier, 2019). Relatively long cochlear canals (State 1) are seen in *Ornithorhynchus*, *Henkelotherium* (Ruf et al., 2009), *Dryolestes* (Luo et al., 2012), *Vincelestes*, *Didelphis*, *Erinaceus*, and *Cronopio*

Character 331: Shape of cochlear endocast—State 0, linear (tip points away from vestibule); State1, hook (points back to vestibule); State 2, spiral. This character refers specifically to the orientation of the tip of the cochlear canal relative to its base. Because of our treatment of this character as multistate and unordered, it is unnecessary to posit a plesiomorphic condition for State 0 in these analyses. However, because of the generally linear cochlear canals/recesses seen in early mammaliamorphs (Luo et al., 2016) this is the likley plesiomorphic state; as seen in tritheledontids (see Rodrigues et al., 2013), tritylodontids (Luo, 2001), *Morganucodon (*Graybeal et al 1989), docodonts (Ruf et al 2013; Panciroli et al., 2018), *Ornithorhynchus* (Schultz et al 2017)*, Priacodon* (Rougier et al 1996) and the Höövör petrosals (Harper and Rougier 2019). Hook-shaped cochlear canals (State 1) have the tip of the cochlear canal pointing dorsally, and back toward the vestibule; as seen in *Henkelotherium* (Ruf et al., 2009), *Dryolestes* (Luo et al 2012), and *Vincelestes* (Rougier et al., 1992). Spiral cochlear canals (state 2) have their apical tip pointing in a direction generally

orthogonal/tangential to the vestibule; as seen in *Didelphis*, *Erinaceus*, *Cronopio Coloniatherium* (Rougier et al, 2009), *Peligrotherium* (Paez-Arango, 2008), and *Necrolestes* (Ladevèze et al 2008).

Phylogenetic Estimates

As a presentation of the phylogenetic information available within the updated dataset described above, a randomized phylogenetic analysis was performed using the program PAUP (Swofford, 2003) implemented using the HPC phylogenetic facility CIPRES (Miller et al., 2015). The 329 parsimony-informative characters available in this matrix were partitioned into 44 ordered (Wagner parsimony model; corresponding to the ordered characters used in Rougier et al., 2011) and 287 unordered (Fitch parsimony model) characters. For each bootstrap replicate a heuristic search was performed using random taxon addition and TBR (tree bisection and reconnection) to maneuver across the space of potential phylogenies (Wiley et al., 1991). For each of 1000 bootstrap (complete character resampling with replacement) randomizations ten iterations of the heuristic addition sequence were performed and one optimal topology was retained per sequence.

Figure 4 shows the 50% majority rule consensus tree resulting from this bootstrap analysis. With the character matrix used here, this phylogeny represents a parsimony tree-length of 1417 steps, and an average character Consistency index of 0.323, Retention index of 0.657, and Rescaled Consistency Index of 0.212. As can be seen, these results demonstrate that the additional inner ear character information and bootstrap randomization significantly reduces the amount of resolution attainable, compared to the original analyses of this dataset presented by Rougier et al. (2011, 2012) and O'Meara and Thompson (2014). Although there is fairly strong support for the placement of many stem mammaliaform and

cynodont taxa, and the monophyly of Australosphenida, Tribosphenida (Boreosphenida), and Meridiolestida, the majority of mammalian taxa are included in one of two poorly supported polytomies. The more inclusive of these polytomies generally represents the crown mammalian clade, with the group "Yinotheria" (Chow and Rich 1982) (australosphenidans and shuotheriids) as its only resolved descendant lineage.

The second major polytomy loosely represents the mammalian clade Cladotheria. In this group the descendent lineage Meridiolestida is well resolved, and the less-well-sampled lineage Tribosphenida somewhat less so (but more strongly supported). In addition to these major groups, many singleton lineages representing taxa traditionally grouped in the clade Dryolestoidea, and the South American mammal *Vincelestes*, also emerge. Therefore, while these results do not provide any resolution among cladotherian taxa, there is no support for the purposed meridiolestidan-spalacothere relationship suggested by Averianov et al. (2013). Other small groups recovered by this parsimony method include Morganucodonta, Triconodontidae, and Spalacotheroidea (although without the basal taxon *Tinodon*). Additionally, the sister-relationship between both Höövör petrosals, and their location within the basal mammalian polytomy, do not support either previously purposed affinities of these taxa as early spalacotheres or eutriconodonts (Rougier et al., 1996; Harper and Rougier, 2019.

Using the Bayesian model specifications described within Materials and Methods, the program MrBayes (Ronquist et al., 2012), as implemented on the CIPRES XSEDE cluster (Miller et al., 2015), was used to approximate the posterior distribution of the FBD-Mka model. Four independent runs, each using four sampling chains and a temperature parameter of 0.15, were run through 60 million steps for the MCMC approximation of its posterior distribution. For each independent run the MCMC state was logged every 5000 steps, and convergence diagnostics were checked using the MCMC program Tracer (Rambaut et al.,

2018) for the parameter logs of each run, independently (using a 10% burn-in) and for all four trace files combined. All four runs had reached stationarity and Effective Sample Sizes (ESS) for all parameters were well above 200 (the lowest being 616 for overall clock-rate in one particular run).

A DensiTree representation (Bouckaert, 2010) of an uncalibrated prior sample and the posterior sample is shown in Figure 5, with a corresponding summary tree of all compatible clades found in the posterior sample shown in Figure 5B. Because of the nine topological constraints used in the estimation of the posterior, most interior nodes or the resulting summary phylogeny show exceptionally high support values, with only 9 clades having associated posterior probabilities lower than 0.8 (Fig. 6). The most weakly-supported of these groups are the clade uniting all non-mammaliaform cynodonts and its sub-clade uniting all non-mammalianform "mammaliamorph" taxa (Rowe, 1988) to the exclusion of *Probainognathus*; the sister relationship of *Megazostrodon* and *Dinnetherium*; the clade uniting the *Spalacotherium* with zhangheotheriids, and the clade uniting the "eutriconodontan" taxa.

FIGURE 4. Majority rule summary tree of MP bootstrap analysis using PAUP. Numbers on interior nodes are percentage bootstrap support.

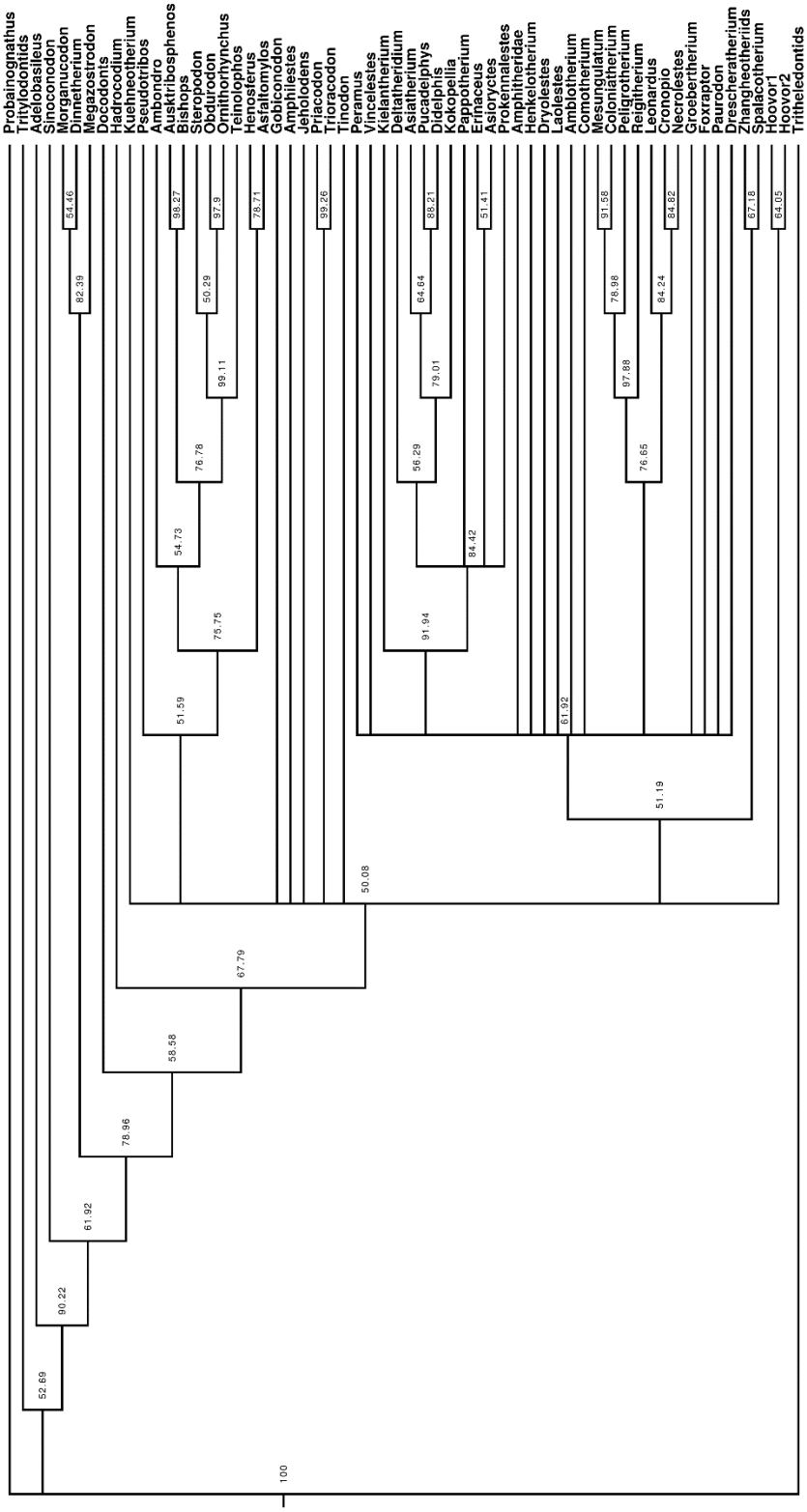

FIGURE 5. Results of constrained Bayesian analysis using MrBayes. **A**, DensiTree representation of uncalibrated FBD prior sample; **B**, Bayesian consensus phylogeny of all compatible clades found in FBD posterior sample, bars represent upper and lower 95% bounds for node ages.

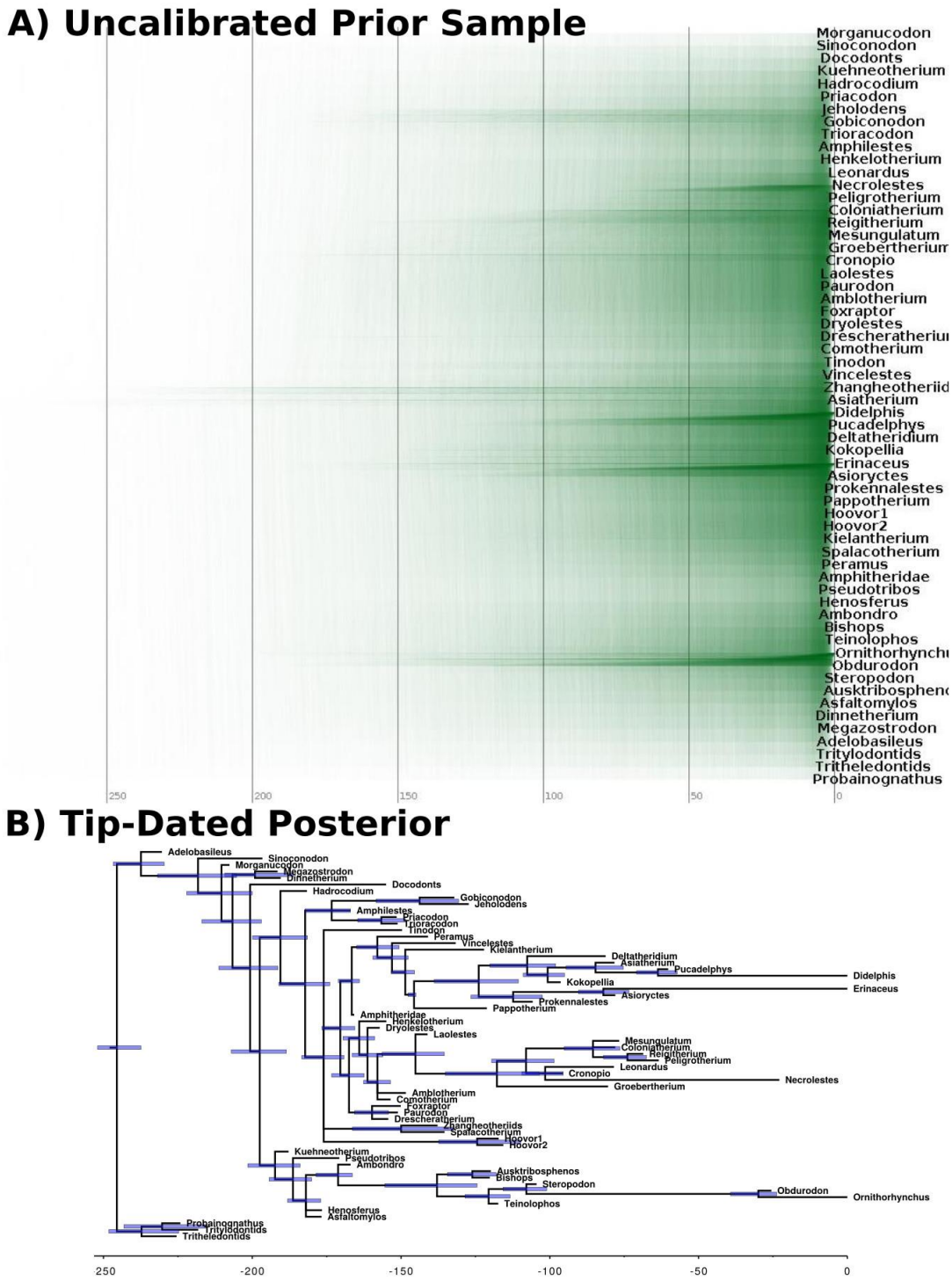

FIGURE 6. Bayesian consensus phylogeny used in subsequent macroevoltuionary analyses. Black circles represent clade constraints used in MCMC estimation; white circles show clades with less than 0.8 posterior probability.

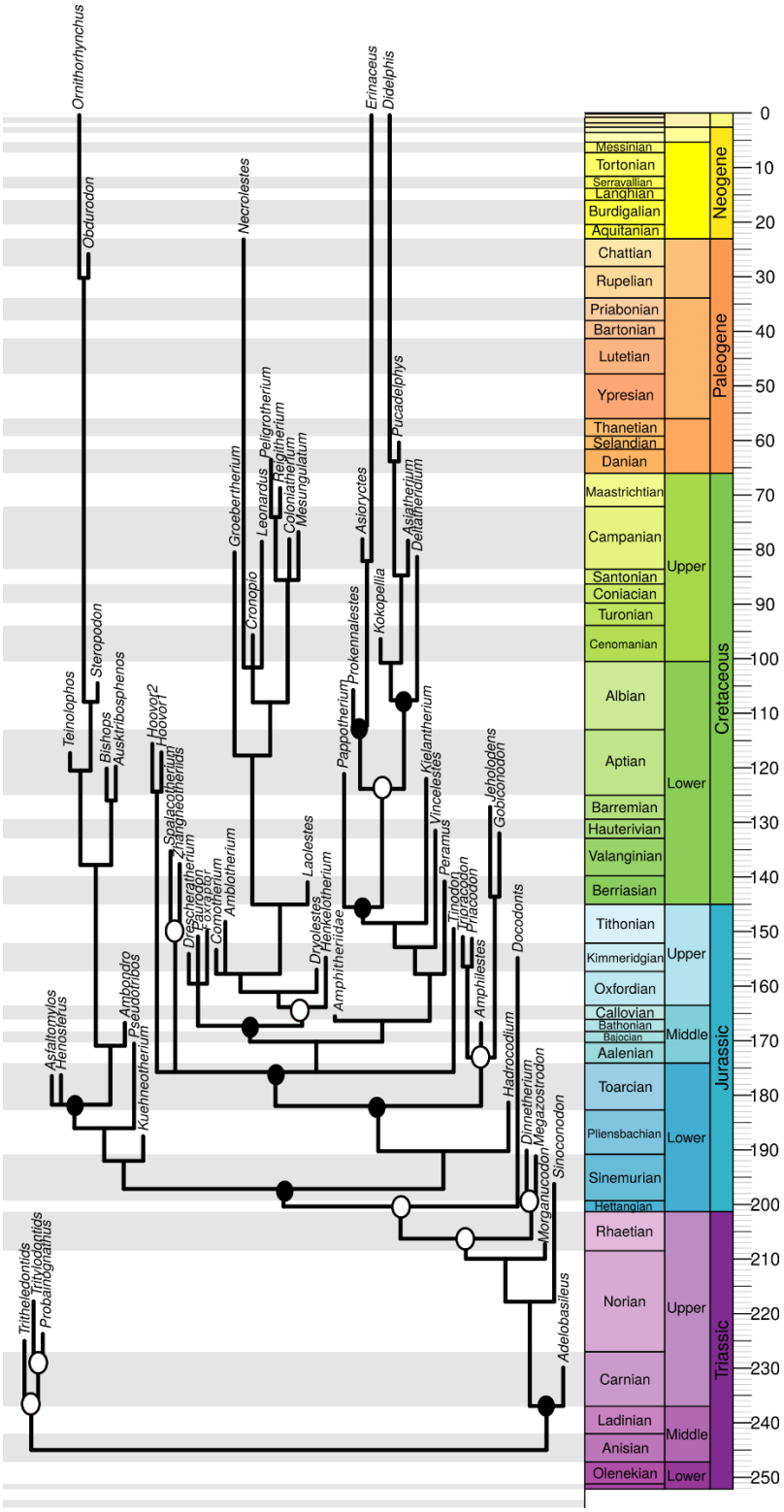

Morphometric Results

As a proof-of-concept evaluation of the SPHARM protocols described above, a sensitivity analysis based on the repeated sampling of multiple molariforms for three Mesozoic lower jaw specimens was performed. These specimens correspond to three of the OTU taxa included in Rougier et al (2012): *Docodon victor* (YPM 11826), *Dryolestes priscus* (USNM 2722), and *Laolestes eminens* (YPM 13719). These taxa were chosen because of the very similar and approximately "average" molariform shapes represented by the molars of *Dryolestes* and *Laolestes*, and apomorphically extreme molariform shapes seen in *Docodon*. Because of limitations in preservation only molars 2 and 5-7 were analyzed for *Dryolestes*, molars 2–6 and 8 for *Laolestes*, and molars 2–6 for *Docodon*. Each analyzed tooth postion was cropped and processed three separate times, with each replicate serving as a separate sample in the subsequent spherical parameterization. These molariform surfaces were registered in a common Fourier shape space using the average molariform shape from the full (N =29) taxon sample as the target specimen, so as to not unfairly bias the variance in the projected PC scores of either *Docodon* or dryolestid molars in the resulting shape space.

The resulting principal components of this inter and intra toothrow shape variation create an extremely steep scree-plot of explained variance, with PC1 explaining 62% of total variance, and PC2 11%, PC3 6%, and PC4 3% of total variance, respectively. As would be expected, PC1 clearly separates the molars of *Docodon* (with negative PC1 scores) from the dryolestids (with positive PC1 scores). Conversely, the second axis of shape variation is mostly associated inter-speciic differences between the two dryolestid genera and with intra-toothrow variation. As can be seen in Figure 7A, the rotated PC2 value differentiates most molariform positions belonging to *Dryolestes* (with positive PC2 values) from those belonging to *Laolestes* (with negative PC2 values), and is highly correlated with the sequential positioning of molar positions within the tooth row of *Docodon*. From PC2 scores near 0,

consecutively more distal molar positions of *Dryolestes* generally have more positive values, while consectutive molars of *Laolestes* generally have more negative positions. The ultimate molar of *Laolestes* (m8) is an exception, and has PC2 values well within the range of *Dryolestes*. This is likely influenced by the "ultimate molar effect" on tooth shape seen in the m8 of *Laolestes*, making its shape relatively abberant with respect to the preceding molar positions. This is also supported by the extremely negative values taken by the m8 of *Laolestes* in PC3 (Fig. 7B).

These results clearly display the effectiveness of the SPHARM protocols described above for the registration of intra-tooth-row and interspecific differences between molariform surfaces. The result that the majority of sample variance is reasonably aligned with the axis separating the PC scores of *Docodon* and dryolestids suggests that the methods used here have the capability of discriminating species-level differences in crown shape irrespective of positional differences in the representative molar elements sampled. Additionally, at least in the case of *Docodon*, the variation caused by the necessarily artificial closure of tooth surfaces required for use in the SPHARM method does not seem to disrupt the natural morphological gradient apparent in the corresponding PC2 scores of *Docodon*. This preliminary analysis therefore positively recommends the preceding SPHARM protocols for use in wider interspecific (i.e. macroevolutionary) samples of molariform shape variation, and demonstrates the unique effectiveness of spherical harmonic registration compared to alternative morphometric approaches for the quantitative analysis of dental morphology. For instance, it would be difficult to design a classical morphometric or landmark/semilandmark-based registration protocol capable of producing results comparable to those presented in Figure 7, using shape data as disparate as the molar morphology of *Docodon* and *Laolestes*.

With the full (N=29) taxon sample of representative lower left molariform surfaces, using *Tinodon* as the alignment target specimen, the SPHARM registration protocol also produces a fairly steep scree-plot of the principal components of molariform shape variation. Under this registration, the first five PCs of shape variation explain 26.2%, 20.2%, 16.3%, 7.0% and 6.3% of total shape variance, respectively (see Supplementary Data Table 1S). Additionally, as can be seen in Figure 8A, the grand sample-average shape resulting from this registration corresponds to a molariform tooth with vaguely triangulated principal cuspids and some development of a talonid or distal cingulid. This is likely an artifact caused by the unavoidable relative over-abundace of OTUs from the "middle section" of Mesozoic mammalian phylogeny, which tend to have more symmetrodont and generalized tribosphenic molariforms, relative to the under-sampled earliest mammaliaformes, which tend to have a linear "triconodont" arrangement of primary cusps. It should be emphasized that the average shape does not correspond with any sampled or known mammalian taxon, and therefore "average" in terms of shape does not correspond to "primitive" or any other actual biological quality. As can be seen in the scatter-plots for PC scores 1-3 (Fig. 8B,C) most sampled OTUs plot some distance away from the origin of the graph and therefore no individual or group could be regarded as having an "average" molariform shape. Because of the sharp drop in explained variance per component after the first three, only three PCs shown in Figure 8B,C; however PCs 4 and 5 are also used for subsequent shape analysis (Fig. 1S). Because of the significant imaginary component to the PC scores for PC1 and PC5, the real and imaginary components of these PCs were rotated to align along a single axis using a separate covariance-matrix PCA, and the resulting rotated PC scores were used for subsequent analysis (similar to PC2 in Fig. 7A). Additionally, while the average specimen produced by this SPHARM registration is fairly unrealistic, these first three shape specifiers

are interpretable using terms commonly used to describe the natural variation in dental anatomy.

For instance, as can be seen in Figure 8B, PC1 can be regarded as an indicator of the relative elongation and linearity of the molariform crown. Highly positive OTUs on this axis are the spalacothere *Spalacolestes* and several dryolestoid taxa, all of which have tightly trangularized lower molars. Conversely, the stereotypically "triconodont" taxa *Trioracodon*, *Morganucodon*, and *Gobiconodon* all have highly negative scores for PC1. Possibly because of the necessary elongation of the molar crown caused by the presence of a highly developed talonid, all "tribosphenic" taxa, except for the two ausktribosphenid taxa (*Ausktribosphenos* and *Bishops*), take negative values along PC1 even though these forms also show highly triangulated principal cusps. Therefore, despite prior categorizations of molariform shape emphasizing the relative triangulation of principal cuspulids, the single most important specifier of molariform shape in this sample is mostly influenced by the relative length to width of the crown surface, with negative values having a greater relative length and positive values having labiolingually widened crowns, either because of tight triangualtion and/or the presence of labial projections (such as the exodaenodont lobes seen in *Reigitherium*, *Peligrotherium* and the ausktribosphenids).

The second principal component axis (Fig. 8C) is generally associated with the height versus width ratio of the crown surface. Surfaces corresponding to highly positive scores on this axis are relatively thin, have high relief, and have longer crests compared to OTUs with lower scores. It is tempting to assert that PC2 also corresponds to molars with sharper shearing surfaces (Evans and Sanson, 2014), but the inability of the SPHARM method to reliably register sharper (high-frequency) components of molar shape makes the correlation of PC2 with molar sharpness only speculative. However, it is apparent that many of the

sampled OTUs with hypothesized insectivorous/carnivorous feeding strategies (*Gobiconodon*, *Deltatheridium*; Kielan-Jaworowska et al., 2004) score highly on PC2. At the extreme negative end of the PC2 axis are the monotremes *Obdurodon* and *Steropodon* and the highly derived meridiolestidan taxa *Peligrotherium* and *Reigitherium* (considered to be sister taxa in Paez-Arango, 2008; Harper et al., 2018). These lower molars in these taxa are very low-crowned, rectangular, and have reduced/absent paraconids. These derived features, combined with the relatively young age for all taxa with the lowest PC2 values, suggest that PC2 may also correlate with degree of omnivory/herbivory generally. While there is no systematic error involved with the registration of bunodont crown shapes using the SPHARM method, the hypothesized correlation with herbivory can not be supported due the lack of relevant dietary information in these extinct forms.

The third principal component is more difficult to interpret. On one hand, all "tribosphenic" OTUs in this sample have negative scores on this axis, and the eigenmode corresponding to negative two standard deviations along this axis closely resembles a "typical" tribosphenic molar (Fig. 8A). On the other hand, there seems to be no obvious anatomical features uniting OTUs with positive scores along this axis, and the close proximity of the "pre-tribosphenic" taxon *Vincelestes* with the "triconodont" taxa *Gobiconodon* and *Morganucodon* is particularly confusing. The eigenmode corresponding to positive two standard deviations along this axis appears to be vaguely triconodont but does not resemble an actual molariform surface, as seen in the sampled taxa or otherwise. A conservative description of the shape variation captured by PC3 would be that this axis loosely quantifies the relative inflation of the three primary cuspids compared to surrounding accessory structures within the crown surface, such as the distal talonid. As such, surfaces with high positive scores on PC3 have principal cuspids (especially the protoconid and metaconid, or

their homologs in triconodont taxa) wider relative to peripherial structures on the tooth crown, while highly negative PC3 scores are associated with crowns with closely compressed principal cuspids which are much higher and labiolingually thinner than surrounding accessory structures.

PCs 4 and 5 are even more difficult to interpret, and only account for a small percentage of total shape variation in the sample (7% and 6%, respectively). These axes seem to be related to the sculpturing of larger features on the crown surface, but no general statements can be made about the morphology of taxa within certain ranges of these PC scores.

Having a combined ~75% of total shape variance described by the first five principal components of the 18-degree SHARM coefficients is obviously not an ideal situation for the concise representation of all significant shape variation using as few specifiers as possible. While the eigenmode surfaces corresponding to PCs 1-3 (Fig. 8B,C) demonstrate that the kinds of shapes reproducible within this subspace are representative of the major contours and broad outlines of the "triconodont," "symmetrodont," and "tribosphenic" molariform types sampled for this analysis, it is also apparent that most of the occlusally significant shape variation at the apices cuspids and cingulids is not well reconstructed. This is also apparent from Figure 3 which contrasts the parametric surfaces generated from the full set of 18-degree SPHARM coefficients, with their reconstruction using only their first five PC scores. Anatomical features which are particularly poorly reconstructed using these PCs include: 1) the lengths and shapes of the apices of principal cuspids, especially the paraconid; 2) the presence and extent of labial cingulids, exodaenodont lobes, or labial accessory culpulids; and 3) the height and salience of distal cuspids, such as the hypoconulid, hypoconid and entoconid or their homologs. These features are obviously significant

contributors to most of the functionally relevant aspects of dental topography (i.e. Shearing Quotient, Relief Index, Orientation Patch Count, Dirichlet Normal Energy, etc.; Evans, 2013), and their absence, or unrealistic reconstruction, using only the first five PCs of shape variation makes feeding inferences using high-level dental characteristics in this sample entirely intractable. It is unclear if the incorporation of a greater proportion of total variance, using higher degree spherical harmonic coefficients, would produce accurate (or at least consistently offset) reconstructions of these dental topography metrics; the considerable computational resources required to examine this are not available for the present analysis.

FIGURE 7. Scatterplot showing PC scores of intra-and-inter specific lower molar shape variation from lower jaw specimens of *Dryolestes priscus* (Dr), *Laolestes eminens* (La) and *Docodon victor* (Do). Shaded triangles represent PC scores for three replicated measurements of same tooth; numbers next to taxon label represent molar position. **A**, scatterplot showing real component of PC1 on x-axis versus rotated PC2 score on y-axis. **B**, scatterplot showing real component of PC1 on x-axis versus real component of PC3 on y-axis. Occlusal view surfaces corresponding to positive/negative two standard deviations along each axis are shown along margins of each scatterplot.

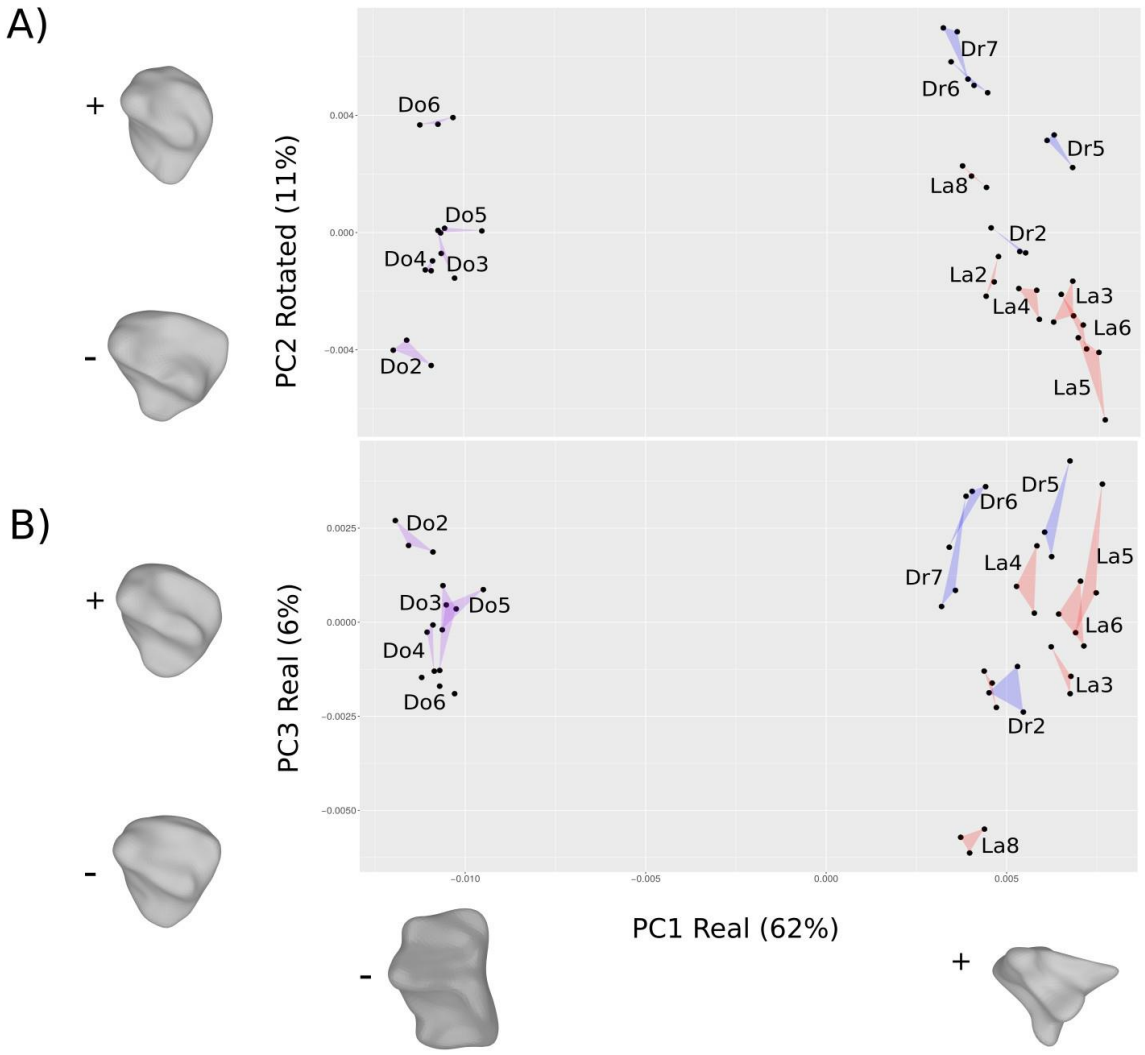

FIGURE 8. Principal axes of molariform variation in the 29 taxa shown in Fig. 3. **A**, eigenmode surfaces for representing shapes positive and negative two standard deviation units along PC axes 1-3, all surfaces shown in oblique labial view, surface shown in center represents sample average molariform shape; **B**, scatterplot of PC1 vs PCs; **C**, scatterplot of PC1 vs 3. Abbreviations of taxon names are shown next to corresponding point values.

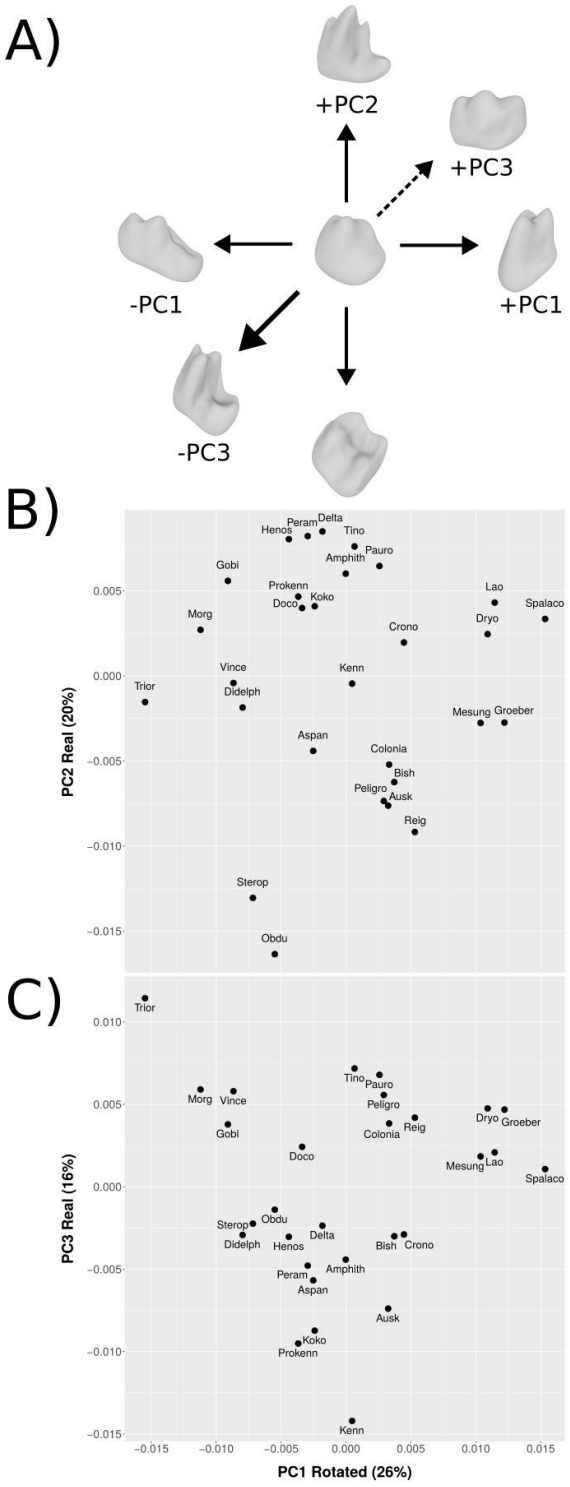

Comparative Results

Relative support for several macroevolutionary scenarios (models) of lower molariform shape change (as represented by the first five PCs of shape variation described above) were estimated using methods outlined in Clavel et al. (2015) for the R package mvMORPH, and the constrained Bayesian summary tree presented in previous sections (Tables 2,3). The input phylogeny used for this analysis was processed to drop all unsampled OTUs and to reformat it as a "SIMMAP-like" object using functions provided by the R packages "ape" and "phytools" (Paradis et al., 2004; Revel, 2012). Because of the small absolute values taken by the PC scores generated by SPHARM analysis, all PC scores were multiplied by 10,000 to avoid floating point errors and make matrix operations more tractable for the mvMORPH optimizer; all resulting variance-covariance estimates for these analyses (Tables 4,5) are reported for units of 10,000 times the original PC score, but estimated ancestral PC scores produced by these models were divided by 10,000 before their subsequent use. All considered macroevolutionary scenarios were evaluated using the mvBM function in mvMORPH, set to use the "pseudoinverse" method for likelihood calculation, and a maximum of 1,000,000 optimization iterations.

Evolutionary scenarios of a shift in evolutionary mode were implemented using the "BMM" family of macroevolutionary models. Points in mammalian phylogeny representing a switch between BM processes were modeled for the interior nodes defining the common ancestor of the clades Tribosphenida (Boreosphenida), Zatheria, Cladotheria, Trechnotheria, and Theriimorpha, respectively (because of the presence of only two sampled OTUs outside of crown Mammalia, a shift in BM process could not be modeled for this node). A group of skeptical "null-model" evolutionary scenarios were also tested in which a single BM process was imposed over the entire phylogeny (the "BM1" family of models), with three levels of

constraints imposed on the corresponding evolutionary variance-covariance matrix (Polly, 2004). These models assumed a completely unconstrained variance-covariance matrix (BM1), a complete lack of evolutionary covariance but separate variances between PCs (BM1-Diagonal), and no-covariances and one single variance parameter for all PCs (BM1-EqualDiagonal), respectively.

When these models are compared using the Akaike Information Criterion (AIC; as calculated using the aicw function provided in mvMORPH) it is apparent that the most likely scenario for the trait evolution of the principal components of lower molariform shape corresponds to a switch in multivariate BM process at the node corresponding to the clade Theriimorpha (Table 2). This BMM-Theriimorpha model receives over one-third of the Akaike weight among the models considered, followed by the similar BMM-Zatheria model and the simplified BM1-EqualDiagonal model. Macroevolutionary scenarios modeling shifts in BM process at other interior nodes have even less support than the skeptical "null-model" BM1-EqualDiagonal scenario, and are not considered to have sufficient support for further interpretation. However, it should also be noted that the amount of absolute difference in AIC value between the "top-three" tested models are within 2 units, indicative of only "weak" support for the most likely BMM-Theriimorpha (e.g., see Raftery, 1999). Additionally, when these models are compared using the AIC metric corrected for small sample sizes (AICc; Cavanaugh, 1997; Table 3), which penalizes additional parameters more heavily compared to the traditional AIC value, the relative support for the BMM-Theriimorpha model drops below that seen for all of the skeptical BM1 models (Table 3). While this makes support for the BMM-Theriimorpha model ambiguous, this model is used as the most realistic scenario of multivariate trait evolution for all subsequent interpretation and ancestral character state reconstructions because of the unrealistically constrained

covariance assumptions involved with the skeptical BM1 family of models (Tables 4,5). Ancestral character state estimates for PCs 1–5 were generated using the BMM-Theriimorpha model estimates as input for the "estim" trait estimation function in mvMORPH (Figs 9–13).

TABLE 2. Ranking and relative weights for macroevolutionary models evaluated using AIC value.

	AIC	Difference	Relative Weight	AIC weight
BMM-Theriimorpha	1564	0	1	0.36200
BMM-Zatheria	1565	0.74	0.6907	0.25005
BM1-EqualDiagonal	1565	1.61	0.4478	0.16209
BMM-Tribosphenida	1566	2.04	0.3599	0.13027
BM1-Diagonal	1568	3.88	0.1435	0.05194
BMM-Trechnotheria	1568	4.56	0.1021	0.03696
BM1	1573	8.69	0.0130	0.00470
BMM-Cladotheria	1574	10.41	0.0055	0.00199

TABLE 3. Ranking and relative weights for macroevolutionary models evaluated using corrected-AIC value (AICc).

	AIC	Difference	Relative Weight	AIC Weight
BM1-EqualDiagonal	1566	0	1	0.839
BM1-Diagonal	1569	3.31	0.191	0.16
BM1	1579	13.25	0.00133	0.00111
BMM-Theriimorpha	1587	20.90	0.0000289	0.0000242
BMM-Zatheria	1588	21.64	0.00002	0.0000167
BMM-Tribosphenida	1589	22.95	0.0000104	0.00000872
BMM-Trechnotheria	1591	25.47	0.00000295	0.00000247
BMM-Cladotheria	1597	31.31	0.000000159	0.000000133

TABLE 4. Estimated BM variance-covariance matrices for non-theriimorphan taxa, corresponding to the BMM-Theriimorpha model (estimates correspond to input values of 10,000 times PC score).

	PC1 rotated	PC2 real	PC3 real	PC4 real	PC5 rotated
PC1 rotated	66.62614	11.679797	-29.005298	-32.491639	18.091951
PC2 real	11.67980	79.832859	-7.156907	-4.469631	-2.227187
PC3 real	-29.00530	-7.156907	54.224741	-16.532794	-7.452602
PC4 real	-32.49164	-4.469631	-16.532794	70.219023	-7.033498
PC5 rotated	18.09195	-2.227187	-7.452602	-7.033498	7.189630

TABLE 5. Estimated BM variance-covariance matrices for the clade Theriimorpha, corresponding to the BMM-Theriimorpha model (estimates correspond to input values of 10,000 times PC score).

	PC1 rotated	PC2 real	PC3 real	PC4 real	PC5 rotated
PC1 rotated	134.167613	11.12943	-17.430603	9.090009	-14.077228
PC2 real	11.129433	46.47016	-27.461241	-4.053030	29.843391
PC3 real	-17.430603	-27.46124	99.903017	25.104051	3.517686
PC4 real	9.090009	-4.05303	25.104051	78.835773	32.092535
PC5 rotated	-14.077228	29.84339	3.517686	32.092535	75.523581

As can be seen in Figures 9-13, the reconstructions for consecutively nested nodes at the root of Mammaliaformes and among stem therians are extremely similar. As reconstructed, the range of molariform shapes seen especially in the earliest therians could conceivably be encompassed within the range of variation in molariform shape seen within a typical extant therian genus. This may reflect the fact that the diversity of molariform shape is an unrepresentative proxy of the deep phylogenetic divisions between early therian taxa included in this analysis; and that, within the Cretaceous at least, molariform diversity is not a reliable indicator of standing or future biodiversity (also see Polly et al., 2005). An analogous situation in modern eutherians can be seen among stereotypically "insectivoran" mammals such as the eulipotyphlans and tenrecoids, whose deep phylogenetic divisions were traditionally unappreciated based solely on dental (and other morphological) characterizations (Rose, 2006; also see Price et al., 2011). A more likely explanation for the similarity among these early therian ancestral reconstructions is the inability of the first five SPHARM PCs to accommodate the most evolutionarily labile and quickly changing aspects of lower molariform shape.

These ancestral morphological reconstructions are also broadly consistent with the qualitative ancestral reconstructions generated from the Bayesian summary phylogeny described above (see Fig. 2S), and the discrete lower molariform data available in the Rougier et al. (2012) character matrix (as analyzed by the "apolist" command in PAUP; Swofford, 2003). The following paragraphs provide comparisons between the qualitative ancestral character-state predictions based on unambiguous parsimony-based reconstructions, with the ancestral tooth shapes estimated using the first five PC scores of the sampled SPHARM coefficients (using the "estim" function of mvMORPH; Figs. 9−13). However, it should be reiterated that, because of the inability of SPHARM coefficients to precisely reconstruct

sharp or localized features, the presence/absence of minute cuspulids and basal cingulids (i.e. characters 70 – 74, and 144 in Rougier et al., 2012) are not reliably reconstructed in ancestral SPHARM surfaces across the whole phylogeny. This causes a particular problem for the reconstruction of the deepest (most rootward) nodes in the phylogeny of the 29 included taxa, especially the nodes representing the common ancestors of Mammalia and Mammaliaformes (Fig. 9).

The reconstruction of the aultralosphenidan common ancestor (Fig. 10) by both methods is also weakly congruent. Only one of the three unambiguously reconstructed character states predicted for this node (Character 61, Posterior cusp c is more than 40% of cusp a) can be seen in the estimated SPHARM surface for this node. The two other parsimony unambiguous reconstructed character-states for this node (Character 86: Rear portion of molariform rimmed with three major cusps, and Character 87: Hypoconulid elevated above the cingulid level) are not visible in this ancestral surface, most likely because of the poor ability of the SPHARM method to reconstruct small localized features generally.

The common monotreme ancestor (node uniting *Steropodon* and *Obdurodon*; Fig. 10) has three of its five unambiguous character-state reconstructions visible in its SPHARM ancestral surface. These reconstructed character-states are: Character 86 rear portion of molariform presenta as a transverse V-shaped basin with two major cusps; Character 120 metacristid oriented transverse. Additionally, Character 75 (Postcingulid present, horizontal above the gum level) can be reasonably reconstructed even though the presence/absence of cingulids is not usually reliably determinable in these SPHARM results. Both Character 74 (relating to the cingulid shelf) and Character 84 (Hypoflexid very deep, >60% of the talonid width) can not be reconstructed from the SPHARM surface for this node.

The unambiguously reconstructed apomorphies of the "eutriconodont" common ancestor (node uniting *Gobiconodon* and *Trioracodon*; Fig. 9) are not well reconstructed by the corresponding SPHARM ancestral surface, with only one out of three reconstructed character-states visible. The two unreconstructed character-states (Characters 73, and 74) relate to presence/absence of lower molariform cingulids. Character 120 (Metacristid parallel to lower jaw axis) is reasonably visible in the SPHARM ancestral surface (despite the absence of a corresponding lower jaw).

The cladotherian common ancestor (Fig. 11) is also not well reconstructed for the same reasons, with four out of five unambiguous character-states (Characters 70-74) corresponding to the absence of cuspulids and cingulids which can not be confirmed in the corresponding ancestral SPHARM surface. Character 62 (Cusp c taller than b) can be seen in the ancestral SPHARM surface, however.

The node representing the common ancestor of amphitheriids and crown therians (Fig. 11) has three of its six unambiguously apomorphic character-states visible in its corresponding SPHARM ancestral surface. These characters are related to the expansion of the talonid region of lower molariforms (Character 64, Cristid obliqua present; Character 87, Hypoconulid elevated above the cingulid level; and Character 94, Hypoconulid/protoconid height ratio between 25% and 35%). Conversely, the three character-states that can not be seen in the SPHARM ancestral surface are related to the presence of smaller cuspids (Characters 72 and 88) and the extent of the hypoflexid (Character 84). Additionally, the one unambiguous character state for the zatherian common ancestor (Character 107, m1 oblong with strong labial bulge; Fig. 13) can not be definitively identified in its corresponding SPHARM ancestral surface; and only one of the two unambiguous character states for the common ancestor of *Vincelestes* + Theria (Fig. 13) can be seen in its SPHARM surface

(Character 83, talonid wide), however it is not clear if the other corresponding character state (Character 85, talonid basin present) can be applied to this surface.

The crown therian common ancestor (Fig. 13) has two of its three unambiguously reconstructed character-states reflected in its corresponding SPHARM ancestral surface. These character-states are related to the talonid region of the lower molar (Character 66, Pre-entoconid cristid of talonid in alignment with the metaconid; and Character 86, rear portion of molariform rimmed with three major cusps). As is the character-state which is not reflected in the SPHARM model (Character 90, Entoconid present but far from hypoconulid, at least equal to one cusp length); however, this is likely because of the poor ability of SPHARM surfaces to reconstruct the position and height of cuspids in general. All ancestral nodes nested within Theria show very poor agreement between parsimony ancestral reconstructions and estimated ancestral SPHARM surfaces.

The large clade Dryolestoidea (Fig. 11) has only one of its three unambiguously reconstructed character-states poorly reflected in its corresponding SPHARM ancestral surface. However, this character (Character 120, Metacristid oriented transverse) is difficult to confirm because of the lack of shape information related to the relative placement of the surrounding dentary bone. The two character states that are not reflected in the SPHARM surface (Character 76, Interlocking mechanism between two adjacent lower molars absent; and Character 123, Distal metacristid absent) are related to the absence of localized features on the crown surface which are not well-reconstructed by the SPHARM method. The node representing the common ancestor of *Dryolestes* and the meridiolestidans (Fig. 12) has one of its two unambiguous character-states visible in its corresponding ancestral SPHARM surface (Character 111, Buccal side of crown much taller than lingual side). The other unambiguous

character-state (Character 144) is related to the presence of lower molariform cingulids, and is not visible in the corresponding SPHARM surface.

The South American dryolestoid clade Meridiolestida (here including *Cronopio* and the mesungulatoids; Fig. 13) has both of its unambiguously reconstructed character-states reflected in its corresponding SPHARM ancestral surface. These characters (Character 81, Procumbent paraconid absent; and Character 82, Paraconid and metaconid bases approaching each other becoming confluent) are related to the configuration of the major trigonid cuspids. The meridiolestidan subclade Mesungulatoidea (here including *Mesungulatum* + *Colonitatherium* + *Reigitherium* + *Peligrotherium*; Fig. 13) has only two of its six unambiguously reconstructed character-states reflected in its corresponding SPHARM surface. These characters (Character 107, outline of m1 rectangular or slightly rhomboidal; and Character 108, Crown length/width subequal) are related to the general shape and outline of the lower molars. Conversely, three of the character-states which are not reflected in the mesungulatoid SPHARM surface (characters 71, 73, and 75) are related to the presence and extent of cingulids and cuspids which are not well reconstructed by SPHARM. The fourth unreconstructed character-state (Character 120, Metacristid oblique) is also not reconstructed with enough definition in the corresponding SPHARM surface. All other nodes in the summary phylogeny lack an association between unambiguously reconstructed character-states and their corresponding ancestral SPHARM surface.

While ambiguous, the quality of ancestral reconstructions provided by these SPHARM surfaces is more than adequate to categorize lower molariform shape into traditional "morphotypes" as signified by the common specifiers "triconodont", "symmetrodont' or "tribosphenic" (Osborn, 1888, 1907). These specifiers refer to the relative conformation of cusp apices within a crown's surface; specifically whether the three

primary cusps present in most mammaliaforms ("cusp a" or protoconid, "b" or paraconid, "cusp c" or metaconid) are in a linear relationship, a triangular relationship, or a triangular relationship with a distal appendix termed a talonid (Fig. 14). Further, the relative length and shape of the talonid as a trenchant (linear) or basined structure is also apparent using by these methods. As such, the point estimates for PC scores pertaining to the internal nodes in the phylogeny presented here (Figs. 9–13) can be seen as indicators of the qualitative properties of the lower molariform dentition seen in ancestral mammalian taxa (Fig. 14). However, the fact that the coefficient of variation values corresponding to these point estimates are large, (i.e. standard error values are near the magnitude of reconstructed PC score; see Supplementary Information Table 2S) implies that these reconstructions should only be considered as very approximate.

FIGURE 9. Reconstructed ancestral surfaces at root of phylogeny using BMM-Theriimorpha model. For this and following figures interior nodes show ancestral SPHARM reconstructions using PCs 1-5. Tips show original 18 degree SPHARM surfaces.

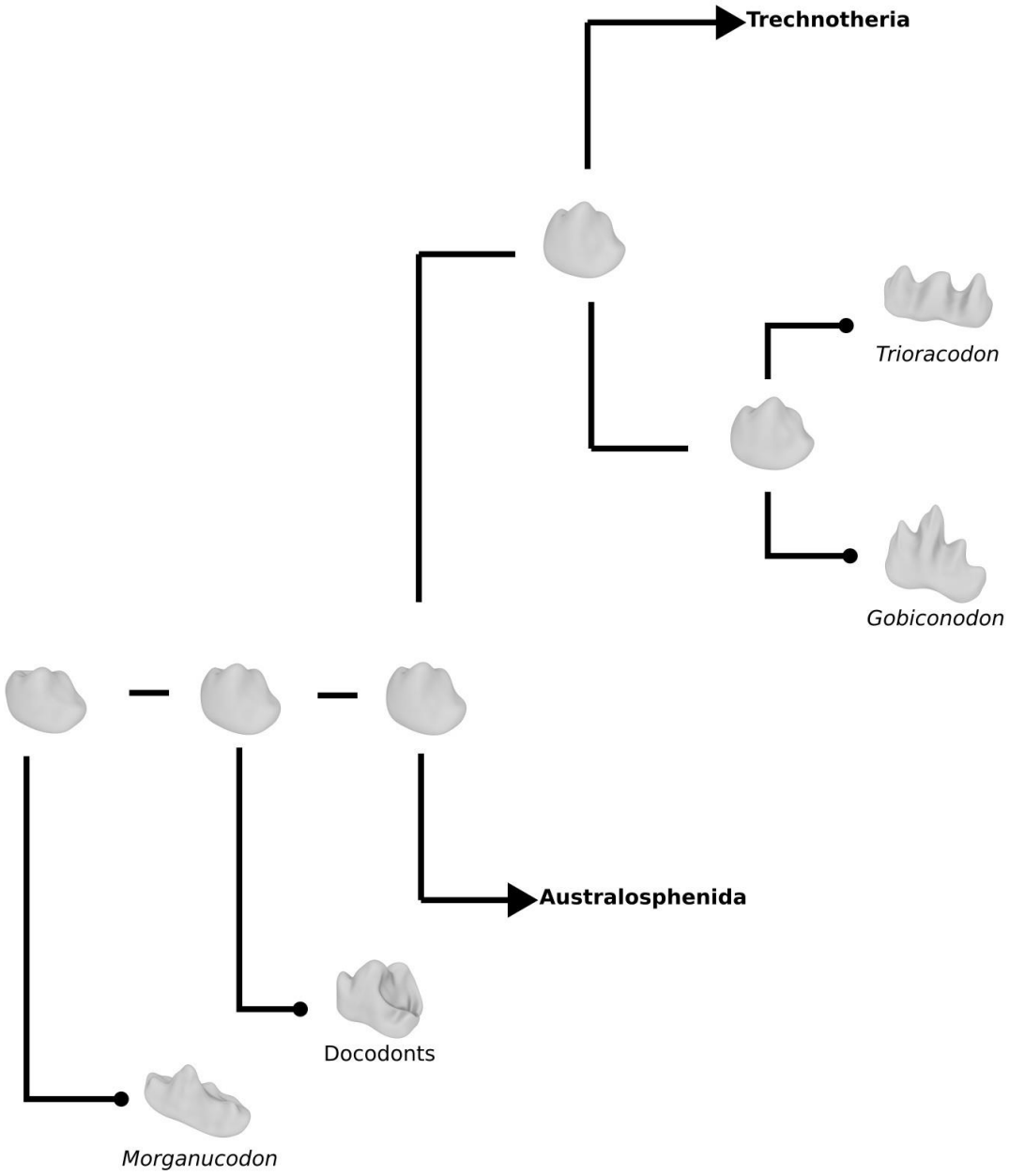

FIGURE 10. Reconstructed ancestral surfaces for clade Australosphenida using BMM-Theriimorpha model.

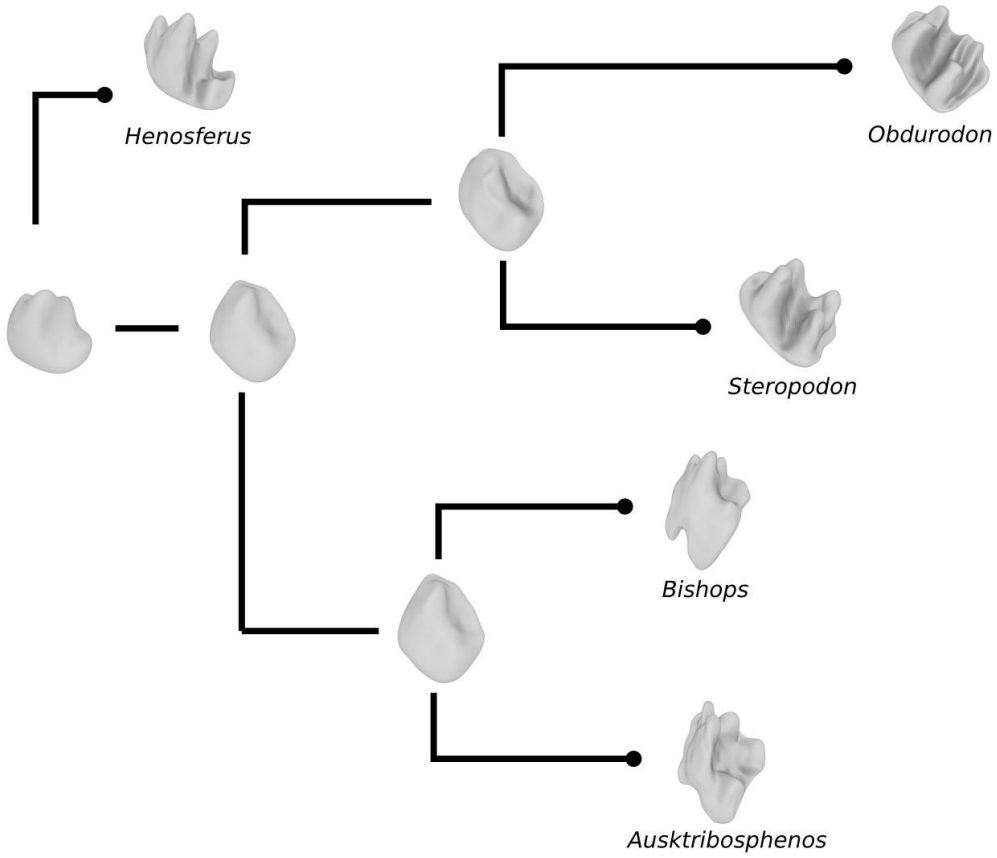

FIGURE 11. Reconstructed ancestral surfaces for clade Trechnotheria using BMM-Theriimorpha model.

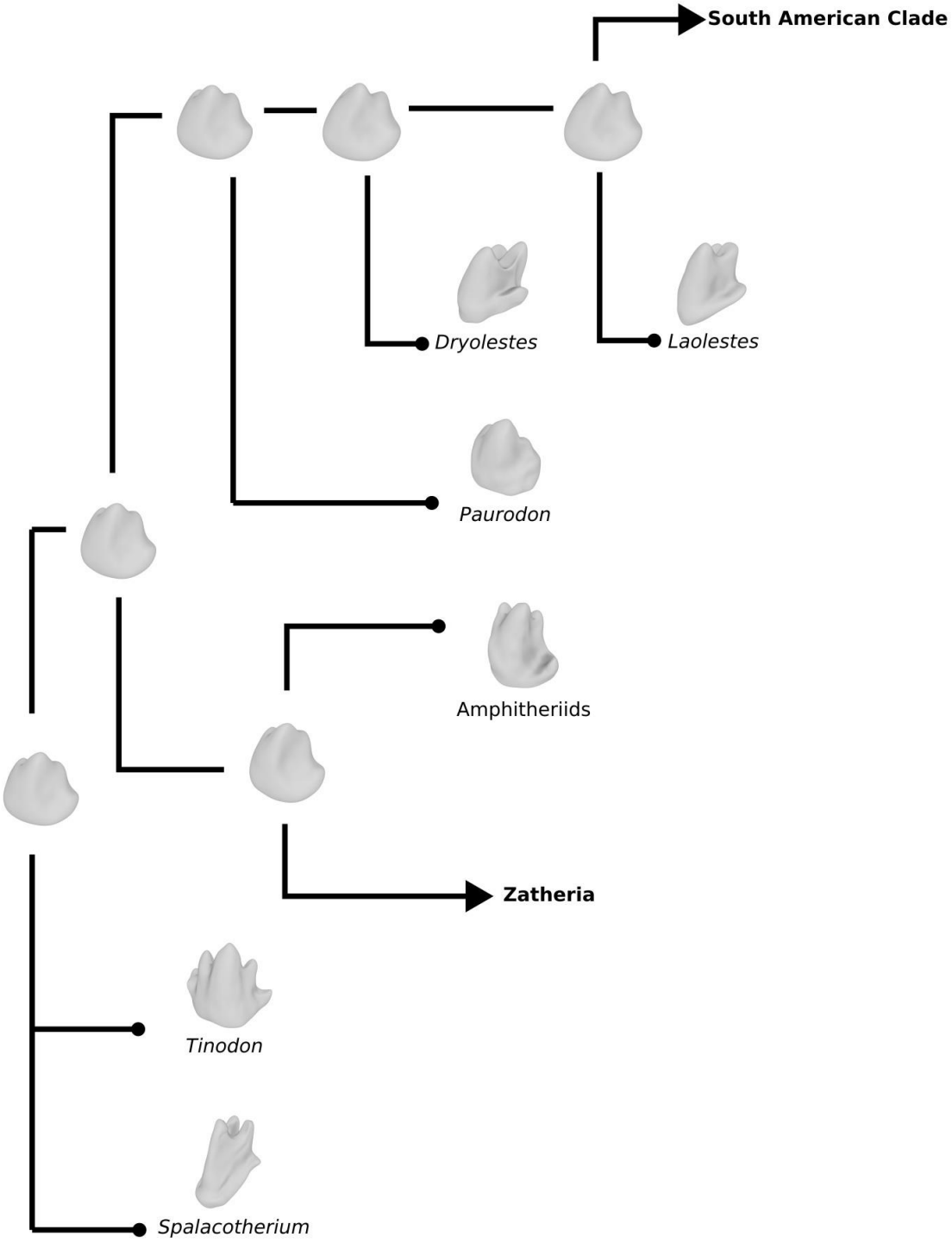

FIGURE 12. Reconstructed ancestral surfaces for South American endemic Dryolestoids using BMM-Theriimorpha model.

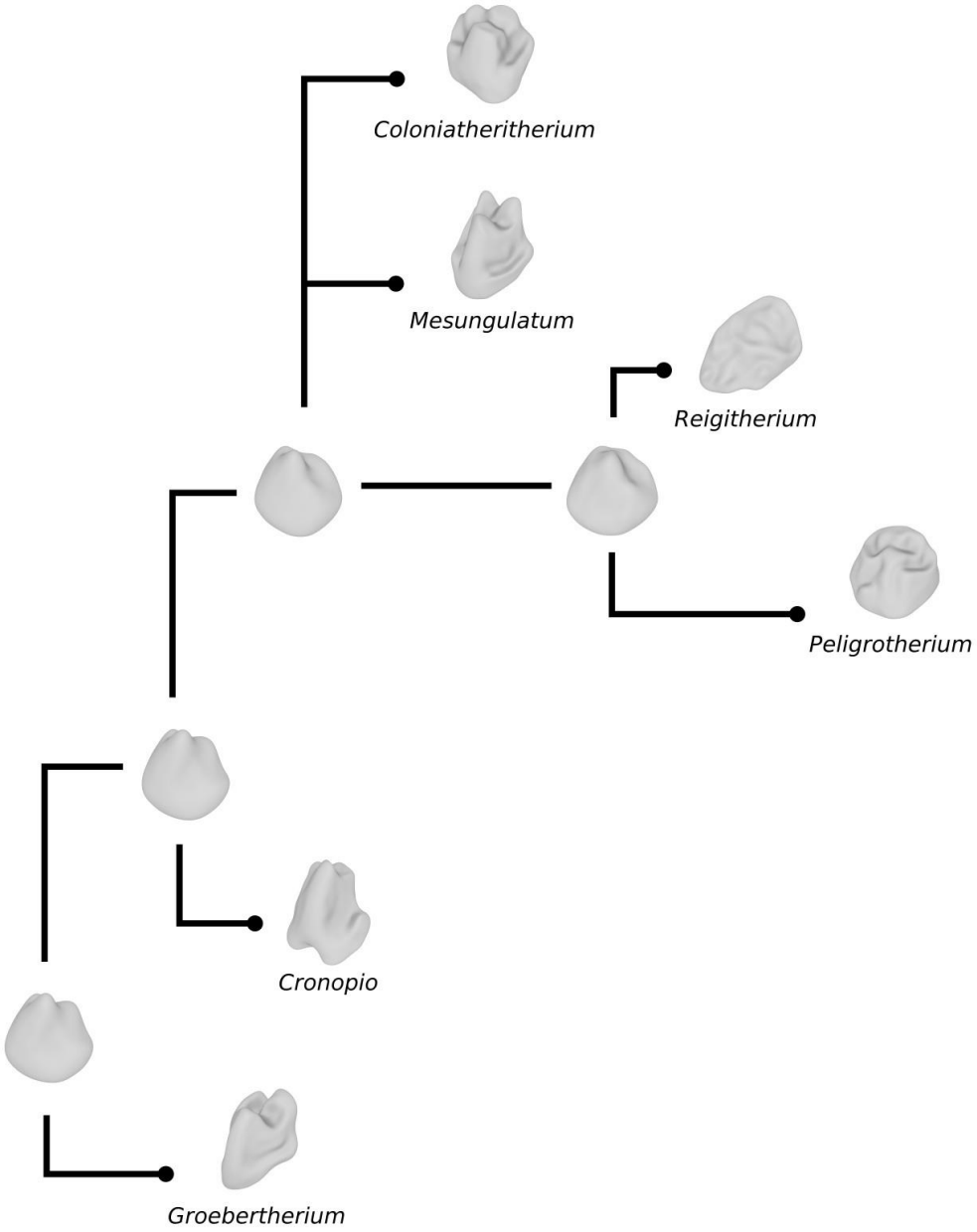

FIGURE 13. Reconstructed ancestral surfaces for clade Zatheria using BMM-Theriimorpha model.

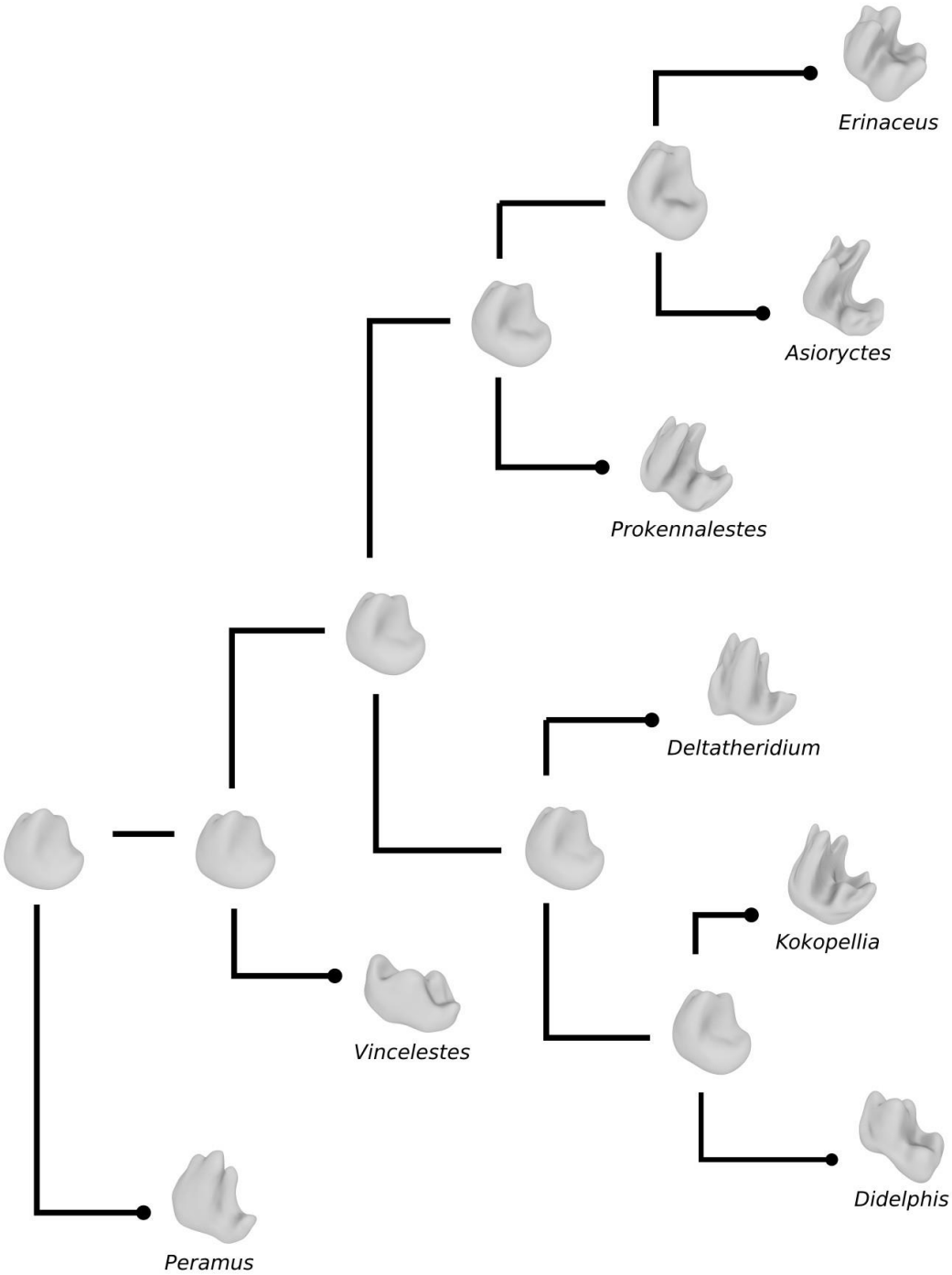

FIGURE 14. Reconstructed ancestral surfaces in lingual view for major mammaliaform clades, using BMM-Theriimorpha model.

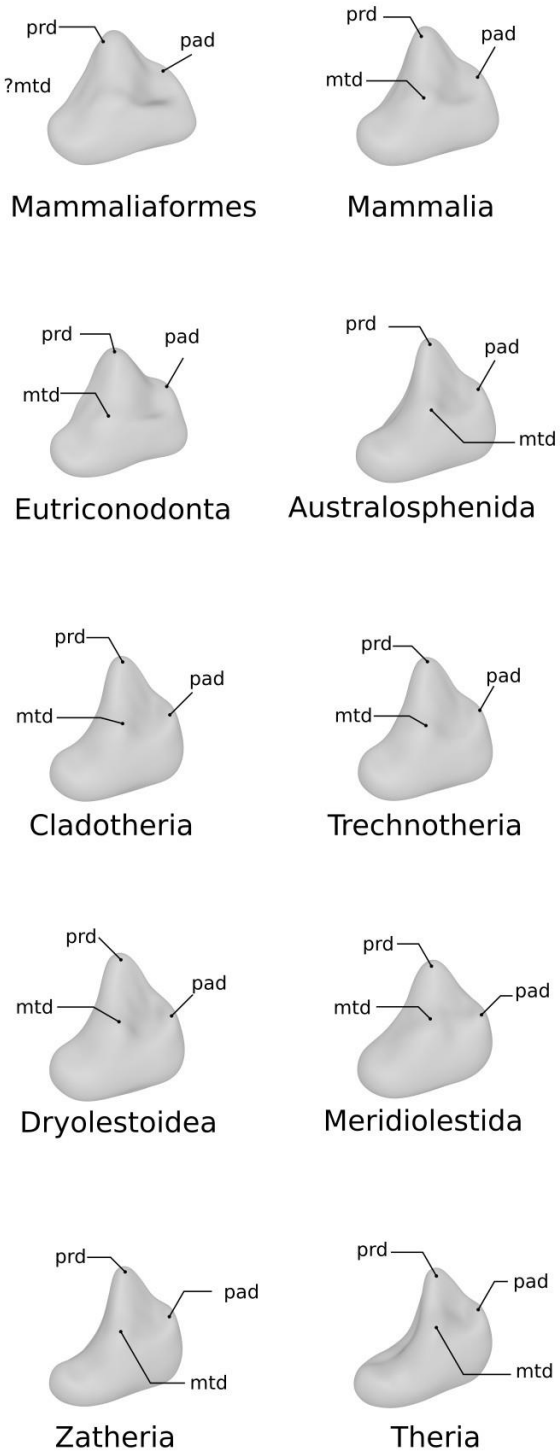

DISCUSSION

This report presents the first analytical attempt to quantify and temporally calibrate estimates of molariform shape across the entire clade Mammaliaformes. As such, much of the morphological information measured and compiled for this report should be seen only as another step towards the type of macroevolutionary studies required for a complete and unbiased understanding of molariform shape evolution (see also Polly, 2004; Wood et al., 2007). The relatively unresolved phylogenetic results (as seen in the parsimony analysis, Fig 4) and ambiguously supported macroevolutionary models (as seen in Tables 2,3) suggest that definitive conclusions regarding the tempo and mode of lower molariform shape change can not be made solely from these data.

Probably the most surprising result of this analysis is lack of direct support for a shift in evolutionary mode within Tribosphenida, the clade containing all living toothed mammals. The wide literature on the function and feeding implications of the tribosphenic molar (Crompton and Sita-Lumsden, 1970; Crompton, 1971; Lucas, 2004; Davis, 2011) has cultivated an assumption that the evolutionary trajectory of tribosphenic shape change should be qualitatively different than that seen in earlier forms. This makes intuitive sense, given the likely shape constraints on tribosphenic lower molars caused by their functional requirements to accommodate an opposing upper protocone (Polly et al., 2005); however, the likely convergent acquisitions of the "tribosphenic" condition (as in australosphenidans), and "pseudotribosphenic" condition (in docodont and shuotheriid groups not analyzed here; Luo, 2007) suggest that the evolutionary process of shape change between these categories may be more gradual and continuous than originally appreciated. The best supported of the macroevolutionary scenarios tested above also suggest a lack of punctuational change in

evolutionary mode beginning with Tribosphenida (Tables 2,3). This is either because the best supported model of lower molariform shape change (according to AIC value) suggests an evolutionary punctuation at a deeper and more inclusive node in mammaliaform phylogeny (Theriimorpha), or because the best supported model (according to corrected AIC value) posits a single evolutionary process for the whole of the clade Mammaliaformes. Therefore, under either result, the attainment of the "fully tribosphenic" character state by the clade Tribosphenida can be considered similar to the attainment of the character state of a "fully coiled" cochlear canal – usefully preservable and diagnostic features but not indicative of a major change in evolutionary process relative to taxa with preceding states of this character.

The addition of the 14 additional inner ear characters to the character matrix used by Rougier et al. (2011, 2012) and O'Meara and Thompson, (2014), also does not seem to have added any resolving power to the phylogenetic estimates presented above (see MP phylogeny; Fig. 4). This is perhaps unsurprising given the above mentioned known homoplasy in this character complex (Luo et al., 2016), and the incomplete character scoring of these characters in most fossil taxa. This does not vitiate the value of these characters for the estimation of evolutionary rate parameters within likelihood-based estimation, and these characters are likely to be even more valuable when larger numbers of OTUs can be reliably scored. However; the constrained Bayesian phylogeny used for the comparative methods described above (Figs. 5,6) presents the best current time scaled representation of the consensus relationships for the included Mesozoic mammaliform taxa. In particular, our use of the Fossilized Birth-Death prior and the asymmetric Mk likelihood parameterization for binary characters with this character matrix allowed for a greater amount of temporal information and rate variation to be incorporated relative to the previous Bayesian analyses of this dataset in O'Meara and Thompson (2014). While this does not necessarily translate

into a significantly greater marginal likelihood for this more parameterized model relative to those estimated by O'Meara and Thompson (2014), the direct representation of fossil sampling rate, speciation rate, and extinction rate makes the constrained FBD phylogeny presented above particularly appropriate for subsequent use in macroevolutionary comparative methods.

Even though support is quite poor, the comparative results suggesting a switch in BM process within the clade Theriimorpha are interpretable given what is known from the fossil record of the included OTUs. For both non-theriimorphs and theriimorphs (Tables 4 and 5) PCs 1 and 2 show little macroevolutionary covariance, suggesting that the relative elongation of the molar crown is unaffected by the relative height of its principal cusps. However, within the theriimorphs the "temperature" (variance) of trait evolution increases for all PCs except PC2, reflecting the greater variety of crown shapes seen in this group, but more quadrate crown seen within the most derived non-theriimorphan molars (the monotremes). In particular, PC1 has less negative correlation with PC3 because many theriimorphans can have a highly triangulated trigonid without large talonid, unlike the included non-theriimorphs; although the inclusion of the "pseudotribosphenic" shuotheriids in future analyses may alter this result. Within theriimorphans PC2 has a stronger negative covariance with PC3, likely related to the taller, more apiculate crowns seen in the included northern tribosphenic taxa relative to the southern tribosphenic OTUs. In theriimorphs PC3 also has a positive instead of negative covariance with PC4.

The increased variation and altered covariation of lower molariform shape evolution in theriimorphans compared with non-theriimorphan taxa supports the recognition of this clade as an evolutionary radiation, in terms of molar morphology. Interestingly, from the vaguely triangular crown morphology estimated for the theriimorphan common ancestor by

the BMM process (Fig. 9) the descendant theriimorph lineages adopt tooth forms in all major categories (triconodont, symmetrodont, and tribosphenic; Fig. 14). If the major Mesozoic clades Multituberculata and Gondwanatheria are also correctly included in Theriimorpha (Rowe, 1993) then it is even more apparent that no single dental apomorphy can be credited with the success and diversity of this group. Other features, such as mediolateral separation of postdentary elements from the mandible, may therefore have facilitated the wider "diffusion" of molar morphologies throughout the morphological "wave-space" (Kielan-Jaworowska et al., 2004).

Whatever the causal drivers for this unique estimated mode of lower molar evolution within Theriimorpha, it is apparent that the recovered pattern and parameterizations of lower molariform shape evolution would not have been possible without recourse to the explicitly "physical" models of shape variation and transformation described above. It is hoped that this report will motivate future studies using spherical harmonic registration and thermodynamic models of trait alteration to better understand evolutionary processes in the light of the mammalian dentition.

ACKNOWLEDGMENTS

I would like to sincerly thank Mark McPeek (Dartmouth College) for making the the SPHARM package available, and his assistance with my application of it to the mammalian dentition. Additionally, I thank April Wright (Southeastern Louisiana University), and Gary Rosner and Robert Scharpf (both at Johns Hopkins Bloomberg School of Public Health), for generously lending their time and expertise with the Bayesian and computational aspects of this project.

This work was performed in part at the Duke University Shared Materials Instrumentation Facility (SMIF), a member of the North Carolina Research Triangle Nanotechnology Network (RTNN), which is supported by the National Science Foundation (Grant ECCS-1542015) as part of the National Nanotechnology Coordinated Infrastructure (NNCI).

LITERATURE CITED

Allin, E. F. Evolution of the mammalian middle ear. Journal of Morphology 147:403–437.

Archibald, J. D., and D. H. Deutschman. Quantitative analysis of the timing of the originand diversification of extant placental orders. Journal of Mammalian Evolution 8:107–124.

Archibald, J. D. 2011. Extinction and Radiation: How the Fall of the Dinosaurs Led to the Rise of Mammals. Johns Hopkins University Press, Baltimore, Maryland, 107 pp.

Atkinson, K., and W. Han. 2012. Spherical Harmonics and Approximations on the Unit Sphere: An Introduction. Springer, Berlin, 256 pp.

Averianov, A. O, T. Martin, and A. V. Lopatin. 2013. A new phylogeny for basal Trechnotheria and Cladotheria and affinities of South American endemic Late Cretaceous Mammals. Naturwissenschaften 100:311–326.

Bapst, D. W. 2014. Preparing paleontological datasets for phylogenetic comparative mehtods. pp. 515–544 in L. Z. Garamszegi (ed) Modern Phylogenetic Comparative Methods and Their Application in Evolutionary Biology: Concepts and Practice. Springer, Berlin.

Bell, M. A., and G. T. Lloyd. 2015. strap: an R package for plotting phylogenies against stratigraphy and asserting their stratigraphic congruence. Palaeontology 58:379–389.

Benoit, J., P. R. Manger, V. Fernandez, and B. S. Rubidge. 2017. The bony labyrinth of late Permain Biarmosuchia: palaeobiology and diversity of non-mammalian Theriapsida. Palaeontologia Africana 52:58–77.

Bouckaert R. R. 2010. DensiTree: making sense of sets of phylogenetic trees. Bioinformatics 26:1372–1373.

Cavanaugh, J. E. 1997. Unifying the derivations for the Akaike and corrected Akaike information citeria. Statistics and Probability Letters 30:201–208.

Chow, M., and T. H. V. Rich. 1982. *Shuotherium dongi*, n. gen. And sp., a therian with pseudo-tribosphenic molars from the Jurassic of Sichuan, China. Australian Mammalogy 5:127–142.

Clavel, J, G. Escarguel, and G. Merceron. 2015. mvMORPH: an R package for fitting multivariate evolutionary models to morphometric data. Methods in Ecology and Evolution 6:1311–1319.

Close, R. A., M. Friedman, G. T. Loyd, R. B. J. 2015. Benson. Evidence for a mid-Jurassic adaptive radation in mammals. Current Biology 25:2137–2142.

Cohen, K. M., S. C. Finney, P. L. Gibbard, J. and X. Fan. 2013. The ICS International Chronostratigraphic Chart 36:199–204.

Conith, A. W., M. J. Imburgia, A. J. Crosby, and E. R. Dumont. 2016. The functional significance of morphological changes in the dentitions of early mammals. Journal of the Royal Society Interface 13:1–7.

Crompton A. W., and A. Sita-Lumsden. 1970. Functional significance of the therian molar pattern. Nature 227:197–199.

Crompton, A. W. 1971. The origin of the tribosphenic molar. Zoological Journal of The Linnean Society 50:65–81.

Crompton, A.W. 1978. Molar structure and occlusion in Cretaceous therian mammals; pp. 249-287 in P. M. Butler, K. A. Joysey (eds.), Development, Function and Evolution of Teeth. Academic Press, London, U.K.

Crompton, A. W., and P. Parker. 1978. Evolution of the mammalian masticatory apparatus: the fossil record shows how mammals evolved both complex chewing mechanisms and an effective middle ear, two structures that distinguish them from reptiles. American Scientist 66:192–201.

Crompton, A. W., and Z. X. Luo. 1993. Relationships of the Liassic mammals *Sinoconodon*, *Morganucodon oehleri*, and *Dinnetherium;* pp. 30–44 in F. S. Szalay, M. J. Novacek, and M. C. McKenna (eds.), Mammalian Phylogeny: Mesozoic Differentiation, Multituberculates, Monotremes, Early Therians and Marsupials. Springer, New York, New York.

Cúneo, R., J. Ramezani, R. Scasso, D. Pol, I. Escapa, A. M. Zavattieri, and S. A. Bowring. 2013. High-precision U-Pb geochronology and a new chronostratigraphy for the Cañadón Asfalto Basin, Chubut, central Patagonia: implications for terrestrial faunal and floral evolution in Jurassic. Gondwnan Research 24:1267–1275.

Davis, B. M. 2011. Evolution of the tribosphenic molar pattern in early mammals, with comments on the "dual-origin" hypothesis. Journal of Mammalian Evolution 18:227–244.

Einstein, A. 1905. On the movement of small particles suspended in stationary liquids required by themolecular-kinetic theory of heat. Annalen der Physik 17:549–560.

Evans, A. R., and G. D. Sanson. 1998. The effect of tooth shape on the breakdown of insects. Journal of Zoology 246:391–400.

Evans, A. R., D. Jones, A. G. Boyer, J. H. Brown, D. P. Costa, S. K. M. Ernest, E. M. G. Fitzgerald, M. Fortelius, J. L. Gittleman, M. J. Hamilton, L. E. Harding, K. Lintulaasko, S. K. Lyons, J. G. Okie, J. J. Saarinen, R. M. Silby, F. A. Smith, P. R. Stephens, J. M. Theodor, and M. D. Uhen. 2012. The maximum rate of mammal evolution. PNAS 109:8187–4190.

Evans, A. R. 2013. Shape descriptors as ecometrics in dental ecology. Hystrix, the Italian Journal of Mammalogy 24:133–140.

Felsenstein, J. 1985. Phylogenies and the comparative method. American Naturalist 125:1–15.

Felsenstein, J. 2003. Inferring Phylogenies. Sinauer Associates, Sunderland, Massachusetts, 664 pp.

Frey, E., and K. Kroy. 2005. Browian motion: a paradigm of soft matter and biological physics. Annalen der Physik 14:20–50.

Gavryushkina, A., T. A. Heath, D. T. Ksepka, T. Stadler, D. Welch, and A. J. Drummond. 2016. Bayesian total-evidence dating reveals the recent crown radiation of penguins. Systematic Biology 66:57–73.

Graybeal, A., J. J. Rosowski, D. R. Ketten, and A. F. Crompton. Inner-ear structure in *Morganucodon*, an early Jurassic mammal. 1989. Zoological Journal of the Linnean Society 96:107–117.

Gill, P. G., M. A. Purnell, N. Crumpton, K. R. Brown, N. J. Gostling, M. Stampanoni, and E. J. Rayfield. 2014. Dietary specializations and diversity in feeding ecology of the earliest stem mammals. Nature 512:303–305.

Gillooly, J. F., A. P. Allen, G. B. West, and J. H. Brown. 2005. The rate of DNA evolution: effects of body size and temperature on the molecular clock. Proceedings of the National Academy of Sciences 102:140–145.

Greaves, W. S. 2012. The Mammalian Jaw: A Mechanical Analysis. Cambridge University Press, Cambridge, U.K., 114 pp.

Grossnickle, D. M., and E. Newham. 2016. Therian mammals experience an ecomorphological radiation during the Late Cretaceous and selective extinction at the K-Pg boundary. Proceedings of The Royal Society B 283:1–8.

Gunz, P., P. Mitteroecker, and F. L. Bookstein. 2005. Semilandmarks in three dimensions; pp. 73–98 In D. E. Slice (ed.) Modern Morphometrics in Physical Anthropology. Springer, Boston, Massachusetts.

Halley, J. M. 1996. Ecology, evolution and 1f-noise. Trends in Ecology and Evolution 11:33–37.

Harper, T,. A. Parras, and G. W. Rougier. 2018. *Reigitherium* (Meridiolestida, Mesungulatoidea) an enigmatic Late Cretaceous mammal from Patagonia, Argentina: morphology, affinities, and dental evolution. Journal of Mammalian Evolution https://doi.org/10.1007/s10914-018-9437-x

Harper, T., and G. W. Rougier. 2019. Petrosal morphology and cochlear function in Mesozoic stem therians. PLOS One 14: 1–62.

Harvey, P. H., and A. Purvis. 1991. Comparative methods for explaining adaptations. Nature 351:619–624.

Harvey, P. H., and A. Rambaut. 2000. Comparative analyses for adaptive radiations. Philosophical Transactions of the Royal Society of London B 355:1599–1605.

Hansen, T. F. 2014. Use and misuse of comparative methods in the study of adaptation; pp. 351–379 in L. Z. Garamszegi (ed) Modern Phylogenetic Comparative Methods and Their Application in Evolutionary Biology: Concepts and Practice. Springer, Berlin.

Harrison, L. B., and H. C. E. Larsson. 2015. Among-character rate variation distributions in phylogenetic analysis of discrete morphological characters. Systematic Biology 64:301–324.

Heath, A. M., and B. R. Moore. 2014. Bayesian inference of species divergence; pp. 277–318 in M. H. Chen, L. Kuo, P. O. Lewis (eds.) Bayesian Phylogenetics: Methods, Algorithms, and Applications. CRC Press, Oxfordshire, U. K.

Helmstetter, A. J., A. S. T. Papadopulos, J. Igea, T. J. M. Van Dooren, A. M. Leroi, and V. Savolainen. 2016. Viviparity stimulates diversification in an order of fish. Nature Communications 7:1–7.

Hershkovitz, P. 1971. Basic crown patterns and cusp homologies of mammalian teeth; pp. 95–150 in A. A. Dahlberg (ed) Dental Morphology and Evolution. University of Chicago Press, Chicago.

Hughes, E. M., J. R. Wible, M. Spaulding, and Z. X. Luo. 2015. Mammalian petrosal from the Upper Jurassic Morrison Formation of Fruita, Colorado. Annals of the Carnegie Museum 83:1–17.

Hunt, G., and M. T. Carrano. 2010. Models and methods for analyzing phenotypic evolution in lineages and clades; pp. 245–269 in J. A. Alroy, G. Hunt (eds.), Quantitative Methods in Paleobiology. Paleontological Society Papers, Volume 16, Cambridge, U. K.

Hunt, G. 2012. Measuring rates of phenotypic evolution and the inseparability of tempo and mode. Paleobiology 38:351–373.

Jernvall, J., J. P. Hunter, and M. Fortelius. 1996. Molar tooth diversity, disparity, and ecology in Cenozoic ungulate radiations. Science 274:1489–1492.

Juuri, E., M. Jussila, K. Seidel, S. Holmes, P. Wu, J. Richman, K. Heikinheimo, C.-M. Chuong, K. Arnold, K. Hochedlinger, O. Klein, F. Michon, and I. Thesleff. 2013. Sox2 marks epithelial competence to generate teeth in mammals and reptiles. Development 140:1424–1430.

Kermack, K. A.1963. The cranial structure of the triconodonts. Philosophical Transactions of the Royal Society of London B 246:83–103.

Kermack, K. A., F. Musset, and H. W. Rigney. 1981.The skull of *Morganucodon*. Zoological Journal of the Linnean Society 71:1–158.

Kermack, K. A., and F. Musset. The ear in mammal-like reptiles and early mammals. Acta Palaeontologica Polonica 28:147–158.

Kielan-Jaworowska, Z., R. L. Cifelli, and Z. X. Luo. 2004. Mammals From The Age of Dinosaurs: Origins, Evolution, and Structure. University of Colombia Press, New York, New York, 630 pp.

Laaß, M. 2015. The origins of the cochlea and impedance matching hearing in synapsids. Acta Palaeontologica Polonica 61:267–281.

Ladevèze, S., R. J. Asher, and M. R. Sánchez-Villagra. 2008. Evidence for metatherian affinities and comparisons with the extant marsupial mole. Journal of Anatomy 213:686–697.

Lande, R. 1976. Natural selection and random genetic drift in phenotypic evolution. Evolution 30:314–334

Langton, C., and Levin, V. 2017. The Intuitive Guide to Fourier Analysis and Spectral Estimation with MATLAB. Mountcastle Academic, Chicago, U.S.A., 320 pp.

Larsson, H. C., T. A. Dececchi, and L. B. Harrison. 2012. Morphological largess: can morphology offer more and be modeled as a stochastic evolutionary process; pp. 83–115 in R. J. Asher, J. Müller (eds.), from clone to bone: the synergy of morphological and molecular

tools in palaeobiology. Cambridge University Press, Cambridge, U.K.

Lempert, J., P. E. Meltzer, E. G. Wever, M. Lawrence, and J. H. T. Rambo. 1952. Structure and function of the cochlear aqueduct. AMA Archives of Otolaryngology 55:134–145.

Lewis, P. O. 2001. A likelihood approach to estimating phylogeny from discrete morphological character data. Systematic Biology 50:913–925.

Lucas, P. W. 2004. Dental Functional Morphology: How Teeth Work. Cambridge University Press, Cambridge, U.K., 355 pp.

Luckett, W. P. 1993. An ontogenetic assessment of dental homologies in therian mammals; pp. 182–204 in F. S. Szalay, M. J. Novacek, and M. C. McKenna (eds.), Mammalian Phylogeny: Mesozoic Differentiation, Multituberculates, Monotremes, Early Therians and Marsupials. Springer, New York, New York.

Luo, Z. X., A. W. Crompton, and S. G. Lucas. 1995. Evolutionary origins of the mammalian promontorium and cochlea. Journal of Vertebrate Paleontology 15:113–121.

Luo, Z. X. 2001. The inner ear and its bony housing in tritylodontids and implications for evolution of the mammalian ear. Bulletin of the Museum of Comparative Zoology 156:81–97.

Luo, Z. X., Z. Kielan-Jaworowska, and R. L. Cifelli. 2004. Evolution of dental replacement in mammals. Bulletin of the Carnegie Museum of Natural History 36:159–176.

Luo, Z. X, 2007. Transformation and diversification in early mammal evolution. Nature 450:1011–1019.

Luo, Z. X. 2011. Developmental patterns in Mesozoic evolution of mammal ears. Annual Review of Ecology Evolution, and Systematics 42:355–380.

Luo, Z. X., C. X. Yuan, J. Q. Meng, and Q. Ji. 2011. A Jurassic eutherian mammal and divergence of marsupials and placentals. Nature. 476:442–445.

Luo, Z. X., I. Ruf, and T. Martin. 2012. The Petrosal and inner ear of the Late Jurassic cladotherian mammal *Dryolestes leiriensis* and implications for ear evolution in therian mammals. Zoological Journal of the Linnean Society 166:433–463.

Luo, Z. X., J. A. Schultz, and E. G. Ekdale. 2016. Evolution of the middle and inner ears of mammaliaformes; pp. 139–174 in J. A. Clack, R. R. Fay, and A. N. Popper (eds.), Evolution of The Vertebrate Ear: Evidence from The Fossil Record. Springer, Cham, Switzerland.

Lynch, M. 1990. The rate of morphological evolution in mammals from the standpoint of the neutral expectation. American Naturalist 136:727–741.

MacPhee, R. D. 1981. Auditory Regions of Primates and Eutherian Insectivores: Morphology, Ontogeny and Character Analysis; in F. S. Szalay (ed.) Contributions to Primatology, Volume 18. S. Karger, Basel, 282 pp.

MacRobert, T. M. 1967. Spherical Harmonics: An Elementary Treatise on Harmonic Functions with Applications. Pergamon Press, Oxford, U.K., 368 pp.

Manley G. A., 2000. Cochlear mechanism from a phylogenetic viewpoint. Proceedings of the National Academy of Sciences 97:11736–11743.

Manley, G. A. 2017. The mammalian Cretaceous cochlear revolution. Hearing Research 352:23–29.

Manley, G. A. 2018. The foundations of high-frequency hearing in early mammals. Journal of Mammalian Evolution 25:155–163.

Martin, T. 1997. Tooth replacement in Late Jurassic Dryolestidae (Eupantotheria, Mammalia). Journal of Mammalian Evolution 4:1–18.

McKenna, M. C. 1976. Comments on Radinsky's "later mammal radiations"; in R. B. Masterson, M.E. Bitterman, C. B. G. Campbell, and N. Hotton (eds.), Evolution of Brain and Behavior in Vertebrates, Volume 1. Lawrence Erlbaum Associates, Hillsdale, New Jersey.

McKenna, M. C., S. K. Bell. 1997. Classification of Mammals: Above the Species Level.

Colombia University Press, New York, New York, 631 pp.

McPeek, M.A., L. Shen, and H. Farid. 2009. The correlated evolution of three-dimensional reproductive structures between male and female damselflies. Evolution: International Journal of Organic Evolution 63:73– 83.

Meng, J., and R. C. Fox. 1995. Osseus inner ear structures and hearing in early marsupials and placentals. Zoological Journal of the Linnean Society 115:47–71.

Meng J., Y. Hu, Y. Wang, C. Li. 2003. the ossified Meckel's cartilage and internal groove in Mesozoic mammaliaforms: implications to the origin of the definitive mammalian middle ear. Zoological Journal of the Linnean Society 138:431–448.

Miller, M. A., T. Schwartz, B. E. Pickett, S. He, E. B. Klem, R. H. Scheuermann, M. Passarotti, S. Kaufman, and M. O'Leary. 2015. A RESTful API for access to phylogenetic tools via the CIPRES science gateway. Evolutionary Bioinformatics 11:43–48.

Mills, J. R. E. 1967. A comparison of lateral jaw movements in some mammals from wear facets on the teeth. Archives of Oral Biology 15:645–661.

Mitchell, J. S.2015. Extant-only comparative methods fail to recover the disparity preserved in the bird fossil record. Evolution 69:2414–2424.

Novacek, M. J. 1986. The primitive eutherian dental formula. Journal of vertebrate paleontology 6:191–196.

O'Leary, M. A., and S. G. Kaufman. 2012. Morphobank 3.0: Web application for morphological phylogenetics and taxonomy. http://www.morphobank.org.

Olson, E. C. 1944. Origin of mammals based upon cranial morphology of the therapsid suborders. Special Papers of the Geological Society of America 55:1–136

O'Meara, B. C. and J. M. Beaulieu. 2014. Modelling stabilizing selection: the attraction of Ornstein-Uhlenbeck models; pp. 381–393 in L. Z. Garamszegi (ed), Modern Phylogenetic Comparative Methods and Their Application in Evolutionary Biology: Concepts and Practice. Springer, Berlin.

O'Meara, R. N. and R. S. Thompson. 2014. Were there Miocene meridiolestidans? Assessing the phylogenetic placement of *Necrolestes patagonensis* and the presence of a 40 million year ghost lineage. Journal of Mammalian Evolution 21:271–284.

Osborn, H.F. 1888. The evolution of mammalian molars to and away from the tritubercular type. American Naturalist 22:1067—1079.

Osborn, H. F. 1907. Evolution of mammalian molar teeth. Macmillan, New York, U.S.A., 250 pp.

Oxnard, C., and P. O'Higgins. Biology clearly needs morphometrics. does morphometrics need biology?. Biological Theory 4:84–97.

Paez-Arango, N. 2008. Dental and craniomandibular anatomy of *Peligrotherium tropicalis*: the evolutionary radiation of South American dryolestoid mammals. M. Sc. thesis, University of Louisville, Louisville, Kentucky, 107 pp.

Palci, A, and M. S. Y. Lee. 2018. Geometric morphometrics, homology and cladistics: review and recommendations. Cladistics 35:230–242.

Panciroli, E., J. A. Schultz, and Z. X. Luo. 2019. Morphology of the petrosal and stapes of *Borealestes* (Mammaliaformes, Docodonta) from the Middle Jurassic of Skye, Scotland. Papers in Palaeontology 5:139–156.

Paradis, E. J. Claude, and K. Strimmer. 2004. APE: analyses of phylogenetics and evolution in R language. Bioinformatics 20:289–290.

Paradis, E. J. 2014. An Introduction to the phylogenetic comparative method. pp. 3–18 in L. Z. Garamszegi (ed) Modern Phylogenetic Comparative Methods and Their Application in Evolutionary Biology: Concepts and Practice. Springer, Berlin.

Patterson, B. 1956.Early Cretaceous mammals and the evolution of mammalian molar teeth. Fieldiana Geol 13:1-105

Polly, P. D. 2004. On the simulation of the evolution of morphological shape: multivariate shape under selection and drift. Palaeontologia Electronica 7:1–28.

Polly, P. D., S. C. Le Comber, T. M. Burland. 2005. On the occlusal fit of tribosphenic molars: are we underestimating species diversity in the Mesozoic?. Journal of Mammalian Evolution 12: 283–299.

Price, S. A., S. S. B. Hopkins, K. K. Smith, V. L. Roth. Tempo of trophic evolution and its impact on mammalian diversification. Proceedings of the National Academy of Sciences 109:7008–7012.

Pyron, R. A. 2016. Novel approaches for phylogenetic inference from morphological data and total-evidence dating in squamate reptiles (lizard, snakes, and amphisbaenians). Systematic Biology 66:38–56.

Raftery A. E. 1999. Bayes factors and BIC: Comments on "A critique of the Bayesian information criterion for model selection". Sociological Methods and Research 27:411–427.

Rambaut A., A. J. Drummond, D. Xie, G. Baele, and M. A. Suchard. 2018. Posterior summarization in Bayesian phylogenetics using Tracer 1.7. Systematic Biology 67:901–904.

Revell, L. J. 2012. phytools: an R package for phylogenetic comparative biology (and other things). Methods in Ecology and Evolution 3:217–223.

Rizk, O. T., T. M. Grieco, M. W. 2013. Holmes, and L. J. Hlusco. Using geometric morphometrics to study the mechanisms that pattern primate dental variation; pp. 126–169 in G. R. Scott, J. D. Irish (eds.), Anthropological Perspectives on Tooth Morphology: Genetics, Evolution, Variation. Cambridge University Press, Cambridge.

Rodrigues, P. G., I. Ruf, and C. L. Schultz. 2013. Digital reconstruction of the otic region and inner ear of the non-mammalian cynodont *Brasilitherium riograndensis* (Late Triassic, Brazil) and its relevance to the evolution of the mammalian ear. Journal of Mammalian Evolution 20:291–307.

Ronquist, F., M. Teslenko, P. Van Der mark, D. L. Ayres, A. Darling, S. Höhna, B. Larget, L. Liu, M. A. Suchard, and J. P. Huelsenbeck. 2012. MrBayes 3.2: efficient Bayesian phylogenetic inference and model choice across a large model space. Systematic Biology 61:539–542.

Ronquist, F., S. Klopfstein, L. Vilhelmsen, S. Schulmeister, D. L. Murray, and A. P. Rasnitsyn. 2012. A total-evience approach to dating with fossils, applied to the early radiation of the Hymenoptera. Systemic Biology 61:973–999.

Rose, K. D. 2006. The Begining of The Age of Mammals. Johns Hopkins University Press, Baltimore, Maryland, 428 pp.

Rougier, G. W., J.R. Wible, and J. A. Hopson. 1992. Reconstructions of the cranial vessels in the Early Cretaceous mammal *Vincelestes neuquenianus*: implications for the evolution of the mammalian cranial vascular system. Journal of Vertebrate Paleontology 12:188–216.

Rougier, G. W., J. R. Wible, and J. A. Hopson. Basicranial anatomy of *Priacodon fruitaensis* (Triconodontidae, Mammalia) from the Late Jurassic of Colorado, and a reappraisal of mammaliaform interrelationships. 1996. American Museum Novitates 3183:1–38.

Rougier, G. W., A. M. Forasiepe, R. V. Hill, and M. J. Novacek. 2009. New mammalian remains from the Late Cretaceous La Colonia Formation, Patagonia, Argentina. Acta Palaeontologica Polonica 54:195–212.

Rougier, G. W., S. Apesteguía, and L. C. Gaetano. 2011. Highly specialized mammalian skulls from the Late Cretaceous of South America. Nature 479:98–102.

Rougier, G. W., J. R. Wible, R. M. Beck, and S. Apesteguía. 2012. The Miocene mammal Necrolestes demonstrates the survival of a Mesozoic nontherian lineage into the late Cenozoic of South America. Proceedings of The National Academy of Sciences 109:20053–20058.

Rowe, T. 1988. Definition, diagnosis, and origin of Mammalia. Journal of Vertebrate Paleontology 8:241–264.

Rowe, T. 1993. Phylogenetic systematics and the early history of mammals; pp. 129-145 in F. S. Szalay, M. J. Novacek, and M. C. McKenna (eds.), Mammalian Phylogeny: Mesozoic Differentiation, Multituberculates, Monotremes, Early Therians and Marsupials. Springer, New York, New York.

Rowe, T. B., Z. X. Luo, R. A. Ketcham, J. A. Maisano, M. W. Colbert. 2016. X-ray computed tomography datasets for forensic analysis of vertebrate fossils. Scientific Data 3:1–25.

Ruf I., Z. X. Luo, J. R. Wible, and T. Martin. 2009. Petrosal anatomy and inner ear structures of the Late Jurassic *Henkelotherium* (Mammalia, Cladotheria, Dryolestoidea): insight into the early evolution of the ear region in cladotherian mammals. Journal of Anatomy 214:679–693.

Ruf, I., Z. X. Luo, and T. Martin. 2013. Reinvestigation of the basicranium of *Haldanodon expectatus* (Mammaliaformes, Docodonta). Journal of Vertebrate Paleontology 33:382–400.

Schultz, J. A., and Martin T. 2014. Function of pretribosphenic and tribosphenic mammalian molars inferred from 3D animation. Naturwissenschaften 101:771–781.

Schultz, J. A., U. Zeller, and Z. X. Luo. Inner ear labyrinth anatomy of monotremes and implications for mammalian inner ear evolution. Journal of Morphology 278:236–263.

Shahid R., G. G. Gil, and S. Hoffmann. 2018. Inner ear morphology of basal-most mammaliaform *Morganucodon*. The FASEB Journal 32(1, Supplement):780.

Shen, L., H. Farid, and M. A. McPeek. 2009. Modeling three-dimensional morphological structures using spherical harmonics. Evolution: International Journal of Organic Evolution 63:1003–1016.

Simpson, G. G. 1944. Tempo and Mode in Evolution. Colombia Unversity Press, New York, New York, 239 pp.

Skinner, M. M., P. Gunz, B. A. Wood, and J. J. Hublin. 2008. Enamel-dentine junction (EDJ) morphology distinguishes the lower molars of *Australopithecus africanus* and *Paranthropus robustus*. Journal of Human Evolution 55:979–988.

Slater, G. L. 2013. Phylogenetic evidence for a shift in the mode of mammalian body size evolution at the Cretaceous-Palaeogene boundary. Methods in Ecology and Evolution 4:734–744.

Sterli, J. M. S. de la Fuente, and G. W. Rougier. 2018. New remains of *Condorchelys antiqua* (Testudinata) from the Early-Middle Jurassic of Patagonia: anatomy, phylogeny, and paedomorphosis in the early evolution of turtles. Journal of Vertebrate Paleontology 38:1–17.

Sutton, M. D., I. A. Rahman, and R. J. Garwood. 2014. Techniques for Virtual Paleontology. Wiley, Oxford, U. K., 200 pp.

Swofford D. A. 2003. PAUP* 4.0. Sinauer Associates, Sunderland, Massachusetts.

Tarver, J. E. and P. C. Donoghue. 2011. The trouble with topology: phylogenies without fossils provide a revisionist perspective of evolutionary history in topological analyses of diversity. Systematic Biology 60:700–712.

Thenius, E. 1989. Zähne und gebiß der säugetiere. In J. Neithammer, H. Schliemann, D. Stark (eds.), Handbook of Zoology: A Natural History of The Animal Kingdom, Volume VIII Mammalia. Walter de Gruyter, Berlin.

Thorne, J. L., and H. Kishino. 2002. Divergence time and evolutionary rate estimation with multilocus data. Systematic Biology 51:689–702.

Vandebroek, G. 1961. The comparative anatomy of the teeth of lower and non specialized mammals, part 1; pp. 215–320 in G. Vandebroek (ed.), International Colloquium on the Evolution of Lower and Non Specialized Mammals. Koninklijke Vlaamse Academie voor Wetenschappen, Letteren en Schone Kunsten van Belgie, Brussel.

Vasseur, D. A., and Yodzis, P. 2004. The color of environmental noise. Ecology 85:1146–1152.

Wagner, P. J., and J. D. Marcot. 2010. Probabilistic phylogenetic inference in the fossil record: current and future applications; pp. 189–211 in J. A. Alroy, G. Hunt (eds.), Quantitative Methods in Paleobiology. Paleontological Society Papers, Volume 16, Cambridge, U. K.

Wible, J. R. 1991. Origin of mammalia: the craniodental evidence reexamined. Journal of Vertebrate Paleontology 11:1–28.

Wible, J. R., G. W. Rougier, M. J. Novacek, and M. C. McKenna. 2001. Earliest eutherian ear region: a petrosal referred to *Prokennalestes* from the Early Cretaceous of Mongolia. American Museum Novitates 3322:1–44.

Wible, J. R., G. W. Rougier, M. J. Novacek, M. C. McKenna, and D. Dashzeveg. 1995. A mammalian petrosal from the Early Cretaceous of Mongolia: implications for the evolution of the ear region and mammaliamorph interrelationships. American Museum Novitates 3149:1–19.

Wible, J. R., and G. W. Rougier. 2017. Craniomandibular anatomy of the subterranean meridiolestidan *Necrolestes patagonensis* Ameghino, 1891 (Mammalia, Cladotheria) from the early Miocene of Patagonia. Annals of the Carnegie Museum 84:183–252.

Wiley, E. O., D. R. Brooks, D. Seigel-Causey, and V. A. Funk. 1991. The Compleat Cladist: A Primer of Phylogenetic Procedures. University of Kansas Museum of Natural History, Lawrence, Kansas, 159 pp.

Wood, A. R., M L. Zelditch, A. N. Rountrey, T. P. Eiting, H. D. Sheets, and P. D. Gingerich. 2007. Multivariate stasis in the dental morphology of the Paleocene-Eocene condylarth *Ectocion*. Paleobiology 33:248–260.

Wright, A.M., G. T. Lloyd, and D. M. Hillis. 2016. Modeling character change heterogeneity in phylogenetic analyses of morphology through the use of priors. Systematic Biology 65:602–611.

Zelditch, M. L., D. L. Swiderski, and H. D. Sheets. 2012. Geometric Morphometrics for Biologists: A Primer. Academic Press, Amsterdam, 432 pp.

Zhang, C., T. Stadler, S. Klopfstein, T. A. Heath, and F. Ronquist. 2016. Total-evidence dating under the fossilized birth-death process. Systematic Biology 65:228–249.

Supplementary Data: Models of craniodental transformation in early mammals.

TABLE 1S. Real component of first three PC scores for taxa used in macroevolutionary analyses. For PCs 1 and 5 both real and imaginary components of the PC score were significant, and PC scores corresponding to a diagonal axis in the complex plane is listed. To reconstitute the complex values for PC1 multiply the listed PC1 value by 0.849338958154313 for the real component, and by -0.527847832392391 for the imaginary component. To reconstitute the complex values for PC5 multiply the listed PC5 value by 0.630017888359048 for the real component, and by 0.776580620636136 for the imaginary component.

OTU	PC1 rot	PC2 real	PC3 real	PC4 real	PC5 rot
Morganucodon	-0.011230977731608	0.002754	0.005945	0.004212	-0.00059762151621
Docodonts	-0.003406259467934	0.004034	0.002465	0.007802	0.003416964959516
Ausktribosphenos	0.003222458432016	-0.007579	-0.007351	-0.001694	0.004209233267434
Henosferus	-0.004422693274816	0.008083	-0.002996	0.002052	0.001204166976166
Bishops	0.003695854651292	-0.006199	-0.002962	-0.00748	0.004459784888477
Steropodon	-0.007192373526478	-0.013009	-0.002192	0.000866	0.002632237934742
Obdurodon	-0.005506863415404	-0.016314	-0.001347	0.001449	0.001184811489464
Gobiconodon	-0.009120090494352	0.005631	0.003828	-0.005165	0.00107600468726
Trioracodon	-0.015496846095549	-0.001494	0.011485	-0.005598	-0.007158337647152
Tinodon	0.000632344737196	0.007653	0.007219	-0.002283	0.00542827677539
Peramus	-0.002969749713009	0.008259	-0.004744	-0.004181	-0.000269017930471
Vincelestes	-0.008691637503463	-0.000375	0.005839	0.001245	-0.001205348381369
Deltatheridium	-0.001840636344033	0.008534	-0.002319	-0.003606	0.002839082206232
Kokopellia	-0.002432542363691	0.004139	-0.00869	0.001281	-0.001589835248085
Didelphis	-0.007986524073879	-0.001816	-0.002882	0.003014	0.004202053712157
Erinaceus	-0.002547976299366	-0.004368	-0.005639	0.003864	-0.001068599938677
Asioryctes	0.000448646619982	-0.000412	-0.014164	0.000698	-0.006228410170911
Prokennalestes	-0.003700938469326	0.004704	-0.009468	0.002403	-0.005244152574934
Amphitheridae	-4.36E-05	0.006054	-0.004373	-0.002844	7.02E-05
Dryolestes	0.01088234648013	0.002498	0.004799	0.003319	-0.004998597330039
Laolestes	0.011427610593485	0.004355	0.002126	0.00014	-0.003651391533178
Mesungulatum	0.010339836740357	-0.002724	0.00188	0.000327	0.001647980338765
Coloniatherium	0.003296552851843	-0.005167	0.003882	0.003888	0.002829089453937
Reigitherium	0.005280345676848	-0.009129	0.004233	-0.008327	-0.007483981473141
Peligrotherium	0.002887817101566	-0.007312	0.005611	0.002207	0.000499032659608
Groebertherium	0.012179893777205	-0.002699	0.004722	0.004393	-0.003342920014762
Paurodon	0.002551477093201	0.006502	0.006833	0.003083	0.004990866387447
Cronopio	0.004435100171646	0.002006	-0.002855	-0.003216	0.00100653887635
Spalacotherium	0.015309441347091	0.003392	0.001116	-0.001849	0.001141880720532

TABLE 2S. Ancestral PC score reconstruction values for interior nodes in summary phylogeny, "node num" referrers to interior node number seen if Figure 2S. Reconstructions based on BMM-Theriimorpha model of trait change.

Node num	PC1 rot	PC2 real	PC3 real	PC4 real	PC5 rot
30	-0.01033878	0.003054361	0.0053284558	0.0038824609	-0.0002973871
31	-0.007152459	0.004127036	0.0031265964	0.0027055806	0.0007748376
32	-0.006345383	0.004494552	0.002432527	0.0019490023	0.000948682
33	-0.004285227	0.00468954	0.0032923461	-0.0013595303	0.001403223
34	-0.007717918	0.003278525	0.0054001179	-0.0029215527	-0.0007683783
35	9.485596E-06	0.005158772	0.002094185	-0.001327443	0.001228826
36	0.001613656	0.00529208	7.1968E-05	-0.0010246556	0.0001950262
37	6.481693E-05	0.00588354	-0.0035337408	-0.0024881288	4.975178E-05
38	-0.00227267	0.005430762	-0.0028575509	-0.0020548543	-0.0004886701
39	-0.003409127	0.004353912	-0.0019251011	-0.0011921514	-0.0008603698
40	-0.002948263	0.004414366	-0.0069697552	0.0005980035	-0.002590968
41	-0.002590754	0.004988958	-0.0067453067	0.0001174297	-0.0009137876
42	-0.002635576	0.004306384	-0.0078056996	0.0008862536	-0.001185089
43	-0.003019151	0.004030466	-0.0091311527	0.0016496109	-0.004468389
44	-6.535675E-05	-7.723004E-05	-0.0132446046	0.0009363768	-0.005816421
45	0.003633753	0.004911781	0.0017561572	0.0002480682	-0.0002364801
46	0.008338932	0.003501038	0.0034150839	0.0018809268	-0.003133214
47	0.01054078	0.003784829	0.0022788567	0.0004645713	-0.003312865
48	0.008319996	0.0004332231	0.0013754672	0.000239701	-0.001341883
49	0.006514883	5.565331E-05	0.0001757946	-0.0009287676	-0.0001130554
50	0.006152005	-0.004362825	0.0029358717	0.0005493739	0.0006732337
51	0.004870292	-0.007547907	0.0042831983	-0.0035476604	-0.003527459
52	-0.004568315	0.006059356	-0.0017713147	0.0016834707	0.0013205
53	-0.0007075751	-0.005991876	-0.0037291734	-0.0020749085	0.003324962
54	0.002619096	-0.006691109	-0.004816461	-0.0041437122	0.004132533
55	-0.006487919	-0.0124322	-0.0023139789	0.0005952506	0.002648635

TABLE 3S. Ancestral PC score reconstruction standard error values for interior nodes in summary phylogeny, "node num" referrers to interior node number seen if Figure 2S. Reconstructions based on BMM-Theriimorpha model of trait change, values correspond to values of 10,000xPC score.

Node num	PC1 rot	PC2 real	PC3 real	PC4 real	PC5 real
30	0	0	0	0	0
31	18.447182	19.83037	16.734896	18.725627	6.138486
32	19.25306	20.381959	17.544852	19.360437	6.473021
33	20.649691	15.252322	20.161586	17.203236	8.025936
34	30.033718	18.57003	26.563546	23.395499	20.993426
35	22.173795	13.758836	19.647431	17.29348	15.410003
36	18.07048	10.746293	15.673	13.897717	13.374888
37	9.859609	5.808547	8.512201	7.560276	7.387717
38	24.761303	14.573204	21.367213	18.980912	18.576661
39	28.652802	16.863114	24.724993	21.963789	21.496862
40	32.43714	19.090011	27.990342	24.864544	24.336578
41	28.584973	16.822908	24.666257	21.911677	21.446437
42	21.567797	12.693139	18.611066	16.532693	16.181665
43	24.720976	14.548859	21.331977	18.949749	18.547397
44	21.555722	12.686033	18.600646	16.523437	16.172606
45	20.332684	12.011467	17.577613	15.604502	15.181347
46	18.614742	10.961377	16.067259	14.271578	13.956052
47	20.372682	11.989983	17.579929	15.616664	15.284689
48	34.238763	20.150302	29.544976	26.245567	25.68829
49	29.19982	17.184761	25.196816	22.382986	21.907737
50	19.715098	11.602784	17.012354	15.112516	14.791642
51	19.609908	11.540877	16.921584	15.031882	14.712721
52	16.43873	17.948074	14.842101	16.848939	5.410246
53	23.783519	26.033077	21.456483	24.4157	7.813058
54	13.557489	14.840391	12.230844	13.918191	4.453608
55	14.283201	15.634843	12.885525	14.663251	4.691987

FIGURE 1S. Scatterplot showing lower molariform variation along PCs 4 and 5. Tooth surfaces correspond to "eigenmode" surfaces representing positive and negative two standard deviations along each axis.

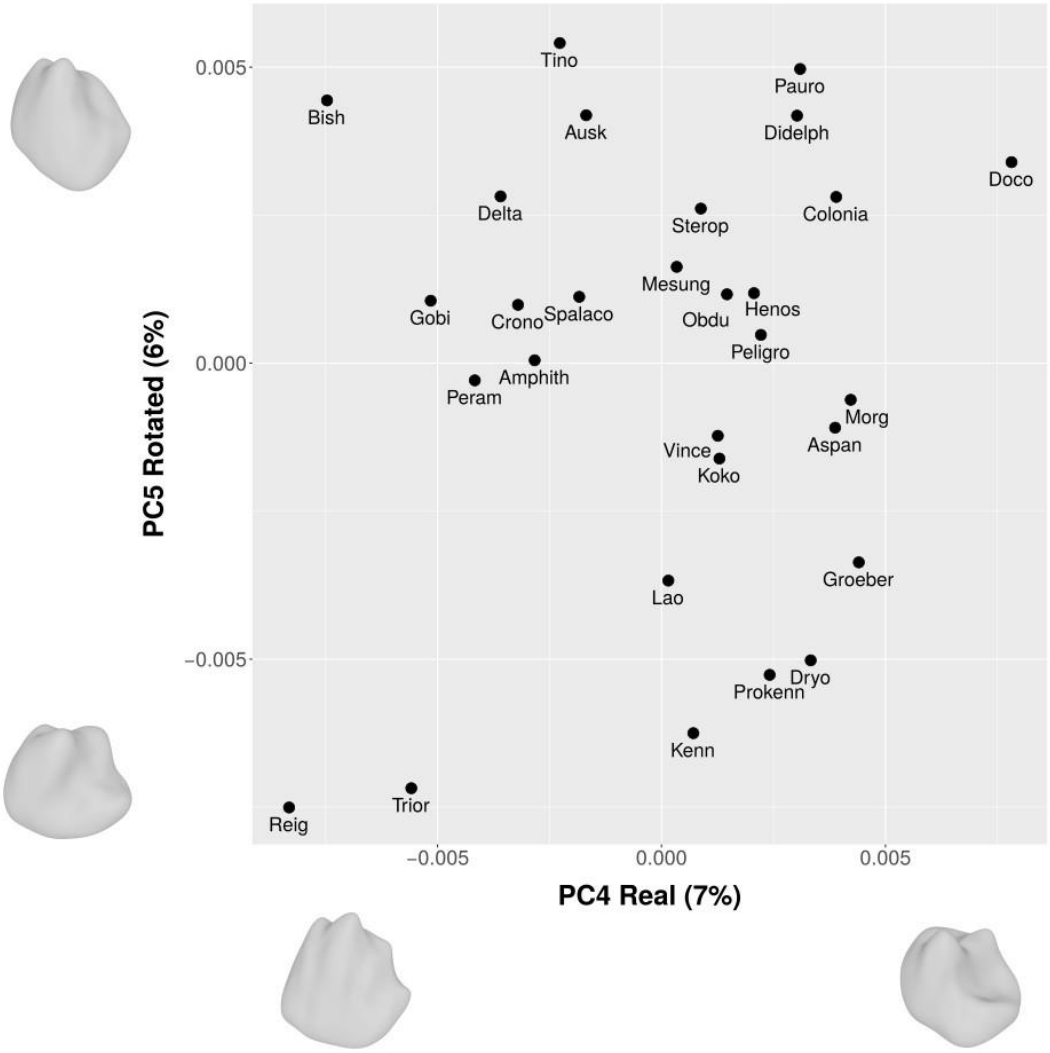

FIGURE 2S. Example of constrained Bayesian summary phylogeny used for ancestral state reconstructions shown in Table 2S. Node labels refer to "node num" index shown in Table 2S.

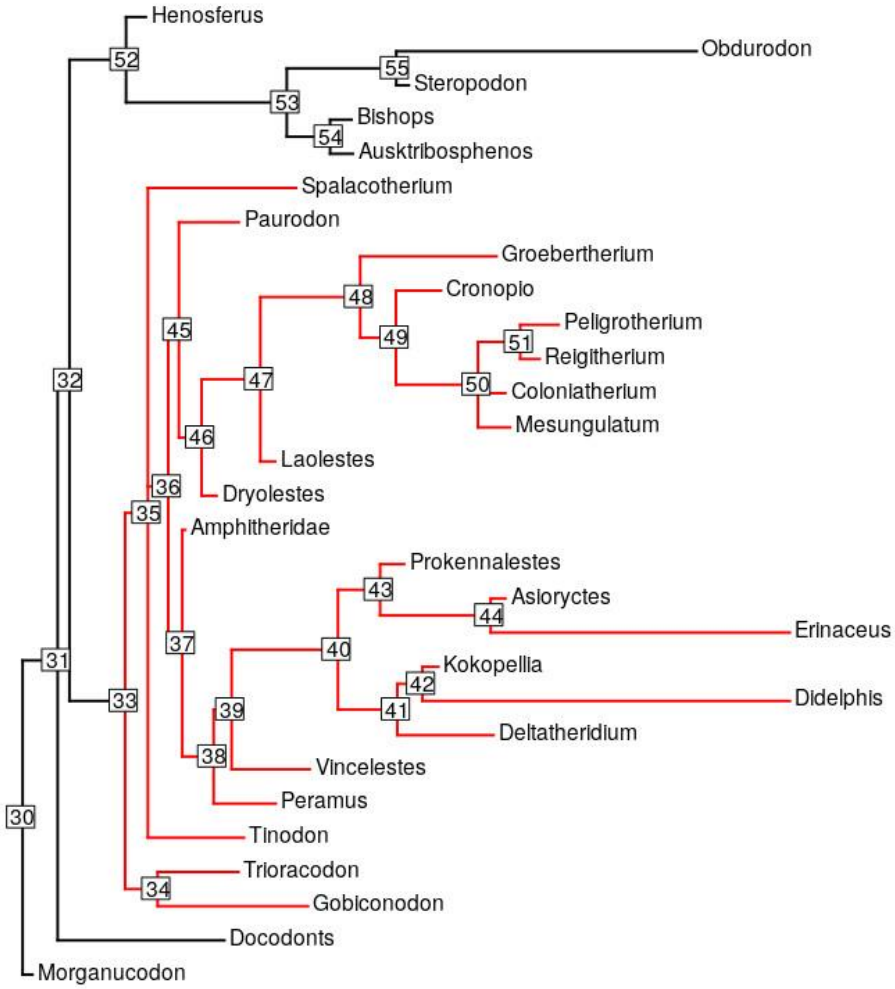

%Example Script for Reconstructing Ancestral Tooth Surfaces From Arbitrary PC Scores and The Output from SPHARMGUI (here shown only for PCs 1 and 2):

% For each PC, X is an N by 2 matrix with the real and imaginary components of the PC %scores.

%Then for each PC do:
[coeff,score] = pca(X)

PCX_real_loading = coeff(1,1) % Loading of real component of PCX with rotated scores

PCX_imag_loading = coeff(2,1) % Loading of imaginary component of PCX with
% rotated scores

PCX_Rotated_Scores = score(:,1) % vector of scores for PCX, rotated in complex plane

% If a particular PC has no significant imaginary component then PCX_real_loading = 1,
% and PCX_imag_loading = 0. In this case the pca() step is unnecessary

%The following shows steps to create a tooth surface crresponding to ancestral values
% estimated by mvMorph and the eigenmode output from SPHARM. Shown for only PCs 1 % and 2 but extendable to include others:

R_avg % the real(fvec) for PC1_0.mat
I_avg % the imag(fvec) for PC1_0.mat

R_pc1 % the real(fvec) for PC1_1.mat
I_pc1 % the imag(fvec) for PC1_1.mat

R_pc2 % the real(fvec) for PC2_1.mat
I_pc2 % the imag(fvec) for PC2_1.mat

eigenval_1 % eigenvalue corresponding to PC1 from PCSummary.dta

eigenval_2 % eigenvalue corresponding to PC2 from PCSummary.dta

AncPC1 % an arbitrary rotated PC1 score such as estimated by mvMORPH

AncPC2 % an arbitrary rotated PC2 score such as estimated by mvMORPH

R_r = R_avg + ((AncPC1*PC1_real_loading)/sqrt(PC1_eigenvalue))*(R_pc1 – R_avg) + ((AncPC2*PC2_real_loading)/sqrt(PC2_eigenvalue))*(R_pc2 – R_avg) ;

I_r = I_avg + ((AncPC1*PC1_imag_loading)/sqrt(PC1_eigenvalue))*(I_pc1 – I_avg) + ((AncPC2*PC2_imag_loading)/sqrt(PC2_eigenvalue))*(I_pc2 – I_avg) ;

fvec = complex(R_r , I_r) ; % the reconstructed fvec

landmarks = zeros(6,3) ; % this is just because the Make surfaces from SPHARM models needs an object named landmarks

save anctooth dg faces fvec landmarks vertices % the matrices dg, faces, and vertices come from the PC1_0.mat eigenmode

%Then use SPHARMGUI to recreate .STL file from anctooth.mat

#NEXUS
[Character Data and MrBayes commands used for Chapter 3]

BEGIN DATA;
DIMENSIONS NTAX=60 NCHAR=331;
FORMAT DATATYPE = mixed(Standard:2 5 9 17 22 24 25 27 30 36 40 42 47 49 52 55-57 60 62 63 65 66 70 73-78 82-84 86 90 93-96 100 101 107 108 110 112 114-116 119 120 126 127 129 133 135 136 140 144 146 155 157 166 171 178 184 186 187 201 206 207 209 212 214 216 222 228 230-232 237 240 242-245 247 252 254 263 265 268-270 272-273 276 277 281 287 289 291 294 298 299 308 310 325 331 , Restriction:1 3 4 6-8 10-16 18-21 23 26 28 29 31-35 37-39 41 43-46 48 50 51 53 54 58 59 61 64 67-69 71 72 79-81 85 87-89 91 92 97-99 102-106 109 111 113 117 118 121-125 128 130-132 134 137-139 141-143 145 147-154 156 158-165 167-170 172-177 179-183 185 188-200 202-205 208 210 211 213 215 217-221 223-227 229 233-236 238 239 241 246 248-251 253 255-262 264 266 267 271 274-275 278-280 282-286 288 290 292-293 295-297 300-307 309 311-324 326-330) GAP = - MISSING = ? SYMBOLS = " 0 1 2 3 4 5";
MATRIX
Probainognathus 0(1 2
3)000000?00000??00000???0?0000000000000?0??????????0??00?00????????00??0?00?0000???00????????200
????0?000001100??????0000????0010?0?00?000?0??0?0??????0000?00?00?0????0?000000?000000000000000?0
??000000?00000???00???0?100000??000??000000000000001101000?000?00?000000000000000000000000000000
000000000000000?00000?00000???0?????????????
Tritylodontids 0(1 2 3)000010?00000??00000???0?3000?110?2??1??0??????0?0???(2
3)????4????????00??0?00??0?????????????????00??????100511402??????2???????????0?120011????0?3??????00
00?00000?0000000000000000000(0
1)000000?0000000000000000000??00100000??000??00000001?000100000101?100?000001000100000000(0
1)0010000000000000000(0 1)01010?00000?00000???00?000010??0?00
Tritheledontids
1?000000?000000?000000001?20000000001?0?0?????????0?0??00?00????????00??0?00?0?000??00????????240
????0?00?001100??????000?????0010?0?00?001?0??0?0??????00100?0??0?00?1101000000?000000000000?0?
?0?000???0?????????????1000100?000??0?000001?0000001000000?000?00000000100?110100000000000000000
10?001?001?????????011100???000000010??0?00
Adelobasileus
1???0???0?????????0?00????????0?????????????????????0
????0??0???
????????????10??????01?0????000001002010110000?000000000001????0?????0?1110?00??1101120??????01????
????????10?????????????????
Sinoconodon
1?000000?000000000000001100000000001?10100100000000012000?00000???0010(0
1)00000100000??000??0????200????0?00?101000?0?0?0000?????00(0 1)0?0?(0
1)10000?0??001?0000000101000?00?000000000000000000000000000????000000??0????????????10001000011
000000000001112000000101?000000100111000011011011010000011000000000001010000000000010??00??0???
???0???
Morganucodon 10000100?00000000000000(0
1)1000021000?01?13001000000000101200?11000???0012001202000000??000??0????240????0?00?10100100?0?00
00?????0000?0?110010?1??001?0000000101000000?10?1?0010?000?000000000000000?0000100010?0?000000000??
??100110(0 1)(0
1)012110100000000111201010011201000001011101102?101101101000001100111011000101000000000010010??00010
0011000?00
Megazostrodon
10000100?000000000000000201100?000?01??300101000000101200?12000???0012000102000000??000??0????2
40????0?00?10100100?0?0000?????0000?0?110000?0??001?0000000100?0000?1????0?100000?0000000000000?0
000001000?00000000000?000010?110??01201010?000001111101?10011201000001011101?0?21?11?11?10??001?001
?10???????1???????0110?10??0?????????????
Dinnetherium
10000111000000000000000022011 00?0?0?0???300100000000101200?11020???0012011201000000??000??0????24
0????0?00?10100100?0?0000?????0000?0?110010?0??001?0000000101?????????????????????????????????????

??????????????????????????????12110???000001111?1?10011201000001011107?10?21??1??1?????????????????????
?1???????00?????????????????????

Docodonts

10000010?000000000000001101102100000 1??10010000000100120 0?11??0???0012002100000000??000??0????21
0????0?00150130100?0?00100???00000?0?11001001001?10000000000?????????????100????00?00?0100000????
?0?000?0?????????????1001201101200010000000111001???0102010000011011 0????2?021122110000007 1011111
10000000???10??010010??000100011010?00

Hadrocodium

1?101???300?10000?000000102??2?0?0?01??0?0?1100010?001100?12000???001?000000000000??000??0????200
????0?00?10100100?0?0000?????0000?0?1100?0?0??001?0000000???
??????????????????1100210101212????00000111?11021000211000001 0?11?????2??21122110010011112121 01?00
?21??11111??00?10??0???0??????????

Kuehneotherium

10000110?000000000000000?100101?0?01???13?0?0100000010?3120120200?0111101120101000000000000???0110
???00?0002001011100?0010000?01000?0?(0
1)1001??100101??00?00000???
??

Pseudotribos 1(1
3)0001110000?00000??0001?10010?0?0?11??3100100100111102211120100?0110101220001000000011000??20020
10100000030120211 00?011001000100 10(0
1)1100?1010010110000000?????????000000000010100000000001000????0?10?000?????????????????1????????????
??

Ambondro ???0??1?????????????????????????????????????0?0200011???21?131?11021?00011200
?100002114110100(1
2)1???????????301?0211?11?110?00???????0?1100????0010???00??0?????????????????????????????????????
??
??????????????????????????????

Ausktribosphenos 1010011121(0
1)0100010010?0?112012?????????3?01101210011??121?131021221?000012000200002114110211 23????????????50
1?0212???0110?11???????0?1100?????00???00?00???
??
????????????????????

Henosferus 1000011121(0
1)000002001000011211 2?0?0?1???3?001001000?00?122?131211021?00110001010000211411 0(1 2)(0
1)021???????????0301?0211?100110?00?01????0?1100?00???00??000000?01?????????????????????????????
??
??????????????1?????????????????????

Asfaltomylos 10000?11210??0002001010(0
1)112112???????????0???0100011??121?13??112?1?00110001110000211411 0(1
2)0021?????????????01?0211??00110?10??1????0?1100????0000???00000?????????????????????????????????
??
????????????????????????????????????

Bishops

10101111211010001001010111211 2???0?????3?01101210011??121?131021221?000012001100002114110211 23??????
??????501?0212???0110?11???????0?1100????0000???00?00???
??
??????????????????????????

Steropodon 1(0 1
2)?0101?????????????????????01?????????????????????0?????121?1311211?1?00101120020001220311 00??23???????
?????501?0212?210020?00???????0?1100????0011?0??0??0???
??
??????????????????????????

Teinolophos ??10111121001000200111011120 12?????????????????????221?1311211?1?00001120
12000(1
2)22031100??23????????????501?0212?210020?00???????0?1100??2?0011???????0?????????????????????????
??
??

Obdurodon ??10201031001100201110l?112111?1???2???0?00110200110011211?1311211?1?00101(0
1)200210?022031100??23010???????0?50140212?210(0
2)200100?100000?1200??2100113?00000002121???
0000111001212????000011111111210012010000000000?????2??2112211121?111012121111012?211??????1??0010??0
?????????????
Ornithorhynchus
10102?10?1111100201?111111?111?1???2???0????????0???011???1?????????0???1?200210??220?1100??23010????
???0050040???????(0
2)2??????100000?12001?21??0?30??00?1101??1101110000000010100000000010000001?11000002010000000021l
1110000101001212120000001111111121001201000000000002012?2112112211121?111012121111000211110111??0001
0??0111100111111?10
Gobiconodon
13101110???0?1102011011110100l?110111?120001?010000101200?12010???0111010001000?00??0000?0????210??
????000101001l0?0?00000?????020?01110001?0??001?0000000101?????00????1?21?1?1?1110000110000??00000
000100100?????????1100120110l2?10???000??1?1?11???????0?0??00????????????21??????0??1012001?0?1?0?
?01???????00???10??0?????????????
Amphilestes
13101110???1?110200?0?1110210??0?0?0??120001101000010?200?12010??00?11010001000?00??0000?0????2???
??????0?10100110?0?0000??????????0?1100???0??001?000000?????0???
??1?????????????????
??????????????????????????????
Jeholodens 1?10(1
2)?10?????110?0?100121010?1?010?11??010?10000000101200?12010???00110?0001?00000??000000????2(0
1)0??????00?10?00110?0?00000??00?0(0
2)0?011100?1?0??001?0000000?????0??10????112111??01110??0110100000?0000001000001?000010100?0012?11
0???(0
1)?1?????????????????????????????????122????1??????0??11???11??01?0??1???????????00?????????????????
Priacodon
11101010???1?110201100121011010?010?000?10000101010020120l?11110???00111000031l00?00??0000?0????210??
????11?10100100?0?00000??00?000?02110010?0??001?0000000101?????????????????????????110100?????????
??????????????????1?????????2110101000001111?11100??20??00??10121?????2??21???????????11???2?????????
??????00???10??010000011000100
Trioracodon 11101010???1?110201100121010011??010??120000101000020110l?11110???0011(0
1)00003100?00??0000?0????210??????11?10100100?0?00000??00?000?02110010?0??001?0000000?????????????
??0?????????????121101??000001111?1110011201?00??1012??????
2???1???????????11???????????1?1101110?????10??0???0??????????
Tinodon
10101110???0?11010??0111113111?0?0?1???10001001000010?212?120100?0110101120101000000010000??00110??
?00?00020010111?0?001010?001000?021100??01??001??00?00???
??
????????????????????????????
Peramus 1(1
2)10111141001100210100011121l2?0?010???3000011101001011210131201001100010001010(0
1)0001021110??01010?000000003011021111001101O?0011(0
1)01011100??01??00100000000???1??????????
??
Vincelestes 12102?11(1 4)1001100110101011121l(0
2)?1101000?000001010101101122013010100110010000001000010121000?0101110000?0003011021111001100000
010001021100?101??002100000101000111l?112111121111101111010011110000101110011101011001212??0?11002111
012121011111001111110211012120110011021?????21?110?11101000(0
1)12001211110??11??????001001000011010112111011
Kielantherium 1(1
2)1010114100?10011110?0??1311??????0???200001000?0000?22101302010111l00(0
1)1000101000011141l000?0100110000000030110212110112010000110010(0
1)1100??01??0021?00??0???
??

Deltatheridium
13102?113101110111010101313111?011100011000010101001012210131201011100110001110000111411110101021100
1)10000030120212210112010000110010111001001??00210000000100???
????????1211?12?????111?21111121222??111002123221???00212?000111021?????21?211110101??0112?1?200211??
1????0???001000?000?????????????
Asiatheriidae 13101?113101110111010101?1311(0
2)??11??00?10000101010010122111310012111001100111101002114111111130111022000003012021221011200100011
0010011100??01??00210000000???????101????11210111?21111120221111?0101?111111101????????2011102111112
122???111??2?2322????00?121??1111??1?????21?21111010???01???11200?????21??????????100?000???????????
??
Kokopellia
13?01?113??1?1??11110?????301??0?0?0???1?000101010011??2211131101211100110011110100211411111103021101200
0000030120212210112001000210010(0
1)11001001??0021?00?000???
??
Pucadelphys 13101?113101110111010111311(0
2)?011100011000010101001012211131001211100110011110100211411121113031102211000301202122101120010002
1001001100100?1??00210000000???111110112111121011112111112022111?1101111111110121111202?011102111112
1222??111002123221???00212100011102?????21?211110101110112011200211?210?????????1100?000???????????
???
Didelphis
12102?113101110111010111313011101110001111001010100101221113100121110011001111010021141112111303110201
1100030120212210112001000200010011001001?00210000000112111110112111121011112111112022111111101111
1111101211112020201110211111212222111110021232211???00212000111102111111212211110101110112001200211121
0011011121010?00011011112111112
Pappotherium ???0??1?????????????????????????????????0?010001000???2101310010111001100010
1?10000111411111002031100100000301202122101110110001100100110??01??0021??00000?????????????????????
??
??
Erinaceus
12102?111101110011010101313112110011?10000001100000111211130001211100110021010000211?1?11113111112
2000005014021221111200100010001021100110111103100000001121111101121111210111121111120221010101111111
2111122121110202011102111112122221111212123221?1100212011001102111111212211110101100112011210211122 1
0110111210100?11111011112111112
Asioryctes 1(1
2)102?111100110011010101313112?000100012000110100000101211130001011100110001210000111411111003021111
1200000301202122101120110001100100110010010000210000000???01111?????????????????????????0101??????
????10122?2111020?011102111112122???1121?2123221?1100212010001102?????21?211110101110112011210211??
110110111??0000?111?????????????
Prokennalestes 1(1
2)101011110011001111000131211 2?0?0?0???300011010000010121113000101110011000121000011141111100303111
110000?30120212210111011000110010011001?0100002100000001 00???????????????????????????????????????
????????????????????1????????12122211112012 12??21?110021??11??11021?????2???????????1????1?????????????
??????00???11000???1???2??????
Zhangheotheriids
12101010???0?110200101111110111?010111?111011001001010132201201 00?0110100120101000000000000???0020??
?00?000411201110 0?011000?001110001110111110010100000000????1100010101112111110111101(0
1)111100000001111011000011001211?2110012111012 11????111001?11?112100121200000 1?121?????21??1????1?0??
01???1???0111?????????????????000?????????????
Amphitheridae
101111114100110020010101112112?0?0?0???3?00010100010??321?13100100110011000101001001021110??01110??
?00?000401102111100110 10?00110000?1100??0???002000000000???
??
????????????????????????????
Henkelotherium 10111011110011002001010111301(0
2)10?010??1100000010101101321012100 0?0110010000001001000000000??00000???0000004012121110?012011?0

0101000211001000001020000000001000?????1????112111?1?11110?00111000??00111101110l0????1?????101?12?11
012121111?110(0 1)11(0 1)???121?002??011??110(1 2)?????????(1
2)1??????11?01?????????????????????0?0011?00?11011?12???011

Dryolestes
1011111111001100200101011130101000101?120000001010110132101210000?01100100000010010000000000??00000
???000000421212111O?012011?012010002111110000010200000000100?????????????????????????????111100??????
?????????????????????1?????????????11???
????????001???????11011?12???011

Laolestes 1011111111001100200101011130l(0
2)?0?010???2?000001010110132101210000?01100100000010010000000000??00000???000001421212111O?012111?11
211000211111110001020000000100???1?????????
??00?????????????????
?

Amblotherium 1011111111001100200101011130l(0
2)?0?010???200000010101107321012100?01100100000010010000000000??00000???000001421212111O?012011?0
011?000111111110001020000000???
??
?

Comotherium ???1?????????????0?????????????????????????????????3??012???????10???????
??0?????????????000???0000004??2121110??1??1??002100001111?1?10????200??0??0?????????????????????
??
??

Mesungulatum ??11??1????????0????0?????????????0?????2?1012?2011011210121000?01100002
020010001000000000??000(0
1)0???00?0?15112121110?0?1111?122011?021101??00111020???1100???
??
????????????????????????????????

Coloniatherium
11112?111101?10011010?????3102????1000?102110121200101121012100O?01100002020010001000000000-?00000?
??00?00151121211l0?011011?122011?0211011?001110201111100100???
??????????????????????????212201111(1
2)00111??1111010212?11?01112??????2?????????????????????????????????????00?????0001101?1?2111??2

Reigitherium
11112?1????1???011?10?????2112?????0???2?10111211002011210121000?0100010202001000200000000??00040??
?00?000521412101O?011001?122001?1211011?01112020?11?000???
??
????????????????????????????

Peligrotherium 10112?1111011100110101O?(1
3)13102??1?1000?102111121210201121012100O?01100002020010001000000000??00040???00?00151141211l0?01(1
2)011?122011?121101100011202011110O0?????????????????????????????10?????????0?????????????0??
0?0???1212201111001111(1 2)(1 2)21101011(1 2)?2?11?01112??????2??21?2??1?0??0012001?10(0 1)11?(1
2)11??0011?????1100001101???211???2

Groebertherium ???1???0??210121000?0110010101
0?1001000000010??00000???00?00(0 1)4212121110?0?2101?022111?0(0
1)1111???0011020????0???
??0?????????????????????

Leonardus ?(1 2)?12?1?????????????????????????????(1 2)?1?01101100201(1
2)210121000??1100100000020001000000?0????000???00?00142121211l0?0?2001?122001?021(1
2)31??10000?100000111???0???????????????
??

Foxraptor
00?11011???1???01??10??????10??0?0?0???1000111101001??2210131000?01?00100000(1
2)1001000020000??20????????????510?0211?0?0?20?1????0???0?1100?0????00??000?00?????????????????????
??
??

Paurodon 0?111111???0?1?01??10?????(2
3)11??0??10???0100011101011O?2210130000?0110010000001001000020010--

20??0?-???????4112021110?0?20?1???????00?1100???0??00??000?01??
???
????????????????????????????????????

Cronopio

10112?113101110010010011111101??1?1001?211001120100200121012100 0?0110010000002000100000000--00000?-
-
00?0004212121110?012011?002011?0200211110000000000111???
????????????????0001201111212201111 10(0 1)111??1011010212?11?01112??????21(0 2)01??0?100?100?????1?0(0
1)10??2????01?1??0011000011?11102111112

Drescheratherium ???????????????????????????????0??001?11???????????002??01????????10?????
??010????????????????000???00?001???2?2111??????1??11100000011????100?0?200??0??0?????????????????????
??1??
?????01???

Necrolestes 10112?11(2
3)1011100110101?1113112?001?000?11001010110020112201211 00?0110010000002000 10000-0-0----000?--
00?10042(0 1)2121110?-120?1?001001?020021?1100000000000011111(0
1)0?1?1?1??????1????1?2110010112011??0??111010??0?????????????0??0211111212211?1111?111??1011011212011
0011021??????1?111(1 2)101????001(1 2)12?110?0???211??01??0?00110000??01???2?????2

Spalacotherium

12101010???0?11020?10111112111?0??100??201010010011101321012010 0?011010012110100000000000???0000??
?00?0004(1
2)12121110?012000?001110?011101?01?0010100000?00???
???
?????????????????????

Hoovor1 ??
???
??1??11101011 00111??110?00110??00??1102??????????????????????
???????????????????????????????11000100100100

Hoovor2 ??
???
???1?01110101?00111??1000??????00??1102?????????????????????
?????????????????????????????????11000100110100

;
END;
begin mrbayes;

calibrate

Probainognathus=uniform(201,237) [Late Triassic ; PBDB]
Tritylodontids=uniform(201,237) [Late Triassic ; PBDB]
Tritheledontids=uniform(201,237) [Late Triassic ; PBDB]
Adelobasileus=uniform(227,337) [Carnian ; Keilan-Jaworowska et al., 2004]
Sinoconodon=uniform(190,199) [Sinemurian ; Keilan-Jaworowska et al., 2004]
Morganucodon=uniform(190,237) [Late Tr -Sinemurian ; Keilan-Jaworowska et al., 2004]
Megazostrodon=uniform(174,201) [Early Jurassic ; Keilan-Jaworowska et al., 2004]
Dinnetherium=uniform(174,201) [Early Jurassic ; Keilan-Jaworowska et al., 2004]
Docodonts=uniform(152,157) [Kimmerid for Haldanodon ; Keilan-Jaworowska et al., 2004]
Hadrocodium=uniform(174,201) [Early Jurassic ; Keilan-Jaworowska et al., 2004]
Kuehneotherium=uniform(174,237) [Late Triassic-Early J ; Keilan-Jaworowska et al., 2004]
Pseudotribos=uniform(164,174) [Middle Jurassic ; PBDB]
Ambondro=uniform(166,168) [Bathonian ; Keilan-Jaworowska et al., 2004]
Ausktribosphenos=uniform(113,125) [Aptian ; Keilan-Jaworowska et al., 2004]
Henosferus=uniform(174,183) [Toarcian ; Cuneo et al., 2013]
Asfaltomylos=uniform(174,183) [Toarcian ; Cuneo et al., 2013]
Bishops=uniform(113,125) [Aptian ; Keilan-Jaworowska et al., 2004]

Steropodon=uniform(100,113) [Albian ; Keilan-Jaworowska et al., 2004]
Teinolophos=uniform(113,125) [Aptian ; Keilan-Jaworowska et al., 2004]
Obdurodon=uniform(23,28) [Chattian, for O.insignis ; PBDB]
Ornithorhynchus=fixed(0)
Gobiconodon=uniform(100,140) [Valanginian-Albian ; Keilan-Jaworowska et al., 2004]
Amphilestes=uniform(166,168) [Bathonian ; Keilan-Jaworowska et al., 2004]
Jeholodens=uniform(125,129) [Barremian ; Keilan-Jaworowska et al., 2004]
Priacodon=uniform(145,157) [Kimmeridgian-Tithonian ; Rougier et al., 1996]
Trioracodon=uniform(145,157) [Kimmeridgian-Tithonian ; Keilan-Jaworowska et al., 2004]
Tinodon=uniform(100,163) [Late Jurassic-Early K ; Keilan-Jaworowska et al., 2004]
Peramus=uniform(100,145) [Early Cretaceous ; Keilan-Jaworowska et al., 2004]
Vincelestes=uniform(130,133) [Hauterivian ; Keilan-Jaworowska et al., 2004]
Kielantherium=uniform(100,125) [Aptian-Albian ; Keilan-Jaworowska et al., 2004]
Deltatheridium=uniform(72,84) [Campanian ; Keilan-Jaworowska et al., 2004]
Asiatherium=uniform(72,84) [Campanian ; Keilan-Jaworowska et al., 2004]
Kokopellia=uniform(94,113) [Aptian-Cenomanian ; Keilan-Jaworowska et al., 2004]
Pucadelphys=uniform(56,66) [Early Paleocene ; PBDB]
Didelphis=fixed(0)
Pappotherium=uniform(100,125) [Aptian-Albian ; Keilan-Jaworowska et al., 2004]
Erinaceus=fixed(0)
Asioryctes=uniform(72,84) [Campanian ; Keilan-Jaworowska et al., 2004]
Prokennalestes=uniform(100,125) [Aptian-Albian ; Keilan-Jaworowska et al., 2004]
Zhangheotheriids=uniform(100,145) [Early Cretaceous ; Keilan-Jaworowska et al., 2004]
Amphitheridae=uniform(164,174) [Middle Jurassic ; Keilan-Jaworowska et al., 2004]
Henkelotherium=uniform(152,157) [Kimmeridgian ; Keilan-Jaworowska et al., 2004]
Dryolestes=uniform(145,164) [Late Jurassic ; Keilan-Jaworowska et al., 2004]
Laolestes=uniform(133,157) [Kimmeridgian-Valanginian ; Keilan-Jaworowska et al., 2004]
Amblotherium=uniform(140,157) [Kimmerid-Berri ; Keilan-Jaworowska et al., 2004]
Comotherium=uniform(152,157) [Kimmeridgian ; Keilan-Jaworowska et al., 2004]
Mesungulatum=uniform(66,84) [Campanian-Maastrichtian ; Keilan-Jaworowska et al., 2004]
Coloniatherium=uniform(66,84) [Campanian-Maastrichtian ; Rougier et al., 2009]
Reigitherium=uniform(66,84) [Campanian-Maastrichtian ; Bonaparte, 1990]
Peligrotherium=uniform(56,66) [Early Paleocene ; Paez-Arango, 2008]
Groebertherium=uniform(66,84) [Campanian-Maastrichtian; Keilan-Jaworowska et al., 2004]
Leonardus=uniform(66,84) [Campanian-Maastrichtian ; Keilan-Jaworowska et al., 2004]
Foxraptor=uniform(145,157) [Kimmeridgian-Tithonian ; Keilan-Jaworowska et al., 2004]
Paurodon=uniform(145,157) [Kimmeridgian-Tithonian ; Keilan-Jaworowska et al., 2004]
Cronopio=uniform(94,100) [Cenomanian ; Rougier et al., 2011]
Drescheratherium=uniform(152,157) [Kimmeridgian ; Keilan-Jaworowska et al., 2004]
Necrolestes=uniform(14,23) [Aquit-Langh; ~Santacrucian Rougier et al., 2012]
Spalacotherium=uniform(100,145) [Early Cretaceous ; Keilan-Jaworowska et al., 2004]
Hoovor1=uniform(100,125) [Aptian-Albian ; Wible et al., 1995]
Hoovor2=uniform(100,125) [Aptian-Albian ; Rougier et al., 2016]
;

charset multi = 2 5 9 17 22 24 25 27 30 36 40 42 47 49 52 55-57 60 62 63 65 66 70 73-78 82-84 86 90 93-96 100 101 107 108 110 112 114-116 119 120 126 127 129 133 135 136 140 144 146 155 157 166 171 178 184 186 187 201 206 207 209 212 214 216 222 228 230-232 237 240 242-245 247 252 254 263 265 268-270 272-273 276 277 281 287 289 291 294 298 299 308 310 325 331;

charset asymbin = 1 3 4 6-8 10-16 18-21 23 26 28 29 31-35 37-39 41 43-46 48 50 51 53 54 58 59 61 64 67-69 71 72 79-81 85 87-89 91 92 97-99 102-106 109 111 113 117 118 121-125 128 130-132 134 137-139 141-143 145 147-154 156 158-165 167-170 172-177 179-183 185 188-200 202-205 208 210 211 213 215 217-221 223-227 229 233-236 238 239 241 246 248-251 253 255-262 264 266 267 271 274-275 278-280 282-286 288 290 292 293 295-297 300-307 309 311-324 326-330;

ctype ordered: 2 5 27 40 42 49 56 57 65 78 82 83 93 100 101 114 115 120 126 135 136 144 146 178 184 186 187 201 207 209 228 230 231 237 240 242 244 273 276 277 281 287 289 308; [from Rougier et al 2011, but renumbered from omeara et al 2014, eg no 127 no of molarif postcanines; 130 lower molarif roots is binary]

constraint eutheria_monophyly 100=Erinaceus Asioryctes Prokennalestes;

constraint metatheria_monophyly 100=Deltatheridium Asiatherium Kokopellia Pucadelphys Didelphis;

constraint theria_monophyly 100=Deltatheridium Asiatherium Kokopellia Pucadelphys Didelphis Pappotherium Erinaceus Asioryctes Prokennalestes;

constraint trechnotheria_monophyly 100=Tinodon Peramus Vincelestes Kielantherium Deltatheridium Asiatherium Kokopellia Pucadelphys Didelphis Pappotherium Erinaceus Asioryctes Prokennalestes Zhangheotheriids Amphitheridae Henkelotherium Dryolestes Laolestes Amblotherium Comotherium Mesungulatum Coloniatherium Reigitherium Peligrotherium Groebertherium Leonardus Foxraptor Paurodon Cronopio Drescheratherium Necrolestes Spalacotherium Hoovor1 Hoovor2;

constraint theriimorpha_monophyly 100=Gobiconodon Amphilestes Jeholodens Priacodon Trioracodon Tinodon Peramus Vincelestes Kielantherium Deltatheridium Asiatherium Kokopellia Pucadelphys Didelphis Pappotherium Erinaceus Asioryctes Prokennalestes Zhangheotheriids Amphitheridae Henkelotherium Dryolestes Laolestes Amblotherium Comotherium Mesungulatum Coloniatherium Reigitherium Peligrotherium Groebertherium Leonardus Foxraptor Paurodon Cronopio Drescheratherium Necrolestes Spalacotherium Hoovor1 Hoovor2;

constraint australosphenida_monophyly 100=Ambondro Ausktribosphenos Henosferus Asfaltomylos Bishops Steropodon Teinolophos Obdurodon Ornithorhynchus;

constraint dryolestoid_monophyly 100=Henkelotherium Dryolestes Laolestes Amblotherium Comotherium Mesungulatum Coloniatherium Reigitherium Peligrotherium Groebertherium Leonardus Foxraptor Paurodon Cronopio Drescheratherium Necrolestes;

constraint hadro_and_crown_monophyly 100=Hadrocodium Kuehneotherium Pseudotribos Ambondro Ausktribosphenos Henosferus Asfaltomylos Bishops Steropodon Teinolophos Obdurodon Ornithorhynchus Gobiconodon Amphilestes Jeholodens Priacodon Trioracodon Tinodon Peramus Vincelestes Kielantherium Deltatheridium Asiatherium Kokopellia Pucadelphys Didelphis Pappotherium Erinaceus Asioryctes Prokennalestes Zhangheotheriids Amphitheridae Henkelotherium Dryolestes Laolestes Amblotherium Comotherium Mesungulatum Coloniatherium Reigitherium Peligrotherium Groebertherium Leonardus Foxraptor Paurodon Cronopio Drescheratherium Necrolestes Spalacotherium Hoovor1 Hoovor2;

constraint mammaliaformes_monophyly 100=Adelobasileus Sinoconodon Morganucodon Megazostrodon Dinnetherium Docodonts Hadrocodium Kuehneotherium Pseudotribos Ambondro Ausktribosphenos Henosferus Asfaltomylos Bishops Steropodon Teinolophos Obdurodon Ornithorhynchus Gobiconodon Amphilestes Jeholodens Priacodon Trioracodon Tinodon Peramus Vincelestes Kielantherium Deltatheridium Asiatherium Kokopellia Pucadelphys Didelphis Pappotherium Erinaceus Asioryctes Prokennalestes Zhangheotheriids Amphitheridae Henkelotherium Dryolestes Laolestes Amblotherium Comotherium Mesungulatum Coloniatherium Reigitherium Peligrotherium Groebertherium Leonardus Foxraptor Paurodon Cronopio Drescheratherium Necrolestes Spalacotherium Hoovor1 Hoovor2;

```
partition all= 2:multi,asymbin;
set partition=all;

        lset applyto=(1) coding=variable rates=gamma;
    lset applyto=(2) coding=variable rates=gamma;

        unlink statefreq=(all) revmat=(all) shape=(all) pinvar=(all) tratio=(all);

        prset brlenspr = clock:fossilization;
        prset speciationpr = exp(10);
        prset extinctionpr = beta(1,1);
        prset fossilizationpr = beta(1,1);
        prset sampleprob = 0.00006; [5000 living species, 3 sampled]
        prset samplestrat = diversity;
        prset treeagepr = uniform(201,252); [Triassic origin of Probaingnathia ]
        prset clockvarpr=igr;
        prset igrvarpr=exp(10);
        prset clockratepr=lognorm(-5.521461,1.00400801); [derived from 1 change in tree height,in
logn distributuion 250. eg lognormal(ln(1/250), e^(1/250))]
        prset applyto=(all) ratepr=variable;



    calibrate theria_monophyly = offsetexponential(145,151); [calculated mean for 95% of the offset
exponential probability in late Jurassic for Juramaia]

    prset topologypr = constraints(eutheria_monophyly, metatheria_monophyly, theria_monophyly,
dryolestoid_monophyly, trechnotheria_monophyly, theriimorpha_monophyly,
australosphenida_monophyly, hadro_and_crown_monophyly, mammaliaformes_monophyly);
    prset nodeagepr = calibrated;


mcmcp temp=0.15 nruns=4 nchains=4 ngen=60000000 samplefr=5000 printfr=10000;
mcmc;

sump;
sumt contype=allcompat;

end;
```

5 Summary

The content of the preceding chapters is designed to be comprehensive and self-contained with respect to the specific aspects of craniodental morphology covered in each section. Introductions to the problems, approaches, and results covered in each of these sections can be found in the introductory material for each chapter, and in the introductory front-matter for this dissertation. The focus of this summary section is to provide a synthetic review of several tentative inferences and implications for future research that can be gathered from a holistic view of all three chapters together, and to provide recommendations for future studies of craniodental adaptation and homoplasy. These thoughts can be roughly organized into three themes centered on the methods, anatomy, and taxa described in the previous chapters.

The value of "high-level" and "homology-free" descriptors of dental morphology

The analyses of molariform morphology presented in chapters 1 and 3 demonstrate the usefulness of Dental Topography Analysis (DTA, as implemented in the R package MolaR; Pampush, 2016; Pampush et al., 2019) and spherical harmonic registration (as implemented in the MATLAB package SPHARM; Shen et al., 2009) for the quantitative study of Mesozoic mammalian dentitions generally. This is unsurprising given the fact that these shape descriptors are agnostic to, and therefore work with, any triangularized surfaces irrespective of the living or extinct status of the specimen they are generated from. In the case of DTA, the main challenge for this dissertation comes with interpretating the output of these algorithms as ecometrics (Evans, 2013); i.e., as autecological descriptors for extinct

taxa outside of the phylogenetic bracket of all extant tooth-bearing mammals. As emphasized in Boyer (2008), Bun et al. (2011); Pineda-Munoz and Alroy (2014); Pineda-Munoz et al. (2017); inter alios, dietary-preference categorizations based on shape descriptors in extinct forms require abundant statistical control from empirical correlations of these metrics with the feeding habits observed in comparable and closely related extant species. Often the precise relationship between a DTA variable, such as Relief Index (Boyer, 2008), Orientation Patch Count (Evans et al., 2007), and Dirichlet Normal Energy (Bun et al., 2011), and dietary-preference-group shows taxon-specific effects which must be included as factors in discriminate function analyses of diet in extinct taxa (Evans et al., 2007, Bun et al., 2011). For most groups of Mesozoic mammals these taxon-specific effects will forever remain indiscernible, because of the lack closely related or even analogous living representatives. The unique crown shapes, occlusal relationships, and mandibular articulations seen in early mammaliaforms give strong reasons to suspect that the mechanics of mastication in these early forms would be drastically different from that seen in even the most plesiomorphic living therians (Crompton and Hiiemae, 1970; Hiiemae, 1985); thus blurring the significance of DTA for the reconstruction feeding strategy. However, even with these empirical limitations, the macroevolutionary analysis and ancestral reconstruction of these DTA metrics as continuous morphological traits does provide an interesting perspective on the origin and diversity of broadly construed mammalian feeding categories (e.g. Wilson et al., 2012; Conith et al., 2016; Chen et al., 2019). For instance, the relative appropriateness of early mammalian molariforms for "stress-limited defenses" versus "displacement-limited defenses" in food material properties (Lucas, 2004) could reasonably be gauged through the comparison of RI, DNE, and similar metrics.

The application of SPHARM analysis to Mesozoic dental remains is fortunately not limited by the lack of comparable living representatives. And, as the analysis in Chapter 3 shows, the ability of SPHARM to simultaneously accommodate triconodont and symmetrodont morphologies not seen in modern taxa is a great advantage of this method relative to classical and landmark-based morphometric methods. For example, aside from the the possible placement of type-2 landmarks on the apices of the protoconid/cusp "a" and metaconid/cusp "c", only the poorest quality (type-3) landmarks would be able to be consistently located on all sampled molariforms. The use of redundantly registered, or "degenerate," landmarks would also be possible for several structures such as the "amphiconid" in *Reigitherium* which may represent a connate paraconid and metaconid (Rougier et al., 2012). This small set of possible landmarks precludes the useful application of "homology-based" morphometric methods, where a strict relationship between measured quantity (distances, angles, or coordinates) and anatomical structure must be defined a priori. The large amount of qualitative variation in the sampled molariforms used in Chapter 3 therefore necessitates the use of "homology-free" (Polly, 2008) morphometric protocols, wherein no fixed association between the information digitized and underlying anatomy is required. The most common of these methods is the sliding semilandmark approach outlined in Gunz et al. (2005); where the geometric information of a semilandmark's position parallel to a linear curve, or two-dimensional sheet, is discarded, and allowed to "slide" toward a sample-defined global optima according to an arbitrarily selected criterion (Procrustes Distance or Bending Energy). The problem here comes with the difficulty of defining diagnostic curves (e.g., crests, cingulids, tissue boundaries) and surfaces which would be consistently present in a wide sample of early mammaliaformes; where major lower molariform features (such as the paracristid, protocristid, trigonid basin, talonid, talonid

basin, cristid obliqua, postcristid, entocristid, cingulids, paraconid and accessory cuspulids, etc.) are all variably present. Therefore, the required definition of sets of semilandmarks with respect to "typical" landmarks, in addition to the requirement that all sampled surfaces contain the same number of registration points (landmarks and semilandmarks), vitiates the effectiveness of semilandmark analysis in samples as disparate as the molariforms of early mammaliaforms. It is unknown how useful the newly automated "pseudolandmark" method described in Boyer et al. (2015a) would be at relaxing these requirements; however, this is an interesting approach deserving of further investigation.

The SPHARM protocol described in Chapter 3 is shown to be a highly flexible approach for the registration of the molariforms sampled, eliciting a much wider morphospace of possible crown surfaces than the more traditional methods described above. The results of this analysis show that the inconsistent presence of cusps (such as the absent paraconid in *Reigitherium* and monotremes), crests (e.g. the protocristid in most taxa), surfaces (e.g., the lack of talonid basins in non-tribosphenic taxa), and even large regions (e.g., the lack of a talonid altogether in "triconodonts") can be accommodated within the SPHARM Fourier-based morphospace. This is not to say that all this molariform variation can be accommodated well, and as mentioned in Chapter 3 the reconstruction of particularly sharp features such as cingulids, crests, and the apices of cusps is not realistically handled using only the first five principal components of Fourier-space shape variation generated by this approach. The term "homology free" in Fourier-based analyses such as this is also potentially misleading because of the implicit assumptions of biological correspondence required for the standardization and orientation of the sampled surfaces (Klingenberg, 2008). For SPHARM in particular, the required topological correspondence of all sampled shapes with a closed (genus-zero) spherical parameter space entails implicit homology

assumptions regarding the connectivity of the objects analyzed. In the case of the molariform dentition the "closure" of the free edges of cropped crown surfaces to meet this requirement may also limit the applicability of SPHARM to the complete range of molariform variation seen in nature. For example, points in morphospace with considerable topographic variation within the artificially closed region of a molariform surface have no biological significance, creating "dead-zones" where sampled and reconstructed molariforms should not occupy, or cross during their evolutionary or developmental trajectories. These required topological assumptions cause individual geometries (shapes) to be treated as instantiations of their corresponding abstract topology. For SPHARM the linear (shortest) distance between two empirically sampled instantiations of a spherical topology are calculated regardless of whether these samples, or the geometries occupying the intervening space between these two samples, is biologically reasonable or not. The analyses of molariform shape described in Chapter 3 produced no sampled or reconstructed molariform surfaces with significant shape variation within the artificially closed-off bottom region; however, currently not enough is known about the morphospaces elicited by SPHARM to be sure if this will be a source of problems for future studies (McPeek, 2009).

The variables manipulated in both DTA (OPC, RI, DNE, etc.; Pampush et al., 2019) and SPHARM quantify abstract characteristics of shape beyond measured geometry (Evans, 2013). By discarding the originally digitized coordinate information encoded by their input, these methods trade precise positional information about the transformed point values used to represent a sampled surface for information that is hopefully more biologically interpretable. This naturally raises questions regarding the level of mutual information attainable between the two approaches, or more specifically, how precisely can reconstructed SPHARM surfaces reflect original DTA measurements. While this question has not been

addressed by previous studies, and the inability of SPHARM to realistically reconstruct sharper features on a crown surface gives some cause to be pessimistic, the potential covariance between DTA and SPHARM variables could assist in ancestral reconstructions of molariform shape such as those provided in Chapter 3. This is not to suggest that tooth surfaces regenerated from best-fit spherical harmonic coefficients would accurately reflect the value of DTA variables measured from original surface scans, but through use of spherical harmonic coefficients of increasing degree some consistent offset may be found between DTA variables measured from the original surface and its SPHARM reconstruction. Other research projects which could unlock the ecometric and morphometric value of unworn crown surfaces in early mammaliaforms could be to use the SPHARM-MAT (Shen, 2010) and SPHARM-PDM (Styner et al., 2006; Gao et al., 2014) implementations for spherical harmonic analysis, and the measurement of additional DTA metrics such as shearing quotient (Hogue and ZiaShakeri, 2010; Boyer et al., 2015b) in Mesozoic groups. Finally, further research into the large-scale patterns of serial homology across mammaliaform groups with widely varying dental formulas, and the accession of surface information from rare and important Mesozoic specimens into online public repositories (such as morphosource.org), would provide the greatest contribution toward reducing the most important sources of statistical error for future analyses of crown morphology in Mesozoic mammaliaforms.

Function and homoplasy in early mammalian cochleae

The otic capsule serves as a "developmental craton" throughout the evolutionary history of the mammalian skull. Appearing early in development, the mesenchymal housing of the

primordial otocyst suppresses the development of adjacent somitomeres and quickly gains prominence within the initiating cranium (Moore 1981). During its subsequent ossification, the otic capsule bears the impressions of many of the embryonic and adult structures it forms amongst, making the periotic skeleton one of the most phylogenetically and functionally informative structures available in the fossil record (Mason, 2016; Luo et al., 2016).

Chapters 2 and 3 of this dissertation take advantage of the information-dense morphology of the internal and external surfaces of the petrosal bone to address several hypotheses regarding the evolution of the mammalian ear. Based on the descriptions and analysis provided, questions such as "can complex structures be expected to show less homoplasy than simple ones?" (Luo and Martin, 2005), or "do important adaptations appear synchronously with the emergence of major mammalian clades?" (Luo, 2007) can both be answered with a resounding no, for the case of the mammalian inner ear.

The lack of strong phylogenetic signal seen in the 14 updated inner ear characters used in the phylogenetic estimations described in Chapter 3 may be an inevitable byproduct of increased character conflict caused by the better characterization of incompletely preserved fossil taxa. As discussed in Chapter 2, the fact that the cochlear canal in the earliest stem therians appears to have lost the lateral curvature and terminal inflation present in earlist stem mammaliaforms, and the convergent appearance of fully coiled cochleae in therians and meridiolestidans, point to the evolutionarily labile nature of the complex cochlear endocast.

The plesiomorphic appearance of the earliest stem therian cochlear endocasts is surprising given the hypothesized necessity for small-bodied mammals to utilize high-frequencies for precise sound source localization (Heffner and Heffner, 1992). For reasons

outlined in Chapter 2, the lack of primary bony lamina and the short cochlear length seen in the stem therians described in this dissertation suggest that the selective pressure for high-frequency perception was not as critical to the autecological strategy of early mammals as it is to most small therians today. This may reflect the more ambulatory and/or diurnal habits of the earliest mammals, where rapid and precise sound localization would be less advantageous relative to other sensory modalities. Conversely, the convergent appearance of complex internal armatures and spiral morphology within the cochleae of both therians and meridiolestidans may be an indication of the wider capacity of cladotherian mammals to adapt to novel high-frequency niches appearing within the Late Jurassic and Early Cretaceous. Possible future research trajectories which may help elucidate the nature of cochlear evolution during the Mesozoic would be to test the possible competition for space among venous sinuses and cochlear contents within the pars cochlearis (Luo, 1995), through the use of volumetric measurements and the description of petrosal remains from the earliest mammals outside of the stem therian lineage (e.g., australosphenidans and early monotremes; Musser, 2003).

The fossil evidence summarized in Chapter 2 also provides a valuable constraint on estimates of frequency sensitivity in ancestral mammals produced by the neurobiological literature. These prior estimates, based on the geometrical (e.g., ideal transformer model; Fleischer 1978; Mason 2016) and/or material properties of the middle ear and empirical correlations among extant model organisms (Rosowski, 1992), have typically produced unrealistically high upper frequency estimates. One particularly influential instance of this is the statement in (Masterson, 1969): "the results show that high frequency hearing [above 32 kHz] is a characteristic unique to mammals and, among members of this class one which is commonplace and primitive". Based on the morphology of the early crown mammalian

fossils described here, and the auditory performance of living monotremes (Ashwell 2013), this statement is obviously false (see also Manley, 2012 for other criticism of this paper). A later and more paleontologically informed report by Rosowski and Graybeal (1991) provides a similarly high estimated upper frequency limit, extrapolated from the observed negative correlation between length of the basilar membrane and upper detectable frequency in a sample of extant therians.

While the low high-frequency limitations of early mammals suggested by the fossil record and comparative hearing research summarized above are suggestive, more basic research (including investigations of the possible presence and strength of the endolymphatic potential in modern monotremes; Manley 2017) is required before inferences on the performance and phylogenetic context of complex features of therian cochlear physiology (such as the endolymphatic potential) in ancestral mammals can be usefully understood. The evolution and development of complex abneural structures within the mammalian cochlea is however an excellent field of inquiry which stands to benefit from paleontological, neurobiological, and molecular input. This research trajectory has a unique potential to return societal dividends through the illumination of several of the most common causes of age-related hearing loss. Diseases such as metabolic presbycussis (Schuknecht et al., 1974), are a likely byproduct of the relatively recent evolutionary construction of the stria vascularis, and the propensity of more recently acquired traits to be particularly liable to pathology (Nesse and Williams, 1994).

Window into Western Gondwana

Prior to the Late Jurassic-Early Cretaceous opening of the South Atlantic, the South American landmass represented the western extent of a wider Gondwanan biogeographic region (Rougier et al., 2011). Because of the likely appearance of most major crown mammalian lineages earlier in the Jurassic (Kielan-Jaworowska, 2004), the Mesozoic mammals of South America have a unique potential for determining the relative importance of vicariance versus dispersal during the initial diversification of Mammalia. The presence of South American australosphenidans, "eutriconodontans" and haramiyidans within the Jurassic, and dryolestoids (including meridiolestidans), allotheres (multituberculates and gondwanatheres) and *Vincelestes* within the Cretaceous, show that the diversity of Mesozoic lineages in this region was comparable to that seen in North America, Asia, or any other continental province. A complete and accurate understanding of the phylogenetic relationships linking these Jurassic and Cretaceous groups with each other, and with better known holarctic groups, is therefore a necessary prerequisite for any macroevolutionary study of mammalian trait evolution. As the phylogenetic analyses presented in Chapter 3 show, the goal of a fully resolved global phylogeny of Mesozoic mammals will require much wider character and taxon sampling than is currently available in published datasets. The reduced resolution provided by the 14 additional characters of the labyrinthine endocast used in this dissertation also suggests that a redoubled effort to populate currently missing character information, rather than the addition of new characters, would be the most useful strategy for overcoming the topological ambiguities caused by existing character conflicts.

Biogeographic reconstructions contingent on a well supported phylogeny of global mammalian diversity include the originally "Pangean" or holarctic distribution of Zatherian/prototribosphenidan mammals such as *Peramus* and *Vincelestes*; the possible relationships between Southern and Northern tribosphenic mammals (Rich et al., 2002;

Rowe, 2008); and the hypothesized descent of South American endemic meridiolestidans from the Late Cretaceous holarctic radiation of spalacotheres (Averianov et al., 2013). In addition to these systematic issues, further research into the "evolutionarily precocial" nature of South American mammal faunas, and their possible relation to the early diversification of angiosperms, would provide a valuable reference with which to compare the ecological expansion of mammals in the Northern Hemisphere. As the description of the highly complex dentition in *Reigitherium* shows, mammals in the Southern Hemisphere attained a higher level of herbivorous adaptation than their contemporaneous "pretribosphenic" or "symmetrodont" relatives in the Northern Hemisphere (also see Chen et al., 2019). Future sampling and analyses of the alpha-level taxonomy of the La Colonia fauna, which yielded the new specimens of *Reigitherium* described here, would provide better insight into the environmental significance of these herbivorous adaptations.

6 Bibliography for Introduction and Summary

Archibald J.D., and A. O. Averianov. 2012. Phylogenetic analysis, taxonomic revision, and dental ontogeny of the Cretaceous Zhelestidae (Mammalia: Eutheria). Zoololgical Journal of the Linnean Socociety 164:361–426.

Ashwell, K. W. 2013. Auditory and vestibular systems; pp. 219–233 in K. Ashwell (ed.), Neurobiology of Monotremes. CSIRO Publishing, Collingwood, Australia.

Axelsson A. 1988. Comparative anatomy of cochlear blood vessels. American Journal of Otolaryngology 9:278–145.

Baker, J., A. Meade, M. Pagel, M., and C. Venditti. 2015. Adaptive evolution toward larger size in mammals. Proceedings of the National Academy of Sciences 112:5093–5098.

Bonaparte, J. F., New Late Cretaceous mammals from the Los Alamitos Formation, northern Patagonia. Geographic Research 6:63–93.

Boyer, D. M., J. Winchester, and R. F. Kay. 2015. The effect of differences in methodology among some recent applications of shearing quotients. American Journal of Physical Anthropology 156:166–178.

Chen, M., C. A. E. Strömberg, and G. P. Wilson. 2019. Assembly of modern mammal community structure driven by Late Cretaceous dental evolution, rise of flowering plants, and dinosaur demise. Proceedings of the National Academy of Sciences 116:9931–9940.

Clauset, A., and S. Redner. 2009. Evolutionary model of species body mass diversification. Physical Review Letters, 102:1–4.

Clavel, J, G. Escarguel, and G. Merceron. 2015. mvMORPH: an R package for fitting multivariate evolutionary models to morphometric data. Methods in Ecology and Evolution 6:1311–1319.

Conith, A. J., M. J. Imburgia, A. J. Crosby, and E. R. Dumont. 2016. The functional significance of morphological changes in the dentitions of early mammals. Journal of the Royal Society Interface 13:1–7.

Cooper, N., and A. Purvis. 2010. Body size evolution in mammals: complexity in tempo and mode. American Naturalist 175:727-738.

Crompton, A. W., and K. Hiiemae. 1970. Molar occlusion and mandibular movements during occlusion in the American opossum, Didelphis marsupialis L. Zoological Journal of the Linnean Society 49:21–47.

Evans, A. R., G. P. Wilson, M. Fortelius, and J. Jernvall. 2007. High-level similiarity of dentitions in carnivorans and rodents. Nature 445:78–81.

Evans, A. R. 2013. Shape descriptors as ecometrics in dental ecology. Hystrix 24:133–140.

Fleischer, G. 1978. Evolutionary principals of the mammalian middle ear. Advances in Anatomy, Embryology, and Cell Biology 55:5–70.

Gao, Y., T. Riklin-Raviv, and S. Bouix. 2014. Shape analysis, a field in need of careful validation. Human Brain Mapping 35:4965-4978.

Gunz, P., P. Mitteroecker, and F. L. Bookstein. 2005. Semilandmarks in three dimensions; pp. 73–98 In D. E. Slice (ed.) Modern Morphometrics in Physical Anthropology. Springer, Boston, Massachusetts.

Heffner, R. S., and H. E. Heffner. 1992. Evolution of sound localization in mammals; pp. 691-715 In D. B. Webster, R. R. Fay, A. N. Popper (eds.), The Evolutionary Biology of Hearing. Springer-Verlag, New York, New York.

Hiiemae, K. 1985. Mastication, food transport and swallowing; pp. 262–290 In M. Hildebrand, D.M. Bramble, K. F. Liem, D. B. Wake (eds.), Functional Vertebrate morphology. Belknap Press, Cambridge, Masschusetts.

Hogue, A. S., and S. ZiaShakeri. 2010. Molar crests and body mass as dietary indicators in marsupials. Australian Journal of Zoology 58:56–68.

Kielan-Jaworowska, Z., R. L. Cifelli, and Z. X. Luo. 2004. Mammals From The Age of Dinosaurs: Origins, Evolution, and Structure. University of Colombia Press, New York, New York, 630 pp.

Klingenberg, C. P. 2008. Novelty and "homology-free" morphometrics: whats in a name?. Evolutionary Biology 35:186–190.

Luo, Z. X. 2007. Transformation and diversification in early mammal evolution. Nature 450:1011–1019.

Luo Z.X, J. A. Schultz, and E. G. Ekdale. 2016. Evolution of the middle and inner ears of mammaliaformes: the approach to mammals; pp. 139–174 in J. A. Clack, R.R. Fay, A. N. Popper (eds), Evolution of the Vertebrate Ear: Evidence from the Fossil Record, Springer, Cham, Germany.

Manley, G. A. 2012. Evolutionary paths to mammalian cochleae. Journal of the Association for Research in Otolaryngology 13:733–743.

Manley, G. A. 2017. The mammalian Cretaceous cochlear revolution. Hearing Research 352:23–29.

Manley, G. A. 2018. The foundataions of high-frequency hearing in early mammals. Journal of Mammalian Evolution 25:155–163.

Masterson, B. H. Heffner, and R. Ravizza. 1969. The evolution of human hearing. Journal of the Acoustical Society of America 45:966–985.

Mason, M. J. 2016. Structure and function of the mammalian middle ear II: inferring structure from function. Journal of Anatomy 228:300–312.

Martin, T., and Z. X. Luo. 2005. Homoplasy in the mammalian ear. Science 307:861–862.

Martin, T., F. Goin, L. Chornogubsky, J. Gelfo, and J. Schultz. 2013. Early Late Cretaceous (Cenomanian) mammals and other vertebrates from the Mata Amarilla Formation of southern Patagonia (Argentina). Society of Vertebrate Paleontology Annual Meeting Abstracts.

Meng, J., Y. Hu, Y. Wang, and C. Li. 2003. The ossified Meckel's cartilage and internal groove in Mesozoic mammaliaforms: implications to origin of the definitive mammalian middle ear. Zoological Journal of the Linnean Society, 138:431–448.

Mitchell, J. S.2015. Extant-only comparative methods fail to recover the disparity preserved in the bird fossil record. Evolution 69:2414–2424.

Musser, A. M. 2003. Review of the monotreme fossil record and comparison of palaeontological and molecular data. Comparative Biochemistry and Physiology Part A: Molecular & Integrative Physiology 136:927–942.

Nesse, R. M., and G. C. Williams. 1994. Why We Get Sick: The New Science of Darwinian medicine. Vintage Books, New York, New York, 298 pp.

Oxnard, C. and O'Higgins, P. 2009. Biology clearly needs morphometrics. Does morphometrics need biology?. Biological Theory 4:84–97.

Paez-Arango, N. 2008. Dental and craniomandibular anatomy of *Peligrotherium tropicalis*: the evolutionary radiation of South American dryolestoid mammals. M.S. thesis, University of Louisville, Louisville, Kentucky, 107 pp.

Pampush, J. D., J. M. Winchester, P. E. Morse, A. Q. Vining, D. M. Boyer, and R. F. Kay. Introducing molaR: a ner R package for quantitative topographic analysis of teeth (and other topographic surfaces). Journal of Mammalian Evolution 23:397–412.

Pampush, J. D., J. K. Cromwell, A. Karme, S. A. Macrae, R. F. Kay, and P. S. Ungar. 2019. Comparing dental topography software using platyrrhine molars. American Journal of Physical Anthropology 169:179–185.

Pascual R., F. J. Goin, P. González, A. Ardolino, and P. F. Puerta. 2000. A highly derived docodont from the Patagonian Late Cretaceous: evolutionary implications for Gondwanan mammals. Geodiversitas 22:395–414.

Pineda-Munoz, S., and J. Alroy. 2014. Dietary characterization of terrestrial mammals. Proceedings of the Royal Society B 281:1–7

Pineda-Munoz, S., Lazagabaster, I. A., Alroy, J., & Evans, A. R. (2017). Inferring diet from dental morphology in terrestrial mammals. Methods in Ecology and Evolution 8:481–491.

Polly, P. D. 2004. On the simulation of the evolution of morphological shape: multivariate shape under selection and drift. Palaeontologia Electronica 7:1–28.

Polly, P. D., S. C. Le Comber, and T. M. Burland. 2005. On the occlusal fit of tribosphenic molars: Are we underestimating species diversity in the Mesozoic? Journal of Mammalian Evolution, 12:283–299.

Rich, T. H., T. F. Flannery, P. Trusler, L. Kool, N. A. Van Klaveren, and P. Vickers-Rich. 2002. Evidence that monotremes and ausktribosphenids are not sistergroups. Journal of Vertebrate Paleontology 22:466–469.

Rose, K. D. 2006. The Begining of The Age of Mammals. Johns Hopkins University Press, Baltimore, Maryland, 428 pp.

Rosowski, J. J., and A. Graybeal. 1991. What did *Morganucodon* hear?. Zoological Journal of the Linnean Society 101:131–168.

Rosowski, J. J. 1992. Hearing in transitional mammals: predictions from the middle-ear anatomy and hearing capabilities of extant mammals; pp. 615–631 In: D. B. Webster, R. R. Fay, A. N. Popper (eds.), The evolutionary Biology of Hearing. Springer, New York.

Rowe, T. 1988. Definition, diagnosis, and origin of Mammalia. Journal of Vertebrate Paleontology 8:241–264.

Rougier, G. W., J. R. Wible, and J. A. Hopson. Basicranial anatomy of *Priacodon fruitaensis* (Triconodontidae, Mammalia) from the Late Jurassic of Colorado, and a reappraisal of mammaliaform interrelationships. 1996. American Museum Novitates 3183:1–38.

Rougier, G. W., A. M. Forasiepe, R. V. Hill, and M. J. Novacek. 2009. New mammalian remains from the Late Cretaceous La Colonia Formation, Patagonia, Argentina. Acta Palaeontologica Polonica 54:195–212.

Rougier, G. W., S. Apesteguía, and L. C. Gaetano. 2011. Highly specialized mammalian skulls from the Late Cretaceous of South America. Nature 479:98–102.

Rougier, G. W., J. R. Wible, R. M. Beck, and S. Apesteguía. 2012. The Miocene mammal Necrolestes demonstrates the survival of a Mesozoic nontherian lineage into the late Cenozoic of South America. Proceedings of The National Academy of Sciences 109:20053–20058.

Rowe, T., T. H. Rich, P. Vickers-Rich, M. Springer, and M. O. Woodburne. 2008. Proceedings of the National Academy of Sciences 105:1238–1242.

Saarinen J. J., A. G. Boyer, J. H. Brown, D. P. Costa, S. K. M. Ernest, A. R. Evans, M. Fortelius, M. J. Hamilton, L. E. Harding, K. Lintulaakso, S. K. Lyons, J. G. Okie, R. M. Sibly, P. R. Stephens, J. Theodor, M. D. Uhen, and F. A. Smith. 2014. Patterns of maximum body size evolution in Cenozoic land mammals: eco-evolutionary processes and abiotic forcing. Proceedings of The Royal Society B 281:1–10.

Schuknecht H. F., K. Watanuki, T. Takahashi, A. A. Belal, R. S. Kimura, D. D. Jones, and C. Y. Ota. 1974. Atrophy of the stria vascularis, a common cause for hearing loss. The Laryngoscope 84:1777-1821.

Shen, L., H. Farid, and M. A. McPeek. 2009. Modeling three-dimensional morphological structures using spherical harmonics. Evolution: International Journal of Organic Evolution 63:1003–1016.

Shen, L.2010. SPHARM-MAT v1.0.0 documentation. http://www.nitrc.org/projects/spharm-mat.

Simpson, G. G. 1928. A Catalogue of the Mesozoic Mammalia in the Geological Department of the British Museum. Trustees of the British Museum, London, 215 pp.

Simpson, G. G. 1929. American Mesozoic Mammalia. Memoirs of the Peabody Museum of Natural History 3:1–235.

Slater, G. L. 2013. Phylogenetic evidence for a shift in the mode of mammalian body size

evolution at the Cretaceous-Palaeogene boundary. Methods in Ecology and Evolution 4:734–744.

Smith, F. A., A. G. Boyer, J. B. Brown, D. P. Costa, T. Dayan, S. K. M. Ernest, A. R. Evans, M. Fortelius, J. L. Gittleman, M. J. Hamilton, L. E. Harding, K. Lintulaakso, S. K. Lyons, C. McCain, J. G. Okie, J. J. Saarinen, R. M. Silby, P. R. Stephens, J. Theodor, M. D. Uhen. 2010. The evolution of maximum body size of terrestrial mammals. Science 330:1216–1219.

Smith, F. A., and S. K. Lyons.2011. How big should a mammal be? A macroecological look at mammalian body size over space and time. Philosophical Transactions of the Royal Society of London B 366:2364–2378.

Tarver, J. E. and P. C. Donoghue. 2011. The trouble with topology: phylogenies without fossils provide a revisionist perspective of evolutionary history in topological analyses of diversity. Systematic Biology 60:700–712.

Wible, J. R., G. W. Rougier, M. J. Novacek, M. C. McKenna, and D. Dashzeveg. A mammalian petrosal from the Early Cretaceous of Mongolia: implications for the evolution of the ear region and mammaliamorph interrelationships. 1995. American Museum Novitates 3149:1–19.

Wilson G.P., A. R. Evans, I. J. Corfe, P. D. Smits, M. Fortelius, and J. Jernvall. 2012. Adaptive radiation of multituberculate mammals before the extinction of dinosaurs. Nature 483:457–460.

Curriculum Vita for Ph. D Cantidates
Johns Hopkins University School of Medicine

Anthony (Tony) Harper — August, 2019

DOB: 8 August 1984
Born in Pasadena, California

Educational History:

Ph.D.	2019	Functional Anatomy and Evolution	Johns Hopkins SOM
M.Sc.	2012	Evolutionary Biology	San Diego State University
B.S.	2007	Environmental Geology	UC Santa Cruz

Scholarships fellowships, or other external funding:

None

Publications, peer reviewed:

• 2019. **Harper T,** Rougier GW. Petrosal morphology and cochlear function in Mesozoic stem therians. PLOS One 14(8): e0209457.https://doi.org/10.1371/journal.pone.0209457

• in review. Luckett WP, Hong-Luckett N, **Harper T**. Initiation and early development of the postcanine dentition in the dasyurid marsupial *Dasyurus viverrinus*. Memoirs of the Museum Victoria.

• 2019. Luckett WP, Hong-Luckett N, **Harper T**. Microscopic analysis of the developing dentition in the pouch young of the extinct marsupial *Thylacinus cynocephalus*, with an assessment of other developmental stages and eruption. Memoirs of the Museum Victoria 78: 1-21.

• 2018. **Harper T**, Parras A, Rougier GW. *Reigitherium* (Meridiolestida, Mesungulatoidea) an enigmatic Late Cretaceous mammal from Patagonia, Argentina: Morphology, affinities, and dental evolution. Journal of Mammalian Evolution.doi.org/10.1007/s10914-018-9437-x

• 2011. Archibald JD, Zhang Y, **Harper T,** Cifelli R. *Protungulatum*, Confirmed Cretaceous Occurrence of an Otherwise Paleocene Eutherian (Placental?) Mammal. Journal of Mammalian Evolution 18(3): 153-151

• 2004. Kapahi P, Zid BM, **Harper T**, Koslover D, Sapin V, Benzer S. Regulation of lifespan in *Drosophila* by modulation of genes in the TOR signaling pathway. Current Biology 14(10): 885-890

Publications, chapters, and other non-peer reviewed:
None

Posters, abstracts, etc.:

• 2019. The Origin of Mammalian High Frequency Hearing: Modeling Cochlear Function from the Fossil Record. University of Louisville, Department of Anatomy and Neurobiology, Invited Speaker.

• 2018**. Harper T**, Rougier, G. W. Cretaceous Stem-Therian Petrosals from Mongolia Provide Earliest Evidence for Modern Cochlear Physiology. Society of Vertebrate Paleontology Annual Meeting, Albuquerque. Presentation.

• 2017. **Harper T**, Rougier G. Systematic and Functional Implications of New Material from The Late Cretaceous Mammal *Reigitherium*. Society of Vertebrate Paleontology Annual Meeting, Calgary. Poster

• 2016. **Harper T**, Perry J. Comparative Myology and Adductor Leverage in Phalangeriform Possum Jaws. International Congress of Vertebrate Morphology Meeting, Washington DC. Poster

• 2016. **Harper T**, Hu H, Passey B. Carbon Isotope Compositions of *Kryptobaatar* Enamel and Ecologically Widespread 13 C Enrichment in Upper Cretaceous Mongolia. Society of Vertebrate Paleontology Annual Meeting, Salt Lake City. Poster

• 2015. **Harper T**. New Taeniodont Remains from The Early Eocene Willwood Formation, Bighorn Basin, Wyoming. Society of Vertebrate Paleontology Annual Meeting, Dallas. Poster

• 2011. **Harper T**. Three Dimensional Mesowear Analysis of Late Cretaceous Eutherians. Society of Vertebrate Paleontology Annual Meeting, Las Vegas. Poster

Inventions, Patents, Copyrights:
None

Service and Leadership:
2018 "Science Outside the Lines" outreach program at Henderson-Hopkins Middle School